



University of HUDDERSFIELD

University of Huddersfield Repository

Bryant, David

Thermo-elastic Deformation of a Vented Brake Disc

Original Citation

Bryant, David (2010) Thermo-elastic Deformation of a Vented Brake Disc. Doctoral thesis, University of Huddersfield.

This version is available at <http://eprints.hud.ac.uk/id/eprint/9076/>

The University Repository is a digital collection of the research output of the University, available on Open Access. Copyright and Moral Rights for the items on this site are retained by the individual author and/or other copyright owners. Users may access full items free of charge; copies of full text items generally can be reproduced, displayed or performed and given to third parties in any format or medium for personal research or study, educational or not-for-profit purposes without prior permission or charge, provided:

- The authors, title and full bibliographic details is credited in any copy;
- A hyperlink and/or URL is included for the original metadata page; and
- The content is not changed in any way.

For more information, including our policy and submission procedure, please contact the Repository Team at: E.mailbox@hud.ac.uk.

<http://eprints.hud.ac.uk/>

**Thermo-elastic Deformation of a
Vented Brake Disc**

David Bryant

A thesis submitted to the University of Huddersfield

in partial fulfilment of the requirements for

the degree of Doctor of Philosophy

University of Huddersfield in collaboration with

Bentley Motors Limited

January 2010

Copyright Statement

- i. The author of this thesis (including any appendices and/or schedules to this thesis) owns any copyright in it (the "Copyright") and s/he has given The University of Huddersfield the right to use such Copyright for any administrative, promotional, educational and/or teaching purposes.
- ii. Copies of this thesis, either in full or in extracts, may be made only in accordance with the regulations of the University Library. Details of these regulations may be obtained from the Librarian. This page must form part of any such copies made.
- iii. The ownership of any patents, designs, trade marks and any and all other intellectual property rights except for the Copyright (the "Intellectual Property Rights") and any reproductions of copyright works, for example graphs and tables ("Reproductions"), which may be described in this thesis, may not be owned by the author and may be owned by third parties. Such Intellectual Property Rights and Reproductions cannot and must not be made available for use without the prior written permission of the owner(s) of the relevant Intellectual Property Rights and/or Reproductions.

Abstract

The subject of retarding a moving vehicle or object in a controlled manner has been investigated over hundreds of years with many different solutions being developed over the years. As time has progressed a common overall design has almost uniformly been agreed upon for vehicle use; a brake disc and caliper or brake drum arrangement. As vehicle refinement has improved there has been increasing focus on the refinement of such designs with regards to their noise, vibration and harshness (NVH) characteristics. Whilst brake noise has had significant research analysing its cause, effect and solutions, brake judder has had less research focussed upon it. The principal reason for past research priorities and the recent interest in judder is because of the increased demands being placed on brakes – higher power absorption with lighter structures. The subject of this thesis was to address the least known phenomena of brake judder, that of the thermo-elastic deformation of vented brake discs. The research utilised experimental, analytical and empirical methods to give a broader understanding of the transient deformation process, both thermo-plastic and thermo-elastic, of a high performance vehicle disc brake.

Initial characterisation of thermal judder was carried out on-vehicle where it was identified that brake pressure could be used as a reliable indicator to show the developing nature of this phenomenon. The brake pressure pulsation was shown to change from low order (first or second order) to high order (up to eighth order) over the duration of a high speed vehicle brake test which involved up to thirty braking events. The pressure pulsation indicated a link to brake disc deformation with the magnitude and order of brake pressure variation increasing with increasing disc temperature. The highly dynamic, transient, nature of brake disc distortion was also investigated on a bespoke quarter car suspension brake dynamometer. Thermo-elastic wave-like deformation was shown to occur during the process of a single braking event with the order of deformation corresponding to the brake pressure variation. The order of this wave-like deformation was shown to be linked to the amount of energy transferred into the braking system with higher energy braking events resulting in higher order deformation. Thermal images of the brake disc have shown an equispaced formation of hot-spots on the inboard and outboard friction ring surfaces which was linked to the disc waveform. The wave-like deformation was attributed to circumferential buckling of the brake disc as suggested by Lang [1]. This resulted from rapid thermal expansion of the friction rings due to the sudden

influx of heat during braking. Thermal gradients between the hot and cold regions of the brake disc constrained the radial thermal expansion of the friction ring and caused compressive stresses to build up. When the tangential load causing the stress was in excess of the critical buckling load, buckling of the brake disc occurred with the mode order of the buckled disc related to the temperature of the friction ring. Stress relieving of the brake disc was shown to occur during brake testing on the brake dynamometer causing a thermo-plastic effect. This “in service” stress relieving effect removed the retained stresses resulting from the casting and machining processes and allowed the disc to adopt a second order mode of deformation. Data from the on-vehicle and dynamometer testing was used to generate and validate finite element analysis simulations which were used to investigate thermal inputs and heat dissipation from the brake disc. These findings were then combined with that of an associated aerodynamic study [2] to generate a modified brake disc vent profile which reduced the surface temperature variation, thermal gradients and maximum disc temperature. On-vehicle testing of the prototype design showed an average 14% reduction in maximum disc temperature and it was proposed that this would reduce the propensity for the disc to generate judder by reducing the thermal deformation of the brake disc.

Table of Contents

1. INTRODUCTION	19
1.1. AIMS	21
1.2. OBJECTIVES	21
1.3. THE BRAKE SYSTEM	22
1.3.1. <i>The Brake Disc</i>	22
1.3.2. <i>The Brake Caliper</i>	24
1.4. RESEARCH BRAKING SYSTEM.....	24
2. LITERATURE REVIEW	26
2.1. INTRODUCTION TO BRAKE JUDDER	26
2.1.1. <i>Cold Judder</i>	26
2.1.2. <i>Hot Judder</i>	28
2.1.3. <i>Drone</i>	29
2.2. TYPES OF DISC DEFORMATION.....	30
2.2.1. <i>Coning</i>	30
2.2.2. <i>Run-out</i>	31
2.2.3. <i>Wave</i>	32
2.3. DISCUSSION OF CURRENT AND PAST RESEARCH.....	32
2.3.1. <i>Mathematical Modelling</i>	32
2.3.2. <i>Physical Testing</i>	34
2.3.3. <i>Hot spotting</i>	39
2.3.4. <i>Finite Element analysis</i>	42
2.3.5. <i>Multi-body dynamics</i>	43
2.4. SUMMARY	45
3. ON-VEHICLE TESTING AND ANALYSIS.....	46
3.1. INTRODUCTION	46
3.2. VEHICLE TESTING	46
3.2.1. <i>Theory</i>	47
3.2.2. <i>Equipment</i>	49
3.2.3. <i>Procedure</i>	51
3.2.4. <i>Results</i>	57
3.2.4.1. <i>Fourier Analysis Method</i>	58
3.2.4.2. <i>Fourier Analysis and Subjective Test Data Comparison</i>	62
3.2.4.3. <i>Brake Pressure Variation</i>	67
3.2.4.4. <i>Pad and Caliper Vibration</i>	75
3.2.4.5. <i>Run-out</i>	78
3.2.5. <i>On-Vehicle Testing and Analysis Summary</i>	80
3.2.6. <i>Post On-Vehicle Test Analysis</i>	81

3.2.6.1. CMM Scanning	81
3.2.6.2. Braking System Temperature	85
3.2.6.3. Buckling Mechanism.....	88
3.2.7. Discussion.....	93
4. BRAKE DYNAMOMETER TESTING AND ANALYSIS.....	95
4.1.1. Dynamometer selection.....	95
4.1.2. Brake Dynamometer Uses.....	96
4.1.3. Brake Judder Dynamometer Description	96
4.1.4. Specifications.....	99
4.1.5. Instrumentation.....	100
4.1.5.1. Pressure Measurement	100
4.1.5.2. Displacement Measurement.....	101
4.1.5.3. Thermocouples	103
4.1.5.4. Thermal Camera	103
4.2. DYNAMOMETER MID-SPEED TESTING	105
4.2.1. Methodology	105
4.2.2. Procedure	106
4.2.3. Results.....	108
4.2.3.1. Clamping Method.....	126
4.2.3.2. Stress Relieving.....	130
4.2.4. Mid-Speed Dynamometer Testing Discussion	135
4.3. DYNAMOMETER HIGH SPEED TESTING	139
4.3.1. Methodology.....	139
4.3.2. Results.....	139
4.3.3. Discussion.....	144
4.3.4. Thermal Imaging.....	144
4.4. DYNAMOMETER HIGH SPEED TESTING DISCUSSION	149
4.5. EXPERIMENTAL DESIGN AND TESTING SUMMARY	150
5. FINITE ELEMENT ANALYSIS	152
5.1. INTRODUCTION	152
5.2. PROCEDURE	152
5.2.1. Heat Flux.....	154
5.2.2. Energy Calculations	155
5.2.3. Modelling.....	159
5.2.3.1. Material Property Sensitivity Analysis	164
5.3. RESULTS	169
5.4. IMPROVEMENT TO CURRENT DISC DESIGN	173
5.4.1. Introduction	173
5.4.2. Procedure	174
5.4.3. Current Design Analysis.....	174

5.4.4. Design Development.....	177
5.4.5. Thermal Analysis Procedure.....	179
5.4.6. Thermal Analysis Results.....	180
5.5. FINITE ELEMENT ANALYSIS DISCUSSION.....	188
6. CONCLUSIONS.....	190
7. RECOMMENDATIONS FOR FURTHER WORK.....	193
8. REFERENCES	194
9. BIBLIOGRAPHY.....	201
10. APPENDIX	202
10.1. ON-VEHICLE TEST EQUIPMENT.....	202
10.2. ON-VEHICLE TESTING - ACCELEROMETER DATASHEET	205
10.3. DYNAMOMETER TEST EQUIPMENT.....	206
10.3.1. Pressure Transducer (P751-0001).....	206
10.3.2. Displacement Transducer	208
10.3.3. Rubbing Thermocouple.....	210
10.4. FFT MATLAB CODE.....	211
10.5. ON-VEHICLE BPV DEVELOPMENT.....	212

Word count: 46115

List of Figures

FIGURE 1.1: BREAKDOWN OF NVH ISSUES FACING A VEHICLE MANUFACTURER [23].....	20
FIGURE 1.2: GENERAL BRAKE DISC FEATURES.	23
FIGURE 1.3: CROSS SECTION VIEW SHOWING THE VANE ORIENTATION.....	25
FIGURE 2.1: DISC THICKNESS VARIATION CAUSED BY RUN-OUT AND POOR PAD RETRACTION.....	27
FIGURE 2.2: EXAMPLE OF PAD IMPRINTING	28
FIGURE 2.3: EXAMPLE OF SEVERE BLUE SPOTTING ON A BRAKE DISC.....	30
FIGURE 2.4: INBOARD VENTILATED (LEFT) AND OUTBOARD VENTILATED (MIDDLE) AND SWAN NECK (RIGHT).....	31
FIGURE 2.5: THERMAL IMAGE OF HOT SPOTS FORMING ON A BRAKE DISC	41
FIGURE 3.1: DATA LOGGING EQUIPMENT.	50
FIGURE 3.2: CALIPER & BACK-PLATE ACCELEROMETERS (LEFT) AND BRAKE LINE PRESSURE TRANSDUCER (RIGHT).....	50
FIGURE 3.3: DIAGRAM SHOWING THE POSITION OF THE ACCELEROMETER ON THE BRAKE PAD BACK PLATE.	51
FIGURE 3.4: EVALUATION OF DIFFERENT REPLACEMENT BRAKING TESTS TO ACCOUNT FOR SPEED REDUCTION.....	55
FIGURE 3.5: FFT DISTRIBUTION SHOWING TOLERANCE POINT.....	59
FIGURE 3.6: GRAPH SHOWING ORIGINAL BRAKE PRESSURE SIGNAL (GREEN) AND RESULT FROM FOURIER ANALYSIS AFTER TOLERANCE HAS BEEN APPLIED (BLUE).....	60
FIGURE 3.7: BLOCK DIAGRAM OF MATLAB FOURIER ANALYSIS PROCESS.....	61
FIGURE 3.8: RIGHT HAND DISC PRESSURE DOMINANT FOURIER FREQUENCIES (DISC SET 2).	62
FIGURE 3.9: CROSS CORRELATION BETWEEN BRAKE PRESSURE VARIATION AND IN PLANE AND OUT OF PLANE VIBRATION (DISC SET 2).....	64
FIGURE 3.10: SUBJECTIVE SCORES AND MAXIMUM DISC TEMPERATURES. NOTE: PEDAL AND BODY SUBJECTIVE SCORES ARE IDENTICAL (DISC SET 1).....	64
FIGURE 3.11: COMPARISON BETWEEN LEFT AND RIGHT BRAKE DISCS SHOWING BPV DEVELOPMENT (DISC SET 1)	65
FIGURE 3.12: DOMINANT FOURIER FREQUENCIES, MAXIMUM TEMPERATURE AND SUBJECTIVE SCORES FOR RIGHT HAND FRONT BRAKE DISC (DISC SET 2).....	66
FIGURE 3.13: DOMINANT FOURIER FREQUENCIES, MAXIMUM TEMPERATURE AND SUBJECTIVE SCORES FOR LEFT HAND FRONT BRAKE DISC (DISC SET 2).....	66
FIGURE 3.14: RIGHT HAND FRONT BRAKE PRESSURE VARIATION STOP 13 – 1 ST DISC SET.....	68
FIGURE 3.15: RIGHT HAND FRONT BRAKE PRESSURE VARIATION STOP 17 – 1 ST DISC SET.....	68
FIGURE 3.16: RIGHT HAND FRONT BRAKE PRESSURE VARIATION STOP 23 SHOWING THE DOMINANT TWO PRESSURE PULSES – 1 ST DISC SET.....	68
FIGURE 3.17: LEFT HAND FRONT BRAKE PRESSURE VARIATION STOP 13 – 1 ST DISC SET.....	69
FIGURE 3.18: LEFT HAND FRONT BRAKE PRESSURE VARIATION STOP 23 – 1 ST DISC SET.....	69
FIGURE 3.19: RIGHT HAND FRONT BRAKE PRESSURE VARIATION STOP 15 – 2 ND DISC SET.	71

FIGURE 3.20: RIGHT HAND FRONT BRAKE PRESSURE VARIATION STOP 30 – 2 ND DISC SET.	71
FIGURE 3.21: LEFT HAND FRONT BRAKE DISC PRESSURE VARIATION STOP 15 – 2 ND DISC SET.	72
FIGURE 3.22: LEFT HAND FRONT BRAKE DISC PRESSURE VARIATION STOP 30 – 2 ND DISC SET.	72
FIGURE 3.23: DEVELOPMENT OF BRAKE PRESSURE VARIATION BETWEEN STOP 15 AND STOP 30 – 2 ND DISC SET.	74
FIGURE 3.24: TANGENTIAL AND AXIAL BACK-PLATE VIBRATION.	75
FIGURE 3.25: THEORETICAL GRAPH OF BPV AND BTV AS A PAD STRIKES A PEAK ON THE DISC SURFACE – ARBITRARY SCALE.	76
FIGURE 3.26: CORRELATION BETWEEN BRAKE PRESSURE VARIATION AND TANGENTIAL (IN-PLANE) PAD VIBRATION.....	77
FIGURE 3.27: COMPARISON BETWEEN BPV (TOP) AND TANGENTIAL CALIPER VIBRATION (BOTTOM) FOR THE LEFT HAND BRAKE.	78
FIGURE 3.28: LEFT HAND BRAKE DISC RUN-OUT PRE AND POST TESTING.	79
FIGURE 3.29: RIGHT HAND BRAKE DISC RUN-OUT PRE AND POST TESTING.	79
FIGURE 3.30: DISC 1 (LEFT) AND DISC 2 (RIGHT) BOTH SHOWING 2 ND ORDER DEFORMATION (ALL AXES SHOW DISTANCE IN MM).	82
FIGURE 3.31: CMM SURFACE SCAN OF AN UN-USED BRAKE DISC (ALL AXES SHOW DISTANCE IN MM). ..	82
FIGURE 3.32: DISC 1 SHOWING INBOARD DISC FACE (LEFT) AND OUTBOARD FACE (RIGHT) SHOWING 2 ND ORDER DEFORMATION AND DISC PEAKS (ALL AXES SHOW DISTANCE IN MM).	83
FIGURE 3.33: SURFACE VARIATION AT MEAN RUBBING RADIUS AND BRAKE PRESSURE VARIATION.	84
FIGURE 3.34: TEMPERATURE PLOT FOR STOPS 11-13.....	85
FIGURE 3.35: TEMPERATURE PLOT FOR STOPS 14-19.	86
FIGURE 3.36: BRAKE PAD BACK PLATE TEMPERATURE FOR STOPS 14-19.	87
FIGURE 3.37: DISC ANNULUS REPRESENTED AS A STRAIGHT BEAM.	89
FIGURE 4.1: SIDE PROFILE OF JUDDER RIG AND MOTOR.	98
FIGURE 4.2: DETAIL VIEW OF RIG ASSEMBLY SHOWING RIGID SUSPENSION MOUNTING POINTS, BRAKE ASSEMBLY AND SUSPENSION ASSEMBLY.....	98
FIGURE 4.3: GENERAL VIEW OF THE BRAKE JUDDER RIG – RUBBER MOUNT IS VISIBLE BENEATH THE SUSPENSION UPRIGHT.	99
FIGURE 4.4: TRANSDUCER MOUNTING ARRANGEMENT.	101
FIGURE 4.5: GENERAL VIEW OF THERMAL CAMERA ARRANGEMENT.	105
FIGURE 4.6: MEASURING THE INSTALLED RUN-OUT OF THE BRAKE DISC ON THE DYNAMOMETER.....	106
FIGURE 4.7: 18/01/08 DISC 4 BRAKE PRESSURE GRAPH.	107
FIGURE 4.8: 26-09-07 DISC 2, INBOARD DISPLACEMENT, 10 TH STOP, 300°C SHOWING 3 RD ORDER DEFORMATION.	108
FIGURE 4.9: 26-09-07 DISC 2, BRAKE PRESSURE VARIATION 10 TH STOP HOT 300°C.	109
FIGURE 4.10: GRAPH SHOWING THE CORRELATION BETWEEN BRAKE PRESSURE VARIATION AND DISC DISTORTION	110
FIGURE 4.11: BRAKE PRESSURE VARIATION FROM ON-VEHICLE TESTING SHOWING 3 DISTINCT PRESSURE PULSES.....	111

FIGURE 4.12: 26-09-07 DISC 2, FFT BRAKE PRESSURE VARIATION 10 TH STOP HOT 300°C.	111
FIGURE 4.13: 18/01/08 DISC 4 START OF TEST – NO BRAKING APPLIED.	113
FIGURE 4.14: 18/01/08, DISC 4, 1 ST BRAKING EVENT – START OF BRAKING.....	114
FIGURE 4.15: 18/01/08, DISC 4, 1 ST BRAKING EVENT – END OF BRAKING.	115
FIGURE 4.16: 18/01/08, DISC 4, 1 ST BRAKING EVENT – BRAKES RELEASED.	116
FIGURE 4.17: 12/02/08 DISC 4, GRAPHS OF OUTBOARD DISC DISPLACEMENT FOR THE 1ST BRAKING EVENT. READING FROM TOP LEFT; NO BRAKING, START OF BRAKING, END OF BRAKING, BRAKES RELEASED.....	117
FIGURE 4.18: 12/02/08 DISC 4 GRAPHS OF OUTBOARD DISC DISPLACEMENT FOR THE 13TH BRAKING EVENT. READING FROM TOP LEFT; NO BRAKING, START OF BRAKING, END OF BRAKING, BRAKES RELEASED.	118
FIGURE 4.19: CORRELATION BETWEEN DISC DISTORTION AND BPV SHOWING APPARENT 3 RD ORDER DEFORMATION AND BPV.....	119
FIGURE 4.20: CORRELATION BETWEEN DISC DISTORTION AND BPV SHOWING DOMINANT 2 ND ORDER DEFORMATION AND POSSIBLE 2 ND ORDER BPV.	120
FIGURE 4.21: FOURIER ANALYSIS OF THE BRAKE PRESSURE VARIATION – SPEED OF DISC ROTATION 30HZ	121
FIGURE 4.22: FOURIER ANALYSIS OF THE OUTBOARD BRAKE DISTORTION – SPEED OF DISC ROTATION 30HZ	121
FIGURE 4.23: DEVELOPMENT OF BRAKE PRESSURE VARIATION THROUGH A SINGLE 8 STOP TEST SHOWING CORRELATION WITH DISC SURFACE TEMPERATURE.....	122
FIGURE 4.24: GRAPH COMPARING THE MODE ORDER OF OFF-BRAKE DISC DISTORTION TO TEMPERATURE.	123
FIGURE 4.25: INBOARD AND OUTBOARD DISPLACEMENT SHOWING THE DIFFERENCE BETWEEN STOP 1 AND STOP 6 IN A BRAKING SEQUENCE.	123
FIGURE 4.26: GRAPH OF DISC RUN-OUT (COLD) SHOWING SECOND ORDER DEFORMATION.	125
FIGURE 4.27: GRAPH OF DISC RUN-OUT (COLD) SHOWING DOMINANT FIRST ORDER RUN-OUT.	125
FIGURE 4.28: COMPARISON BETWEEN IN STOP ‘HOT’ DEFORMATION (LEFT) AND POST TEST ‘COLD’ DEFORMATION (RIGHT).....	126
FIGURE 4.29: SPACER TO ALTER THE CLAMPING AREA OF THE BRAKE DISC, HUB AND WHEEL (LEFT) AND ASSOCIATED FINITE ELEMENT ASSEMBLY WITH HIGH MESH DENSITY IN CRITICAL AREAS.....	127
FIGURE 4.30: DEFORMATION OF THE BRAKE DISC DUE TO CLAMPING FORCE WITH SPACER FITTED. LARGEST DISC DEFLECTION IS SEEN ON THE RIGHT HAND SIDE.	128
FIGURE 4.31: EFFECT ON THE INSTALLED RUN-OUT OF THE BRAKE DISC OF ALTERING THE CLAMPING AREA BETWEEN DISC AND WHEEL.	129
FIGURE 4.32: GRAPH SHOWING THE SIMILARITIES IN THE DISC WAVEFORM DURING BRAKING WITH AND WITHOUT THE SPACER FITTED.	130
FIGURE 4.33: DISC 3 (INBOARD FRICTION RING) PRE STRESS RELIEVING (LEFT) AND POST STRESS RELIEVING (RIGHT) – SAME SCALE.	131
FIGURE 4.34: DISC 3 ALIGNED INBOARD SURFACE SCAN AT A RADIUS OF 167MM	132

FIGURE 4.35: DISC 3 (OUTBOARD FRICTION RING) PRE STRESS RELIEVING (LEFT) AND POST STRESS RELIEVING (RIGHT) – SAME SCALE	132
FIGURE 4.36: DISC 3 ALIGNED OUTBOARD SURFACE SCAN AT A RADIUS OF 167MM	133
FIGURE 4.37: DISC 6 (INBOARD FRICTION RING) PRE STRESS RELIEVING (LEFT) AND POST STRESS RELIEVING (RIGHT) – SAME SCALE	134
FIGURE 4.38: DISC 6 (OUTBOARD FRICTION RING) PRE STRESS RELIEVING (LEFT) AND POST STRESS RELIEVING (RIGHT) – SAME SCALE	134
FIGURE 4.39: GRAPH SHOWING THE SIMILARITIES BETWEEN THE PRE AND POST TEST INSTALLED RUN-OUT OF A STRESS RELIEVED BRAKE DISC.....	135
FIGURE 4.40: FRICTION MATERIAL DEPOSITION/HOT SPOTTING RESULTING FROM 10TH ORDER DISC DEFORMATION. INBOARD (LEFT) AND OUTBOARD (RIGHT) DISC IMAGES SHOWN WITH REFERENCE LINE.	139
FIGURE 4.41: COMBINED IMAGE HIGHLIGHTING THE HIGH POINTS ON THE INBOARD (RED) AND OUTBOARD SIDE (GREEN).....	140
FIGURE 4.42: CMM SURFACE SCAN OF THE BRAKE DISC SHOWING HIGH AND LOW POINTS.....	140
FIGURE 4.43: OUTBOARD SURFACE VARIATION DUE TO PAD DEPOSITION AS A RESULT OF HOT SPOTTING.	141
FIGURE 4.44: MODAL ANALYSIS OF THE BRAKE DISC SHOWING THE FIRST 3 NATURAL FREQUENCIES...	142
FIGURE 4.45: THERMAL IMAGE OF BRAKE DISC SHOWING THE VANE PATTERN	145
FIGURE 4.46: TEMPERATURE PROFILE AROUND THE DISC SURFACE AT 187MM. THE NUMBER OF PEAKS CORRELATES WITH THE NUMBER OF VANES IN THE VISIBLE PORTION OF THE DISC.....	146
FIGURE 4.47: THERMAL IMAGE SHOWING THERMAL BANDING AND REGIONS OF PAD DEPOSITION.	147
FIGURE 4.48: THERMAL IMAGE OF DISC SHOWING 10 AREAS OF CONCENTRATED HEAT. THE REVERSE SIDE INDICATED THE SAME NUMBER BUT POSITIONED BETWEEN THE OPPOSITE SIDE AREAS. ROTATION CCW.....	148
FIGURE 4.49: THERMAL IMAGE OF DISC SHOWING 9 AREAS OF CONCENTRATED HEAT. THE REVERSE SIDE INDICATED THE SAME NUMBER BUT POSITIONED BETWEEN THE OPPOSITE SIDE AREAS. NOTE LEADING EDGE OF “HOT SPOTS” WERE RADIAL, CCW ROTATION.	149
FIGURE 5.1: GENERAL IMAGE OF THE BRAKE DISC CAD MODEL SHOWING THE MACHINED BALANCE...	153
FIGURE 5.2: IMAGE SHOWING HEAT FLUX APPLICATION TO THE FRICTION RING SURFACES (INBOARD FRICTION RING SHOWN)	154
FIGURE 5.3: STANDARD HEAT FLUX APPLICATION FOR A 3 STOP TEST BASED ON-VEHICLE DATA.....	159
FIGURE 5.4: CONVECTIVE COOLING COEFFICIENT GRAPH WITH DATA OBTAINED FROM CFD.....	160
FIGURE 5.5: HEAT TRANSFER COEFFICIENT FOR CLOCKWISE AND ANTI-CLOCKWISE ROTATION.	161
FIGURE 5.6: BRAKE DISC TEMPERATURES FROM VEHICLE TESTING.	163
FIGURE 5.7: CROSS SECTION THROUGH BRAKE DISC SHOWING EQUAL FRICTION RING THICKNESSES. ...	164
FIGURE 5.8: MESH FOR THE FINITE ELEMENT MODEL.	164
FIGURE 5.9: GRAPH SHOWING SIMULATED BRAKE DISC TEMPERATURE RESULTING FROM VARYING THE BRAKE DISC MATERIAL PROPERTIES.....	166
FIGURE 5.10: GRAPH SHOWING SIMULATED TEMPERATURE AGAINST MEASURED DATA.....	168

FIGURE 5.11: SIMULATED DISC SURFACE TEMPERATURE FOLLOWING THREE HIGH SPEED STOPS.	169
FIGURE 5.12: SIMULATED TEMPERATURE GRADIENT THROUGH A VANE CROSS-SECTION.	170
FIGURE 5.13: RESULTS OF ADJUSTING THE CONVECTIVE HEAT TRANSFER COEFFICIENT BY $\pm 10\%$, APPLICATION OF BRAKING LOADS INDICATED BY DOTTED LINE	171
FIGURE 5.14: SIMULATED SURFACE TEMPERATURE VARIATION DUE TO UNDERLYING VANE GEOMETRY AND BALANCE	175
FIGURE 5.15: THERMAL IMAGE OF BRAKE DISC SHOWING THE VANE PATTERN	176
FIGURE 5.16: TEMPERATURE PROFILE AROUND THE DISC SURFACE AT 187MM CLEARLY SHOWING THE VARIATION DUE TO THE DISC VANES.....	176
FIGURE 5.17: TEMPERATURE PROFILE (EXAGGERATED SCALE) DUE TO VENT GEOMETRY AND PROPOSED VENT CROSS SECTION.....	177
FIGURE 5.18: GENERAL VIEW OF VENT DESIGN	178
FIGURE 5.19: GENERAL VIEW OF THE VENT END PROFILE.....	179
FIGURE 5.20: GRAPH SHOWING COMPARISON BETWEEN SIMULATED AND ACTUAL DATA FOR THE STANDARD BRAKE DISC.	180
FIGURE 5.21: GRAPH SHOWING EVOLUTION OF THE WAVY BRAKE DISC DESIGN	181
FIGURE 5.22: GRAPH SHOWING COMPARISON OF WAVY DESIGN ITERATIONS AND THE STANDARD DISC DESIGN (ALL IDENTICAL MASS).....	182
FIGURE 5.23: CROSS SECTION THROUGH BRAKE DISC. "SLICES" REMOVED FROM THE FRICTION RING SURFACES TO EQUALISE THE DISC MASS SHOWN HATCHED.	183
FIGURE 5.24: WAVY DESIGN 7MM THERMAL SIMULATION	184
FIGURE 5.25: END VIEW OF DISC SHOWING THERMAL GRADIENT (WAVY 7MM).....	185
FIGURE 5.26: AERO DESIGN 1 SHOWING TEMPERATURE DISTRIBUTION (LEFT) AND CONVECTIVE HEAT TRANSFER COEFFICIENT (RIGHT) [2]	186
FIGURE 5.27: IMAGE SHOWING THE ORIGINAL VANE STRUCTURE (LEFT) AND THE PROPOSED AERODYNAMIC VANE STRUCTURE (RIGHT)	187
FIGURE 5.28: BACK-TO-BACK VEHICLE TESTING OF THE PROTOTYPE DISC AND THE STANDARD DISC ...	188
FIGURE 10.1: ON-VEHICLE BPV DEVELOPMENT FOR LEFT HAND FRONT BRAKE DISC FOLLOWING ON- VEHICLE TESTING; SELECTED BRAKING EVENTS BETWEEN STOPS 11 TO 30, ONE REVOLUTION INDICATED BY ARROW.	212

List of Tables

TABLE 2-1: COMPARISON OF HOT SPOT TYPES [48]	40
TABLE 3-1: TYPICAL JUDDER TEST SCHEDULE SHOWING VEHICLE SPEED, DISC TEMPERATURE TO AIM FOR AT START OF BRAKING AND RATE OF VEHICLE DECELERATION.	53
TABLE 3-2: REVISED TEST SCHEDULE.	56
TABLE 3-3: MATERIAL PROPERTIES FOR CAST IRON AT 300°C [23].....	89
TABLE 4-1: MATERIAL PROPERTIES FOR CAST IRON - CONFIDENTIAL.....	102
TABLE 4-2: HIGH SPEED TESTS SHOWING NUMBER OF HOT SPOTS, DISC SPEED AND HOT SPOT FREQUENCY	142
TABLE 5-1 – GG15HC CAST IRON MATERIAL PROPERTIES.	165
TABLE 5-2: CONSTANT MATERIAL PROPERTIES PROVIDED BY THE ANSYS 11 SOFTWARE.....	166
TABLE 5-3: CONVECTIVE HEAT TRANSFER COEFFICIENTS USED FOR THE COOLING SENSITIVITY ANALYSIS	172
TABLE 5-4: THERMAL ANALYSIS RESULTS	183

Acknowledgements

The author would like to thank the following people for their help, support and knowledge without which this research would not have been possible:

Andrew Crampton, John Fieldhouse, Chris Talbot, Jonathan Layfield, Enda Claffey, Adrian Hildred, Jules Kite, Graeme Clark, John Conway, Kevin Lunt, Geoff Skenfield, Peter Norman, Chris Stubbs, Marco Tirovic and Nicolas Sergent.

The author would also like to thank Bentley Motors Limited for their continued collaboration, support and funding in association with the EPSRC throughout this project.

Final special thanks for her support goes to my wife Leone.

Notation

- a – REQUIRED VEHICLE DECELERATION (ms^{-2})
- A_D – ACCELERATION DUE TO DRAG (ms^{-2})
- A_D – RUBBING AREA OF ONE SIDE OF ONE FRONT BRAKE DISC (m^2)
- A_V – VEHICLE FRONTAL AREA (m^2)
- b – FRICTION RING THICKNESS (m)
- C_D – COEFFICIENT OF DRAG
- d – FRICTION RING WIDTH (m)
- D – VEHICLE DRAG (N)
- D_D – MEAN FRICTION RING DIAMETER (m)
- E – YOUNG'S MODULUS (Pa)
- F_F – FRICTIONAL FORCE (N)
- G – ACCELERATION DUE TO GRAVITY (ms^{-2})
- I – SECOND MOMENT OF AREA (m^4)
- I_D – DRIVELINE INERTIA (kg.m^2)
- K – CORRECTION FACTOR
- KE – VEHICLE KINETIC ENERGY (J)
- KE_I – KINETIC ENERGY DUE TO INERTIA OF THE DRIVELINE COMPONENTS (J)
- KE_T – TOTAL KINETIC ENERGY (J)
- L – LENGTH (m)
- L_D – DISC ANNULUS MEAN CIRCUMFERENCE (m)
- L_P – PAD LENGTH (m)
- M_D – BRAKE DISC MASS (kg)
- M_P – BRAKE PAD MASS (kg)
- M_V – VEHICLE MASS (kg)
- n – BUCKLING MODE ORDER
- N – BRAKE PAD NORMAL LOAD (N)
- P_b – BRAKING POWER (W)
- P_{bf} – BRAKING POWER AT ONE SIDE OF ONE ROTOR ON THE FRONT AXLE (W)
- P – BUCKLING LOAD (N)
- P_{crit} – ALLOWABLE BUCKLING LOAD (N)
- \dot{q} – HEAT FLUX (W.m^{-2})
- R_R – COAST DOWN DECELERATION (ms^{-2})
- R_C – COEFFICIENT OF ROLLING RESISTANCE
- R_M – MEAN RUBBING RADIUS (m)
- R_R – ROLLING RESISTANCE (N)

S – SPECIFIC HEAT CAPACITY ($\text{J.kg}^{-1}.\text{K}^{-1}$)
 t_s – STOPPING TIME (s)
 T – DISC TEMPERATURE ($^{\circ}\text{C}$)
 T_B – BRAKING TORQUE (Nm)
 V – VEHICLE VELOCITY (CONSTANT) (ms^{-1})
 V_1 – INITIAL VEHICLE VELOCITY (ms^{-1})
 V_2 – FINAL VEHICLE VELOCITY (ms^{-1})
 V_n – VEHICLE VELOCITY AT TIME n (ms^{-1})
 W – RADIANT EMITTANCE OF A GREY BODY (W.m^{-2})
 X_F/X_R – FRONT/REAR BRAKING RATIO
 \ddot{x} – BRAKE PAD ACCELERATION (ms^{-2})
 \ddot{x}_A – AXIAL ACCELERATION (ms^{-2})
 \ddot{x}_T – TANGENTIAL ACCELERATION (ms^{-2})
 Z – REQUIRED VEHICLE DECELERATION (g)
 ε - STRAIN
 ε_{exp} – COEFFICIENT OF THERMAL EXPANSION
 H_D – RATIO OF HEAT ABSORBED BY THE BRAKE DISC
 ρ – DENSITY OF AIR (kg.m^{-3})
 μ – PAD/DISC COEFFICIENT OF FRICTION
 σ – STEFAN-BOLTZMANN CONSTANT ($\text{W.m}^{-2}.\text{K}^{-4}$)
 σ_D – Stress (Pa)
 ω_1 – INITIAL ANGULAR VELOCITY (rad.s^{-1})
 ω_2 – FINAL ANGULAR VELOCITY (rad.s^{-1})

Terminology

Judder	Mechanically forced vibration of the braking system directly related to wheel speed, typically exhibits itself as a pulsation of the brake pedal, vibration of the steering wheel and floor pan and/or a loud drumming sound generally known as drone.
Drone	High frequency audible brake judder which generally occurs in the region of 100-200Hz [4][11] and is heard within the vehicle cabin. It is often a result of hot spotting of the brake disc at high speeds.
BPV	Brake Pressure Variation – Pressure variation caused by pads striking undulations on the brake disc surface. If the pulsation is large enough it can cause a noticeable pulsation of the brake pedal resulting with brake judder being experienced by the driver. The frequency of vibration can also cause excitation of suspension components at their natural frequency.
BTV	Brake Torque Variation – Torque variation caused due to the brake pads riding over an undulation on the surface of the brake disc, intrinsically linked with BPV. As with BPV this can also cause excitation of the suspension components.
DTV	Disc Thickness Variation – Variation in the thickness of the brake disc friction rings, known to cause brake judder as brake pads ride over the undulations.
Disc	The brake disc; also referred to as the brake rotor, one part of the friction pair. Can come in a variety of different designs, but is essentially a mode of converting the kinetic energy of the vehicle into thermal energy in order to slow the vehicle at a controlled rate.
Swash	When viewed directly ahead a rotating disc will appear to sway from side to side due to run-out. This is known as swash.

- Run-out** Deviation of the surface of the brake disc from an ideal flat plane. Typically a first order wave when traced around the mean rubbing radius of a new brake disc.
- Coning** After heavy thermal input, the brake disc will begin to cone either inboard or outboard depending on the design of the disc. If exaggerated the disc shape would look like a bowl.
- Concentricity** A tolerance which is specified to define how much variation is permitted in the concentricity of the circular features of the brake disc.
- Brake pads** Second part of the friction pair and is clamped against the brake disc to slow the vehicle. It is comprised of the back plate, under-layer and friction material which are all bonded together.
- Caliper** Body which houses the brake pads, pistons and brake fluid. A force applied to the brake pedal creates pressure within the brake fluid. This in turn forces the pistons to clamp the brake pad against the brake disc.
- NVH** Noise, Vibration and Harshness – Brake NVH is typically regarded as refinement issues such as squeal (noise) and judder (vibration).
- Snubber** Used to damp out fluctuations in a pressure signal. Can be either orifice or porous metal type and is used to prevent damage to equipment from pressure spikes.

Foundation Brake

The mechanical components of the braking system which generally comprises (but is not limited to) the brake disc, caliper, drum, brake pads, brake shoes and hand brake mechanism.

1. Introduction

With the increasing trend for more luxury goods and technologies to be included on new motor vehicles their weights have been steadily increasing. Typical features include air conditioning, satellite navigation and electronic stability control (ESP) together with increased safety features and the steady increase in vehicle size to both accommodate these technologies and provide increased cabin space for the driver and passengers. This increase in vehicle weight due to customer expectations has a direct knock-on effect to the kinetic energy of the vehicle when in motion, which results in the requirement for more kinetic energy to be dissipated when braking. This puts ever more thermal loading onto the vehicle brake discs leading to higher operational temperatures which increases the problem of thermal deformation and distortion. Thermal distortion of the brake disc can lead to increased brake judder and drone issues which led to the purpose of this research.

Research into the thermal deformation of vehicle brake discs has been undertaken for many years. Typically the research has focussed on a particular aspect or method of analysis such as finite element analysis (FEA) [3], on-vehicle testing [4], brake dynamometer testing [5][6] or mathematical modelling [7][8][9]. Whilst the focus in these individual areas has provided essential data and referencing for current research work, a more encompassing research direction which covers aspects of on-vehicle testing, dynamometer testing and finite element simulations would provide valuable information to advance the knowledge and understanding of brake disc deformation.

Until recently research efforts regarding brake judder have been overshadowed by other brake related issues such as brake noise for example squeal and groan. Although brake noise still remains a problem for vehicle manufacturers, past research effort has led to a greater understanding of the mechanism which creates the noise and solutions are now more readily available [10][11][12]. This is not the case with brake “judder” as past research has been less focussed towards its occurrence or cause. As brake performance and reduced packaging demands increase then the thermal issues of braking become more of an issue. It is this aspect of thermal judder, rather than cold judder, which is most difficult to investigate as this can manifest itself as high frequency (often referred to as drone) or low frequency excitation, the latter causing excessive vibration in the suspension and steering systems.

Brake judder still poses a serious design problem for the brake refinement engineer with as much as 75% of noise, vibration and harshness (NVH) issues being attributed to judder as can be seen in figure 1.1. It may take the form of cold or hot judder but in both cases it presents itself as a vibration directly related to wheel speed. Cold judder is typically manifested as a low-order vibration, whilst hot judder is typically associated with a higher-order vibration. Both types may be felt by the driver through the brake pedal, steering wheel or vehicle floor pan, with higher ‘drone’ frequencies becoming audible within the cabin. Cold judder tends to be caused by rotor geometry errors arising from off-brake wear such as corrosion, pad imprinting and off brake contact between the disc and pads [13][14]. Hot judder is caused due to a short duration but high thermal input to the brake that results in a thermo elastic deformation, and eventual disc thickness variation (DTV), and thermo elastic instabilities in the form of hot spots. The problem is most prevalent on vehicles in the high performance luxury car market which must dissipate a significant amount of energy through the cast iron brake discs with DTV levels as little as 10 microns causing judder [15][16]. It is therefore of great importance to vehicle manufacturers that research into brake judder on cast iron brake discs continues.

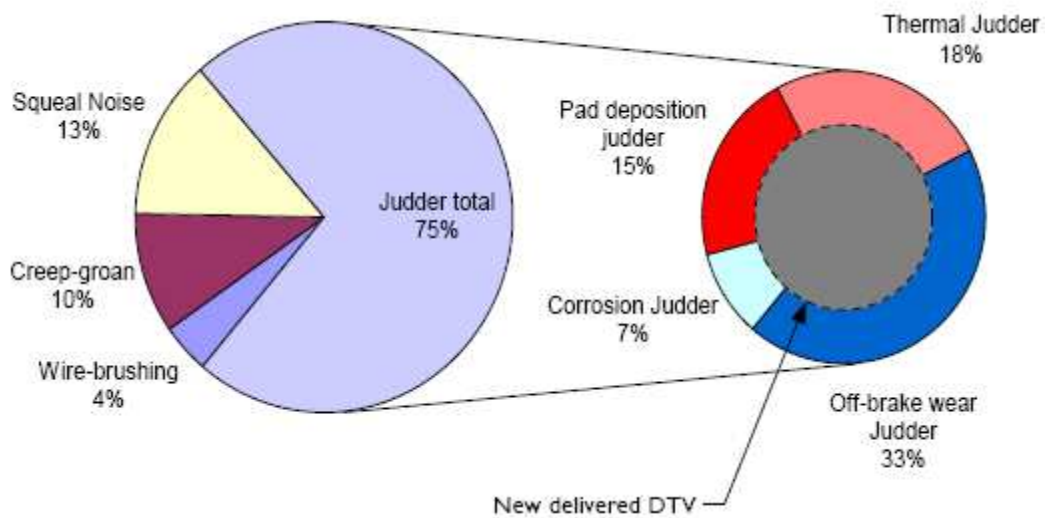


Figure 1.1: Breakdown of NVH issues facing a vehicle manufacturer [23]

1.1. Aims

The following is a list of the primary aims of the research contained within this thesis:

- Advance the understanding of brake judder resulting from thermo-elastic deformation of the brake disc.
- Perform on-vehicle tests to acquire data from a vehicle experiencing brake judder.
- Development of a quarter suspension vehicle dynamometer with a suitable data acquisition system for the analysis of brake Judder.
- Utilise computer simulations to observe and improve the heat distribution of a brake disc.

1.2. Objectives

The research covered in this thesis analysed the thermo-elastic deformation of vented brake discs. The primary aim of the research was to advance the understanding of brake disc thermo-elastic deformation including wave-like deformation causing brake judder. The objective of this was to combine many of the aspects used by the authors in the literature review; mainly on-vehicle testing, dynamometer testing and finite element analysis; this enabled a broad study of brake judder.

The main objective of the on-vehicle testing was to carry out a detailed assessment of brake judder on-vehicle; the findings from this were used to guide the dynamometer testing and analysis. Collaboration with Bentley Motors Limited provided access to vehicle testing and equipment which enabled this objective to be met. One of the objectives of the on-vehicle testing was to identify a method for measuring the occurrence and severity of brake judder. This knowledge was then applied to the brake dynamometer study. The development of a brake dynamometer allowed a more detailed analysis of the thermo-elastic deformation of the brake disc to be carried out in a controlled laboratory environment. The objective of this was to allow for the deformation of the brake disc to be measured during braking and allowed analysis of the thermo-elastic disc distortion.

Computer simulations were used to develop a new disc design. The objective of this was to use the knowledge and information gained from the on-vehicle and dynamometer testing to create a thermal model of the brake disc during transient heating. Modifications were then made to the design to improve the heat transfer through the brake disc to minimise the propensity towards hot spotting and to reduce thermal deformation.

1.3. The Brake System

All vehicles travelling at speed need to slow down to negotiate obstacles on their journey, often they need to achieve rapid deceleration. As aerodynamic and driveline drag on their own are a rather inefficient way to lose speed, the vehicle needs another more efficient method, this is where the braking system comes into play.

Braking systems have advanced greatly over the years from the blocks pushed against wagon wheels with a lever, through to band brakes, drum brakes and more recently disc brakes. All operate by converting the kinetic energy of a vehicle into thermal energy or heat. The rate at which the brakes can convert and dissipate this thermal energy determines their performance and therefore ultimately the rate of braking or deceleration.

Disc brakes are currently considered to be the best compromise between cost, performance, weight and maintenance for many road vehicles. Many vehicles still utilise drum brakes on the rear axle, however this can be due to a number of reasons such as the lower braking power required at the rear axle, the convenience of actuation of a drum brake for the handbrake and cost.

1.3.1. The Brake Disc

Typically one of the most common materials used in the manufacture of brake discs is grey cast iron with high carbon content in the form of flake graphite [17]. Cast iron exhibits a number of advantages over other materials, the main advantages being good conductivity and high specific heat capacity allowing the material to both accept and dissipate large amounts of thermal energy [18]. Other benefits are that it is easy to machine and is a good damping material. These features are due to the carbon content [17] and pearlitic grain structure of the brake disc material which aids the damping of noise such as squeal whilst also exhibiting good thermal properties. Higher performance brake discs tend to have a higher carbon content to enhance

both the conductivity and damping factor and it has also been suggested that there is little difference between the strength of a high and low grade cast iron at high temperatures [19]. Other disc materials include carbon-ceramic (CSiC), popular on high performance sports cars; carbon-carbon, only used on top-end racing cars such as Formula One; and aluminium metal matrix composites (MMC), generally less favourable due to the price and low maximum operating temperature [18].

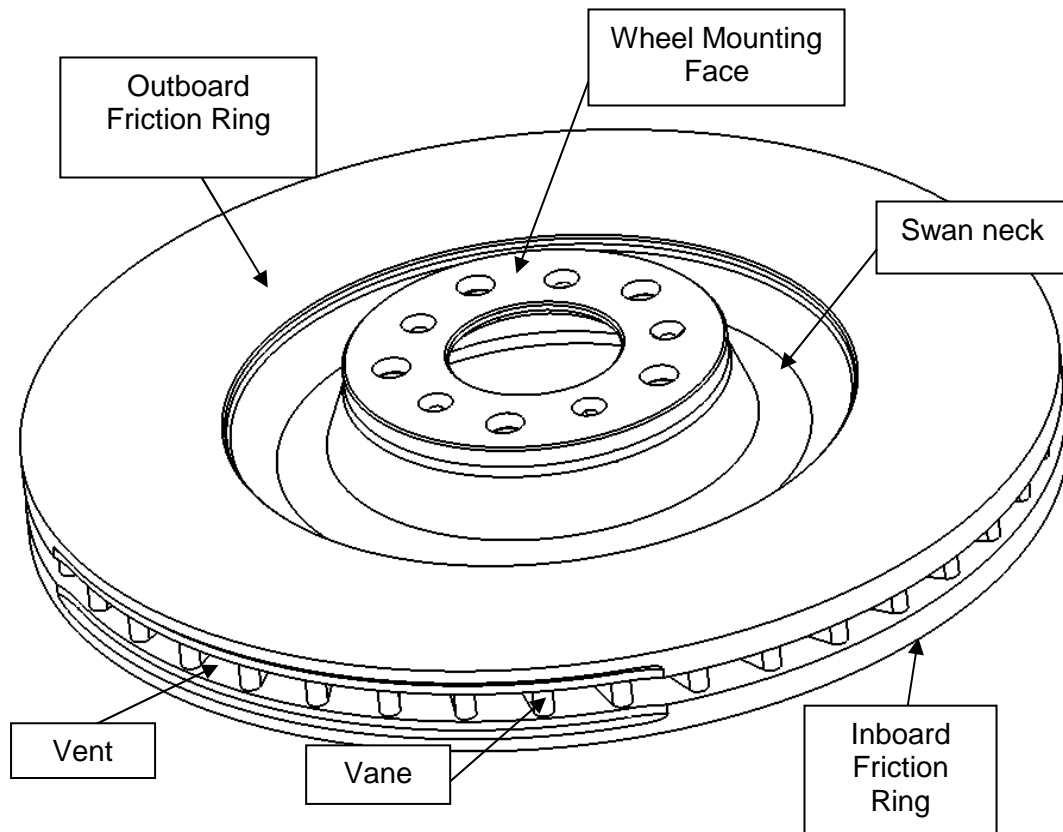


Figure 1.2: General brake disc features.

Figure 1.2 shows a drawing of a vehicle brake disc. Labelled are the inner and outer friction rings, the swan neck and the wheel mounting face, a brief description of some of these features follows.

The inboard brake pad contacts the inboard friction ring to slow the vehicle down. The pad is forced against the friction ring by pistons mounted in the brake caliper. Recently brake disc designs have had a tendency to connect the inboard friction ring indirectly to the hub or swan neck via the vanes. This design feature improves coning performance of the brake disc as a whole, however thermal capacity and heat transfer from the inboard friction ring is reduced as there is limited conduction path

for heat to travel away from the friction ring. Often this is counteracted with the implementation of a thicker friction ring thus increasing the heat capacity/thermal mass.

The outboard or wheel side brake pad contacts the outboard friction ring. The brake pad may be forced against the disc by pistons in the brake caliper or via a sliding type caliper. This face is exposed to the wheel and it is common for engineers to design wheels which actively pump air either onto or away from the disc face to improve cooling.

1.3.2. The Brake Caliper

For road vehicles there are typically two types of caliper in use; the opposed piston or the sliding type caliper. With the opposed piston design both brake pads are forced against their friction rings by hydraulic pressure acting on the pistons. The piston ports will be linked together either via a bridging piece between the two halves of the brake caliper or in many cases through the caliper body itself. In this arrangement both halves of the caliper experience identical fluid pressure and therefore actuation forces.

With a sliding type caliper the inboard pad is moved via hydraulic pressure on the pistons in the caliper, and as it does so the reaction force causes the other half of the caliper to slide inboard and clamp the outboard pad against its friction ring giving the caliper its name. With this caliper arrangement the inboard and outboard pads can experience different actuation forces. Sliding type calipers are often used on passenger vehicles to permit ideal (or close to ideal) location of the suspension lower ball joint to obtain a reduced scrub radius which gives better suspension kinematics. The compact outboard geometry of a sliding type caliper permits this by allowing either the rotor to be positioned further outboard, giving more freedom with the positioning of the lower ball joint [20], or allows a reduced wheel offset; both of which reduce the scrub radius. A fist-type sliding caliper was used in this research.

1.4. Research Braking System

The braking system used for the purpose of this research was that fitted to the front axle of a Bentley high performance luxury grand touring (GT) car. The brake disc was a single piece vented cast iron rotor. The disc had 40 vanes which initially had a radial direction at their inner radius, but then crank through an angle at the entrance

to the air-gap to create a directional or 'handed' disc. Other than the change in direction the vanes may be considered straight. The vanes themselves tapered in thickness along their length with the thicker end being at the outer radius. The friction rings were each 12mm in thickness with the air-gap being a further 12mm to give an overall thickness of 36mm. The disc utilised a swan neck design to connect the friction rings to the hub mounting section, this feature has been shown to reduce disc coning due to thermal distortion [3]. Despite the disc being a "handed" design, the same disc was mounted on either side of the vehicle; this meant that on the left side of the vehicle the disc rotated in a direction which was beneficial to the pumping ability of the vane angle, and on the right it had a reduced benefit. Data presented in section 3.2.6.2 of this thesis, from on-vehicle testing, has identified there to be a 14.4% variation of the whole disc heat transfer coefficient when comparing left and right hand brakes. This corresponded to a temperature variation of between 10-30°C at disc temperatures of up to 652°C. The manufacturer has benchmarked the disc in relation to the direction of revolution and found this performance difference to be small and outweighed by the cost saving.

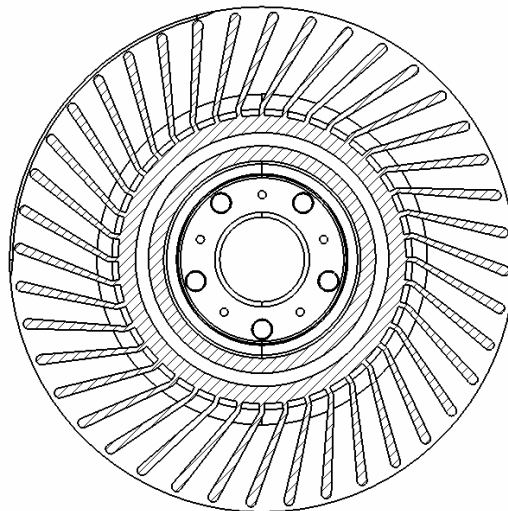


Figure 1.3: Cross section view showing the vane orientation

The brake caliper was a two piston fist-type arrangement with brake pads which exhibited many geometrical features to reduce noise. The caliper was mounted rearwards of the front axle centre line.

2. Literature Review

2.1. Introduction to Brake Judder

Brake judder is now regarded as the primary cause of brake refinement problems, accounting for 75% of all brake refinement. This translates to costs of \$100million (US) a year in warranty claims for European vehicle manufacturers alone [21]; so it can clearly be seen that this is a problem of great financial importance to the automotive industry. The issue of brake judder has grown over recent years. In the year 2000, one parts manufacturer listed brake vibration, or shudder second only to brake noise as a problem or complaint based on J.D. Power and Associates data, listing it in the region of 1-3% of problems compared with 4-5% for brake noise [22]. More recent vehicle manufacturer data has indicated that brake judder can account for up to 75% of all brake noise vibration and harshness (NVH) issues [23].

The mechanism of judder is a forced vibration with a frequency directly related to wheel speed [24]. The vibration emanates from the contact between the brake pad and disc. Variations in the rubbing path of the brake disc will generate, as the pad slides over them, both a brake pressure variation (BPV) and brake torque variation (BTV) which results in high amplitudes of vibration of the wheel hub, the suspension system, the steering wheel and the brake pedal. This vibration is accompanied by a loud “drumming” sound in the driver cabin. It may be divided into several basic causes - that of disc thickness variation (DTV), thermo-elastic deformation of the rotor, variation in rotor/pad deposition and variable rotor corrosion [11].

Judder can be further split into two categories; cold and hot judder. Cold judder will present itself without any significant temperature in the braking system as it is a result of off brake wear or corrosion, whereas hot, or thermal judder, is a result of thermal expansion and deformation on the brake disc [11].

2.1.1. Cold Judder

The causes and effects of cold judder have been well documented [13] and the mechanisms are now well understood and not the focus of this research, it will therefore be suffice to only briefly describe the problem. Cold judder is caused by off brake wear causing permanent DTV due to the following:

- Run-out, where the disc swashes from side to side during running due to poor machining and casting, bolt torque variation or mounting face contamination. The pads will contact the disc in the off-brake condition. Run-out can increase with disc use and it is therefore essential to install the brake disc with as little run-out as possible; usually less than $80\mu\text{m}$ [16]. However a great deal of work has been carried out in industry to minimise the run-out of the brake disc with some authors claiming machining processes which achieve $10\mu\text{m}$ of lateral run-out [25]. Tightening the machining tolerances and ensuring clean mating surfaces can go some way to reducing the installed run-out of the brake disc.

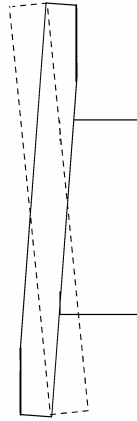


Figure 2.1: Disc thickness variation caused by run-out and poor pad retraction.

- Poor brake pad retraction closely linked with run-out: The brake pads may contact the disc during the off brake condition and cause localised wear if they do not retract far enough back upon release of the brakes. This is especially bad if there is a high level of run-out or the rotor is thermally deformed [15], as the pads will effectively machine flats at points corresponding to the maximum run-out around the disc surface creating DTV as shown in figure 2.1. Improving piston seal roll back characteristics can improve cold judder by allowing the brake pads to retract further, however care must be taken so as to avoid increasing the pad-disc clearance by too much as poor brake response times will result.
- Pad deposition can occur after heavy braking where the brakes are left applied whilst the vehicle is stationary. Pad material will stick to the disc surface causing

what is known as pad imprinting creating a surface undulation large enough to cause judder.



Figure 2.2: Example of pad imprinting

- Uneven corrosion caused while the vehicle is stationary can cause thickness variations on the brake disc surface leading to judder when in use. DTV growth on discs exhibiting corrosion has been shown to develop much faster than discs exhibiting no corrosion [14].

It has been shown that there is a close link between disc run-out and cold judder caused by DTV [13]. Cold judder no longer poses as significant a problem to designers as in the past due to improved quality control and machining processes which have been implemented in order to minimise the problem. It does however require serious consideration to minimise the problem without adversely affecting other features of the braking system such as brake response and cost.

2.1.2. Hot Judder

The most significant form of judder is hot judder or thermo-elastic deformation; it is also the most difficult form to predict. Hot judder has been described by many authors [15][26][5][27]. With disc brakes it can manifest itself in one of two forms; permanent disc deformation, where the disc takes on a wave-like shape resulting in second to fifth order judder relative to rotational speed, and “hot spotting”, (or “blue spotting”) where the disc develops multiple small raised areas of deformation, as a result of rapid heating, followed by rapid cooling, where the localised surface temperature of the rotor exceeds 726°C and is followed by cooling [26] a phase change is caused in the brake rotor material [31]. The structure of the cast iron rotor

changes into martensite at points around the surface, this is known as “hot spotting” or “blue spotting”. It is also possible to observe concave regions of the disc associated with blue spotting. These can be caused by excessive wear of hotter raised areas, which then cool to form a shallow [5]. It is during a subsequent light braking application that judder occurs due to the raised areas with a high order of vibration. The problem of localised heating continues as raised regions of the rotor experience an increased surface pressure distribution which in turn generates a higher temperature causing increased expansion.

Front brake discs present more of a problem to the brake engineer than rear brake discs due to the high proportion of braking carried out by the front brakes. The bias is usually in the region of 70% towards the front brakes to allow for effective and stable braking and means that the rear brakes are required to dissipate much less energy. This allows the rear brakes to be much smaller in size and permits the application of brake drums on the rear axle. There are also an increasing number of vehicle models with front and rear disc brakes [28].

2.1.3. Drone

Brake drone in its simplest form is audible high frequency brake judder. The frequency of brake drone is a function of wheel speed, and therefore as the wheel speed decreases so does the drone frequency. Drone frequency is typically within the range of 100-200Hz [4][11] and the sound can be described as a drumming noise. Brake drone is typically caused by high order or frequency brake judder, often as a result of blue spotting of the brake disc.



Figure 2.3: Example of severe blue spotting on a brake disc.

Studies by Little *et al* [6], Fieldhouse & Beveridge [5] and Lee & Dinwiddie [29] have shown that hot spots on a brake disc exhibit a concave indentation into the brake rotor indicative of a martensitic phase transformation. During a brake application there is significant energy input into the disc for discrete regions to swell and present a raised surface to the brake pad thereby causing an exponential heat increase to the effected area. The raised region would experience a higher contact pressure and therefore localised wear would also be increased. Following cooling the material contracts to form a concave region. The rapid cooling process required to cause martensitic transformation is not only caused by the air cooling of the surface metal, but may be due to sudden heat flow to cooler regions of the brake rotor upon release of the brake pads [30]. Hot spots are usually the cause of higher order judder known as drone which has an audible frequency of around 200Hz. The cause of hot spots is still unclear and much analytical and numerical work has been carried out on the subject [32][27][33]. Lang [1] suggested that wave-like deformation is possibly the cause of hot spotting with typically 6-20 hot spots forming at the waveform peaks. The mechanism of wave-like disc deformation has been investigated in this thesis.

2.2. Types of Disc Deformation

2.2.1. Coning

Coning occurs due to the differential thermal expansion of a brake disc. The outer periphery of the brake disc tends to distort inboard or outboard creating a cone or

bowl shape. The direction of the distortion is dependent upon the design of the brake disc with typically rigid connections between the friction rings and the top hat or bell producing large coning angles due to the inability to distort radially. It has been shown for a vented brake disc [18][17][34] that the inner friction ring should be directly connected to the hub or bell to reduce the coning angle. This has the effect of increasing the distance between the friction ring and the bell therefore reducing its stiffness and allowing radial expansion [3]. With this design the direction of coning is reversed but the magnitude is reduced. Curry [17] also suggested an undercut at the point where the top hat meets the friction ring to reduce coning on a solid brake disc and indicated that this design feature could also be used on a ventilated disc; again this will reduce the stiffness of the friction ring and bell connection. Another solution aimed at reduced coning is the swan neck design. This is a back ventilated design and therefore allows easier direction of airflow to the disc from the inner wheel arch region. The swan neck acts as a spring and allows the brake disc to distort radially rather than axially due to heat input thus reducing the coning angle. Okamura *et al* [3] identified that the axial length of the top hat influences the coning angle of the brake disc, with a longer top hat reducing the coning angle. The swan neck design follows this principle by allowing a longer connection between the hub mounting face and friction ring, whilst promoting better cooling and therefore may be seen as an improvement over front ventilated discs.

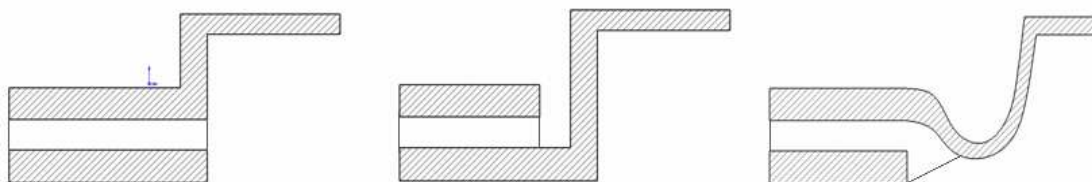


Figure 2.4: Inboard ventilated (left) and outboard ventilated (middle) and swan neck (right)

2.2.2. Run-out

Run-out is a typical first order deformation which is inherent in all new brake discs. It is generally caused by the machining process and large efforts have been made in recent years to reduce the run-out as it has been identified as a major contributing factor to cold judder. Run-out cannot be considered to be a constant value and will vary between an uninstalled brake disc and an installed disc as it is affected by bolt

torque and contamination between the mating faces of the disc and hub. It is therefore necessary to ensure cleanliness when installing brake discs and to guarantee equal torque on all the wheel bolts. Run-out will also change during use as a result of heating and non-uniform expansion of the brake disc. Okamura *et al* [25] have researched into the development of lateral run-out and DTV and have developed a two stage finishing process to limit lateral run-out and DTV to 10 and 5 microns respectively. By improving the machined tolerances of the brake disc they aimed to reduce the development of DTV and lateral run-out during use and therefore reduce the effect this had on brake judder.

2.2.3. Wave

Wave deformation of the brake disc has had little documentation and is believed to be a result of high heat input into a ventilated brake disc [11]. As the disc heats up its expansion is restricted due to the vane geometry which induces a wave-like deformation into the brake disc. Lang [1] suggested that high speed low deceleration braking events can cause hot bands on the brake disc surface which were surrounded by cooler material and would induce compressive stress within the brake disc. This compressive stress would result from the cooler regions of material constraining the thermal expansion of the hot band of material. Lang went on to state that buckling of this compressively stressed region would result in wave-like deformation. However no experimental results were performed by Lang to confirm this mechanism. Wave deformation of the brake disc is believed to cause brake judder as the brake pads rise over the crests of the wave as the disc revolves, this will cause both a brake pressure variation and a brake torque variation.

2.3. Discussion of Current and Past Research

The majority of research into brake judder has been carried out over the last ten or so years, however the problem has been known about for much longer. Presented below is a discussion of the various methods which authors have used to tackle the subject.

2.3.1. Mathematical Modelling

Barber, together with many other authors, has done much research into both brake and clutch judder over the past forty years [35][36][7][37]. Much of the research carried out by these authors has been aimed at developing mathematical models to predict hot spots on brake discs or clutch plates using an eigenvalue and Fourier

reduction approach. The authors have also attempted a coupled approach with the aim of observing the interaction between frictional instabilities and thermo-elastic instabilities (TEI) [8]. The results of which indicate that frictional variations can be caused due to a “flutter instability” at a frequency close to the first natural frequency of the system. This work is of interest as it could possibly be a cause of hot spotting at high speeds and is the focus of Barber’s work.

Barber has also developed a computer program which predicts the formation of hot spots on brake discs. By combining the heat conduction equation with an equation to define a perturbation in the temperature field which has exponential growth with time, the authors developed a finite element matrix equation. When this is solved together with a thermo elastic contact equation the eigenvalues can be used to identify the critical sliding speed above which hot spots will form [36]. The program appears to use simple geometry and from what can be understood from the freely available demonstration version, the program predicts a uniform equispaced distribution of hotspots around the friction ring, which is not necessarily always the case in actual testing of brake discs [33], however the experimental results from Yi *et al* correlate well with this theory [36][7] as well as those of other authors [27][38][29][39]. The testing by Yi *et al* has shown hot spots are created in a uniform equispaced pattern which was antisymmetric [7]. The starting position of the hotspots on various brakes was not consistent and varied between the inner and outer friction ring diameters [36]. The work has shown good correlation between finite element analysis and actual brake testing. The antisymmetric formation of hot spots, as simulated and tested by the above authors, could be caused by wave-like deformation of the friction rings resulting from circumferential buckling due to the compressive stress caused by rapid thermal expansion as stated by Lang [1].

Research by Valvano *et al* [40] used a computer model to predict disc, pad, caliper and hub temperatures that can be used to look at brake disc coning, brake drum bell mouthing and other geometric distortions. The PC tool, FEA and dynamometer temperatures correlated well and had good correlation between FEA and dynamometer studies for disc coning. The PC tool covered more aspects of the thermal modelling of brake systems than Barber and Yi’s work (detailed above), however the work did not look at hot spotting/thermal banding and therefore is limited in its application to brake judder studies. As coning was the main form of thermal deformation predicted by the computational model, it was possible that the model did not take into account constrained thermal expansion of the friction rings which could

cause the wave-like deformation which has been predicted and observed by authors such as Fieldhouse [11][5] and Lang [1].

Whilst the above mathematical modelling looked at the prediction of thermo-elastic deformation and thermo-elastic instabilities of the brake disc, with particular focus on the effect this may have on the braking system, Jacobsson [15][41][42][43][9] has discussed the fact that little research has been carried out into the effect brake vibrations have on the vehicle and how they transfer to the driver. Jacobsson gave good detail of brake judder and what is known as the cause and effect approach [43]. The research focused upon the effect of brake judder and its measurement. Frequency sweep and amplitude functions were applied to assess brake judder. Mathematical models have been developed to identify the level of judder and to discern what order or frequency was being produced. Models were backed up with experimental results whereby caliper vibration was measured using accelerometers. However, the caliper is known to have its own modes of vibration and also exhibits damping and it is unclear whether this has been taken into account. Jacobsson highlighted the current lack of on-vehicle testing, within the field of brake judder, to assess how judder affects the vehicle. In [9] Jacobsson used a combination of amplitude functions and vehicle testing to analyse brake judder. In this paper it was identified that surface DTV was potentially caused by thermal gradients and not absolute disc temperature. This was of importance to the research in this thesis, as whilst not primarily investigating DTV, a hot region around the friction ring surface surrounded by cooler material would have large thermal gradients on either side. These thermal gradients would constrain the thermal expansion of the cast iron which would lead to buckling of the friction ring giving wave-like deformation as indicated by Lang [1]. This mechanism has been described in more detail in section 3.2.6.3.

2.3.2. Physical Testing

In 1972 research was carried out by Rhee *et al* [44] to characterise the microstructure of cast iron friction surfaces. A series of thirty stops were performed from 60mph. Localised changes of the cast iron surface from pearlite to martensite were observed together with transfer and burnishing of pad material onto the disc surface. It was these martensitic transformations which were shown to cause high frequency judder or drone. Prior to this research some authors believed that the cast iron brake rotors had a stable microstructure [44]. The martensitic transformations

found by Rhee *et al*, will have been caused by localised heating of the brake disc to over 726°C followed by rapid cooling as previously described in sections 2.1.2 and 2.1.3. If the brake disc was designed in such a way that the thermal mass is distributed to reduce the localised “overheating” of the brake disc then the martensitic transformations and the associated brake drone would be reduced. Section 5.4 of this thesis focuses on the redesign of the disc vent geometry to achieve this effect.

Whilst the above research by Rhee *et al* used on-vehicle testing, work by Fieldhouse *et al* [5] involved testing two different calipers and two different discs whilst investigating brake judder on a brake dynamometer. Use of a dynamometer for brake testing provided a controllable environment and allowed better access to the braking system. During the dynamometer testing the discs were shown to take up permanent and increasing deformation with a two diameter mode formation. The authors of the paper concluded that this was due to heavy braking preventing uniform thermal expansion of the brake disc. This second order deformation would be caused by the thermal expansion of the friction rings which would generate compressive stress and cause disc buckling resulting in the second order waveform. Research showed the occurrence of hot spots on the disc surface and also blue spots. A pressure damping system was applied to good effect to isolate the driver from pressure pulsations within the brake lines, however this may cause complications if the damper were incorporated into an active braking system (ABS) or an electronic stability program (ESP). The modelling of the braking system on a brake dynamometer used a reduced number of components when compared to a vehicle – Fieldhouse *et al* used only a disc and caliper on the dynamometer as is typical of many brake dynamometer setups, although others do exist [45]. This obviously did not include any of the vehicle suspension system and therefore the effect this may have had on the development of brake judder was un-accounted for. Access to on-vehicle testing of the same braking system would have made validation of the dynamometer testing possible; however this is often not available. The research in this thesis was fortunate enough to include both on-vehicle and dynamometer brake testing to further investigate the permanent 2nd order wave-like deformation found by Fieldhouse *et al*.

Some very interesting and relevant work has been carried out on-vehicle by Kubota *et al* [4]. This work had relevance to this thesis as Kubota *et al* looked at the dynamic disc geometry and temperature distribution during on-vehicle testing, specifically looking at the formation of hot spots. Although the authors of the paper did not

specifically state that wave-like deformation was occurring, their results showed an antisymmetric occurrence of high order surface run-out on each friction ring. This was indicative of wave-like deformation as identified by Fieldhouse *et al* [5] and Lang [1].

Data from Kubota *et al*'s research showed that rumble noise (also known as brake drone) occurred in the frequency range of 150-250Hz and was caused during moderate braking of 0.3g at over 180Kph i.e. a low deceleration high energy braking event. Fourier analysis showed sound pressure levels with 8th-10th order components of rotor revolution increased at vehicle velocity of 160kph. The frequency dropped with decreasing vehicle velocity identifying that this was a mechanically driven vibration such as brake judder.

For on-vehicle tests non-contacting capacitive displacement transducers and infrared temperature sensors were mounted around the brake disc. Displacement sensors were arranged to measure both thickness and waviness. During braking, coning of the brake disc was shown to occur during a single stop. Upon release of the brakes there was no run-out and after cooling in air the coning reduced. This fact that this process occurred during a braking event indicated to the author of this thesis that thermo-elastic deformation was occurring during the process of a braking event which was the cause of the in-stop coning.

Small surface run-out swellings were seen to occur alternately on the inner and outer surfaces. The swellings grew in size with deceleration. Peak run-out swellings were shown to coincide with hot spots indicating large thermal expansion and thermal gradients to occur. These hot spots were identified as the cause of the rumble noise (drone). This work correlates with the work by Barber and Yi, detailed in section 2.3.1, where hot spots were shown to be antisymmetric.

Kubota *et al* listed methods for reducing rumble, these included:

- Adopt a rotor shape that displays little thermal deformation and therefore uniform contact.
- Low pad material compressibility providing a more uniform pad surface contact.
- Uniform rotor surface temperature – high thermal conductivity.

- Narrower pad – Distribute the heat across a higher number of hot spots by raising the number of hot spots to a high order (see below).

The author of this thesis considers that of the above four methods to reduce rumble (or drone), the most effective would be to adopt a rotor shape that displays little thermal deformation and to have a uniform surface temperature. The reason for this is that both of these would reduce the thermal deformation of the rotor and therefore reduce the compressive stress within the friction rings and thus decrease the occurrence or intensity of wave-like deformation and in turn reduce brake judder and drone.

A low pad material compressibility (softer brake pad when observing the author's results) would reduce the variation in the surface pressure distribution (as was identified by Harding *et al* [66]) and therefore help to reduce the surface temperature variation of the disc. This also correlates with the research by Steffen [27].

Narrowing the brake pad effectively raised the order of revolution and lowered the disc run-out. In the paper it was identified that the distribution between hot spots was determined by the spacing of the pad surface pressure distribution. As the order of revolution increased the amount of heat influx per heat spot decreased which in turn lowered the hot spot temperature. A reduction in the pad width (with no change to pad height) can have detrimental effects with regards to the shear strength and power absorption of the lining material [20], therefore these factors must also be taken into account if a reduction in pad width is to be used to reduce hot spotting as suggested by Kubota *et al*.

On-vehicle tests showed that high-order surface run-out components (i.e. hot spots) developed in proportion to the thermal deformation of the rotor. The authors of the paper made the assumption that pad surface pressure differences increase in proportion to rotor thermal deformation. This was a reasonable assumption to make as a variation in the surface profile beneath a brake pad caused by thermal expansion would cause an increase in the brake pressure variation. The larger the temperature variation, the larger the thermal expansion would be and this in-turn would cause a larger brake pressure variation.

To look at the thermal conductivity of the brake disc two rotors with different conductivity were used by Kubota *et al*. A higher conductivity disc was found less likely to produce heat spots. This, the authors identified, was possibly due to the fact

that uniform surface temperature occurs rapidly. Higher conductivity discs are obviously a benefit; however there are other factors to take into account, such as the maximum operating temperature of the disc material defined by its specific heat capacity. Generally disc materials such as aluminium metal matrix composite (MMC) have a higher conductivity than cast iron, however its specific heat capacity is lower which limits the maximum disc temperature [18] and restricts its use to light vehicles.

Recent research into the field has included analysis of motorcycle brakes performed by Kiyotaka Obunai *et al* [46]. The research focused on wave design motorcycle brakes. A number of discs were tested with differing number of waves and differing wave depth. ANSYS Finite element models were used to simulate tests and fast Fourier transform (FFT) and power spectral density (PSD) methods were used to identify judder frequencies in the real world tests. The authors looked at the relationship between BTV and wave number and came to the conclusion that BTV was related to wave number and DTV. After identifying this obvious link the authors did not look further into the cause of DTV. However, as with research by Kubota *et al* [4], this research has shown the possibility to use FFT techniques to identify judder frequencies; this was a technique that was used in this thesis.

A system to measure brake temperature field both in a laboratory and on-vehicle was developed by Litos *et al* [33] for research into thermo-mechanical instabilities. The system measured brake disc temperatures with non-contacting infrared photon detectors. Litos highlighted the benefits of infrared over thermal imaging cameras, notably that infra red has a small size which gives it the capability of measuring small areas, data can be accurately post processed and it has a more accurate temperature measurement over thermal imaging camera. It was noted by Litos that one of the benefits of a thermal camera is that it gives real-time display. In his research Litos took into account the fact that the emissivity of cast iron alters with temperature and developed calibration curves to take this into account. This is usually the main drawback of using non-contacting sensors, as a great deal of time has to be spent calibrating the system. An embedded thermocouple was used for validation of non contact measurements. The research has shown good correlation between temperature field and brake pressure variation. However images of disc flatness measured before and after the braking cycle compared to temperature field, appear to show little or no correlation. Whilst Litos does not draw conclusions on this, the author of this thesis believes that this either indicated that there was no link between disc distortion and temperature field, or, more likely, that the in-stop

distortion was not indicative of the pre and post test distortion. This is a mechanism that has been investigated in this thesis in section 4.2.3.

The sensitivity of a vehicle to brake judder has been highlighted by Gassmann *et al* [47], who performed identical brake testing on similar vehicles with similar suspension geometries. The testing showed that the three vehicles tested exhibited widely different sensitivities to brake judder due to differing transfer paths and local transfer functions. Only vibrations as a result of brake torque variation were identified i.e. steering wheel vibration, and not the vibration of the pedal as a result of brake pressure variation. Dynamic disc geometry variations were listed as the cause of brake judder; however this appears only to have been linked to DTV and not waveform deformation of the brake disc. Dynamic side-face run-out was also listed as a cause; however Gassmann *et al* only linked this to cold judder due to off brake wear. Only first order components of vibration were examined, however the authors clearly identified that the vehicle as a whole can play an important role in the transfer mechanism and therefore the overall sensitivity of the vehicle to brake judder. The authors proposed two methods for reducing brake judder; minimising the excitation or reducing the sensitivity of the vehicle. For the second method they suggested shifting the eigenfrequencies outside of the critical range for the suspension components that lie in the transfer path. Computing power and software development now makes it possible to perform the research carried out by Gassmann *et al* in a multibody dynamics environment. These typically allow relatively fast and economic evaluation of a range of designs. A brief overview of such research is described in section 2.3.5.

2.3.3. Hot spotting

Anderson and Knapp [48] have defined the four types of hot spots which can occur in automotive friction systems; asperity, focal, distortional and regional. The four types can be seen in table 2-1.

Type	Width (mm)	Temperature (°C)	Duration
Asperity	<1	To 1200 peak	<1ms
Focal	5 – 20	750 – 1200 peak	0.5 – 20s
Distortional	20 – 100	100 – 700 delta T	>10s
Regional	50 – 200	10 – 100 delta T	>10s

Table 2-1: Comparison of hot spot types [48]

The authors state that critical focal hot spots are the type which martensite is formed and as such are one such type of hot spot seen on automotive brake discs. Cracking is a serious possibility following martensitic transformation due to the more brittle nature of this phase of cast iron.

Hot spotting has been the focus of Steffen's work [27] in which he attempted to identify a pattern with the presence of hot spots on a brake disc. In this work Steffen varied disc thickness, pad thickness, brake pressure, rotational speed friction ring diameter and initial temperature. An increase in hot spot formation was observed with decreasing disc thickness, decreasing pad thickness and increasing rotational speed. Referring to the buckling mechanism suggested by Lang [1], a reduction in the disc thickness would have reduced its buckling stiffness, and therefore the compressive stress caused during thermal expansion of the brake disc would have caused higher order circumferential buckling. An increase in the rotational speed would have increased the thermal energy being transferred into the brake disc for a given brake pressure. This would have caused larger thermal expansion and higher compressive stress which would again increase the buckling mode order. This mechanism has been described in more detail in section 3.2.6.3 of this thesis. Of interest are the effects of decreasing the pad thickness. It would be assumed that a reduction in the pad thickness would also cause a reduction in the pad stiffness and make the system less sensitive to brake judder and/or hot spotting as the pad would be able to deflect over any undulations on the friction ring surface. However a reduction in the brake pad stiffness may make the system more susceptible to the flutter instability described by Barber [8], and a thickness reduction would decrease the compressibility of the brake pad preventing undulations from being absorbed. Brake pressure and initial brake temperature magnitude were seen to have no effect on the formation of hot spots. Friction ring diameter was only shown to affect the number of hot spots and not their occurrence. An increase in the friction ring diameter resulted in more hot spots being produced. This can be explained by the fact that an increase in the disc diameter will have increased the effective radius of the brake. Therefore the tangential sliding velocity of the brake disc at the effective

radius will also have increased. Therefore, for an identical brake pressure, the heat influx into the brake disc will also have increased, again giving rise to a higher localised thermal expansion and higher compressive stress causing a higher buckling mode shape. The hot spot locations would be at the peaks of the buckled wave form and would be antisymmetric as was found by Steffen. Numerical simulation was used to predict hot spot formation; however, to simplify the calculations Steffen only looked at solid and not ventilated brake discs. Hot spots appeared equispaced on the disc surface for both simulated and experimental tests and Steffen indicated that the hot spots are also antisymmetric on the opposite side of the brake disc in good correlation with Yi *et al*'s mathematical modelling [7] and other physical testing [39]. Steffen also investigated hot spot generation on aluminium brake discs using computer simulations. Hot spot formation was seen to be worse on an identical geometry aluminium brake disc with Steffen suggesting with good reason that this is due to the lower heat capacity and higher coefficient of thermal expansion of aluminium. The higher coefficient of thermal expansion would cause increased compressive stress in the friction ring resulting from circumferential expansion; therefore the buckling mode shape would be higher than an identical cast iron brake at an identical temperature. This contradicts the findings of Kubota *et al* [4] who identified that a higher conductivity brake disc would exhibit a lesser tendency towards hot spotting. However not enough specific details about each of the tests was available to make direct comparisons.

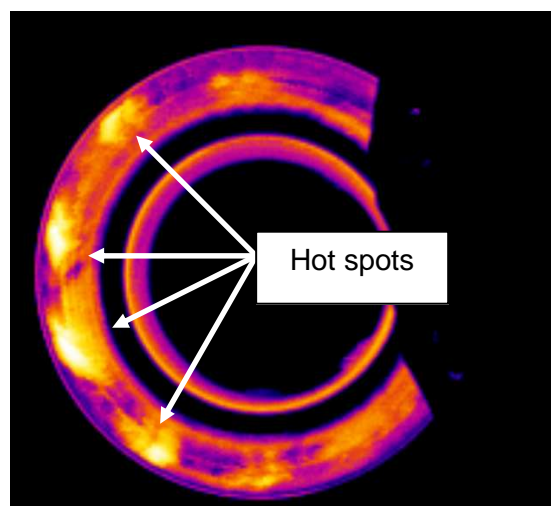


Figure 2.5: Thermal image of hot spots forming on a brake disc

Suryatama *et al* [49] developed a computer simulation technique to investigate hot spots. The authors compared numerical simulations to dynamometer results.

Simulations of 30 and 60mph constant speed drag brake tests were performed, in which the locations of hot spots compared well to tests. The authors identified both coning and waviness of the brake disc to occur in the simulations, however no hot spotting was seen as a result of the waviness and no explanation was given for the waviness of the brake disc. Hot spotting was shown to occur in the simulations when artificial DTV was applied to the disc, and also when bolt torque variations were applied.

2.3.4. Finite Element analysis

Extensive research into the coning of brake discs due to thermal deformation has been researched by Okamura and Yumoto [3]. The initial work focussed upon commercially available brake discs, and gave an interesting brake down of world wide trends in brake disc design. The data showed that Italy and the UK tended to favour outer hat with deep neck designs, whilst France and Sweden tended towards inner hat designs. Both deep neck and inner hat designs were shown to reduce coning, although the inner hat design exhibited poorer cooling as a result of being unable to draw cooling air from inside the wheel arch. Conversely Japan and Korea tended towards an outer hat with neck design which should provide less coning than that of an outer hat alone, but more than a deep neck design. This was a result of the trend for smaller lighter cars in these parts of the world which would reduce the thermal load on the braking system.

The authors present extensive parametric computer aided engineering (CAE) studies identifying which features have the largest effect upon disc coning, thermal stress, mass and friction surface temperature. Disc thickness and vane number were shown to have the largest effect on temperature, whilst the effective friction ring offset had the largest effect on thermal stress and deflection. The authors also demonstrated with the aid of calculations that an increased offset between the hat and friction ring reduced the coning angle and distance, the calculations showing that coning angle is inversely proportional to the hat axial length.

Finite element analysis by Yeo *et al* [50] has benchmarked an FE simulation against steady state data obtained from drag braking on a dynamometer. Convective and conductive coefficients for the vent walls were calculated from the measured data and used to improve the accuracy of the FE simulation. A study of various undercut designs on the top-hat to friction ring mounting section was performed. The results

show that coning is reduced as the arc length of the undercut increases. This goes some way to back up the above findings by Okamura and Yumoto [3] whereby increasing the offset between the hat and friction ring had the effect of reducing brake judder.

Authors such as Barton [18], Day *et al* [51], Tirovic *et al* [52], Qi *et al* [53], Valvano *et al* [40] have developed advanced mathematical models and associated finite element models to study both brake judder and heat dissipation through braking systems amongst other effects such as squeal and contact analysis. To build a fully representative thermal model of the braking system, a lot of time must be devoted to characterising the friction material thermo-mechanical properties through testing and analysis. Qi and Day [53][54] have carried out such simulations which indicated that the contact area ratio between pad and disc had little effect on the average brake pad temperature yet influenced the interface temperature in a non linear way. This highlighted the complex nature of heat generation between the disc and pad. Furthermore, a fully coupled thermo-mechanical model must be developed with correct contact interactions; this must then be validated against known data for the correct frictional heating conditions.

2.3.5. Multi-body dynamics

Some authors [55][56] have used multi-body dynamics models to identify the transmission path and sensitivity of various vehicles to brake judder frequencies. This method has the advantage that the critical components can be identified prior to initial assembly of the prototype vehicle. This will identify early on if there is likely to be any excitation of non-brake system components.

The work carried out by Hussain *et al* [55] looked at the transmission of vibration on a commercial vehicle by applying multi-body dynamic modelling using the ADAMS software package. The results and comparisons by Hussain *et al* with similar experimental data indicated that brake judder transmission could predominantly be longitudinal along the commercial vehicle chassis and that this in turn was linked to the design of the rear suspension. While this work was limited to heavy duty commercial vehicles, it highlighted the fact that suspension design can play an important role in the sensitivity of a vehicle to brake judder.

Singh *et al* [56] attributed brake judder to 'new part' DTV which grows due to cyclic contact with the brake pads. The authors determined that vehicle response was dependent on the magnitude of DTV, suspension sensitivity and other factors including body structure.

The research focused on steering wheel rotational response due to judder with the authors assuming the vehicle body was rigid to simplify the ADAMS full vehicle model.

For the vehicle used, Singh *et al* identified modal frequencies of:

- Wheel hop 10.7Hz
- Wheel tramp mode 11.6Hz
- Suspension fore-aft in phase mode 13.9Hz
- Suspension fore-aft out of phase mode 12.4Hz

It was suggested that these modal frequencies can be excited by brake judder. Out of phase mode was most significant for judder as this gave wheel vibration due to opposing wheel motion.

Singh *et al* only looked at first order judder for simplification; however the modal frequencies identified would correlate to a vehicle speed range of 68-48mph (30-21m/s) for the vehicle used in this thesis. This is a typical motorway deceleration speed range and judder would be experienced as body or steering vibrations at these speeds. Second order judder would reduce the excitation speed by a half to 34-24mph.

Whilst the multi-body dynamics approach can show significant advantages and benefits when analysing and predicting NVH and more specifically brake judder issues, it is limited in its ability to analyse the root cause of the judder and is more suited to identifying vibrations that can arise as a result of a specific vibration pattern. It is possibly suited to a situation whereby the vibration of a specific component is known and the location of the driving force is to be identified, i.e. whether it is the front or rear brake.

Tan *et al* [57] have used the ADAMS package to show that the magnitude of the simulated brake torque variation increased linearly with increasing DTV magnitude. It was also shown that BTV decreased with both a more compressible pad material and a reduced stiffness caliper. Both of these however would reduce brake pedal feel by increasing the compliance and brake pedal travel within the braking system and therefore are not ideal solutions.

2.4. Summary

The literature review has identified the various different approaches that have been taken into the research of thermal judder, from the frequency sweep approach of Jaccobsson [15][41][42][43][9] and Fourier reduction of Barber *et al* [35][36][7], to the theoretical simulations of Valvano *et al* [40], on-vehicle testing of Kubota [4] *et al*, the dynamometer studies of Steffen [27] and Fieldhouse *et al* [5][39] and the multi-body dynamics approaches of Hussain *et al* [55] amongst others. All the different techniques have helped to advance the understanding of thermal judder and whilst the transfer of brake judder vibrations to (and through) the vehicle was not the focus of the research in this thesis, the multi-body dynamics approach to brake judder transfer is an important area of research. It is now widely accepted that brake judder is a mechanically driven instability as a result of disc thickness variations causing a brake torque variation or brake pressure variation. However there has been comparatively little research preformed into the thermal deformation of brake discs causing brake judder and more specifically the wave-like deformation as suggested by Fieldhouse *et al* [5][11], Lang [1] and a major brake disc manufacturer [59]. Lang [1] gave an explanation for the cause of wave-like deformation by relating it to buckling of the disc caused by compressive stress; this was introduced in section 2.2.3. The discussion of the literature in section 2.3 has shown correlation between the buckling mechanism suggested by Lang [1] and the findings of many authors such as Steffen [27], Barber [36], Fieldhouse [5] and Kubota [4]. This therefore gave a good basis for the research into thermo-elastic wave-like deformation of the brake disc which was the focus of this thesis.

3. On-Vehicle Testing and Analysis

3.1. Introduction

Testing of the braking system comprised one of the main and most important aspects of this research. Brake testing was carried out using two methods; on-vehicle and on-dynamometer with the distinct aim of providing comparable data which could be analysed to progress the understanding of brake judder. Within this chapter a detailed discussion of the methodology, experimental setup, test procedure, results and analysis from the on-vehicle testing is presented.

3.2. Vehicle Testing

An essential requirement of any analysis is the need for accurate validation against data which is repeatable, reliable and for which the user is confident in its accuracy. When looking into the field of automotive foundation brake design and analysis a common source of validation is that of a brake dynamometer. However studies have shown [41] that there is an error factor associated with dynamometer testing. It is therefore necessary to quantify the error by means of vehicle testing so that any results can be related back to the vehicle. The validation procedure has been selected to match that already in place to assess a vehicle's judder performance. In doing so the data obtained from dynamometer testing could be immediately compared with expected on-vehicle performance. The test procedure involved a number of high velocity low deceleration repeated braking events; typically braking from 240-50kph. This dissipated a large amount of energy in the form of heat through the brake system giving exactly the conditions thermo-elastic instabilities and thermo-elastic deformations thrive upon. By performing each brake application in quick succession the surface temperature of the brake rotor rapidly increased. High speed stops at a deceleration of 0.3g (0.3 times the rate of acceleration due to gravity) were used to quickly convert a large amount of kinetic energy into thermal energy through the brake system therefore potentially creating large thermal gradients within the rotor material.

Data obtained from the vehicle was limited due to the severity of the test procedure but also due to the harsher environment and constraints that the vehicle suspension dynamics created. However useful data has been obtained in the form of brake line pressures which highlighted axial vibrations caused by brake pressure variation (BPV) and tangential vibration of the caliper & backplate which was proportional to

the brake torque variation (BTV). Embedded thermocouples connected via slip rings constantly record the inner and outer friction ring temperatures at the mean rubbing radius. Moderately high sample rates of 500-1000Hz enabled the various orders of judder to be distinguished.

3.2.1. Theory

The main priority of the on-vehicle testing was to obtain accurate data which could be used for analysis but also validation of the brake dynamometer and finite element simulations. Another objective was to identify a suitable method for measuring and recording both the occurrence of brake judder and its severity. Brake judder is usually attributed to either a brake pressure variation and/or a brake torque variation and therefore these two characteristics presented themselves as the most useful reference sources. Brake pressure variation was measured close to the brake caliper (close to the source) via a pressure transducer tapped into the brake line. Brake torque variation however was more difficult to measure on-vehicle due to the constraints of the test and equipment available (torque wheels are one option for measuring torque variation on-vehicle, however their cost and inability to measure small variations made them prohibitive in this instance). An alternative to directly measuring the torque variation was to measure the vibrations resulting from the torque variation.

Braking torque, T_B , can be defined as the frictional force, F_F , acting at a mean rubbing radius, r_m , on the brake disc as

$$T_B = F_F r_m. \quad 3-1$$

If there was a variation in the brake torque due to judder and the radius was assumed to be fixed, as this was the mean effective radius of the brake pads, then the frictional force must vary. (It must be noted that the effective radius at which the centre of pressure acts, is not fixed but moves during braking. The centre of pressure moves as a result of this wear. However, for simplification, in these calculations it was assumed to be fixed) According to Newton's second law of motion, if the frictional force varied and the mass of the brake pad, m_P , was fixed the tangential acceleration \ddot{x}_T (in-plane motion) of the brake pad must change giving

$$F_F = m_p \ddot{x}_T . \quad 3-2$$

By combining equations 3-1 and 3-2 it can be shown that by measuring the tangential acceleration of the brake pad using an accelerometer, the torque variation can be measured indirectly as

$$T_B = m_p \ddot{x}_T r_m . \quad 3-3$$

Furthermore the axial acceleration, \ddot{x}_A , (out-of-plane motion) of the brake pad can also be related back to the brake torque variation as will be shown. The frictional force was equal to the normal force, N , multiplied by the coefficient of friction, μ , which gave

$$F_F = \mu N . \quad 3-4$$

Again using Newton's second law of motion, the normal force on the brake pad must be proportional to the mass of the pad multiplied by its axial acceleration

$$N = m_p \ddot{x} . \quad 3-5$$

This gave the equation 3-6 which defined the torque variation being proportional to the axial acceleration,

$$T_B = \mu m_p \ddot{x}_A r_m . \quad 3-6$$

This method however relied on the coefficient of friction being constant. It is known that the coefficient of friction will vary with factors such as temperature and lining wear and as a result this method was likely to produce less reliable results. From this point of view it was decided that the most accurate method of measuring brake judder would be to measure the pressure variation, however an exploratory attempt would be made to identify whether measuring vibrations of the brake caliper and/or the brake pad would also produce a feasible method for recording brake judder.

3.2.2. Equipment

To aid the investigation into on-vehicle brake judder a number of measurements were carried out. To achieve this the vehicle was equipped with a range of transducers to provide the data for analysis.

The test equipment consisted of:

- Embedded thermocouples in the front brake discs connected via slip rings which measured inner and outer friction ring temperatures.
- Rubbing thermocouple on the rear brake for calibration purposes.
- Pressure transducers independently measured left and right front caliper brake line pressures (Figure 3.2) allowing brake pressure variation to be measured.
- Biaxial accelerometers mounted on the pad back-plates measured in-plane (tangential to disc revolution) and out-of-plane (axial) vibration.
- Accelerometers mounted on the calipers measured in-plane vibration.
- Thermocouples mounted on the pad back plates for calibration purposes.
- Accelerometer which measured longitudinal vehicle deceleration.
- A GPS sensor and monitoring of the vehicle ECU to measure speed.
- Strain gauge which measured pedal effort.
- String Potentiometer which measured brake pedal travel.
- Roof mounted thermocouple which measured ambient air temperature.
- A modular data acquisition system which recorded 19 separate channels of data.
- A laptop which enabled real-time viewing of brake disc temperatures, vehicle speed and deceleration which therefore improved the repeatability of the test by being able to maintain the correct level of vehicle deceleration throughout the stop. The variation associated with the vehicle deceleration was therefore limited to a maximum of $\pm 10\%$ (typically 0.27-0.33g).

More details of the instrumentation can be found in the appendices in section 10.1.

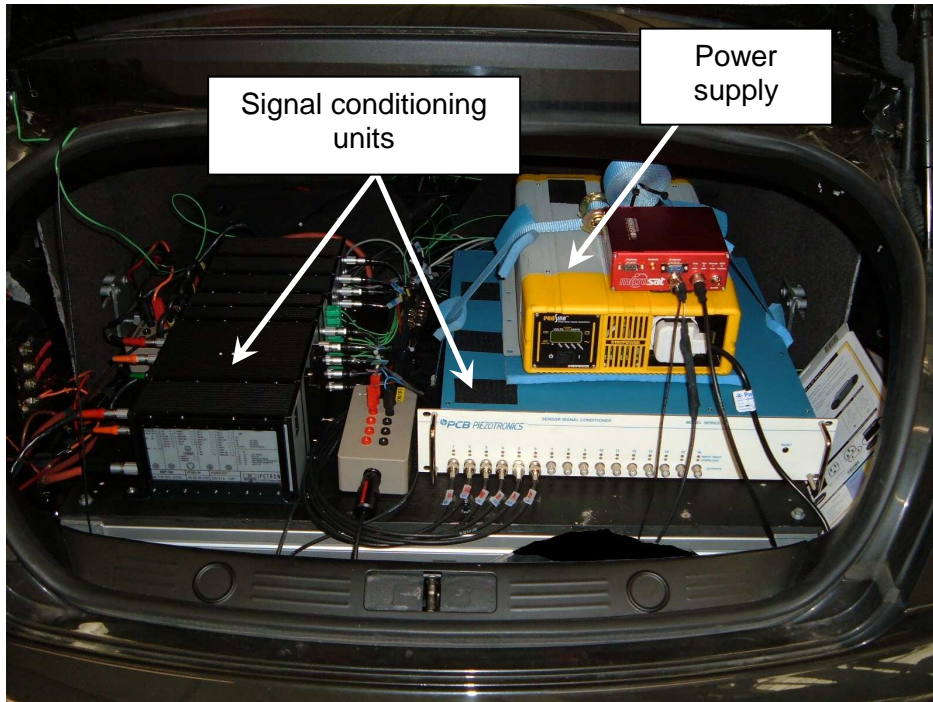


Figure 3.1: Data logging equipment.

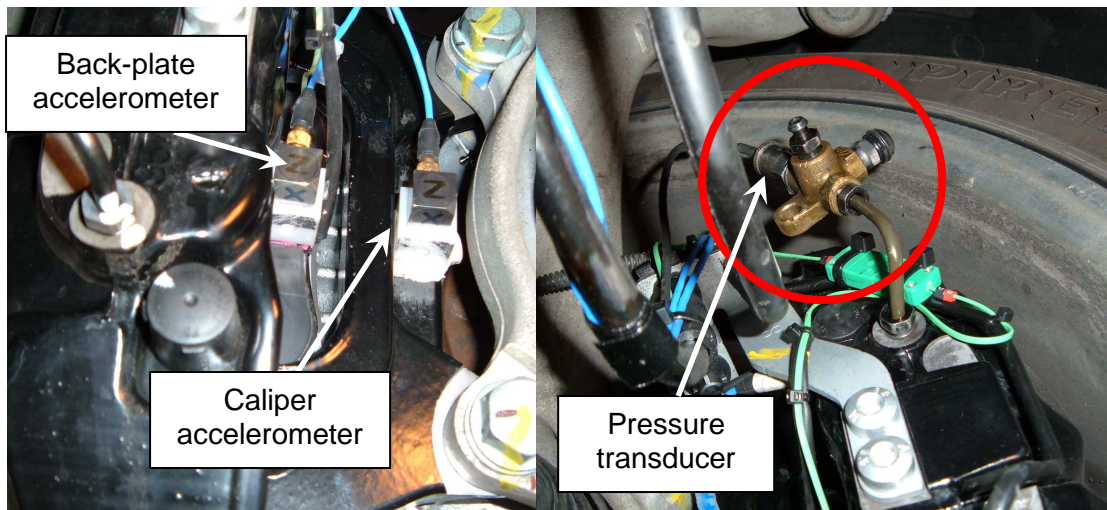


Figure 3.2: Caliper & back-plate accelerometers (left) and brake line pressure transducer (right).

Data was stored directly to a laptop with the capture rate initially set at a frequency of 500Hz due to the limits of the system being used. This was subsequently increased to 1 KHz once the memory requirement had been identified. The acquisition system can be seen in figure 3.1 and was mounted in the luggage compartment of the

vehicle. A subjective scoring system was used for brake drone and pedal, body and steering vibration. In this system a score of 1-10 is given to each of the above mentioned properties with 10 being perfect and 1 being unacceptable. The use of subjective scoring is a normal procedure in industry and is used as a quick and effective measure of the severity of the brake [58].

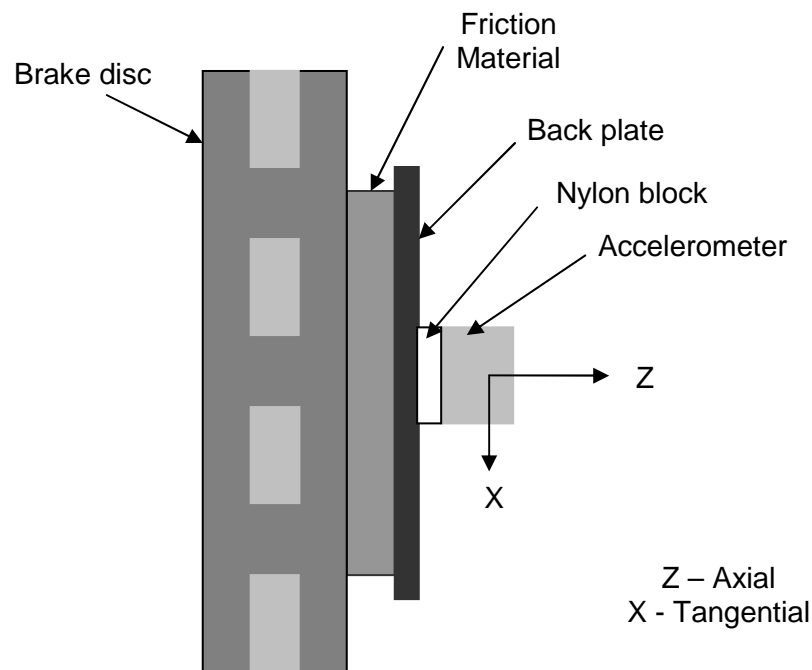


Figure 3.3: Diagram showing the position of the accelerometer on the brake pad back plate.

A diagram of the accelerometer mounting arrangement is shown in figure 3.3 for the brake pad back-plate. The X axis measured tangential pad vibration and the Z axis measured axial pad vibration. The accelerometer was mounted onto a sacrificial nylon block which was then bonded to the pad back plate; this insulated the accelerometer from the high temperatures of the brake pad. The natural frequency of the nylon block was above 250Hz; this was above the frequencies of interest and therefore did not affect the measurements.

3.2.3. Procedure

The vehicle manufacturer used a specific brake testing schedule in order to assess the vehicle's sensitivity to and level of brake judder. The test schedule, shown in

table 3-1, involved a number of low deceleration, typically 0.2-0.4g, high speed braking events performed in quick succession with various starting point temperatures to enable comparison between different vehicles and brake discs. The test schedule was used by the manufacturer for a comparison of various vehicles and therefore lists V_{max} (maximum speed) as a reference for all the braking events allowing the speed to be scaled up or down depending upon the performance of the vehicle. For a standard test performed by the manufacturer the initial and final braking speed for the vehicle used for this research are shown in brackets (km/h). The structure of the test was used for identifying judder issues with a vehicle as the car was required to perform high speed, high energy braking events in fairly quick succession close to or at the maximum speed of the vehicle. This represented a very severe case of braking and would bring out any judder issues caused by hot spotting or thermo-elastic and thermo-plastic deformation due to the high energy dissipation. Measurements of inboard and outboard disc temperatures were recorded throughout the test whilst brake judder severity was assessed by means of a subjective test based on steering, pedal and body vibration and audible drone. The subjective scores were recorded by a qualified test driver to maintain repeatability. Subjective scores were used as a quick and effective method to assess a vehicle's sensitivity to brake judder and also to benchmark the vehicle against others. When sold to the public, it is the vehicle owner and occupants who experience brake judder, therefore subjective scores measured by a trained driver represent the likelihood of customer complaints. Objective data was measured using the brake pressure transducers and accelerometers discussed above. The data recorded from these transducers was then used for correlations with the subjective scores. Brake judder is often a whole vehicle consideration; a juddering brake system on a less sensitive vehicle is not necessarily as big a problem as the same brake system on a sensitive vehicle. It was noted that attempts made by other authors to correlate subjective scores with objective data, when researching brake squeal [60], proved to be more difficult than initially thought, with measured objective data not necessarily correlating with subjective scores taken from a group. Whilst the research in question was related to brake noise rather than vibration (under which judder is classed) there was the possibility that vibrations caused by brake judder may be damped out in the process of being transferred to the driver. Under this situation the subjective scores would be good whilst the brake pressure variation or vibration of the caliper and brake pads would be large. For the data presented in this thesis the correlation between measured brake pressure variation and the subjective scores for pedal vibration was good and is discussed below. Therefore there were no issues with the correlation

between subjective and objective data in this instance. Correlations between pad and caliper vibrations and the subjective scores were not possible due to the amount of road noise picked up within the signals. Attempts were made to remove the road noise however this did not result in a useable signal.

Test Conditions				Subjective Assessment using a 10point Scale					
Stop- No.	Vehicle Velocity $V_a \rightarrow V_e$ km/h	T_a [°C] Start Temperature (Front Axle)	Deceleration z [g]	Brake Drone	Steering Vibration	Pedal Vibration	Body Vibration	T_{max} [°C]	
								Front	Rear
1		80							
2	$0.7v_{max} \rightarrow 50$	150							
3	(210 \rightarrow 50)	200							
4	$0.8v_{max} \rightarrow 50$	80	0.2g						
5	(240 \rightarrow 50)	150							
6		200							
7	$V_{max} \rightarrow 50$	50							
8	(300 \rightarrow 50)	80							
9	$0.8v_{max} \rightarrow 50$	80							
10	(240 \rightarrow 50)	follow on	0.3g						
11		follow on							
12		200	0.4g						
13	$0.8v_{max} \rightarrow 50$	follow on							
14	(240 \rightarrow 50)	follow on	0.3g						
15		follow on							
MIN									

Table 3-1: Typical judder test schedule showing vehicle speed, disc temperature to aim for at start of braking and rate of vehicle deceleration.

The vehicle manufacturer's 'judder' test comprised of high speed braking, often in quick succession, but also extended periods of cooling, at set points, to pre-defined brake temperatures before the next sequence of braking events. It therefore had large amounts of kinetic energy being converted into heat by the brakes from both low and high disc temperatures. This gave a good range of conditions under which to analyse the development of brake judder on the vehicle. However, due to the high vehicle speeds attained it is necessary to perform the test on large foreign high speed test circuits. For the purpose of this research testing was only available at UK testing facilities with restricted speeds of 240km/h (150mph); therefore it was necessary to modify the test schedule to account for this. A basic rule was used to derive three potential test schedules with identical total energy dissipation throughout the duration of the test.

Using this as a guide three test methods were proposed:

- 25 sequential stops 200-30km/h
- 18 sequential stops 240-50km/h
- 28 stops with $V_{\max} = 240\text{km/h}$ following the original manufacturer test schedule with additional 240 – 50 km/h braking events performed to give identical total energy dissipation.

The total energy dissipated during the manufacturer's test was calculated to be 142MJ. This figure was obtained by calculating the kinetic energy dissipated during each braking event, using equation 3-7 below, and then summing the results. Each of the three proposed test methods were designed to dissipate an equivalent amount of energy. Figure 3.4 shows a comparison of the three proposed test methods with all three tests giving the same idealised total kinetic energy (KE) dissipation of the vehicle during braking as defined by the calculation shown in equation 3-7 whereby the kinetic energy of a body is directly proportional to the square of its speed. Therefore the change in kinetic energy when decelerating from an initial speed V_1 , to final speed V_2 , is equal to the final kinetic energy of the vehicle subtracted from the initial kinetic energy

$$KE = \left(\frac{1}{2} m_v V_1^2 \right) - \left(\frac{1}{2} m_v V_2^2 \right). \quad 3-7$$

The calculation used many simplifications in that it did not take into account vehicle drag, driveline losses, inertia effects or rolling resistance, however for this analysis to select a suitable test method it was not necessary to go into this detail. More detailed calculations can be found in section 5.2.2.

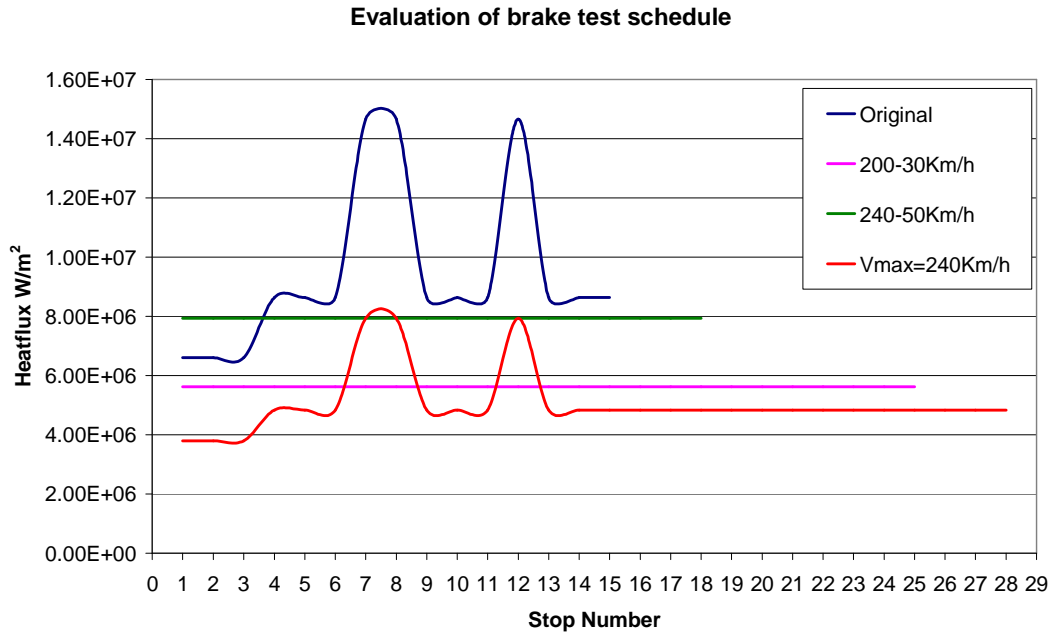


Figure 3.4: Evaluation of different replacement braking tests to account for speed reduction.

It was decided to select the 18 stop test method which was based on the manufacturer's test schedule using a reduced maximum speed of 240km/h for all braking events. By using this method the only significant difference between this test and the manufacturer's original test was the energy difference for the two maximum speed braking events. This was a difference of 6.73MJ for each of the two braking events, this was accounted for by the three additional stops at the end of the test. The test schedule can be seen in table 3-2. This allowed for comparisons with existing test data, whilst the additional repeat braking events towards the end of the test provided valuable data for comparison with the dynamometer testing. The other two tests were discounted as they deviated too far from the original manufacturer's vehicle tests to give good correlation and comparison combined with the much reduced energy dissipation in each braking event. The transducers and associated data acquisition system discussed in chapter 3.2.2 were used for this testing.

All testing was carried out on-vehicle at the Millbrook proving grounds in Bedfordshire to provide the most realistic conditions. The test procedure involved initial bedding-in of the brake system followed by the sequence of braking events set out in the test schedule. During the test it was found that the sensation of judder was masked by vibrations from the poor road surface and that judder did not develop as quickly and

severely as expected, therefore additional braking events were performed at the end of the test where necessary to achieve good data capture on a smoother section of road surface.

The relatively high starting velocity and low decelerations seen in the test dissipated a large amount of thermal energy through the brake discs. During the process of the test, heat rapidly built up in the brake discs and thermal deformations began to appear. Peak temperatures were in excess of 700°C; this was within the domain of blue spotting and hot spotting therefore the test allowed a good assessment of the judder performance of the braking system.

Test Conditions				Subjective Assessment using a 10point Scale						
Stop- No.	Vehicle velocity $V_a \rightarrow V_e$ km/h	T_a [°C] Start Temperature (Front axle)	Deceleration z [g]	Brake Drone	Steering Vibration	Pedal Vibration	Body Vibration	T_{max} [°C]		
								Front	Rear	
1	240→50	80	0.2g							
2		150								
3		200								
4	240→50	80		0.3g						
5		150								
6		200								
7	240→50	50	0.3g							
8		follow on								
9		80								
10		follow on								
11	240 – 50	80	0.3g							
12		follow on								
13		follow on								
14		200	0.4g							
15	240→50	follow on	0.3g							
16		follow on								
17		follow on								
18		follow on								
MIN										

Table 3-2: Revised test schedule.

Two test sessions were scheduled and completed at the Millbrook testing facilities. The first test session used current specification brake discs, whilst the second test used older specification brake discs. The older specification brake discs had the same geometry as the current specification discs; however they were from a different

casting foundry and the required machining tolerances could only be achieved with 100% inspection of parts which was not possible for the volume of brake discs produced. Therefore the probability of the brake discs being outside of the defined tolerances for features such as run-out, DTV, and concentricity was higher and they were known to suffer from poorer judder ratings [23]. By performing a back to back test the current discs could be benchmarked against a set of brake discs which were known to produce worse judder, whilst at the same time maximising the recorded data for analysis. For the first test data was captured at 500Hz, however once the data storage requirement for the test had been identified it was possible to increase the sample rate to 1000Hz for the test using the second set of brake discs. Accelerometers were only mounted on the brake pads for the second test once it had been confirmed in the first test session that they would not be damaged due to heat, therefore comparisons between the two sets of data was not possible for these readings. This was an acceptable compromise as, despite no comparisons being possible, it was still possible to analyse the data from that one test and draw conclusions. Comparisons with other data have been made where possible and where relevant.

3.2.4. Results

The main data obtained from the on-vehicle testing was of good quality with little or no noise which allowed good analysis techniques to be performed. The brake judder vibrations recorded by the accelerometers mounted on the caliper and brake pads were masked by vibrations picked up from the road surface; this was due to the poor quality of the road surface. If the background level of road noise could have been captured it would have been possible to subtract this from the accelerometer data to provide a better signal. However it was not possible to ensure that the vehicle travelled along exactly the same section of road during a brake test for this to be a reliable option; nevertheless it has been possible to make some observations from the raw data.

The analysis of the data included visual comparison of brake pressure variation between different braking events and Fourier analysis of the brake pressure variation and pad and caliper accelerations. The Fourier analysis technique is described in the following section (3.2.4.1) and was used to identify any common frequencies and the nature of brake pressure variation development throughout the test. Subjective scores for pedal, body and steering vibration were also used for overall comparisons

and correlation. Finally computer machine measurement (CMM) was used to create three dimensional surface topography maps of the brake discs post testing enabling comparison of cold disc deformation.

3.2.4.1. Fourier Analysis Method

Fourier analysis was performed on the on-vehicle data using MATLAB software to identify any trends in the judder frequencies over a number of braking events. Fourier analysis of the data would help to identify any frequencies building up which were not visually apparent in the pressure and vibration measurements. To perform the Fourier analysis in this thesis, data had to be partitioned into time periods equal to a single disc revolution. For a steady signal at constant speed it is possible to use multiple disc revolutions for a single analysis, however due to the nature of the tests the brake rotor was never at a constant speed. The only way to achieve a constant brake disc speed whilst measuring brake line pressure is to drag the brake, that is lightly apply the vehicle brakes whilst maintaining a constant speed. However doing this would have rapidly raised the brake temperatures and this would affect the results for each following braking event, not to mention causing unrealistic thermal expansion. Another method would have been to perform a Fourier analysis on all the data as the speed of rotation decreased, and then to plot the Fourier analysis frequencies against disc speed and dominance (or power spectrum) to give a 3D waterfall plot. This would have highlighted the various frequencies that were being excited as a function of wheel speed. However due to the sample rate it was only possible to obtain suitable data with a high enough number of samples per revolution at low speeds towards the end of each braking event. Therefore for each braking event, data for a single revolution was sectioned out at a disc speed of 389 revolutions per minute (r/min) or 50km/h at the very end of the braking period to give approximately 150 data points per revolution. The Nyquist frequency [61], which is the highest frequency that can accurately be represented with a given sampling rate, was 250Hz in the first test (sampling rate of 500Hz) and 500Hz (sampling rate of 1kHz) in the second test. Drone frequencies are typically in the range of 100-200Hz [4][11], therefore the sampling rate used was sufficient to capture the source of any drone frequencies and also the lower frequency judder.

Data sets were sectioned out for each braking event performed during the on-vehicle testing. The first data set to be analysed was the final braking event. The brake pressure signal for this stop showed the greatest response to judder. The data

contained some noise and other external influences which had to be filtered out to provide a better analysis. The data first had to have a least square fit performed upon it to eliminate the effect of the driver varying the brake pressure, this was done using MATLAB. This removed any overall gradient from the signal, bearing in mind that each braking event was performed as close to constant deceleration as possible.

The next step was to perform a Fast Fourier Transform (FFT) analysis, using the built in FFT function in MATLAB [62], which was combined with a tolerance variable. This tolerance eliminated all frequencies from the signal which had a dominance in the power spectrum less than the pre-defined variable. A tolerance band is shown in Figure 3.5; every frequency with dominance less than 15 decibels (db) was set to zero. This was performed to eliminate both noise and all unnecessary frequencies from the signal which caused minimal effects.

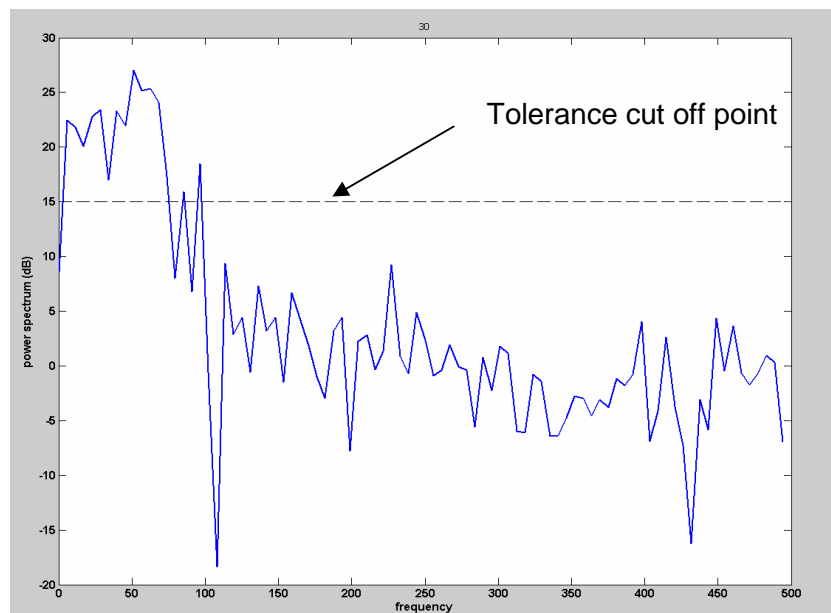


Figure 3.5: FFT distribution showing tolerance point.

An inverse FFT was then performed on the resultant signal to give a new representation of the original brake pressure signal minus the noise and less dominant frequencies. The result from this can be seen in Figure 3.6, which shows the brake pressure variation before and after the removal of the noise and less dominant frequencies.

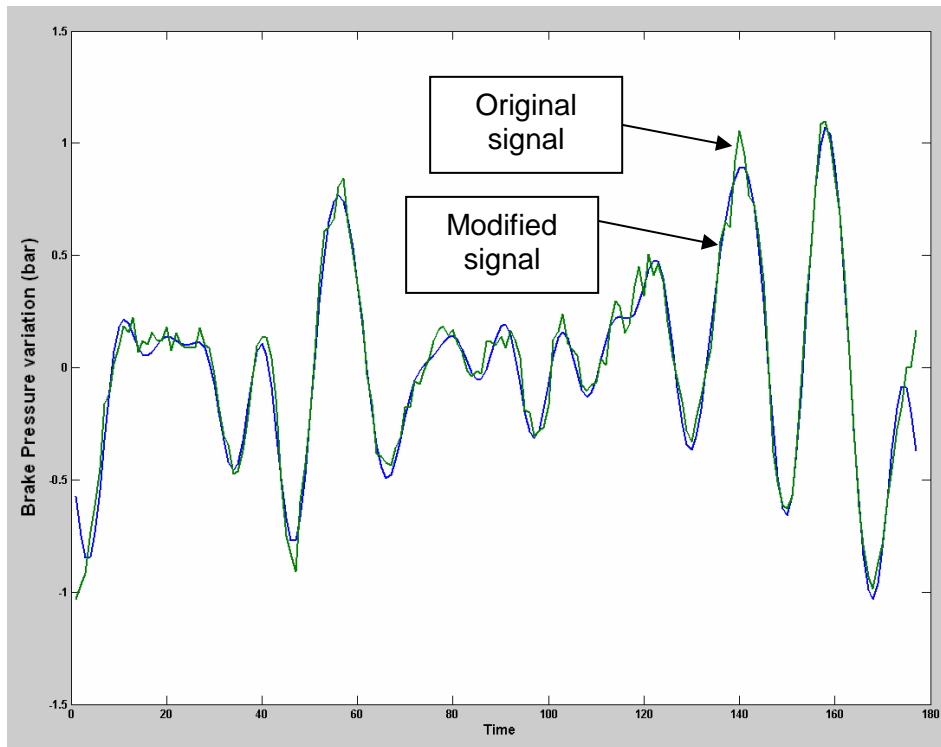


Figure 3.6: Graph showing Original brake pressure signal (Green) and result from Fourier analysis after tolerance has been applied (Blue).

This was repeated for all tolerance values from $n = 1$ up to the maximum value. The most representative output from the inverse FFT on this data set using the fewest dominant frequencies was selected for a tolerance level to use for all the remaining data sets. This ensured that noise was eliminated in all signals, but more importantly a common tolerance was used for all data sets. An example of this process is shown in Figure 3.7.

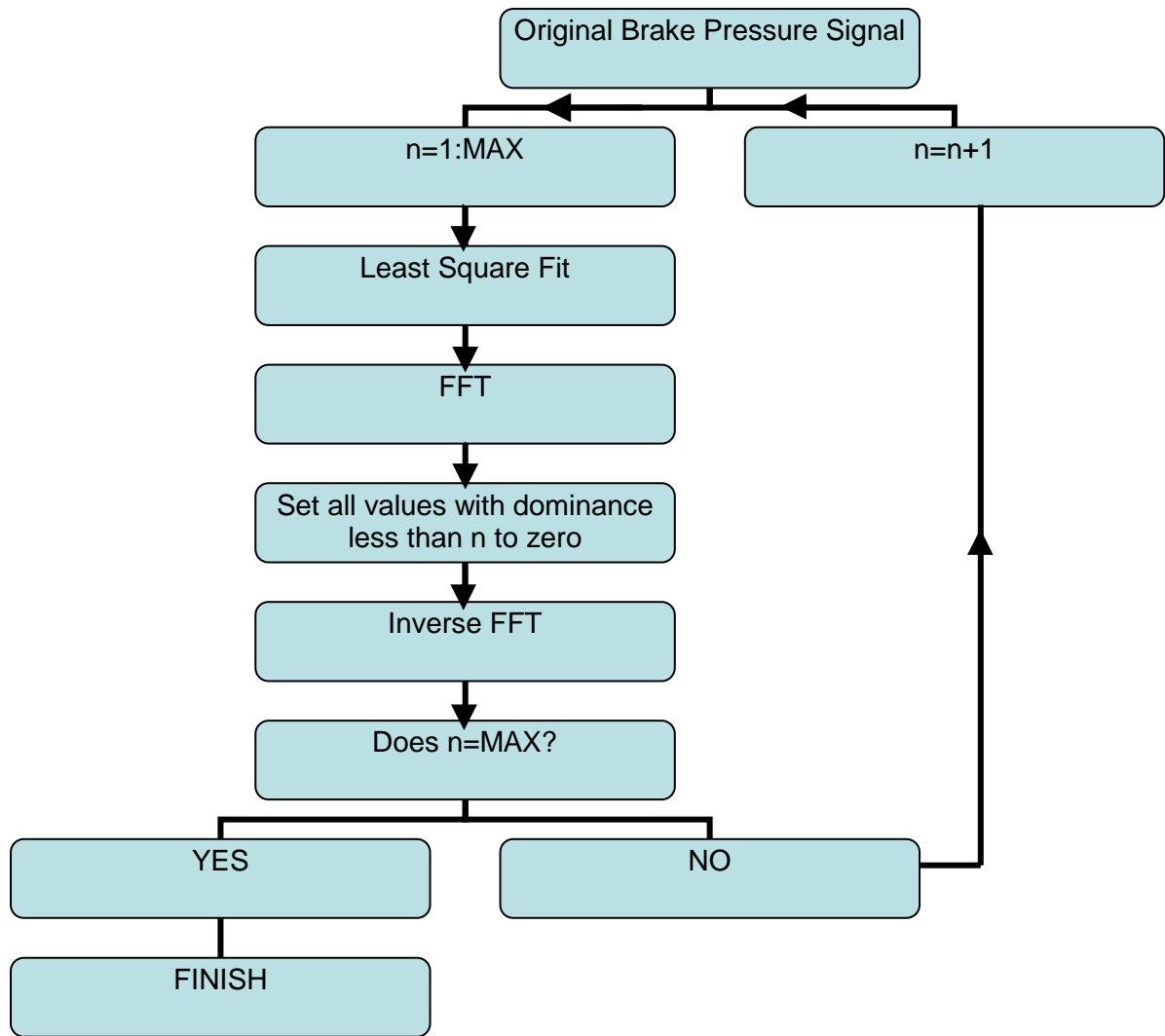


Figure 3.7: Block diagram of MATLAB Fourier analysis process.

Disc revolutions were sectioned out from the test data for each recorded braking event and stored in data sets for pressure variation and in plane and out of plane vibration. This allowed a visual analysis of judder development by analysing the pressure and vibration response, but also enabled Fourier analysis to be performed to enable a more detailed analysis of judder development by examining how the frequencies change over time. The Fourier analysis was able to highlight any excitation frequencies within the braking system caused by judder and also aided correlation. The Fourier analysis MATLAB code which was used for this analysis can be found in the appendices in section 10.4.

3.2.4.2. Fourier Analysis and Subjective Test Data Comparison

The higher sample rate used for the second set of brake discs provided a much better quality of data for Fourier analysis as there was double the number of data points available due to the increased sampling rate. A Fourier analysis of the pressure variation for each braking event using the second disc set is shown in figure 3.8. This graph shows the dominant frequencies which were present within the brake pressure variation measurement for a single disc revolution during each of the braking events that were recorded. It is apparent that there was a significant fall in the number of dominant frequencies following long periods of cooling (stops 21 and 26). This indicated that the brake disc was under-going thermo-elastic deformation and relaxing back to its original un-deformed shape during cooling. This observation is present for both the left and right hand brake disc. It can be seen that as the vehicle number of braking events increased so did the number of dominant frequencies within the BPV data. This was a result of the disc taking up more complex forms of thermo-elastic deformation as temperature built up in the brake disc.

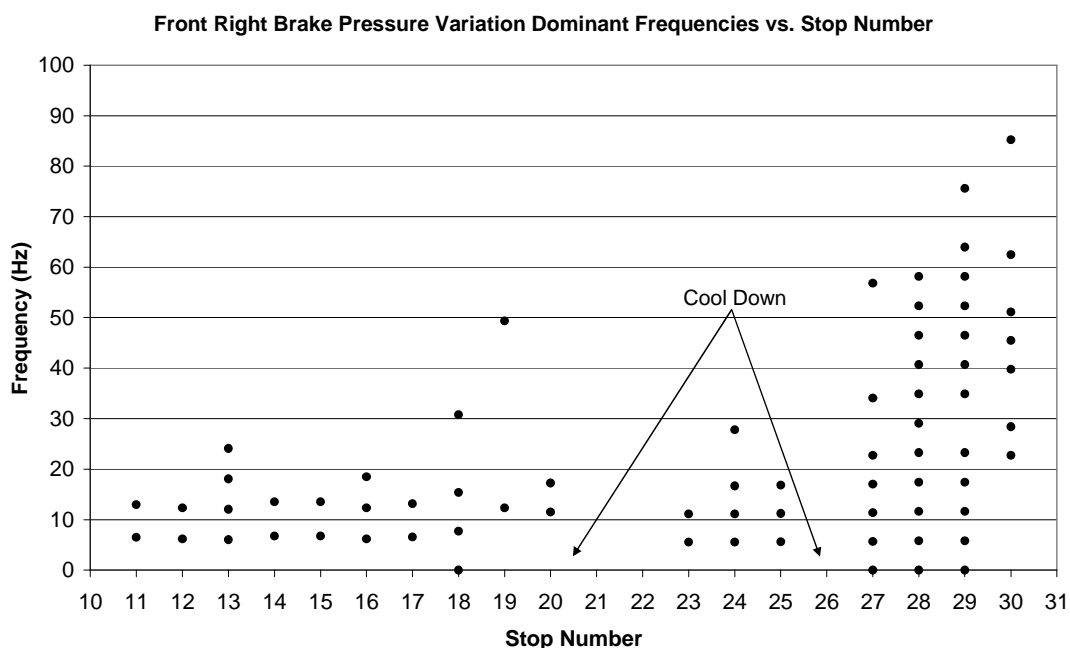


Figure 3.8: Right hand disc pressure dominant Fourier frequencies (disc set 2).

A similar graph showing the dominant Fourier frequencies for pressure and in-plane and out-of-plane pad vibration for each of the recorded braking events is shown in figure 3.9. Cross correlation between pressure and in-plane and out-of-plane pad

vibrations was poor with no common frequencies being detected. This was due to the large amount of noise present within the vibration measurements due to the road surface and vehicle movement. Out of plane pad vibration showed a constant frequency at around 200 Hz for the latter part of the recorded test which occurred for both left and right discs, whilst in-plane vibration showed frequencies consistently below 100 Hz. It is unclear what was causing these frequencies, one argument is that the 200Hz frequency was a drone frequency, but a more reasonable argument was that both frequency groups were caused by the surface roughness of the road. There were also a large number of dominant frequencies present for both in-plane and out-of-plane pad vibrations in the 0-500Hz range during braking events 11-14. An explanation for this is that the larger amplitude thermal distortion of the brake disc would not have fully developed at this stage of the vehicle test, and therefore the pad vibrations were dominated by higher frequency vibrations resulting from the road surface. This was backed up by the temperature of the brake discs which had reached a maximum temperature of 540°C before going through a cooling period prior to braking event 14. Following this the disc temperature rose from 357°C to 652°C during an aggressive braking phase of the test which allowed for minimal disc cooling between repeat braking events (see table 3-2). During this stage larger thermal distortion would have occurred as a result of the larger thermal expansion of the disc at the higher temperatures combined with the limited off-brake cooling periods. When this occurred the lower frequency pad vibrations resulting from brake judder would have begun to dominate the Fourier analysis which is what can be seen to occur following stop 14 in figure 3.9 where all frequencies above 100Hz (apart from the consistent 200Hz frequency) were no longer present.

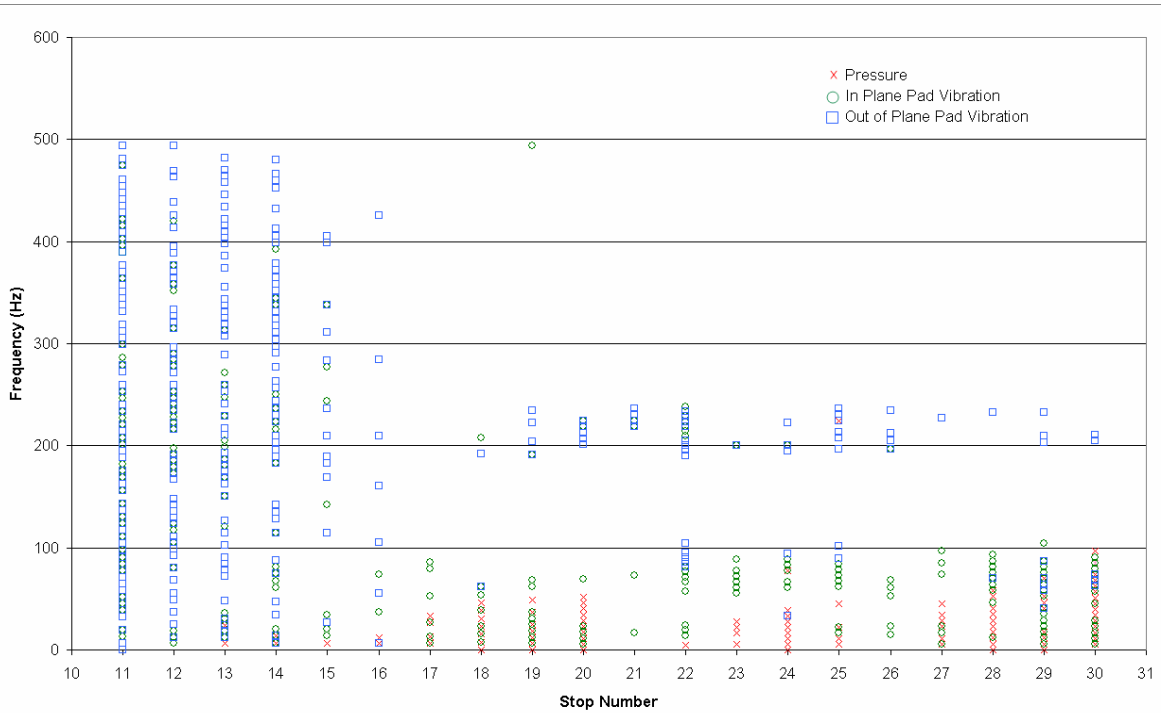


Figure 3.9: Cross correlation between brake pressure variation and in plane and out of plane vibration (disc set 2).

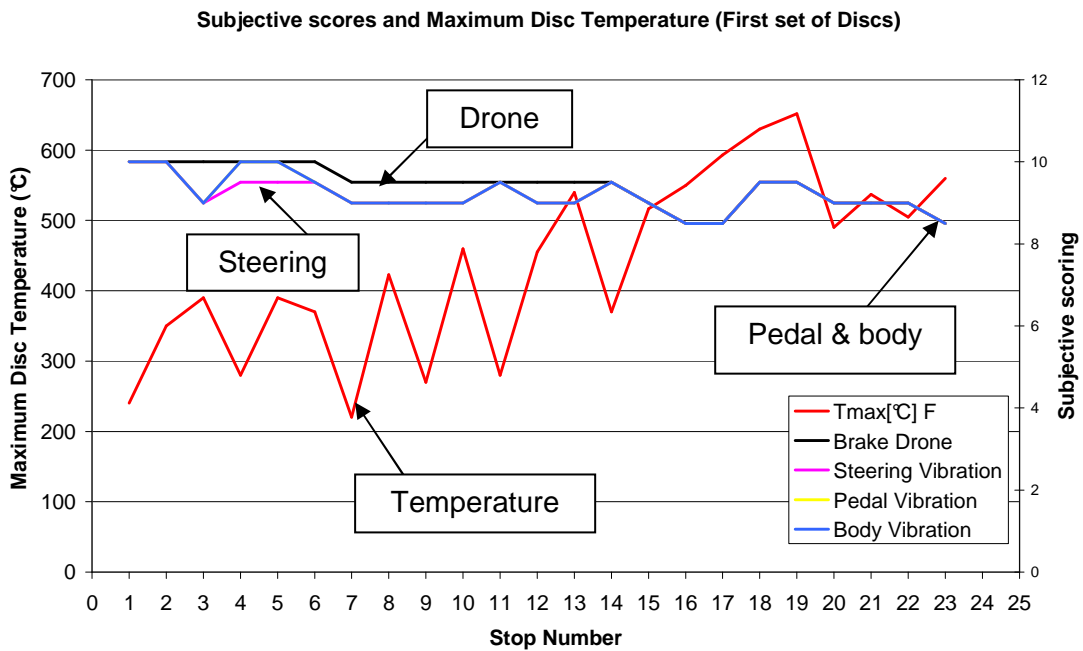


Figure 3.10: Subjective scores and maximum disc temperatures. Note: Pedal and body subjective scores are identical (disc set 1)

Subjective scores for steering, pedal and body vibration along with brake drone were plotted with maximum disc temperature in figure 3.10 for the first set of discs. Subjective scores were rated out of 10 with 10 being perfect running and 1 being completely unacceptable vibrations due to judder. Judder degradation on this set of brake discs was not particularly severe as can be seen from the relatively high subjective scores, although a falling trend is noticed over the duration of the test. A fairly clear correlation between brake pressure variation and maximum in-stop temperature can be seen in figure 3.11 with the brake pressure variation tending to rise and fall with temperature. This is clear indication of thermal judder or thermo-elastic deformation and not cold judder as this trend would not be expected with cold judder. The graph shows the trend of a disc whose pressure rises in response to the expansion of the disc and its surface deformation. Pressure variation is generally the same magnitude between the left and right brakes indicating that the strength of the judder, i.e. the strength of the pulsation of the brake pedal, was coming equally from both halves of the front brake system.

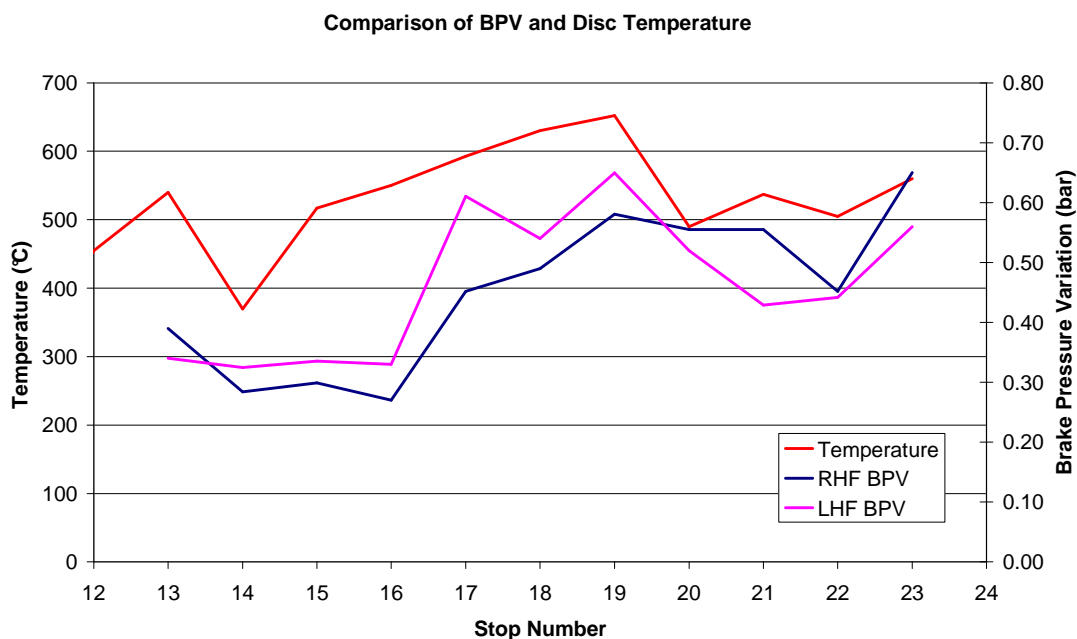


Figure 3.11: Comparison between left and right brake discs showing BPV development (disc set 1)

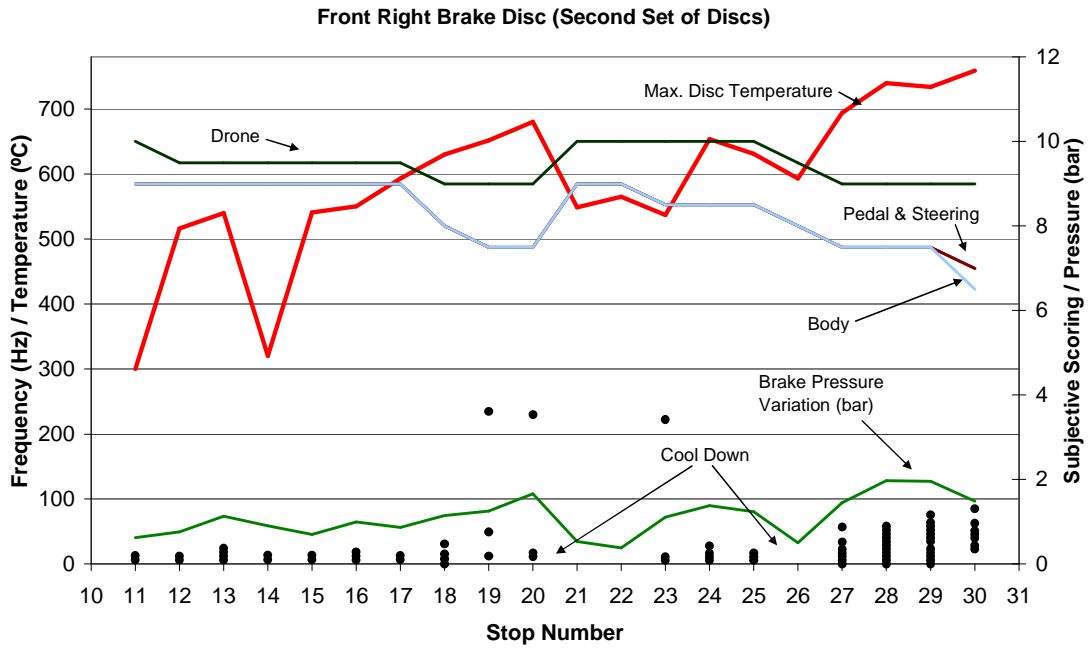


Figure 3.12: Dominant Fourier frequencies, maximum temperature and subjective scores for right hand front brake disc (disc set 2).

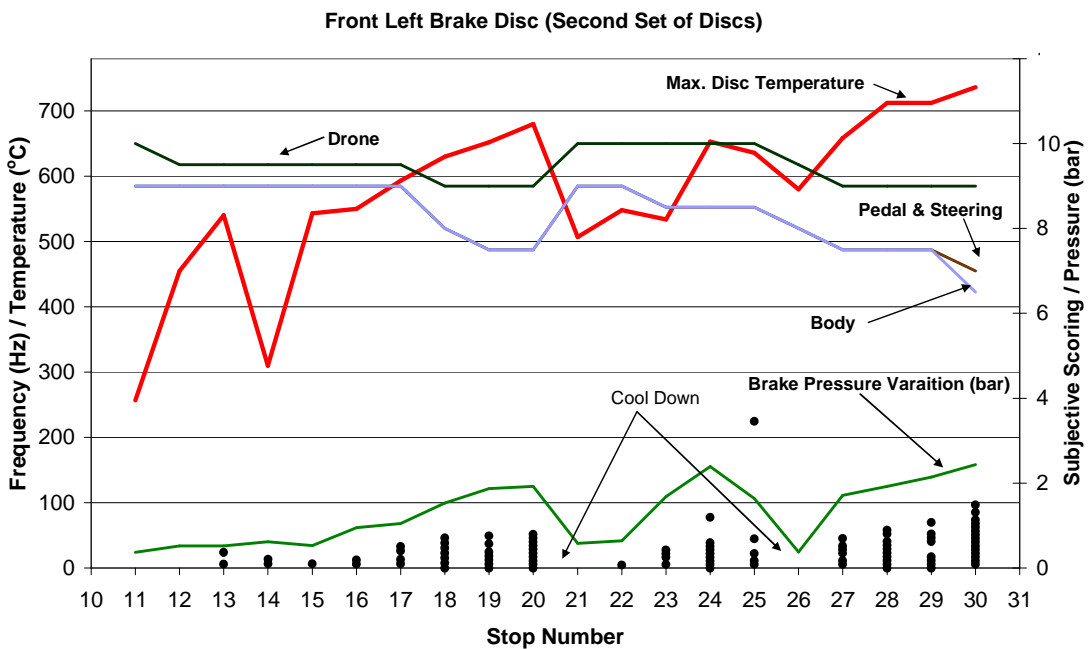


Figure 3.13: Dominant Fourier frequencies, maximum temperature and subjective scores for left hand front brake disc (disc set 2).

Figure 3.12 and figure 3.13 show dominant Fourier frequencies for both the left and right hand front brake discs during the second test. Overlaid are plots of maximum

disc surface temperature and subjective scores for brake drone, steering vibration, pedal vibration and body vibration. Both graphs show common trends which identify that both the number of dominant frequencies and their magnitude rose towards the end of the test together with rising temperature and falling subjective scores. This identified that as the disc temperature increased, the subjective level of brake judder degraded and the number of dominant frequencies increased. The frequency trend is shown more clearly in figure 3.8. This indicated that the disc was under-going increasing thermo-elastic deformation as the brake disc heated up as the deformation was becoming higher order and more complex, therefore explaining the increasing magnitude and number of dominant frequencies picked up by the Fourier analysis. Also indicated on the graphs in figure 3.12 and figure 3.13 is the amplitude of brake pressure variation throughout the recorded section of the test. Again there was clear correlation between BPV and maximum brake disc temperature which was a good indication of hot judder as a result of thermo-elastic deformation of the brake disc. If cold judder were the cause, this correlation would not be expected as discussed earlier in this section. Correlations between the various subjective scores and the amplitude of BPV have also been made; generally the subjective scores were seen to improve when the BPV amplitude fell and vice versa. As with the first test the magnitude of the BPV was comparable between the left and right hand brakes. The subjective scores for this second test were worse than that of the first test. This was expected based on discussions with the vehicle manufacturer and are a result of the generally poorer machined tolerances (discussed in section 3.2.3) of the brake disc. These poorer tolerances would have resulted in uneven thermal expansion and therefore uneven distortion of the brake disc. This would have caused increased BPV therefore the judder would have been worse.

3.2.4.3. Brake Pressure Variation

Brake pressure measurements gave the best response to judder in the form of BPV. Pulsation of the brake pressure as a result of brake judder could be seen, this was a function of the disc rotation and an example of this can be seen in figure 3.14. The accelerometers mounted to the caliper and back plates suffered from high noise levels making data extraction difficult and less reliable than the BPV measurements. Measurement of left and right caliper pressures enabled the type of judder on each brake disc to be identified. The following set of graphs indicates the type of judder present. Data sets for the right hand brake disc from the first test are presented in figure 3.14 to figure 3.16.

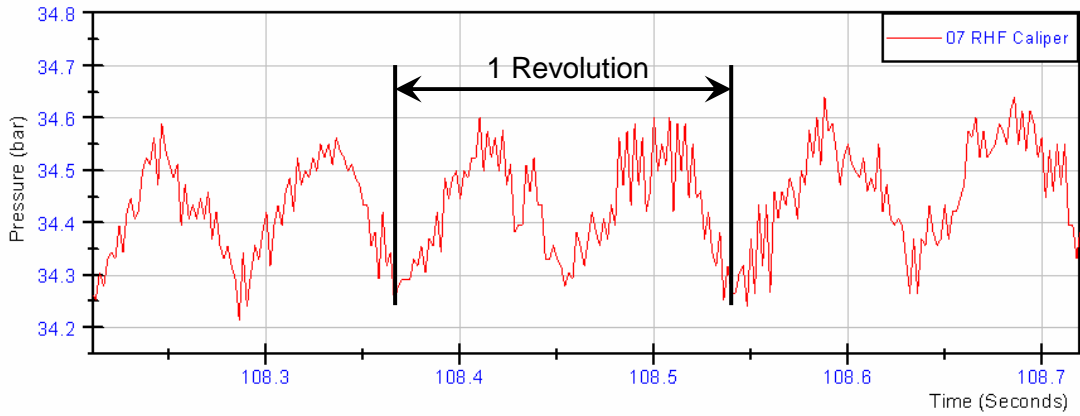


Figure 3.14: Right hand front brake pressure variation stop 13 – 1st disc set.

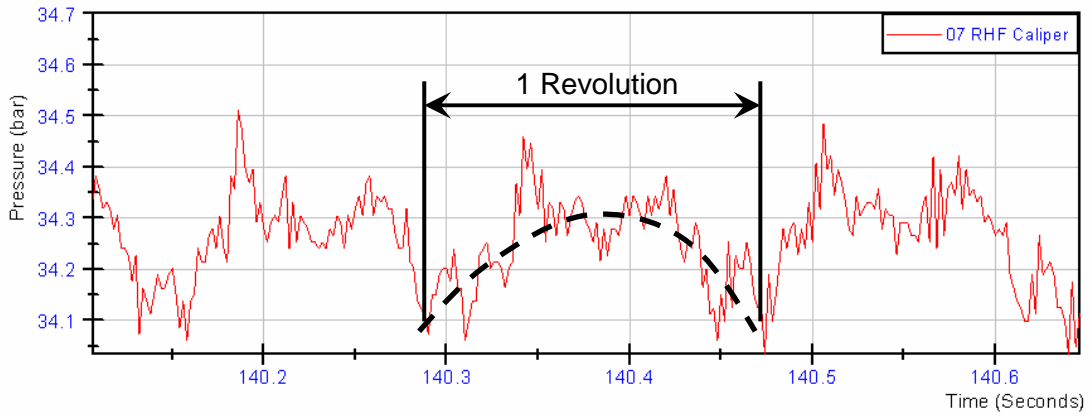


Figure 3.15: Right hand front brake pressure variation stop 17 – 1st disc set.

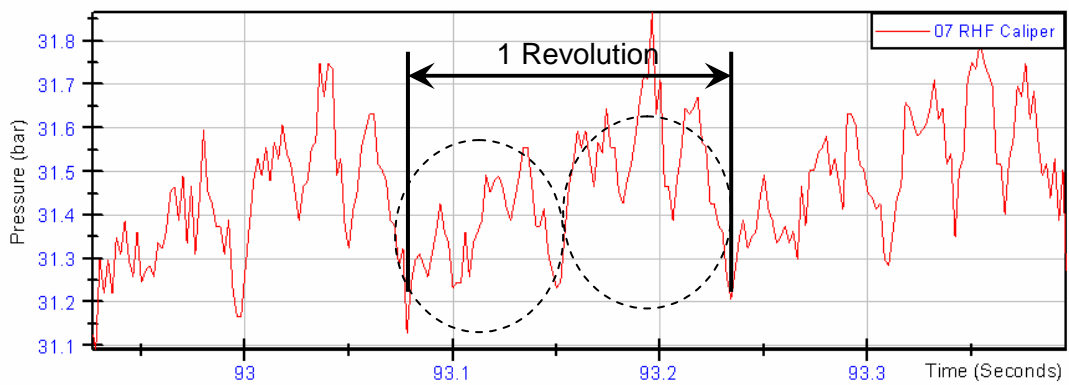


Figure 3.16: Right hand front brake pressure variation stop 23 showing the dominant two pressure pulses – 1st disc set.

Figure 3.14 shows a characteristic pressure pulse response due to dominant 2nd order (or two pulses per revolution) brake judder on the right hand front brake disc. The development of this pulsation can be seen in figure 3.15 and figure 3.16. Figure 3.15 shows that pulse amplitude has increased slightly from approximately 0.3 bar to 0.4 bar, however there is now only one overall clear pulse per revolution as indicated. Figure 3.16, the final braking event in this test, shows that the pressure variation has now transformed to dominant second order with a higher order of pulsation superimposed on top. There was only a small amount of noticeable judder during the above test which was backed up with disc measurements that identified a thickness variation of 5 microns which is below the critical threshold of 10-15 microns [15][16] which is known to cause serious judder. However there is a clear pressure response to the underlying DTV or deformation of the disc.

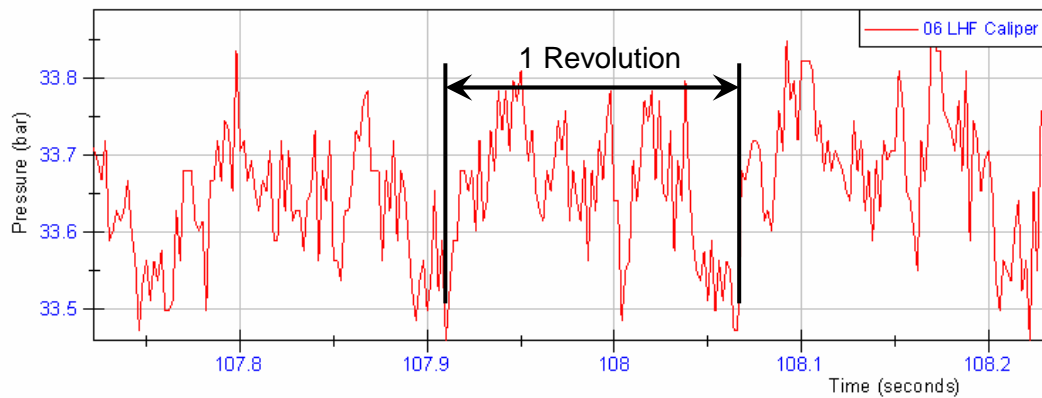


Figure 3.17: Left hand front brake pressure variation stop 13 – 1st disc set.

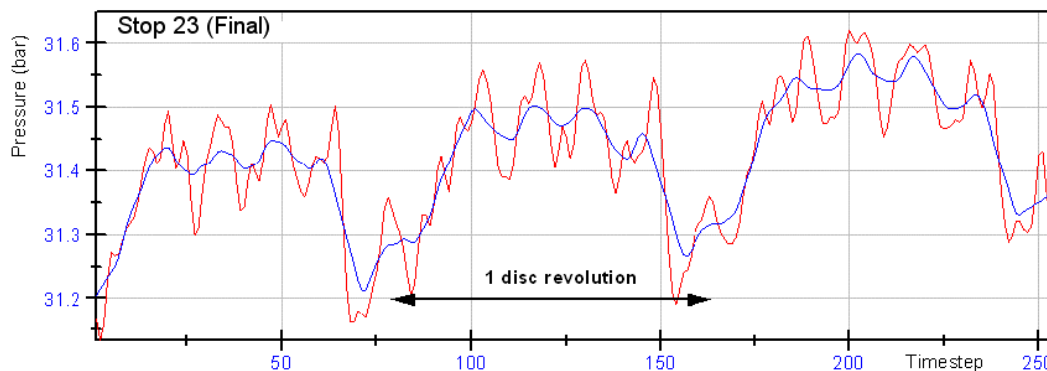


Figure 3.18: Left hand front brake pressure variation stop 23 – 1st disc set.

The development of brake judder on the left hand disc can be seen in figure 3.17 and figure 3.18. Figure 3.17 shows the BPV mid way through the test. It is only just apparent that the pressure pulse was of first order and it was not as clear as the right hand disc during the same stop shown in figure 3.14. The BPV slowly developed throughout the following stops until the final stop as shown in figure 3.18. The BPV by then had developed to dominant first order judder with superimposed fifth order and it was believed that had testing continued this would have developed further. The reasoning for this being that BPV and subjective scores have been shown to be linked to disc temperature (figure 3.10 and figure 3.11), therefore as the results have shown the steady development of judder to this point, it would be expected that judder would become worse if the disc temperature were to have risen further. The figures also show the relative magnitude of the BPV compared to one another. Again it is clear that the pulsation was becoming larger in amplitude as conditioning of the brakes progressed during testing. The pressure variation was in the order of 0.3 – 0.4 bar (0.03–0.04MPa) by stop 23. This was much smaller than the maximum range of ± 0.14 MPa identified in [5] from brake dynamometer testing, however it must be noted that the application pressure in this testing performed for this thesis was far higher in order to overcome the deceleration due to aerodynamic drag and to suitably condition the brake discs, and would therefore suppress the pressure variation. Also the judder felt by the vehicle occupants was very low in these tests as can be seen by the subjective scores which were all above 8.5. This subjective score would have been given a performance rating of “good” and a customer satisfaction rating of “very satisfactory” using a standard rating system [23],[63]. Subjective judder degradation on this set of discs did not progress therefore the test was curtailed after a total of 23 braking events (18 + 5 additional braking events). Again for this brake disc the mean DTV was 9 microns, measured manually with a micron resolution micrometer at ten points around the disc surface when cold, which again was below the critical DTV threshold [15][16]; however the number of measurement locations was only suitable to give a general DTV value with this measurement technique.

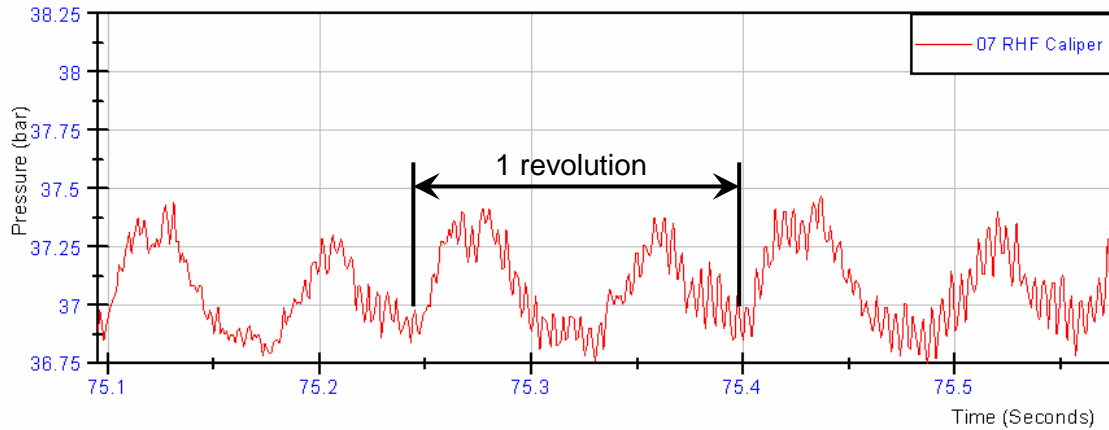


Figure 3.19: Right hand front brake pressure variation stop 15 – 2nd disc set.

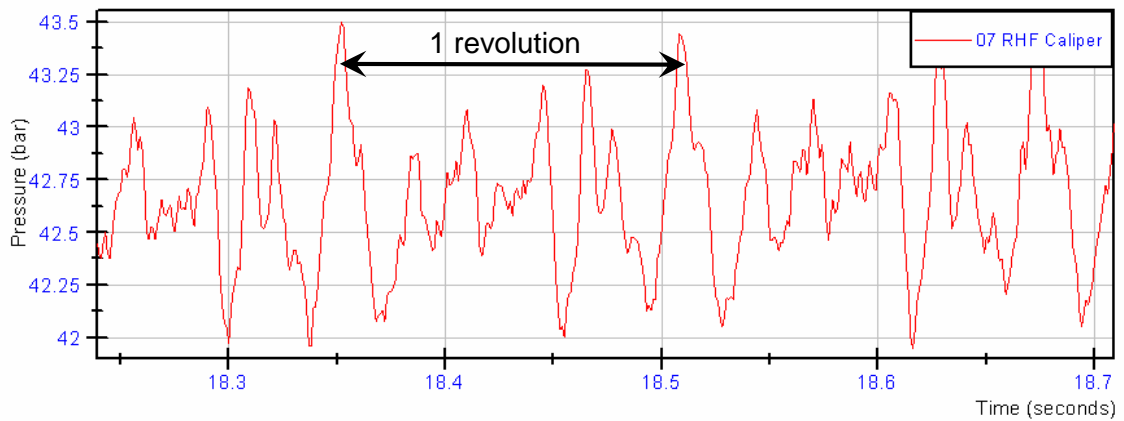


Figure 3.20: Right hand front brake pressure variation stop 30 – 2nd disc set.

Figure 3.19 and figure 3.20 are graphs from a similar test using a different set of brake discs. It can be seen from figure 3.19 that the pressure response is again initially second order, but develops to a much higher order (possible 6th order) by the last stop shown in figure 3.20. The amplitude of the BPV in figure 3.19 is approximately 0.5bar. This is already of similar magnitude to the final stop using the previous brake discs (figure 3.16 and figure 3.18). The development of judder was clearer with the second set of brake discs and therefore an additional 11 braking events were performed to identify any trends. By stop 30, the final braking event, the BPV had progressed to 1.7 bar which correlated well with measurements by Fieldhouse [5] (1.4bar), by which point clear judder was felt by the vehicle occupants with subjective scores as low as 6.5 being recorded for body vibration and a score of 7 for brake pedal vibration.

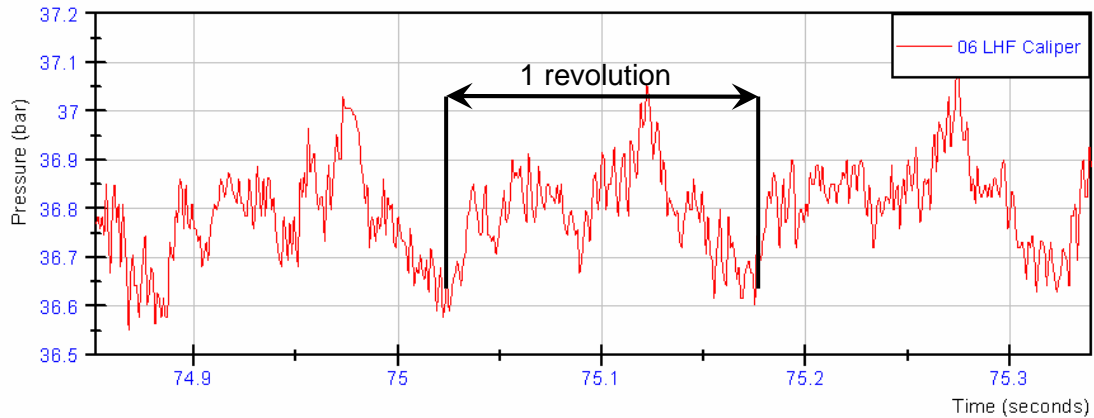


Figure 3.21: Left hand front brake disc pressure variation stop 15 – 2nd disc set.

Again looking at the left hand brake disc for the second set of brake discs the changing nature of the pressure variation can be seen. Figure 3.21 shows the fifteenth stop in the sequence, here the pressure variation was 0.5bar and the signal was showing two major peaks together with many smaller noisier peaks. However by the final stop displayed in figure 3.22 the pressure variation was a very complex signal built up from many dominant peaks. These peaks would be caused either by localised DTV, which may have been a result of hot spots, or localised wear at the peaks of high order wave-like deformation. There was no indication of martensitic transformation following post test analysis which is an indicator of hot spots; therefore it was likely that the cause was wave-like deformation of the disc. The pressure variation was 2.4bar which was larger than that of the right hand disc; however there was no indication of why this should be the case as the right hand disc was consistently the hotter of the two and had larger post test run-out.

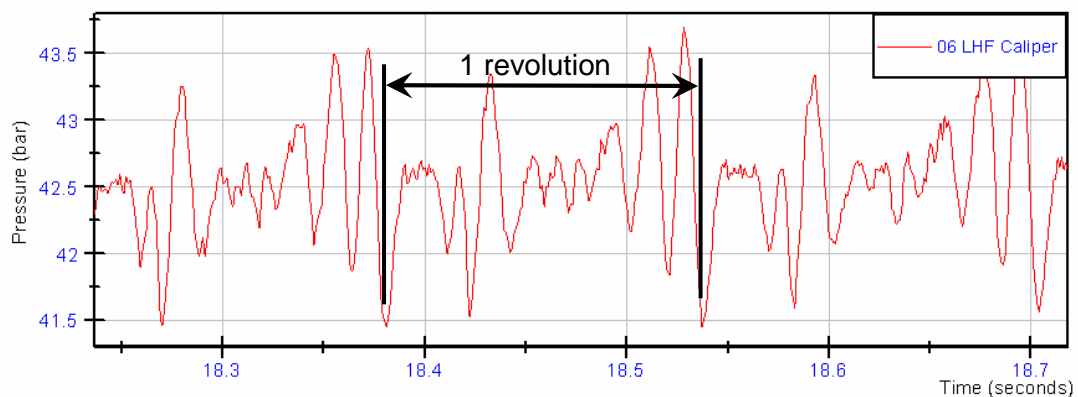


Figure 3.22: Left hand front brake disc pressure variation stop 30 – 2nd disc set.

The results shown indicated a larger tendency towards judder for the second set of brake discs tested, this was backed up by both the subjective scores and BPV amplitude. Both sets of brake discs have exhibited an increasingly complex pressure variation signal as the brake judder develops/increases. For reference the visual change in brake pressure variation for the second set of brake discs throughout the testing can be seen in appendix 10.5. Also of interest was the similar second order deformation indicated for the right hand brake disc in both tests between stops 13 and 15. This compared well with experiments carried out by Degenstein *et al* [65] on a new brake disc whereby the authors obtained the brake torque and associated force variation at the brake pads using transducers mounted between the friction material and backing plate. Their results showed a characteristic second order pulse which was roughly 1.7% of the applied brake torque. Results by Fieldhouse *et al* [5] also showed second order brake pressure variation with associated second order disc deformation following bedding of two different brake disc designs (2-piece pin mounted disc and integral top hat disc). This suggested an initial common mode of deformation independent of disc type or design. Dynamometer tests of the braking system used for the on-vehicle tests has been used to investigate this effect in more detail, the general results and discussion from this can be found in section 4.2 and, more specifically, the link this has to stress relieving in section 4.2.3.2.

Judder was shown to develop from second order (two pulses per revolution) to a much higher order, possibly 8th from analysis of the brake pressure data (Figure 3.23). The relative strength of the pressure variation also increased which correlated well with the recorded subjective scores. The recorded subjective brake judder scores became worse with increasing disc temperature which was also highlighted by the increasing number of dominant frequencies.

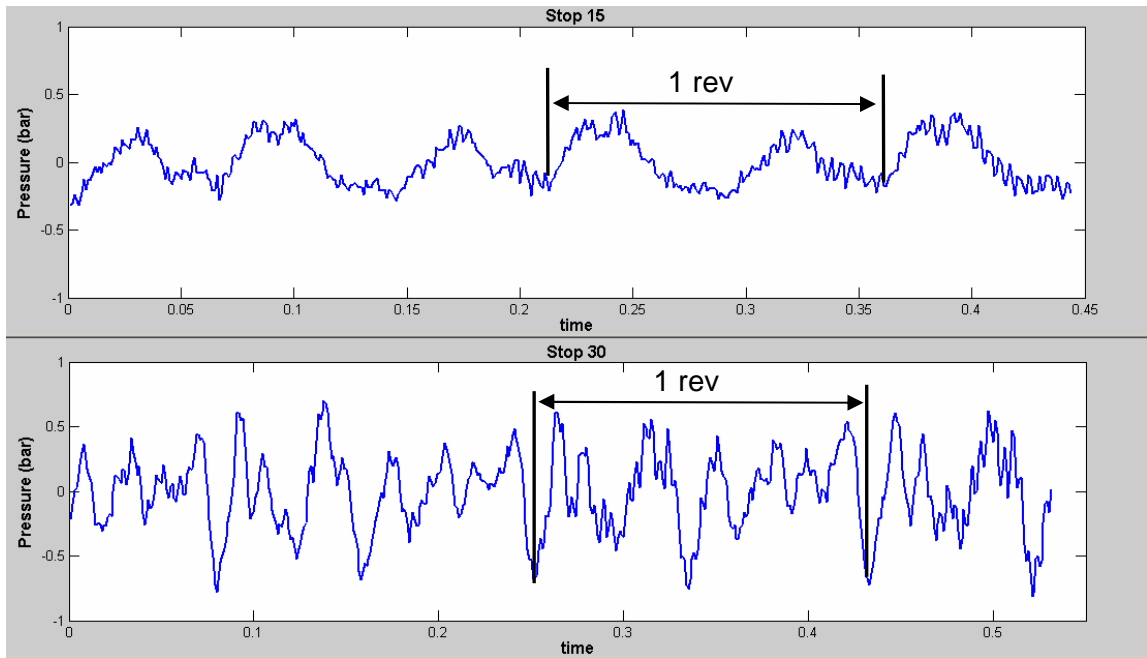


Figure 3.23: Development of brake pressure variation between stop 15 and stop 30 – 2nd disc set.

3.2.4.4. Pad and Caliper Vibration

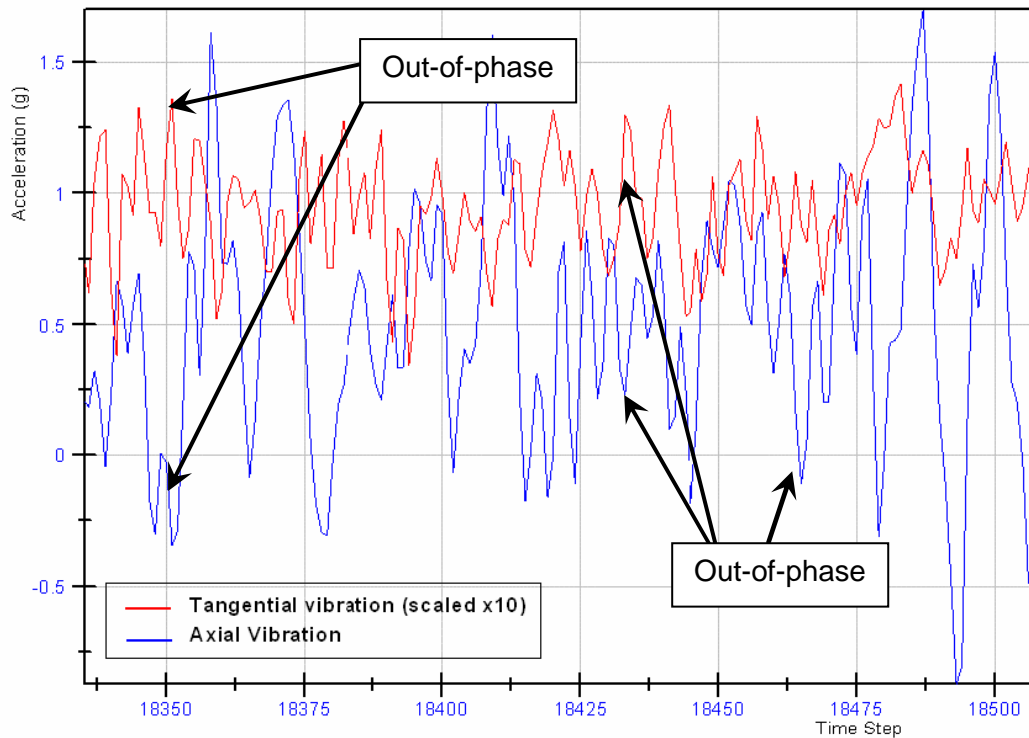


Figure 3.24: Tangential and axial back-plate vibration.

Axial and tangential back plate vibrations are plotted against time step in figure 3.24 for the second set of brake discs. As previously mentioned the vibrations due to judder were masked by road vibrations and the sample shown was a rarity. In theory axial vibration is proportional to BPV and tangential vibration is proportional to BTV due to the relative movement of the brake pad. It can be seen that the two vibration responses to judder appeared to be roughly 180° out of phase at several points throughout the plot. This can be expected as highlighted in figure 3.25 where a theoretical example of a pad striking an undulation of the disc surface is shown. As the pad strikes the raised peak on the disc surface the BTV will be at a maximum and will fall as the pad moves from position 1 to 3. The BPV will do exactly the opposite, rising to a maximum when the pad sits upon the peak. This is an important observation as it highlights the possibility that the two judder responses, BPV & BTV, may combine or subtract to produce excitation frequencies. However this is still a tentative association and further testing in a controlled environment is recommended to confirm this observation.

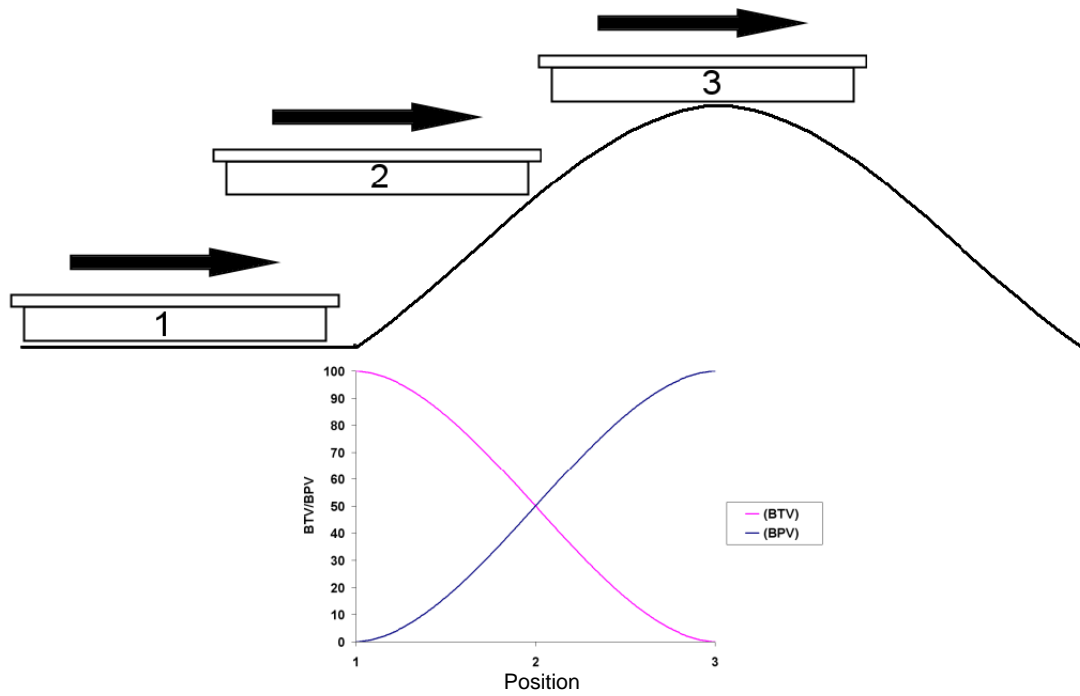


Figure 3.25: Theoretical graph of BPV and BTV as a pad strikes a peak on the disc surface – arbitrary scale.

Throughout the test data there were occasional correlations between tangential or in-plane vibration and brake pressure variation; an example can be seen in figure 3.26. The brake pad appeared to experience a resonant or heterodyne response; however as with all the vibration measurements the pattern disappeared after only a few cycles. The pad vibration pattern bore no resemblance to the BPV signal unlike measurements of the caliper vibration seen in figure 3.27. Out-of-plane vibration of the brake pad gave no correlation to brake pressure variation.

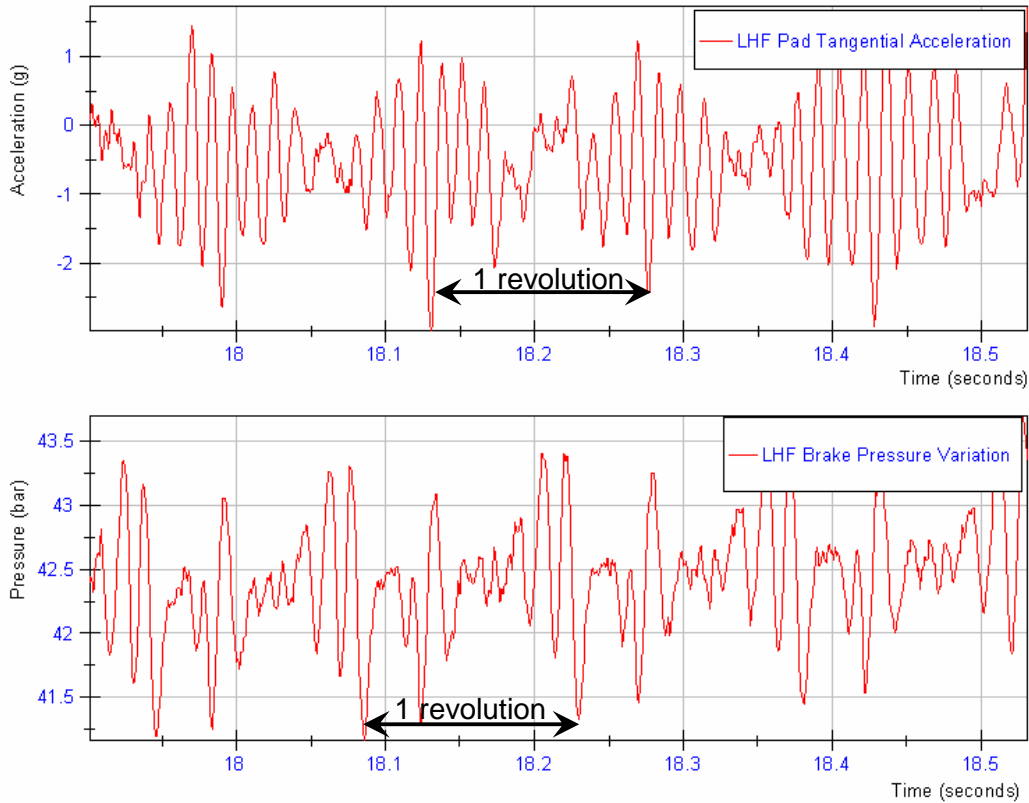


Figure 3.26: Correlation between brake pressure variation and tangential (in-plane) pad vibration

Brake caliper vibrations produced little meaningful data due to excessive noise in the signal. At various points within the test data there was a clear correlation between tangential caliper vibration and BPV with a 0.3 second lag between the two responses as seen in figure 3.27. However there was no clear pattern to the appearance of the caliper vibrations and they rarely matched the brake pressure variation. The caliper is known to have its own damping and modes of vibration; therefore this is one possible reason for the lack of recognisable vibration frequencies. Due to packaging constraints the accelerometer was also positioned at the stiffest point of the caliper, between the mounting holes, which would again reduce the susceptibility to vibrations.

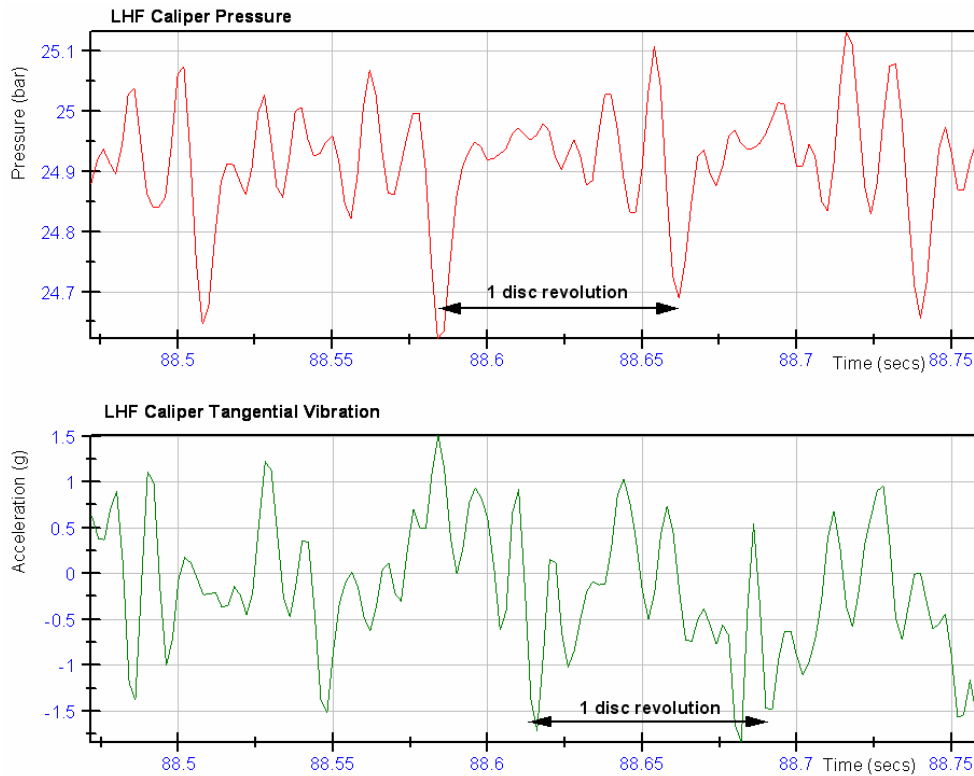


Figure 3.27: Comparison between BPV (top) and tangential caliper vibration (bottom) for the left hand brake.

3.2.4.5. Run-out

Measurements of inboard and outboard disc face run-out were recorded before and after testing. Run-out was measured on-vehicle at the mean rubbing radius of the brake disc (166mm). By measuring the run-out on-vehicle the deformed nature of the disc as a result of the clamping forces of the wheel and wheel bolts could be measured. Measuring at the mean rubbing radius gave a good indication of how the run-out beneath the brake pads was affecting the pressure variation. As might be expected the disc run-out was seen to increase when comparing pre and post test measurements carried out on-vehicle shown graphically in figure 3.28 and figure 3.29, this follows the same trend shown by Fieldhouse *et al* [5]. This increase was a result of thermo-plastic deformation of the brake disc which occurred following thermal deformation during the test. The shape of the wave has also changed slightly as a result of thermo-plastic deformation, this indicated that a stress relieving process may be occurring as a result of the heating and cooling which allowed the disc to adopt a different shape when cold. This effect is analysed in more detail in section 4.2.3.2. DTV comparisons were not possible due to there being no measurements available pre-testing as the brake discs were supplied with a

protective Geomet paint, any thickness variations in this paint would have influenced the DTV measurements.

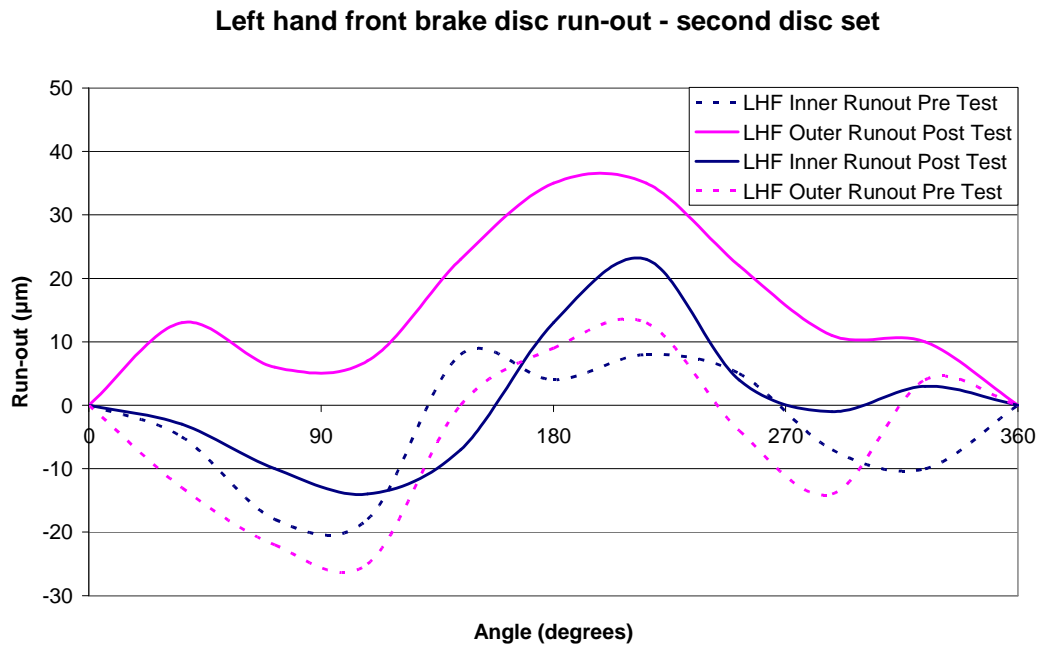


Figure 3.28: Left hand brake disc run-out pre and post testing.

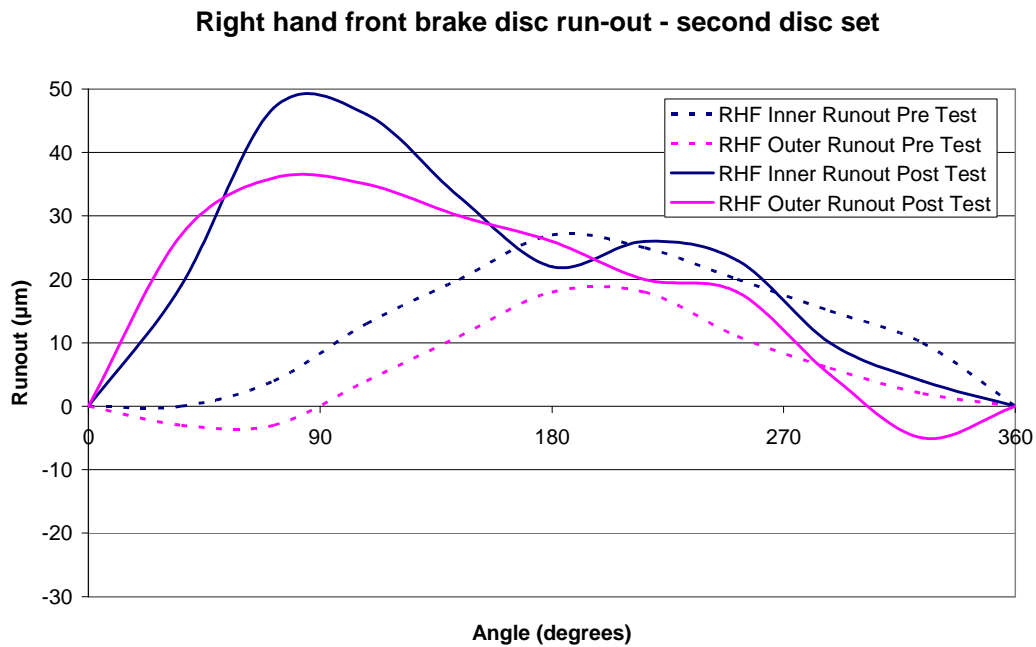


Figure 3.29: Right hand brake disc run-out pre and post testing.

3.2.5. On-Vehicle Testing and Analysis Summary

Of the two sets of brake discs tested the second was found to produce a more noticeable level of judder both subjectively and analytically. As previously discussed in section 3.2.3, this was expected after discussions with the vehicle manufacturer whereby the brake disc would typically achieve a worse subjective judder rating [23]. This was indicated as an important factor by the worse judder subjective scores and brake pressure variation from the on-vehicle testing of the second set of brake discs. This was shown in figure 3.12 and figure 3.13. Both sets of brake discs however did exhibit brake judder and both gave characteristic pressure pulses showing that there were other factors causing the judder. The pressure pulses were found to alter shape over time, as shown in figure 3.14 to figure 3.16, generally starting off as a characteristic single or double pulse per revolution, but developing to a much more complex signal as the test progressed. This indicated that the thermo-elastic distortion of the brake disc was varying with time and caused this change in the brake pressure variation. The dynamometer testing covered in section 4 gives a deeper insight into this process. Post test run-out measurements, discussed in section 3.2.4.5, have shown thermo-plastic deformation of the brake disc to be taking place with both the magnitude and shape of the run-out changing when compared to a new brake disc.

Whilst the energy dissipated throughout the test was close to that of the manufacturer's test (figure 3.4) the peak level was much lower in the highest speed braking events with a difference of 6.73MJ which equated to almost 46% difference in the energy dissipated in that braking event. These high energy braking events play an important role in the accelerated development of brake judder and the absence of them in this testing is a cause of the slow judder development. Testing at full speed using the manufacturers own test procedure would typically give the lower subjective scores earlier in a brake test as a result of the higher energy braking events [23].

Fourier analysis of the data has provided an insight into the development of brake judder over a series of braking events. The analysis has shown the increasing number of dominant frequencies as testing progressed suggesting an increasingly complex mode of disc deformation. The low sampling rate available limited the analysis to a single disc revolution at a time due to the deceleration of the vehicle, however this gave a suitable number of data points per revolution to be able to

identify frequencies of up to 500Hz. To build on this finding it was essential that the testing on the brake dynamometer was performed with a much higher sample rate to enable detailed analysis of higher disc speeds within a controlled environment. Therefore all the dynamometer testing in chapter 4 was performed with a sampling rate of 10kHz.

Measurements of brake pressure variation have been identified to be the most reliable indicator of the development of brake judder. The magnitude and complexity of the brake pressure variation signal has been shown to increase as the subjective brake judder scores decrease, or in other words as the judder gets worse. The pulsation of the brake pressure variation has been shown to change between braking events with the order of pulsation changing from 2nd to 8th order. This identified that there was a dramatic change in the deformation of the brake disc during testing to cause this change in the BPV pulsation. Evidence has also been found to suggest an initial common mode of 2nd order disc deformation, with results correlating to the work of other authors [5][65]. Analysis of the brake pressure variation together with disc deformation therefore formed the basis of the dynamometer testing.

3.2.6. Post On-Vehicle Test Analysis

3.2.6.1. CMM Scanning

Post test CMM scanning of the brake disc surfaces was carried out using a Zeiss coordinate measuring system to record detailed surface geometry. A CMM scan can give a far more detailed picture of the brake disc than a simple run-out or DTV plot. The CMM scan is essentially three dimensional in nature and can identify coning and thickness variations which may not be apparent from a single line scan. Since brake judder is inherently affected by disc thickness variations (DTV) in the circumferential direction, the scans were therefore performed at 5mm radius intervals to give a general overview of radial DTV whilst increased resolution in the circumferential direction provided measurements containing up to 16000 coordinates to give detailed analysis of the circumferential DTV. Using this data a surface map was created using MATLAB to allow for greater visualisation of the surface geometry. The outboard disc face for the front right brake disc from each of the two vehicle tests is shown in figure 3.30. As can be seen the disc on the right exhibited larger coning than the disc on the left (80µm vs. 70µm measured between the inner and outer friction ring radii). The disc on the right was known to have poorer machining tolerances than the disc from the manufacturer shown on the left, as has been

described in section 3.2.3, and this combined with surface run out will cause cold judder [13][16]. However a common point between both discs was the permanent second order run-out or deformation that has formed. This was characterised by two high points (shown in brighter colours) on each disc. A corresponding surface scan of an un-used brake disc is seen in figure 3.31 and the clear first order run-out can plainly be seen (note: the peaks on the left of figure 3.31 are a reference mark).

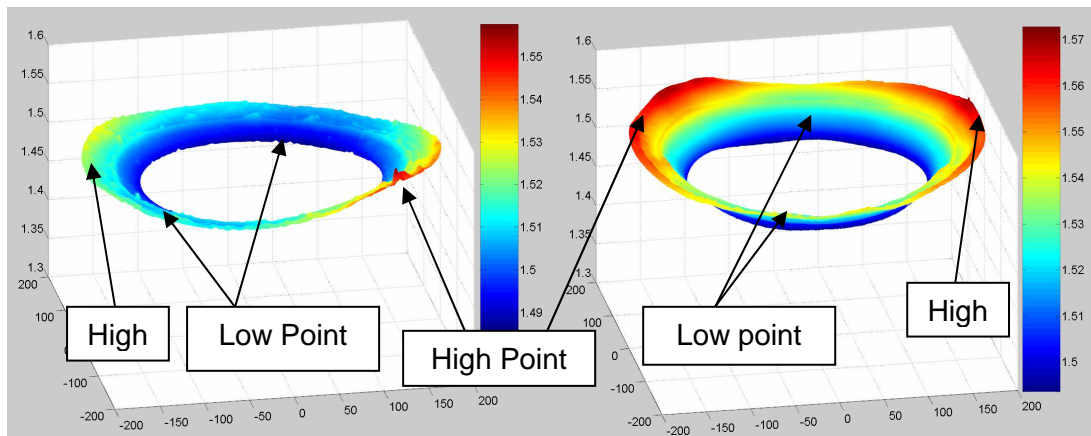


Figure 3.30: Disc 1 (left) and disc 2 (right) both showing 2nd order deformation (all axes show distance in mm).

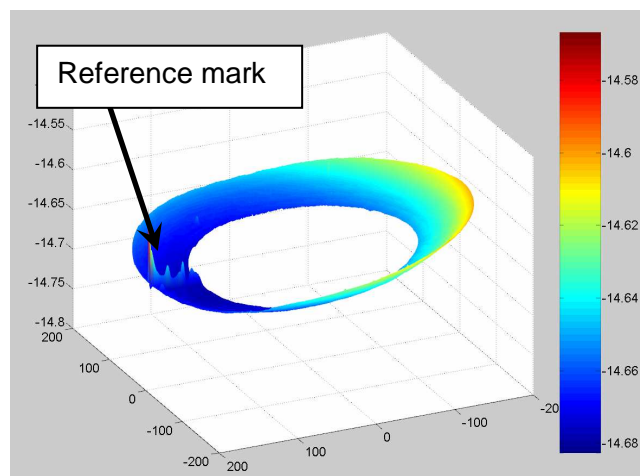


Figure 3.31: CMM surface scan of an un-used brake disc (all axes show distance in mm).

Disc 2 in figure 3.30 showed a large degree of outboard coning when compared to disc 1. The brake discs have a swan neck design which connected the hub to the outboard friction ring for reduced coning. The figure highlights the second order deformation present on both discs after testing. This was interesting to note because

prior to testing both discs exhibited first order run-out. Previous testing carried out by Fieldhouse *et al* [5] using a completely different brake disc had also highlighted second order deformation.

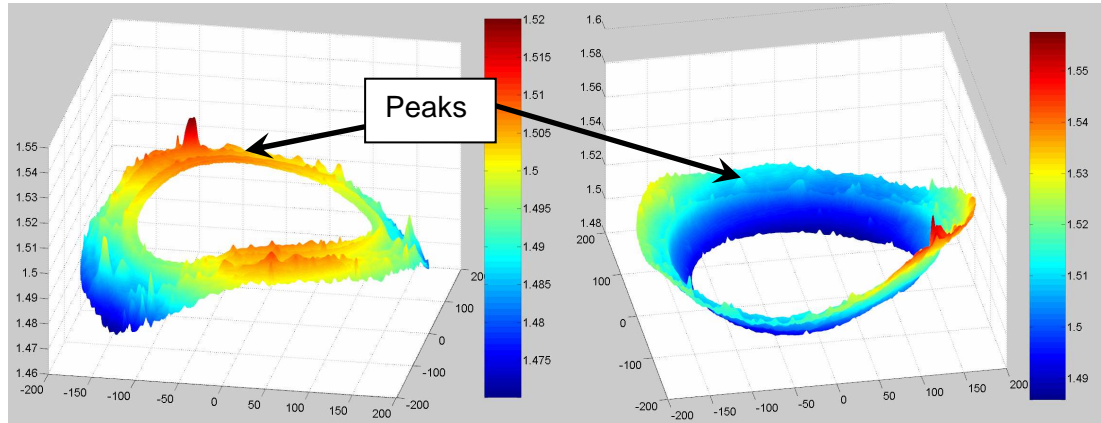


Figure 3.32: Disc 1 showing inboard disc face (left) and outboard face (right) showing 2nd order deformation and disc peaks (all axes show distance in mm).

Brake disc 1 exhibited raised peaks around the friction ring surface. These were observable on both sides of the brake disc as shown in Figure 3.32 on an exaggerated scale. Many of these peaks were in excess of 10microns which was within the threshold for brake judder generation [15][16]. As the pad skimmed over the peaks they would rise in temperature compared with the surrounding material causing them to swell and exacerbate the problem. Some raised sections were also identified as brake pad deposition which was an indication of high temperatures in these regions causing deposition of pad material onto the disc.

Both disc 1 and disc 2 have been shown to develop from first order run-out to second order deformation when measured off-vehicle. This phenomenon may be attributed to disc buckling causing permanent deformation during rapid heating (thermo-plastic behaviour) as suggested by Lang [1]. The outer radius of the friction ring may be allowed to expand radially outwards, however the inner radius of the friction ring is constrained by the cooler swan neck and cannot expand radially inwards. The friction ring itself is constrained in the circumferential direction and therefore any expansion in the circumferential direction is likely to cause buckling if the load exceeds the critical buckling load of the disc. Further discussion of and equations to show this effect can be found in section 3.2.6.3.

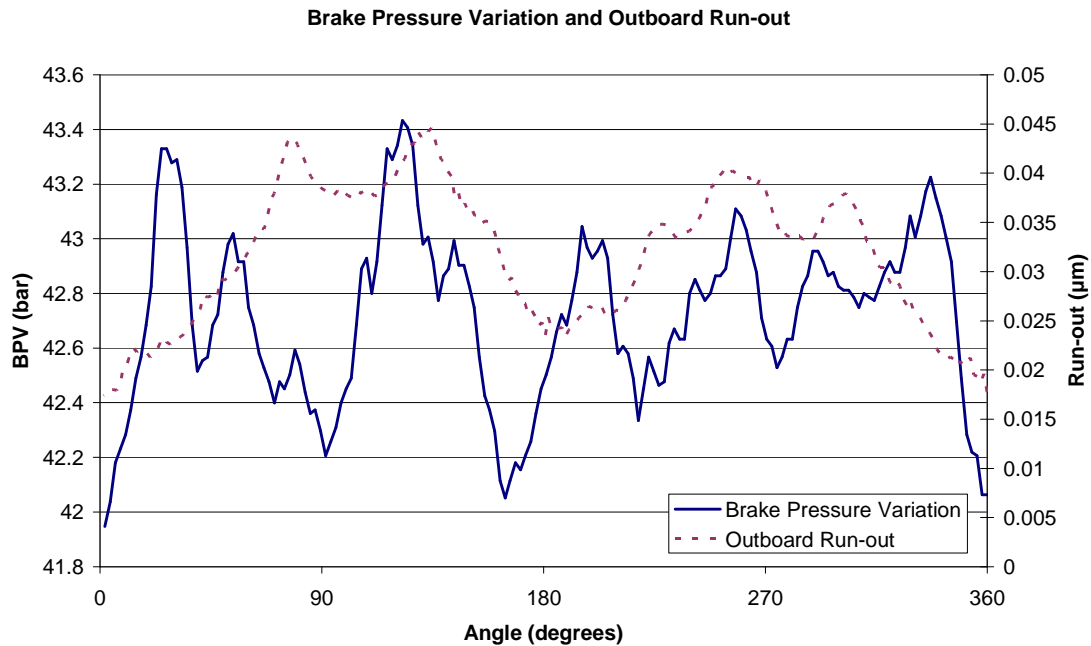


Figure 3.33: Surface variation at mean rubbing radius and brake pressure variation.

The disc surface variation plot around the mean rubbing radius and associated brake pressure variation graphs are shown in figure 3.33 for disc 2. The surface variation was measured using the CMM once the disc had been removed and was compared to the pressure variation during the final braking event. The surface variation plot showed second order deformation with inflection point at 180°. The pressure plot appeared to signify dominant second order judder with inflection at just before 180°, the left hand peak having a further two peaks superimposed upon it (along with many smaller peaks) and the right hand peak having three peaks superimposed upon it. When comparing with the surface plot a similar trend can be seen identifying that this may be the cause of the brake pressure variation. It was important to note that the pressure was recorded whilst the vehicle was slowing down and would therefore account for the point of inflection being ahead of 180° as the disc would slow slightly over the duration of one rotation – therefore if a single revolution was split into two halves, the second half would take longer to occur than the first. In addition to the second order content of both the other similarity was that there were higher order peaks on both plots; however the number and position of each did not correlate. This indicated that there was a high order elastic and/or thermo-elastic wave deformation of the disc taking place during braking which was causing the higher order brake pressure variation seen in figure 3.33. This would explain why the higher order peaks would only be seen dynamically in-stop and not in post test CMM analysis of

the brake disc as the disc would adopt a high order mode of deformation upon heating when the BPV was measured. Upon cooling the disc subsequently relaxed back to its natural state which was when the CMM scan was taken which explained the differences between the two plots. Further insight into this effect can be found in section 4.2.3, where the elastic, thermo-elastic and thermo-plastic effects were investigated during a braking event on the brake dynamometer.

3.2.6.2. Braking System Temperature

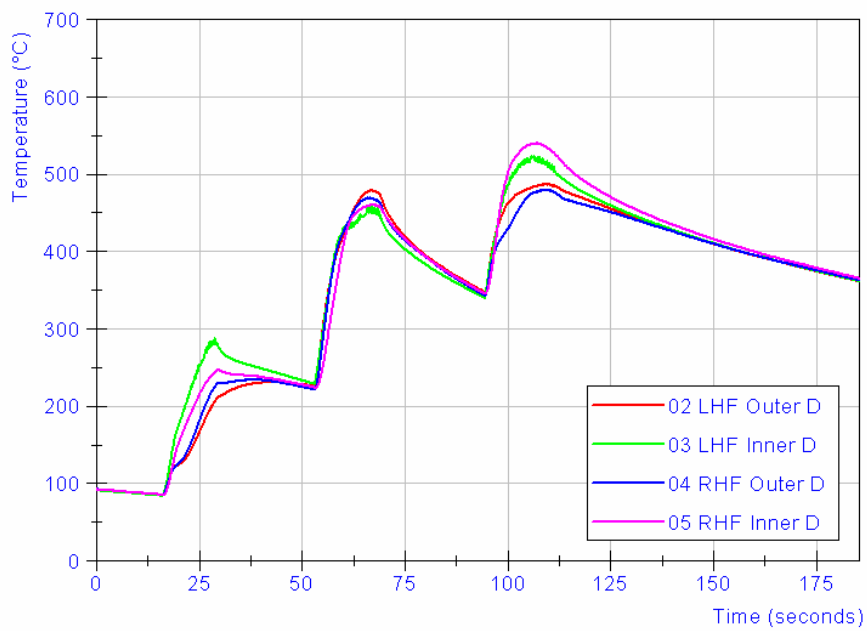


Figure 3.34: Temperature plot for stops 11-13.

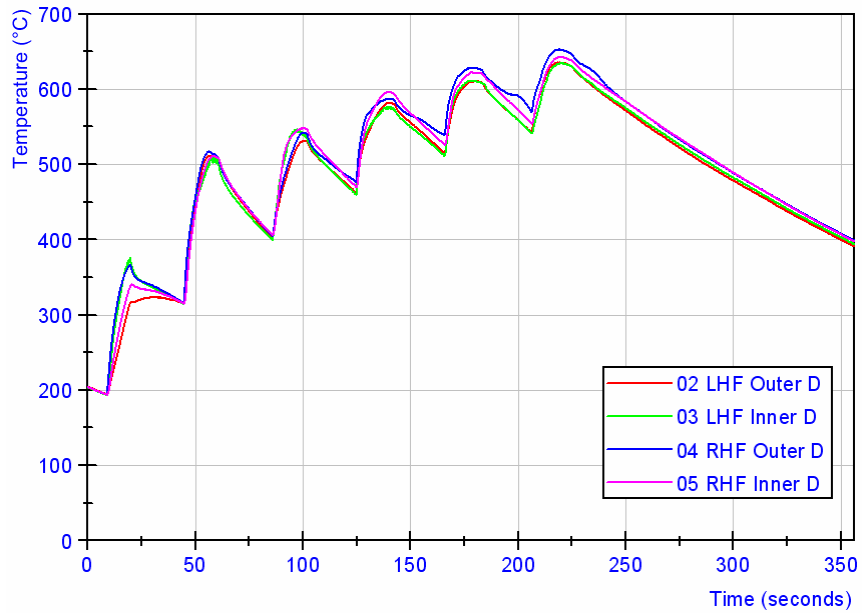


Figure 3.35: Temperature Plot for stops 14-19.

The final aspect to analyse from on-vehicle testing was that of brake disc temperature. As previously discussed, temperature distribution, thermal gradients and dissipation of temperature from the brake disc are generally believed to be major contributing factors to thermal judder [43]. The temperature distribution within the brake disc and rate of heating and cooling causes thermal gradients within the disc. These thermal gradients constrain the expansion of the hotter brake disc material in the radial direction causing the disc to buckle circumferentially due to the compressive stresses. This deformation results in a brake pressure variation which is experienced by the driver as brake judder. This mechanism is described in more detail in section 3.2.6.3. Figure 3.34 and figure 3.35 show typical temperatures seen throughout the test with maximum disc temperature seen here at 652°C. The rapid temperature rise during a short space of time was evident which allowed good scope for disc deformation. For brake judder investigations it was best not to heat soak the brake disc, that is allow the disc to achieve a uniform temperature, as this would have allowed for more uniform disc expansion and deformation to occur.

The data obtained from on-vehicle testing has allowed it to be used for correlations with both FEA and dynamometer simulations with the aim of improving the accuracy of both. Generally for both test sessions the right hand disc was seen to be the hotter of the two front discs typically being 10-30°C hotter. The test was run on an anti-clockwise speed bowl type circuit, therefore there was a small speed differential

between the left and right wheels which would correspond with higher power dissipation on the right hand disc. A computational fluid dynamics (CFD) study from an associated research project [69] on the same braking system has identified there to be a 14.4% difference in the heat transfer coefficient of the brake discs when compared left to right with the left disc performing the better of the two. As mentioned in section 1.4 the same brake disc is mounted on either side of the vehicle. The directional design of the brake disc meant that on the right hand side of the vehicle the mass flow rate, and therefore the convective heat transfer coefficient, was reduced as mentioned by Palmer *et al* [69]. This again would correspond with the increased disc temperature seen on the right hand side of the vehicle.

Also of note was the large temperature variation of 60°C between the inner and outer disc temperature for the first braking event in both figure 3.34 and figure 3.35. These braking events were the first of each 'bank' where the brakes were allowed to cool to 80°C and 200°C respectively prior to the next set of braking events being performed to allow for consistency between test sessions. The data indicated that this cooling procedure actually cooled the brake pads too much so that they contract and no longer conformed uniformly to the brake disc surface. Therefore upon the next brake application there was poor pad-disc contact creating varying temperature profiles between both left and right discs and inboard and outboard faces.

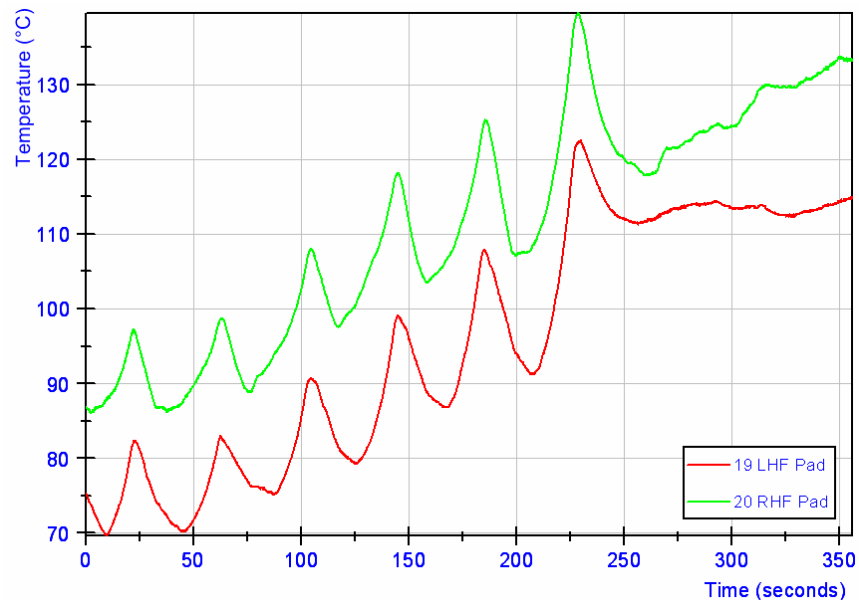


Figure 3.36: Brake pad back plate temperature for stops 14-19.

The corresponding brake pad backing plate temperatures for braking events 14-19 can be seen in figure 3.36, these measurements were recorded during the first vehicle test and identified that in future tests accelerometers could be mounted onto the back plates using nylon blocks for insulation without being damaged by excessive heat (The datasheet for the accelerometers can be found in the Appendices – section 10.2). The results also gave a useful insight into the temperature split between the disc and the brake pad. For stop 19 the maximum disc temperature was 652°C, however the pad back-plate temperature was only 139°C roughly an 80% difference. Again of note was the higher temperature of the right hand brake pad, this was caused by the pad dragging on the brake disc, as was indicated in the region between 250-350 seconds where the pad was still heating up despite there being no brake application and the pad temperature increased by over 16°C – the temperature of the left hand pad only increased by 3°C during this period. The hotter right hand brake disc would also have conducted more heat to the right hand pad when compared to the left during the braking applications.

3.2.6.3. Buckling Mechanism

Non uniform heating, thermal gradients and non-uniform thermal deformation are root causes of hot spotting and brake judder caused by wave-like thermal deformation. This can be explained by consideration of the thermal expansion of a disc annulus. Upon braking the frictional sliding between the brake pad and disc transfers energy into the friction ring surface, this energy is confined to a small annulus. This annulus has a radial width of less than the pad radial width as a result of the deflection of the brake pad when under load from either the caliper pistons or caliper finger ends. Studies of the flexural effects of brake pads when under load have been performed by Harding *et al* [66] showing the non-uniform deflection and reaction load distribution of brake pads when under load. The hot annulus caused by the frictional heating will be constrained in two directions: firstly in the circumferential direction, as the annulus cannot expand into itself in this direction, and secondly in the radial direction, as during the transient heating phase the surrounding disc material will be cooler and will restrict radial expansion. Therefore compressive stresses build up in the friction ring and cause buckling of the disc in the circumferential direction as originally suggested by Lang [1]. Buckling in the radial direction will generally not occur as the second moment of area will tend to be larger in this direction. The circumferential buckling of the disc causes wave-like disc deformation which in-turn causes brake pressure variation (as seen in section 3.2.4.3) as the brake pads slide

over the crest of the disc waves. The mode order of the wave form can be defined from the Euler buckling theory [68]. The calculations based on this theory have previously been presented by the author of this thesis in published papers [39][67]. If the disc is considered to be solid, the annulus can be represented as a straight beam constrained at either end with thickness equal to the disc thickness, width equal to the friction ring width and length equal to the mean circumference of the annulus as can be seen in figure 3.37.

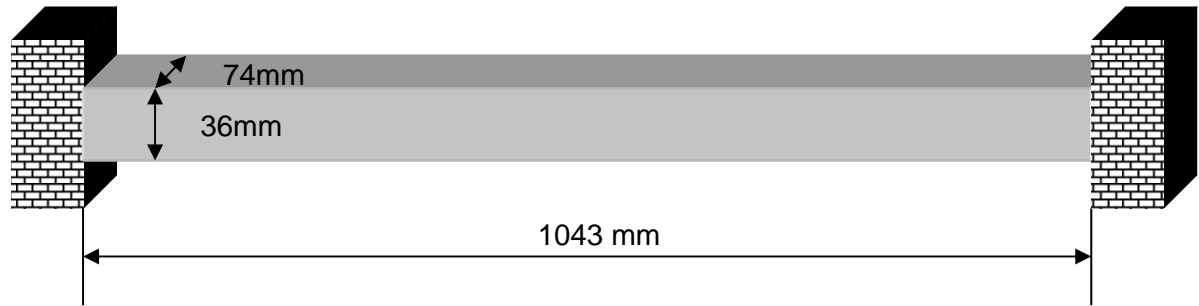


Figure 3.37: Disc annulus represented as a straight beam.

For the brake used in this thesis the mean friction ring diameter was 332mm, therefore the beam length (L_D) was obtained from the disc circumference at the mean friction ring diameter (D_D)

$$L_D = \pi D_D = \pi \times 332 = 1043 \text{ mm} . \quad 3-8$$

Temperature (°C)	Young's Modulus (MPa)	Possion's ratio (-)	Coefficient of thermal expansion $\times 10^{-6}$	Thermal conductivity ($\text{W} \cdot \text{m}^{-1} \cdot \text{K}^{-1}$)	Specific heat capacity ($\text{J} \cdot \text{kg}^{-1} \cdot \text{K}^{-1}$)	Density ($\text{kg} \cdot \text{m}^{-3}$)
300	86300	0.25	11.23	49.5	502	7250

Table 3-3: Material properties for cast iron at 300°C [23]

Assuming a temperature rise (ΔT) to 300°C in a short period, then the expansion of the disc beam (δL_D) was therefore calculated using the coefficient of thermal expansion, ϵ_{exp} , from table 3-3

$$Expansion = \delta L_D = \epsilon_{exp} L_D \Delta T = 11.23 \times 10^{-6} \times 1.043 \times 300 = 3.514 \text{ mm} . \quad 3-9$$

The strain (ϵ) caused by this expansion was found to be

$$\varepsilon = \frac{\delta L_D}{L_D} = \frac{3.514}{1043} = 3369 \mu\text{strain}. \quad \text{3-10}$$

As the disc was constrained in the circumferential and radial directions the stress (σ_D) was calculated using the Young's modulus (E) from table 3-3

$$\text{Stress} = \sigma_D = E \varepsilon = 86300 \times 10^6 \times 3369 \times 10^{-6} = 291 \text{ MN} / \text{m}^2. \quad \text{3-11}$$

This stress acting on a section of 36 x 74mm gave a load of

$$\text{Load} = \text{stress} \times \text{area} = 291 \times 10^6 \times 0.074 \times 0.036 = 0.775 \text{ MN}. \quad \text{3-12}$$

Considering the beam with section 36 x 74mm ($b \times d$) the second moment of area I was found from

$$I = \frac{bd^3}{12} \quad [68]. \quad \text{3-13}$$

Therefore for a beam 1043 mm long the allowable buckling load P_{crit} was

$$P_{crit} = \frac{\pi^2 E I}{L_D^2} = \frac{\pi^2 86300 \times 10^6 \times 0.074 \times 0.036^3}{1.043^2 \times 12} = 0.225 \text{ MN} \quad [68]. \quad \text{3-14}$$

From this calculation, which assumes the disc to be solid, the tangential load imposed on the disc when heated very quickly by 300°C exceeds its critical buckling load by more than three times, therefore buckling would have occurred.

The buckling mode order can be calculated from the Euler buckling theory [68], where n is the number of waveforms in the beam and P is the buckling load

$$P = \frac{n^2 \pi^2 E I}{L_D^2}. \quad \text{3-15}$$

Re-arranging equation 3-15, the mode order of deformation, can be found

$$n = \sqrt{\frac{PL_D^2}{\pi^2 EI}} = \sqrt{\frac{0.77 \times 10^6 \times 1.043^2}{\pi^2 \times 86300 \times 10^6 \times 2.87 \times 10^{-7}}} = 1.85. \quad 3-16$$

A fractional mode order is not possible as the beam ends would be connected together when representing a disc annulus, therefore the disc will adopt the nearest mode order, in this case 2nd order and would display two complete waveforms.

To prevent this buckling the disc thickness would need to be increased to increase its buckling stiffness. The thickness can be calculated from

$$P_{crit} = stress \times area = 291 \times 10^6 \times 0.074 \times t = \frac{\pi^2 \times 86300 \times 10^6 \times 0.074 \times t^3}{1.043^2 \times 12} \quad 3-17$$

$$t = \sqrt{\frac{291 \times 10^6 \times 1.043^2 \times 12}{\pi^2 \times 86300 \times 10^6}} = 67mm$$

The above equations represent a solid brake disc and show that an increase in disc thickness from 36mm to 67mm was required to completely prevent buckling. A vented disc was used for this thesis, therefore the equations to identify the buckling of the disc would be more complex due to the two friction rings which were joined together by the disc vanes. These vanes were angled and would therefore add stiffness in the circumferential direction. Also the calculations would need to take into account the real area of frictional heating beneath the brake pad and the heat penetration depth into the brake disc. The calculations above also assume the friction ring to be independent of the rest of the disc material. In reality this was not the case and the swan neck region of the brake disc would act to increase the buckling stiffness of the friction ring as it would be cooler and therefore would not expand at the same rate as the friction ring, however this was also a cause of the buckling. All these properties will have an effect on the critical buckling load of the brake disc. In summary an increase in the heat penetration depth and the real area of frictional heating would increase the buckling load experienced by the brake disc. Whilst taking into account the effect of the disc vanes, swan neck region and increasing the friction ring thickness would increase the critical buckling load necessary for buckling to occur.

For low orders of disc deformation it would be appropriate to increase the disc thickness to reduce the possibility of buckling. However, if higher order buckling were more of an issue, for example hot spotting, an increase in the buckling stiffness would only activate a lower mode order of deformation and would therefore not eliminate the problem. Therefore in this situation it would be more appropriate to reduce the buckling stiffness of the brake disc to induce higher order buckling. This would increase the number of wave forms beneath the brake pad and therefore reduce the overall pressure pulsation. If two waveform peaks were supporting the brake pad, it is proposed that the pressure pulsation would be reduced as the pad would slide across the top of a pair of peaks rather than sliding up and over each peak. This assumes that all peaks of the waveform were of equal height. However if they were not equal in height then the pressure pulsation would still be reduced as the pad would not have to fully slide up each peak. This is in contrast to the method suggested by Kubota *et al* [4] and Newcomb *et al* [71] whereby a shorter pad was proposed to prevent it bridging two disc antinodes and therefore reduce the heat influx into localised hot spots by reducing the localised contact pressure. However the method suggested by these authors would reduce hot spotting and associated martensitic transformations, whereas the method proposed in this thesis would reduce the pressure fluctuation caused by a high order disc waveform. Therefore for minimum BPV when high order disc deformation is an issue, the pad length should be equal to at least

$$L_p = \frac{L_D}{n} . \quad \mathbf{3-18}$$

Or the buckling mode order should be increased to be at least

$$n = \frac{L_D}{L_p} . \quad \mathbf{3-19}$$

One final method to reduce the possibility of disc buckling would be to reduce the brake disc temperature. This would reduce the thermal expansion of the brake disc and therefore the likelihood of disc buckling. Therefore in section 5.4, finite element analysis has been used to create a disc design which would exhibit a lower maximum disc temperature.

It is proposed in this thesis that the brake judder experienced during the on-vehicle testing was a result of wave-like disc deformation caused by buckling of the brake disc as was originally suggested by Lang [1]. The changing nature of the pulsation of the brake pressure variation with time suggests that the cause of the pulsation is linked to brake disc temperature, with higher order pulsations occurring at higher disc temperatures. This would be caused by the increased thermal expansion of the disc at higher temperatures causing a higher buckling mode order. An investigation to give more understanding into the effect of wave-like deformation caused by buckling was carried out on a brake dynamometer and can be found in section 4.

3.2.7. Discussion

The availability to this research of actual dedicated vehicle testing, which was performed jointly by the author of this thesis and Bentley Motors Limited, has greatly improved the accuracy and validity of the data that can be produced on the brake dynamometer and through simulations by providing representative data that was used for correlations and comparisons in sections 4 and 5 of this thesis. The brake pressure variation as a result of brake judder has been used for correlation purposes to identify whether the brake pressure variation on the brake dynamometer shows similar trends to that of the vehicle testing in chapter 4. Brake disc temperature data has been used to validate the FE simulations in chapter 5.

The on-vehicle research has highlighted some of the various mechanisms causing brake judder and drone in an automotive disc brake system. The order of brake pressure variation has been shown to increase throughout vehicle testing, initially starting with 2nd order judder and progressing to 4th order or higher indicating a rapidly changing disc state. Judder has been shown to develop at different rates on the left and right discs with the left hand disc developing a clear BPV signal later than the right in both tests; however this had no direct result on the final braking event, where the left hand disc had a larger BPV amplitude during the second test.

Whilst cold judder may be occurring during the test, the results have shown a reduction in BPV and the BPV dominant frequencies following cooling of the disc which was an indication of thermal judder as has been described in section 3.2.4.2. If cold judder were dominant in the on-vehicle tests it would be expected that there would be no tail off in the BPV or number and magnitude of the dominant frequencies following cooling. Therefore thermal judder can be confirmed as the dominant mode.

CMM scanning of the brake disc has shown a common 2nd order mode of deformation in two different sets of brake discs following on-vehicle testing when measured “cold” after removal from the vehicle. Prior to testing the discs had a 1st order mode of deformation. This also correlated with research by Fieldhouse *et al* [5] and indicated that there may be a stress relieving process occurring. This was removing the retained stresses from the casting and machining processes and allowed the brake to relax back to a 2nd order mode of deformation following heating and subsequent cooling of the brake during testing on-vehicle. An investigation of this process on the brake dynamometer has been covered in section 4.2.3.2.

Although no measurements of pedal or floor-pan vibrations were made in the vehicle cabin, it was expected that left and right disc judder due to BPV would combine to produce the overall judder felt at the pedal, whilst floorpan and seat rail vibration would depend upon the order of judder present at each disc and the instantaneous rotational speed which would excite any resonant frequencies in the suspension system. Therefore if one disc were displaying 2nd order judder and the other 3rd order, and if at a certain rotational speed the frequency of the 2nd order judder matched the natural frequency of the suspension then that individual disc alone would instigate the vibrations felt through the steering wheel or floor pan.

Pressure and acceleration signals have been analysed using Fourier analysis to extract the individual dominant frequencies which has highlighted the increasing complexity of the BPV signal as judder develops. It has been proposed that wave-like disc deformation was the cause of the brake pressure variation which appeared as brake judder. It has been shown in sections 3.2.4.2 and 3.2.4.3 that the number of pulses per disc revolution was not constant and increased as the testing progressed and with increasing temperature. This indicated thermo-elastic wave-like deformation was the cause of the BPV pulsation.

Large thermal gradients can be provoked within the disc material by performing high speed stops in quick succession, these braking events have been shown in figure 3.12 and figure 3.13 to cause BPV which was recognisable to the vehicle occupants as brake judder. The BPV has been shown to contain high order components of up to 8th order (figure 3.22) which it was proposed was a result of wave-like disc deformation.

Importantly the mechanism of disc buckling which causes wave-like disc deformation has been proposed as the cause of the brake pressure variation which gives rise to brake judder. This mechanism was originally suggested by Lang [1] and the calculations in section 3.2.6.3 have expanded on this to show that buckling of a solid brake disc annulus can occur during a 300°C temperature rise. A relationship between the pad length, disc length and buckling mode order has also been proposed, in equations 3-18 and 3-19, to achieve a reduced BPV when high order buckling is an issue. Using this research as a basis it was possible to apply the findings to a dynamometer study of brake judder in an attempt to advance the understanding under controllable conditions. An investigation into the deformation of the brake disc and its association with brake pressure variation has been carried out and can be found in chapter 4.

4. Brake Dynamometer Testing and Analysis

4.1.1. Dynamometer selection

Brake dynamometers are widely used in industry and research as a means of providing controlled use and analysis of braking systems [70]. A brake dynamometer can provide both a controlled environment and actuation without the need for a test track. Measurement is made easier due to the increased access to the braking system without the constraints of the vehicle body, wheels or steering movement and therefore a wider array of transducers can be used with a higher degree of accuracy; eliminating the possibility of damage due to road debris and large suspension movement. A brake dynamometer however, is not an ideal solution to brake testing and comes with some limitations which have to be “weighed up” when the need for testing arises. There is a limit to how accurately a dynamometer can model a braking system on a vehicle. Traditional dynamometers utilise only the brake disc and caliper assembly mounted to a rigid frame. While this allows quick modification to the rig to accept a wide range of braking systems, it is not particularly representative of the braking system on a vehicle. It has been argued [72] that a full suspension dynamometer presents the most realistic results when carrying out high speed judder tests, allowing excitation frequencies of various suspension components to be investigated. It can be argued that the vehicle suspension has a contributory effect on brake system behaviour, and can certainly be excited by judder frequencies. Dynamometers which incorporate the vehicle suspension are more representative of the on-vehicle braking forces, however these designs tend to be

'one-offs' or bespoke designs allowing little scope for accepting different braking systems without a lot of re-manufacturing and time.

4.1.2. Brake Dynamometer Uses

Brake dynamometers have a range of applications but are typically used for brake noise, vibration and harshness (NVH) issues such as squeal and judder, or endurance and fade testing where they can provide repeatable braking within a controlled environment [73].

4.1.3. Brake Judder Dynamometer Description

The brake dynamometer used in this research was a bespoke design created solely for investigation into brake judder. The still largely undetermined source of brake judder caused by brake disc deformation played an important role in the selection of a suitable brake dynamometer design. A more representative model of the braking system was believed to be achieved through the incorporation of the vehicle suspension into the dynamometer. This would allow the braking system the full range of dynamic movement and displacement as experienced on the vehicle. Correlation and validation between dynamometer and vehicle test data is also improved with a more representative system. The ability to achieve high speeds of rotation also improves correlation by mimicking the high speed low deceleration braking events which typically cause brake judder. To that end the following brake dynamometer has been used for the purpose of this research.

The dynamometer comprised a brake 'rig' and motor as seen in

figure 4.1. The rig consisted of the suspension and braking system mounted on a rigid backplate, seen in figure 4.2, whilst the motor was used to drive the braking system. Briefly the design encompassed the following aspects.

A full quarter car suspension was directly mounted to a 50mm thick rigid steel backplate to eliminate any unwanted vibrations and/or movements. Normally the suspension would be connected to the vehicle subframe and chassis, however there was a limit to how feasible the representation of the system could become. The quarter car suspension would allow investigations into the transmission path of brake judder from the brake assembly, through the suspension to the vehicle structure. It would also allow excitation frequencies of the various components to be analysed

and in this research allowed the suspension and braking system to experience a dynamic range of movement as would be seen on the vehicle during braking. The brake disc itself was directly coupled to a 110kW motor which could drive the discs at speeds up to 2400r/min with a maximum torque of 700Nm. The brake was actuated via a pneumatic proportioning valve which controlled hydraulic pressure in the brake master cylinder and allowed for repeatable brake actuation. Vehicle inertia was not simulated on the dynamometer due to time and financial constraints.

The brake disc itself was clamped to the hub bearing using the centre section of the vehicle wheel; the arrangement can be seen in figure 4.3. This allowed identical mounting conditions, including clamping area, stress and torque, to be replicated, whilst allowing a clear view of the brake disc. This enabled the use of a thermal imaging camera while the disc was in operation without any obstructions to its view of the brake disc surface. This was one area of simplification within the rig as normally there would be a larger rotating mass associated with the wheel and tyre. However due to space constraints and the ability to increase the number of measurements taken it was decided that this was an acceptable design feature. The rotational inertia and mass of the wheel/tyre combination could have been simulated by a larger mass at the wheel centre; however this could affect the run-out of the brake disc due to a larger moment about the wheel centre. This would cause too many problems and so was not implemented. Tyre stiffness was replicated via a rubber support beneath the suspension upright; this can be seen in figure 4.3. The rubber mount was tested in compression and found to have a similar stiffness value to that of an inflated tyre. Stiffness of the mount was 55kg/mm compared with 33.3kg/mm of the tyre.

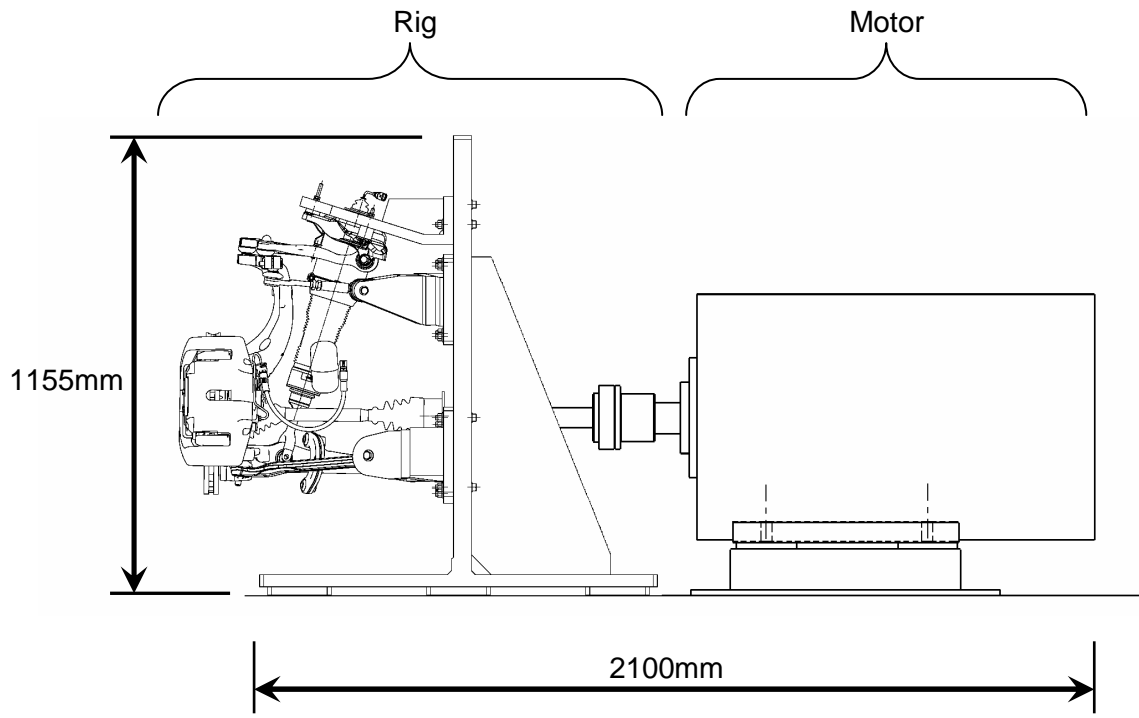


Figure 4.1: Side profile of judder rig and motor.

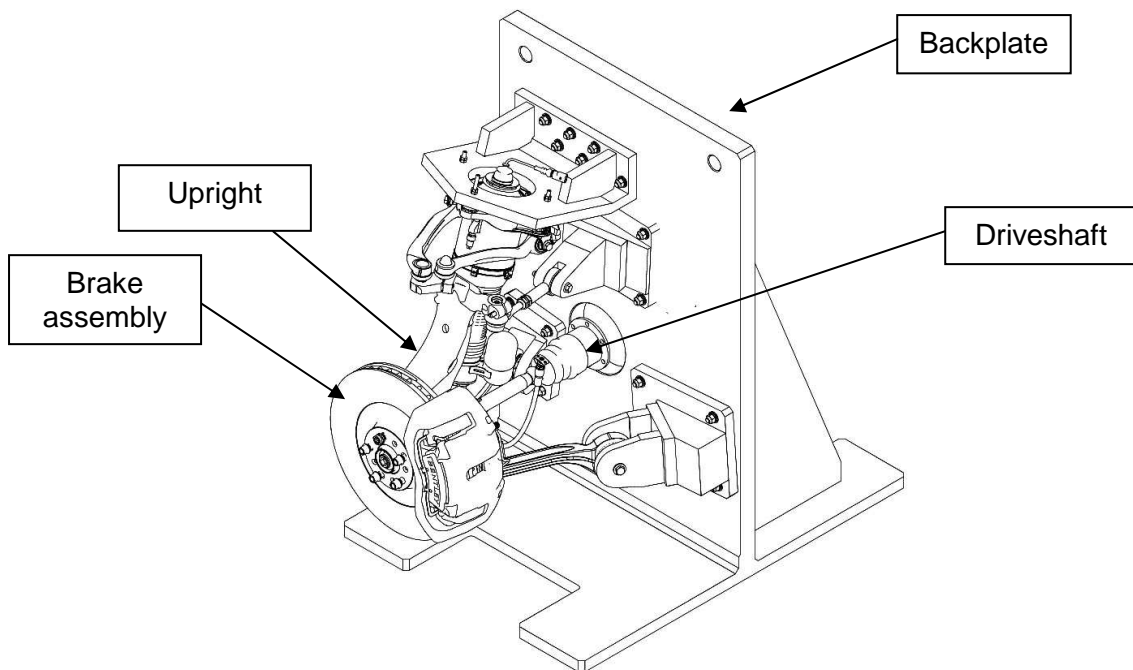


Figure 4.2: Detail view of rig assembly showing rigid suspension mounting points, brake assembly and suspension assembly.

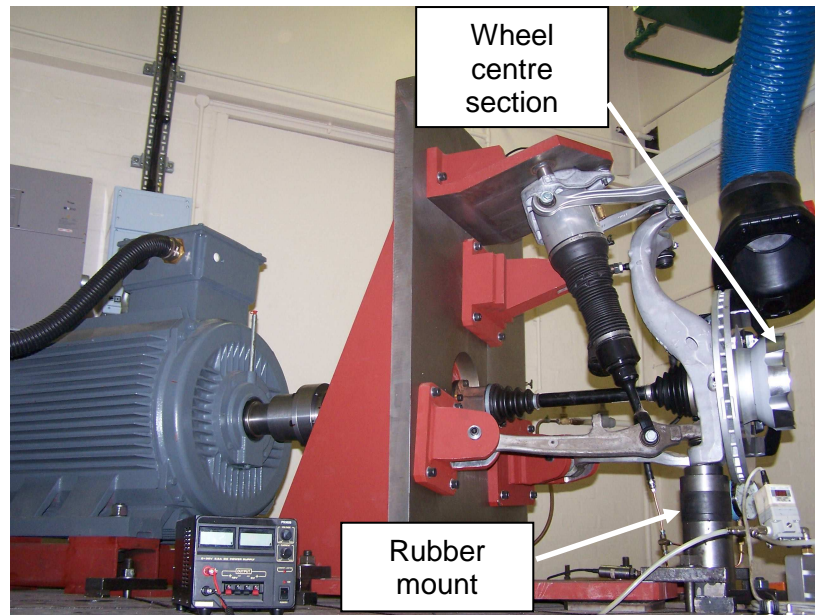


Figure 4.3: General view of the brake judder rig – rubber mount is visible beneath the suspension upright.

4.1.4. Specifications

Test rig specifications:

- 110kW 400V 217amp 3 phase high performance flux vector inverter.
- 110kW 400V motor.
- Speed variable up to 2400r/min and down to 1 r/min
- Max. torque 700Nm
- Constant torque with speed reduction
- Full ¼ car suspension assembly
- 50mm thick steel fabrication provided rigid support for the suspension assembly
- Electronically actuated pneumatic proportioning valve controlled the brake master cylinder
- FLIR S60 Thermal camera capable of 50 frames per second.
 - Temperature range -40 to 160°C, 0-500°C, 350-1500° C

- Schaevitz P751-0001 Pressure transducer
- Analogue pressure gauge
- Bruel & Kjaer MM-0004 non-contacting displacement transducers
- 2 piston fist-type brake caliper
- 405mm cast iron vented brake disc

4.1.5. Instrumentation

4.1.5.1. Pressure Measurement

The on-vehicle testing, shown in section 3.2.4, identified that measurement of the brake pressure variation would be an accurate reference for the identification of brake judder. Therefore it was essential to measure this on the brake dynamometer. To achieve this a pressure transducer was tapped into the brake line close to the caliper where the source of the variation was. The transducer was wired up to a high speed data acquisition card which typically sampled continuously at 10 kHz. The high sample rate allowed for good quality capture of the pressure variation allowing for Fourier analysis to be performed to extract the individual judder frequencies. The transducer had a range of 0-20bar and an accuracy of 0.25% of the full output; typically 0.05bar at full range. The datasheet for the pressure transducer can be found in the appendices in section 10.3.1.

4.1.5.2. Displacement Measurement

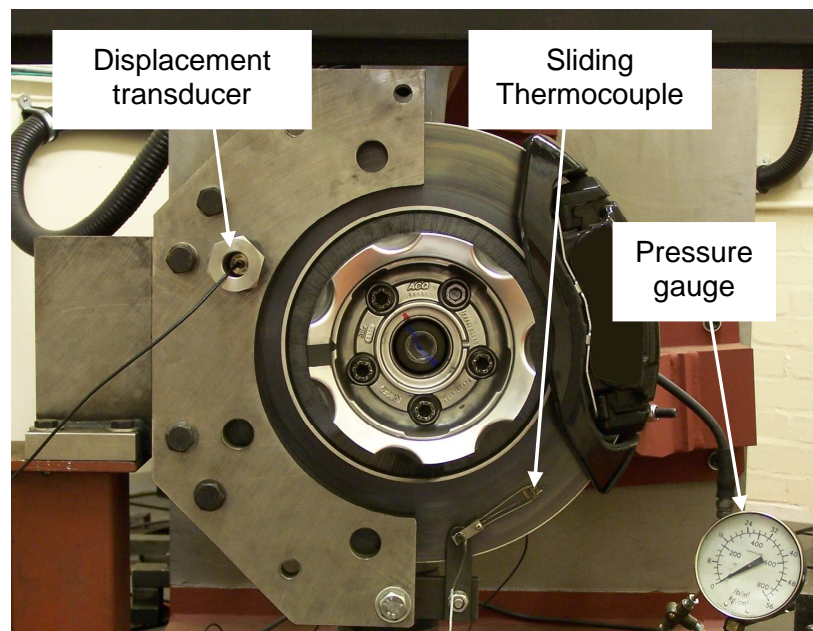


Figure 4.4: Transducer mounting arrangement.

The energy dissipated through the brake disc in the form of heat caused an expansion of the disc material. When considering a beam of material with length L , the expansion of the material in one dimension, ΔL , can be expressed as being directly proportional to the temperature rise, ΔT . The constant that defines this is the coefficient of thermal expansion, ϵ_{exp} , and has units of mm.K^{-1} .

$$\Delta L = L\epsilon_{exp}\Delta T \text{ (mm)} \quad 4-1$$

For cast iron the coefficient is not constant with temperature and must be identified experimentally at a range of temperatures. For the benefit of this project the brake disc manufacturer has supplied temperature dependent material properties for the cast iron brake disc which can be seen in Table 4-1.

Temperature	Young's modulus	Poisson's ratio	Coefficient of thermal expansion	Thermal conductivity	Specific heat capacity	Density
(°C)	(MPa)	(-)	1.00×10^{-6}	($W \cdot m^{-1} \cdot K^{-1}$)	($J \cdot kg^{-1} \cdot K^{-1}$)	($kg \cdot m^{-3}$)
0	96725	0.25	8.84	53.3	457	7250
20	96000	0.25	9	53.1	460	7250
100	93100	0.25	9.65	52.5	474	7250
200	89600	0.25	10.46	51	488	7250
300	86300	0.25	11.23	49.5	502	7250
400	83000	0.25	11.99	49	516	7250
500	79900	0.25	12.75	48	530	7250
1300	58900	0.25	18.83	40	642	7250

Table 4-1: Material Properties for cast iron - CONFIDENTIAL

Expansion of the disc material can cause many geometric deformations of the brake disc such as coning, increased run-out, and wave-like shapes as described in section 2.2. These can all be possible sources of brake judder and it was therefore necessary to record the deformation of the disc over time and its relationship to brake judder. Expansion of a brake disc due to thermal loads is a very complex process. The annular design of the brake disc friction rings essentially meant that the disc was constrained in the 'theta' or angular direction. The vanes between the friction rings also added extra constraints to the system as did the method of connecting the friction rings to the hub face. The distortion of the brake disc due to thermal loads may be small – usually in the region of 0-20microns - however research [15] has shown that this is enough to produce significant brake judder. It was therefore an essential part of the research process that the distortion of the brake disc was recorded in order to gain a better understanding of the mechanism causing brake judder.

To avoid affecting the measurement it was essential that the logging of this displacement, distortion or expansion was taken remotely or non-contacting to avoid influencing the deformation of the brake disc. The high temperatures, high speeds and small displacements involved also limited the use of contacting transducers. The method selected for this research involved the use of non-contacting capacitive displacement transducers. Capacitive transducers were selected due to their availability, compactness and accuracy. It is common for this type of transducer to be used on brake dynamometers and also on-vehicle as shown by Meyer [78] to measure disc thickness variation and geometry changes.

The transducers were mounted on two 30mm thick steel plates with identical but opposite mounting positions as shown in figure 4.4. The thickness of the steel plate reduced the possibility of any experimental error being introduced due to vibrations; a sand filled base also helped to dampen out any vibrations with further isolation being provided by an acoustic well around the bed plate. The arrangement of the transducers allowed for inboard and outboard disc run-out to be measured simultaneously at corresponding positions on each side of the disc, whilst disc thickness variation was calculated from the difference between the two measurements. Connecting the transducers to a high speed data acquisition device gave the benefit that it allowed for the dynamic distortion of the brake disc to be measured. With the aid of these transducers and a sampling rate of 10kHz the dynamic displacement and distortion of the brake disc was recorded.

4.1.5.3. Thermocouples

Whilst embedded thermocouples were used for the on-vehicle testing (see 3.2) sliding surface contacting thermocouples were used for the dynamometer testing. This was because embedded thermocouples were a much more intrusive measurement method than sliding thermocouples. Whilst sliding thermocouples can cause frictional heating in the form of a band this was expected to be relatively small in comparison to the high expected disc temperatures. Embedded thermocouples would possibly cause a hot spot and also the disc geometry had to be altered by drilling one or more holes to mount the thermocouples. Embedded thermocouples also require the use of slip-rings to transmit the signal from the rotating thermocouple. However the slip-rings used for the on-vehicle testing in section 3.2 were not available during the dynamometer testing phase of the research. The datasheet for the rubbing thermocouples can be found in the appendices in section 10.3.3.

4.1.5.4. Thermal Camera

The thermal camera arrangement and location is shown in figure 4.5. The camera was focussed directly at the disc face and was given a clear unobstructed view. It was connected to an external PC for live recording purposes which enabled remote use of the thermal imaging camera while the disc was in operation. The high capture rate of the camera (50fps) when in sequence (video) mode enabled detailed analysis to be performed on the recording. During braking, the surface of a brake disc rapidly changed colour due to pad deposition and thermal inputs. Combined with the

reflective surface of the cast iron, these factors had a large effect on the emissivity of the surface. Without compensation for this, it would have affected the accuracy of the thermal camera measurements because the emissivity of the brake disc was a measure of how much radiation it emitted compared to that of a perfect black body [79]. To solve this problem a sliding (or rubbing) thermocouple was mounted on the surface of the brake disc. This directly measured the surface temperature of the brake disc, and from this value the emissivity of the brake disc was calculated using the thermal camera software.

Other aspects that had an effect on the accuracy of the thermal camera were reflected temperature, distance and atmospheric temperature and humidity:

- **Reflected temperature** is the amount of radiation reflected in the body i.e. radiation from sources other than the target source. If the emissivity of the body is low and its temperature close to ambient, then this can have a large effect on the accuracy. The effect will be that the temperature measured by the camera will be a combination of the temperature emitted by the source and the temperature reflected by the source [79]. For the high temperatures involved in this study the reflected temperature was low in comparison to the emitted temperature. Therefore the reflected temperature only had a small effect on the accuracy of the results; this was measured as 22.5°C. The internal camera software compensated for this value once it was known.
- **Distance** between the camera and the body affected how much radiation was absorbed by the atmosphere before it reached the camera detector. Again the camera could compensate for this once known.
- **Atmospheric temperature and humidity** could also have a varying effect on the accuracy due to the amount of radiation absorbed by the atmosphere before it reached the camera. For the short distance between the object and the camera, the high temperatures involved and the closed lab environment it was acceptable to use the default 50% humidity for this research [79]. Ambient temperature was measured in the room at 25°C to again improve the accuracy of the results.



Figure 4.5: General view of thermal camera arrangement.

4.2. Dynamometer Mid-Speed Testing

4.2.1. Methodology

The data obtained from the on-vehicle testing and analysis identified that it was possible to extract the individual revolutions of the brake disc from the test data. This proved that observing individual revolutions of the disc was a viable means of analysing the brake pressure variation and therefore the brake judder. The on-vehicle test data provided insights into both the development and nature of brake judder through brake pressure variation. The use of a brake dynamometer enabled experiments and analysis with increased repeatability to take place; these both backed-up and build upon the findings from the on-vehicle testing.

Based on the achievements from the on-vehicle testing and analysis it was decided that data should be separated into individual revolutions of the disc to enable a visual analysis of both the brake pressure variation and inboard and outboard disc distortion. Visual correlations between the two were then possible. The speed of the dynamometer was considered steady during a short drag braking event; therefore multiple disc revolutions were used for a more accurate Fourier analysis. It was possible to acquire data at a rate of 10 kHz on the brake dynamometer; this further increased the accuracy and detail of the analysis. This made it possible to identify

dominant orders of pressure variation and/or distortion; these were related to wheel speed.

For the purpose of this research mid-speed testing on the brake dynamometer was carried out at 1200r/min which was half the maximum capable speed of the dynamometer. This was equivalent to a road speed of 154.4km/h or 96.5mph. This speed was selected for the majority of the dynamometer testing as it was in line with the typical speeds seen on unrestricted autobahns in Germany and, although illegal in the UK, is a speed obtained by many drivers of high performance vehicles. Short drag braking applications were selected at these moderately high speeds as they characterised a typical braking application on a motorway where a light braking application is made with low deceleration to slow from high speed of around 112km/h to a complete stop when exiting onto a slip road. For the vehicle used in this thesis, the kinetic energy released into the braking system would be 1.2MJ for the above braking condition due to the high initial speed of the braking event.

It was expected that this dynamometer testing would provide a far better insight into the development of brake judder. The constant speed analysis together with the higher sample rates provided much more consistent data to improve analysis. The much less harsh environment of the dynamometer enabled measurements of disc distortion to take place permitting comparisons with the brake pressure variation.

4.2.2. Procedure

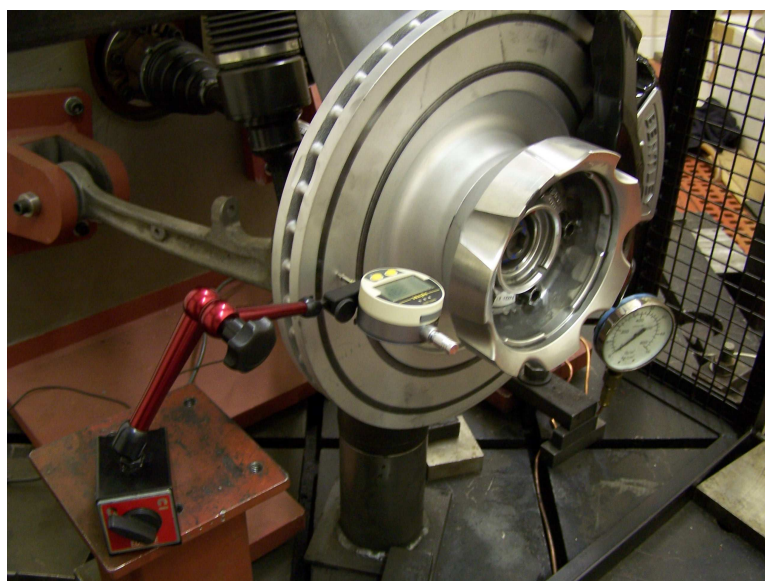


Figure 4.6: Measuring the installed run-out of the brake disc on the dynamometer.

Every time a new brake disc was fitted to the brake dynamometer the installed run-out was measured at the mean rubbing radius on both friction rings using a DTI gauge. This measurement was used for correlation with measurements from the displacement transducers but it was also used as a guide to ensure that the installed run-out was within the manufacturer's specifications. As discussed earlier a disc with smaller run-out would typically exhibit less cold judder than a disc with a higher run-out value. However this was not necessarily the case for hot judder.

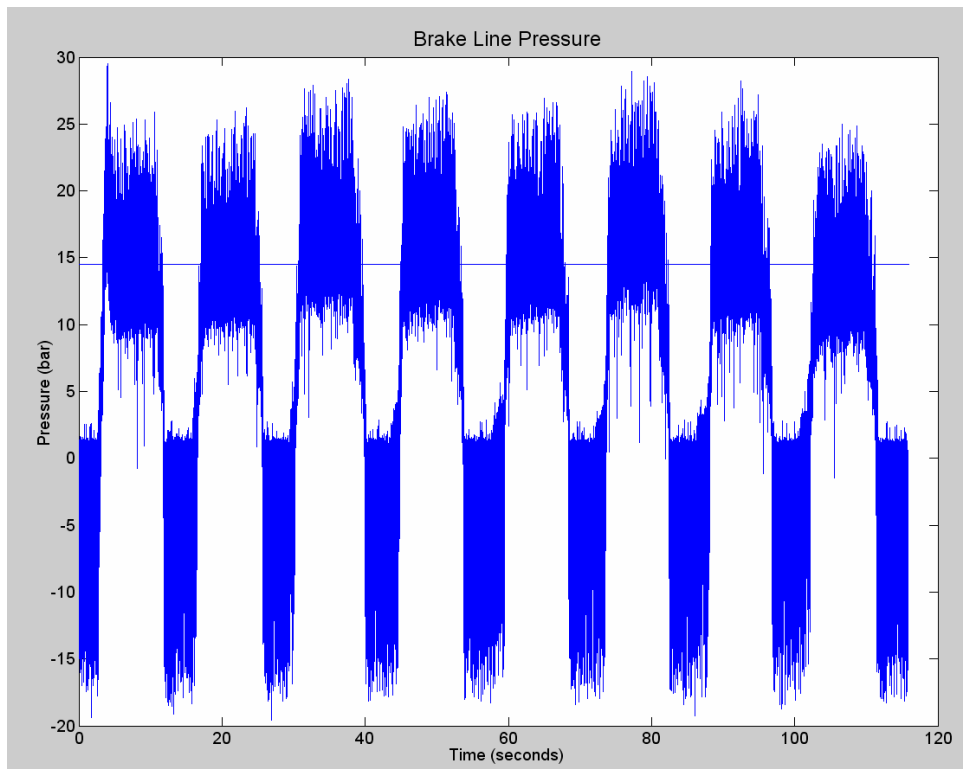


Figure 4.7: 18/01/08 Disc 4 brake pressure graph.

Results from a typical dynamometer test are shown in figure 4.7, which shows the application of the brake pressure. A typical dynamometer test involved 8x8 second braking applications at 16bar and a constant speed of 1200r/min with four seconds between each braking event. Initial trials of this testing regime proved that it could develop significant brake judder in excess of 2bar brake pressure variation. The level of brake judder was so severe that any significant extension to the test was likely to result in damage to the pressure gauge even with a pressure snubber, which was a small orifice which limited the fluid flow rate and therefore dampened out the pressure fluctuations, mounted in-line to damp out the high frequency fluctuations. The repeatability of this test procedure was very good due to its simple design.

Extensions and alterations to the test were also possible by adding extra braking events, scaling the applied pressure or increasing the braking time; all these factors added to the versatility of the test by allowing different rates of energy conversion to be simulated on the test rig.

4.2.3. Results

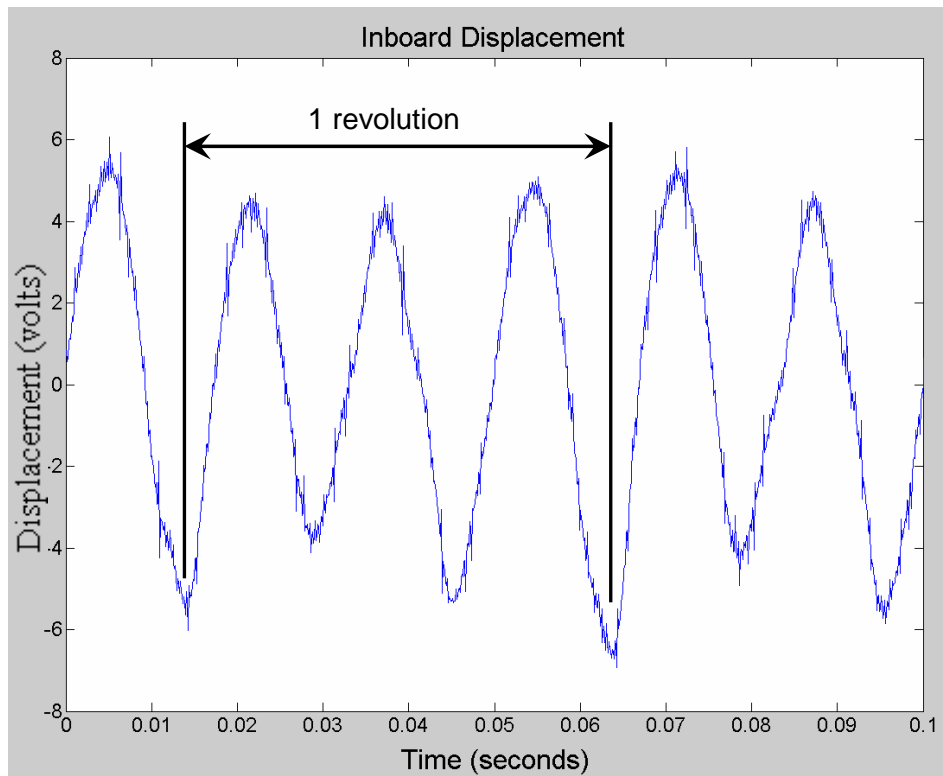


Figure 4.8: 26-09-07 Disc 2, inboard displacement, 10th stop, 300°C showing 3rd order deformation.

Figure 4.8 shows a plot of the inboard brake disc displacement or distortion whilst braking was occurring. A third order wave can be seen, i.e. three peaks per revolution. This brake disc had previously been used for on-vehicle testing and displayed second order deformation (see figure 3.30 section 3.2.6.1) prior to commencing the brake dynamometer test. It was therefore experiencing significant deformation during braking when compared to both its cold state and that of an unused brake disc which would typically exhibit first order deformation when cold. It is this type of behaviour which this research showed to have a strong influence on brake pressure variation and therefore brake judder.

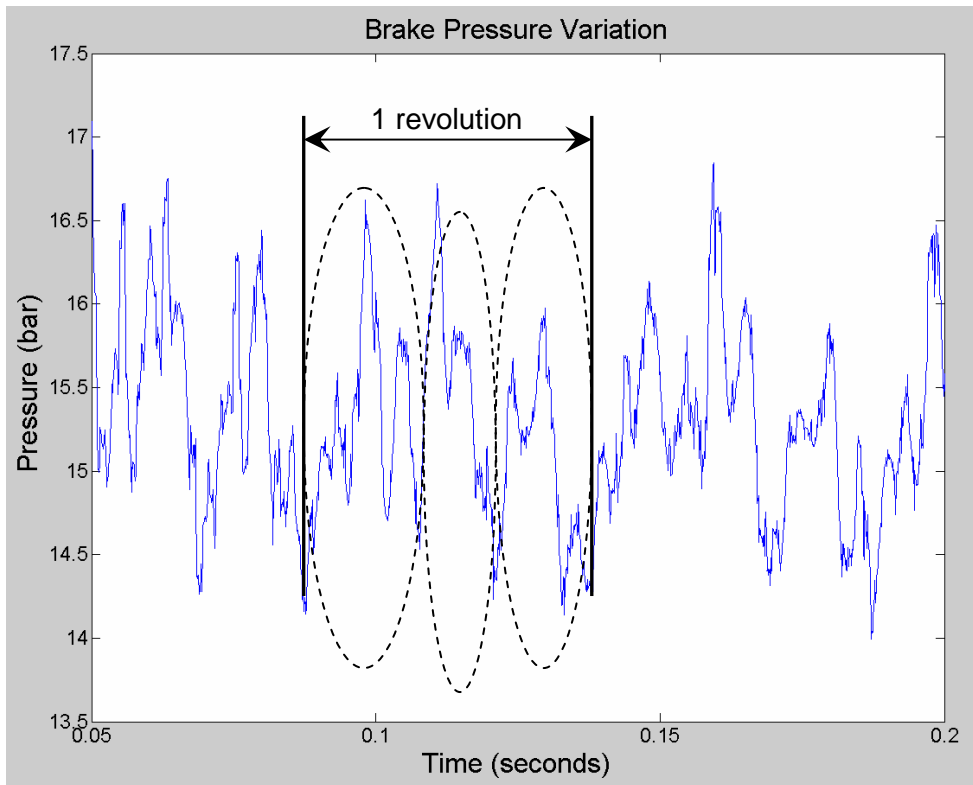


Figure 4.9: 26-09-07 Disc 2, Brake Pressure Variation 10th stop hot 300°C.

Shown in figure 4.9 is the associated brake pressure variation. Of note was the appearance of three semi-distinct pulses within the signal (shown circled). These three pulses were being caused by the peaks of the three waves shown in figure 4.8. The two graphs have been combined and are displayed in figure 4.10 to show this correlation.

Graph of brake pressure variation and disc distortion

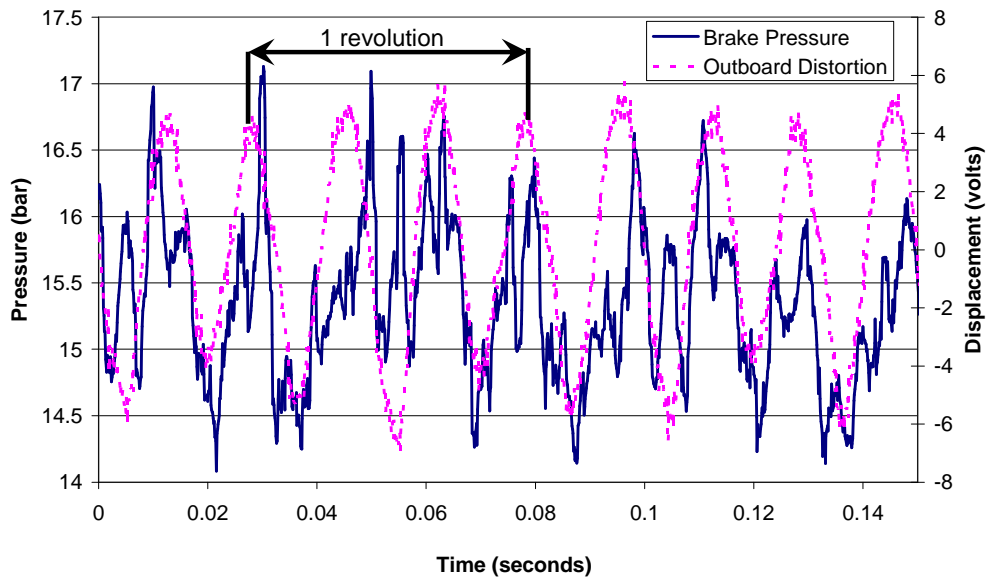


Figure 4.10: Graph showing the correlation between brake pressure variation and disc distortion

There were also many higher frequency pulses superimposed on the BPV signal; it was believed that the cause of these was localised DTV and/or thermo-elastic instabilities on the surface of the brake disc causing hot spots. Displayed in figure 4.11 is a plot of the brake pressure variation from on-vehicle testing. Commonalities were found between the graph in figure 4.11 and the dynamometer testing in figure 4.9 where there were again three distinct pressure pulses appearing within the duration of one disc revolution. Whilst the application pressures were in the order of 2.8 times larger for the on-vehicle testing, the 3rd order judder was still evident. Also apparent was a higher order content; a visual check revealed sixth order in the case of the on-vehicle test and seventh for the dynamometer test. This indicated that similar modes of deformation were occurring in both the on-vehicle testing and the dynamometer testing to cause the similar brake pressure variation pulsations.

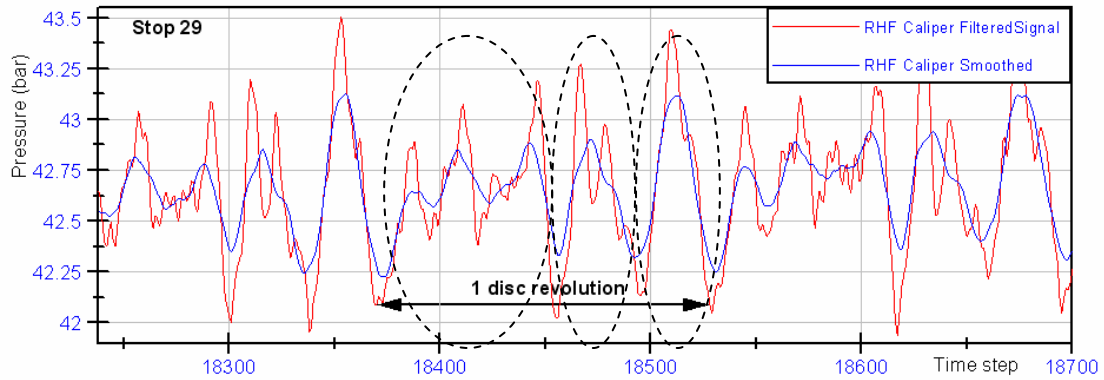


Figure 4.11: Brake pressure variation from on-vehicle testing showing 3 distinct pressure pulses.

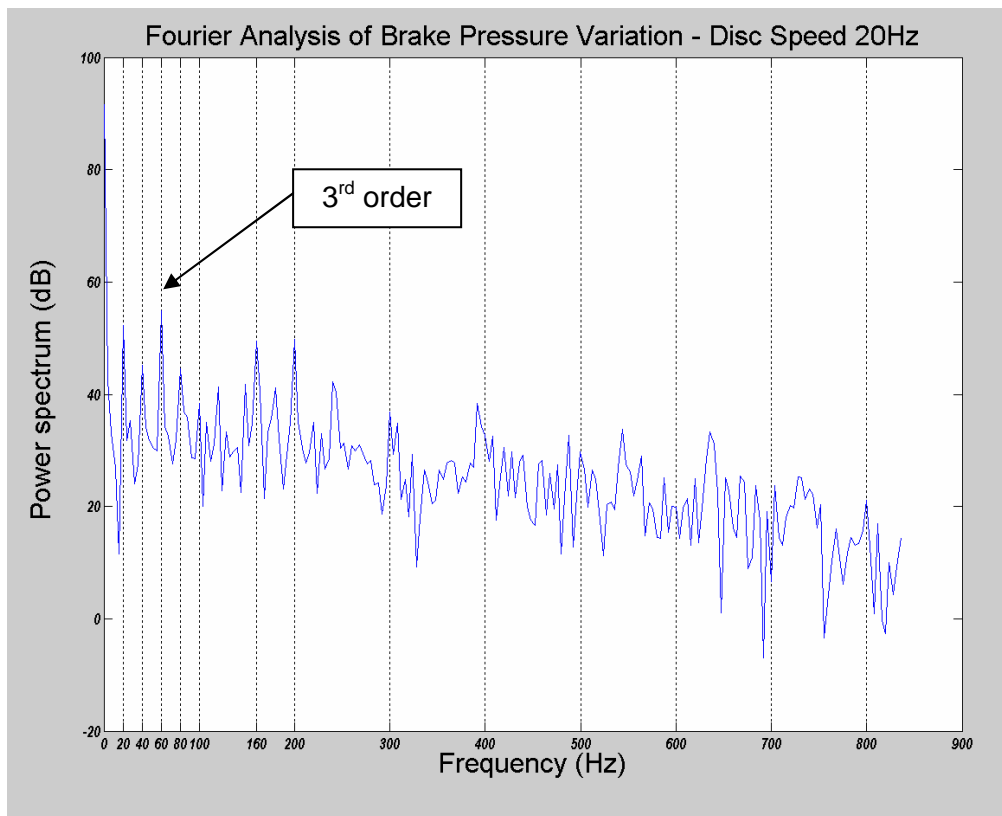


Figure 4.12: 26-09-07 Disc 2, FFT Brake Pressure Variation 10th stop hot 300°C.

It is clearer to see the third order content of the brake dynamometer pressure variation when analysing the FFT of the signal shown in figure 4.12. The third order content was the most dominant frequency within the signal. The disc speed for this test was 1200r/min which was equivalent to a frequency of rotation of 20Hz. In this case the third order content was characterised by a frequency of 60Hz. Also of note

were the other dominant frequencies at 20, 160 and 200Hz or first, eighth and tenth order. The first order content (20Hz) was the first order run-out, however the eighth and tenth order frequencies were of more interest; these were potentially hot spots forming which created localised raised regions of the disc surface as introduced in section 2.3.3. Of note was the fact that this disc later went on to display ten equispaced hot spots on either side of the brake disc, a more detailed analysis and discussion of this can be found in section 4.3. The tenth order frequency picked up in the pressure signal was a precursor to the appearance of the hot spots on the brake disc surface. The 10th order frequency will have been a result of the higher order buckling of the brake disc as proposed in section 3.2.6.3. The following work gave further insight into both the development of the disc deformation and its cause.

For the above test the displacement transducers were mounted with a 2mm offset from the brake disc surface. This was to ensure that the displacement transducers were not damaged, but also to ensure that they did not go into an overload condition due to the temperature being above calibration limits. When mounted at this distance the sensitivity of the transducers was reduced; therefore only the general waveform was detected and not the smaller variations of the brake disc. Mounting the transducers up to 0.6mm from the disc gave results with increased sensitivity as can be seen below.

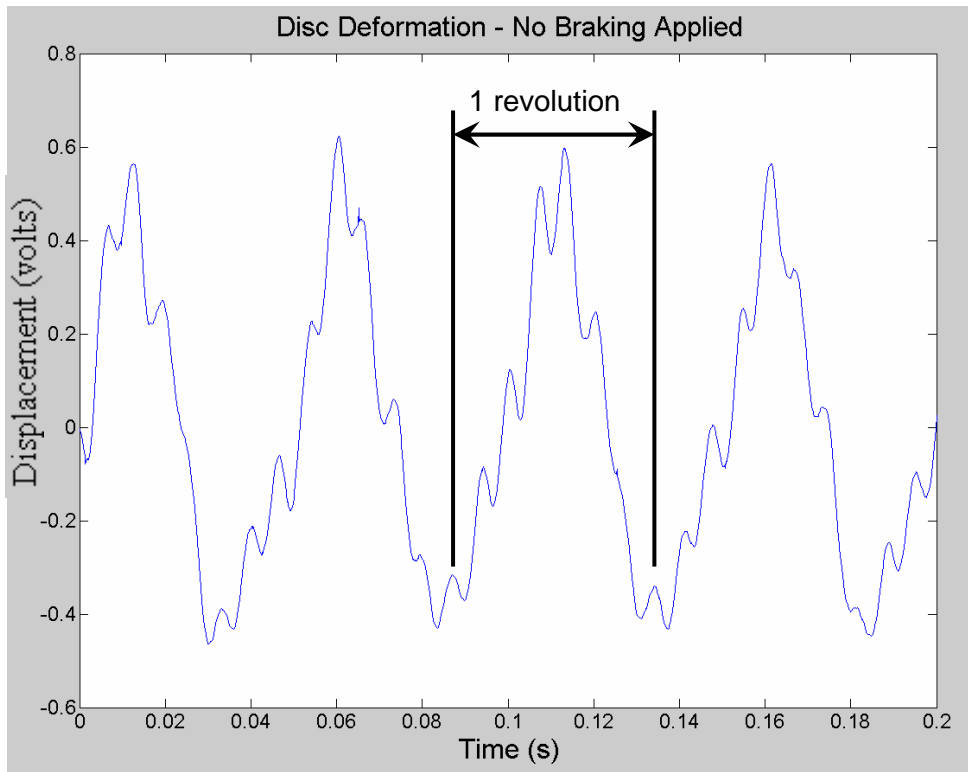


Figure 4.13: 18/01/08 Disc 4 start of test – no braking applied.

For this next set of examples the disc deformation during a single braking event is analysed. From cold the brake disc used for this example exhibited first order run-out as shown in figure 4.13. The displacement transducers were mounted at a 0.8mm offset from the brake disc surface to improve their resolution and sensitivity. The transducers were picking up approximately eight high frequency peaks on the overall waveform with no braking applied. This was a result of a previous test with this disc on the dynamometer (from which only brake pressure variation was recorded) and was likely to be thermo-plastic deformation which has caused a higher order wave form to remain in the disc upon cooling.

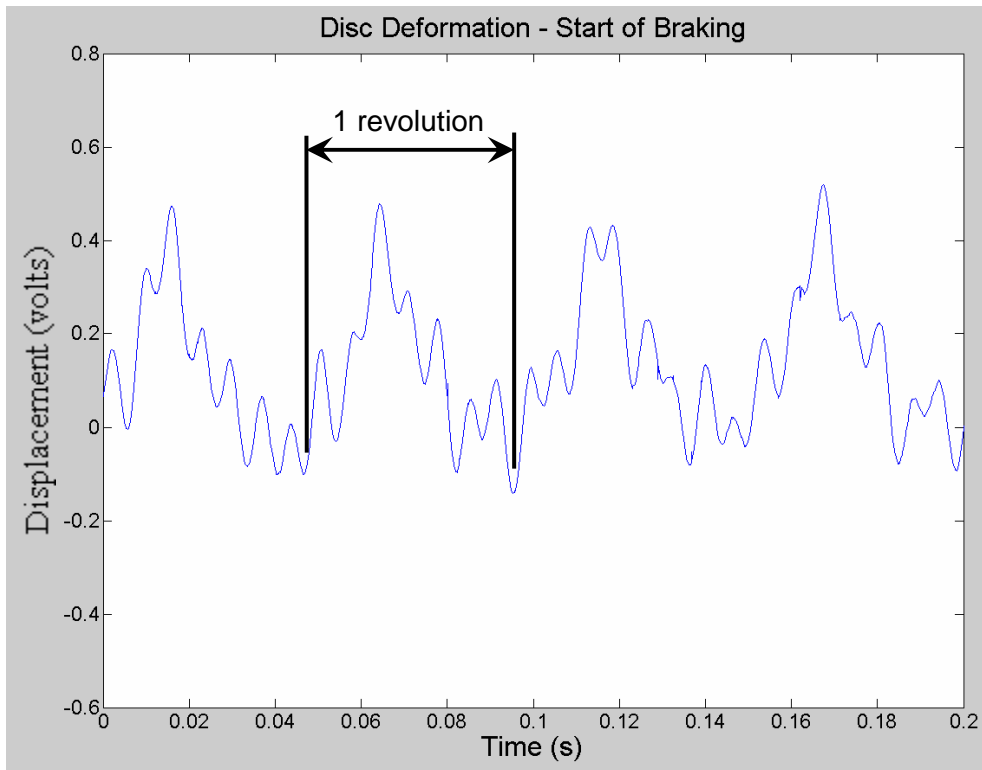


Figure 4.14: 18/01/08, Disc 4, 1st braking event – start of braking.

When the brake was applied during the first braking application the disc shape was still predominantly first order, however a superimposed higher order of displacement was also more apparent as shown in figure 4.14. This was caused by rapid expansion of the raised peaks, seen in figure 4.13, due to non uniform contact and subsequent heating of the brake disc surface. The peaks experienced increased contact pressure from the brake pad and therefore would have an elevated temperature which resulted in further localised expansion. The run-out of the disc at the initiation of braking also appeared to be reduced due to the clamping action of the brake pads.

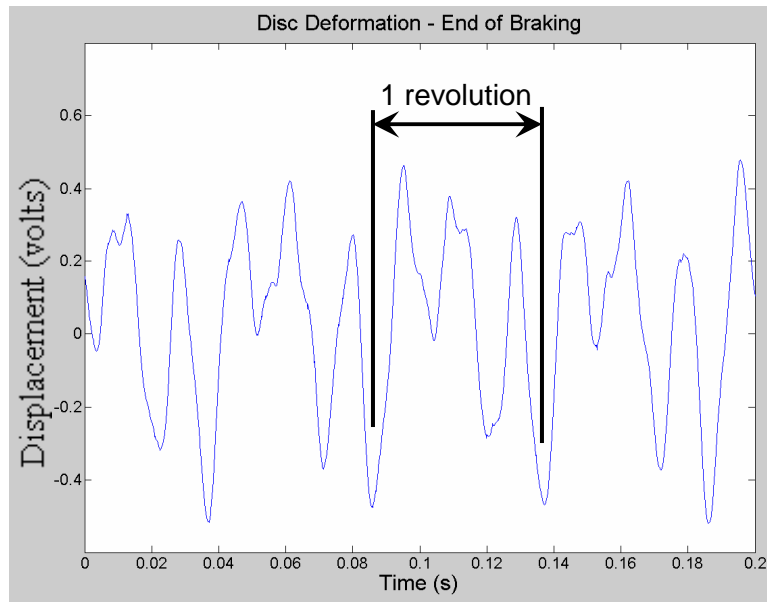


Figure 4.15: 18/01/08, Disc 4, 1st braking event – end of braking.

As braking progressed the order of deformation was seen to change from first order to third order approximately mid way through the braking event. Figure 4.15 highlights the change in disc deformation towards the end of the braking event approximately 7.5 seconds into the 8 second braking event where three peaks are clearly seen per disc revolution. The relative magnitude of deformation of the disc had doubled from the initiation of braking and was the same magnitude as the cold disc.

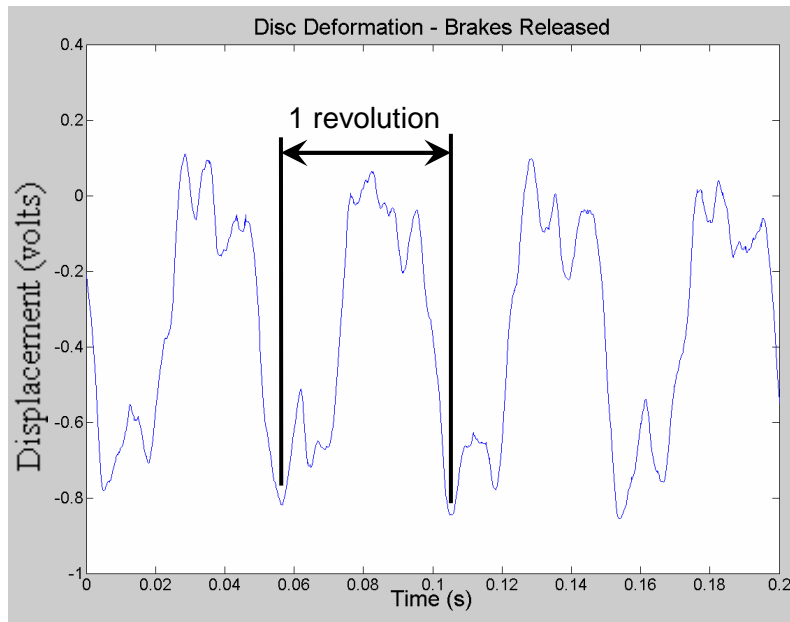


Figure 4.16: 18/01/08, Disc 4, 1st braking event – brakes released.

Immediately following the release of the braking force the disc reverted back to dominant first order deformation shown in figure 4.16. The first order waveform had a slight plateau, caused by wear at the peak of the waveform which was a result of the increased contact pressure between the disc and pad. The images shown indicated the presence of both elastic and thermo-elastic deformation. Elastic deformation was occurring at the onset of the braking loads when there was no heat the brake disc. Thermo-elastic deformation was occurring as the braking progressed and as temperature rapidly built up in the friction rings. The thermal gradients between the hot friction ring and cooler surrounding material prevented uniform expansion of the disc. Therefore compressive stresses caused circumferential buckling of the disc, as was introduced in section 3.2.6.3, which resulted in the third order waveform seen in Figure 4.15. The following examples give more insight into this process.

The sequence of events shown in figure 4.13 to figure 4.16 was a repeatable event which was observed during every test on the brake dynamometer. The graphs shown in figure 4.17 display a subsequent test and show the following sequence; no braking, start of braking, end of braking, brakes released. This is shown for the first stop of the test and it highlighted that the disc distortion was occurring from cold and almost instantaneously. Also of note was the apparent similarity of the waveform between both off-brake periods.

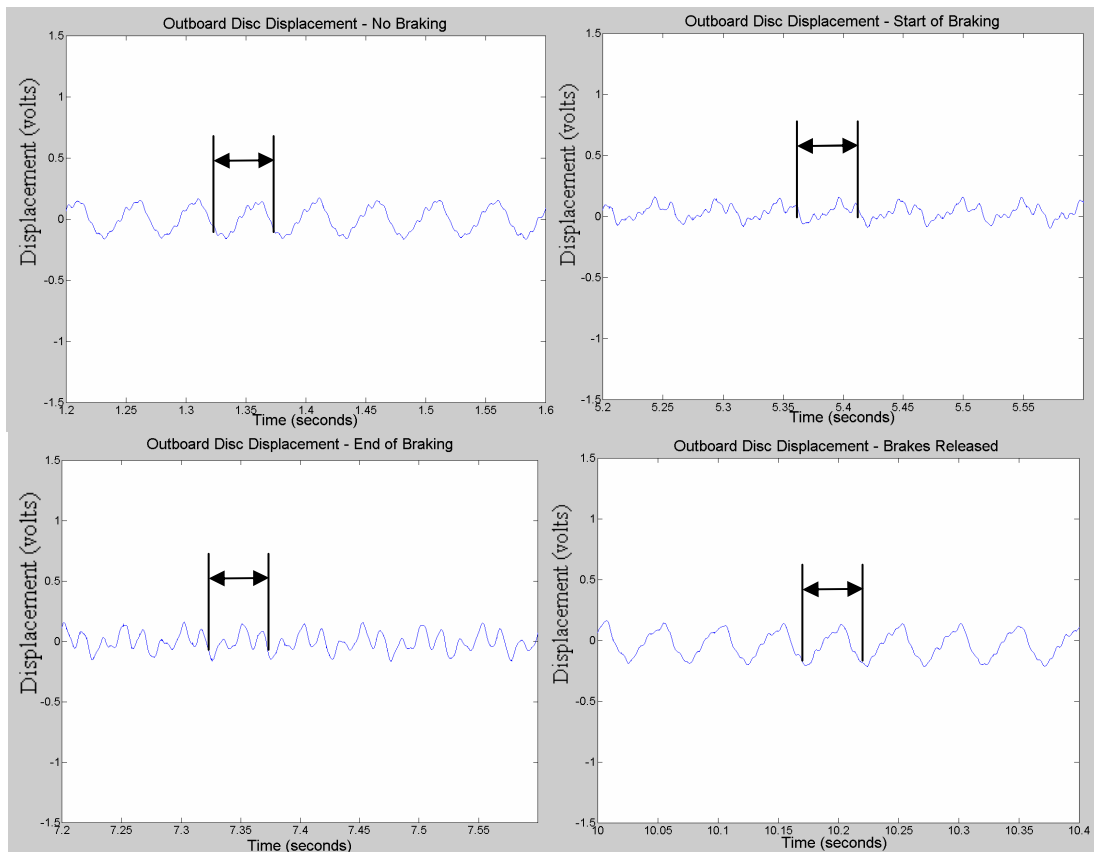


Figure 4.17: 12/02/08 Disc 4, graphs of outboard disc displacement for the 1st braking event. Reading from top left; No braking, start of braking, end of braking, brakes released.

Analysis of later braking events within the test showed that as the temperature increased plastic deformation began to occur, and that during the off-brake periods the disc did not relax back to first order deformation. It is proposed that this was a result of stress relief of the brake disc, whereby the high temperature of the disc during testing caused a stress relieving process to occur which allowed the disc to relax back to its natural state of 2nd order deformation. An in depth analysis of this effect on the dynamometer can be found in section 4.2.3.2. Shown in figure 4.18 is another braking sequence, this time the thirteenth stop. As can be seen the disc had a predominantly second order shape prior to the brake application. As soon as braking was applied the mode order of the wave changes from second order to third order; this was elastic deformation occurring as it is instantaneous with the application of the braking force. The third order wave developed to a stronger more defined wave form by the second half of the braking period due to thermo-elastic deformation. When the braking force was released the disc relaxed back to a predominant second order wave, however there were also signs of a third peak/ third

order component appearing when this graph is compared to the wave form before the braking force was applied.

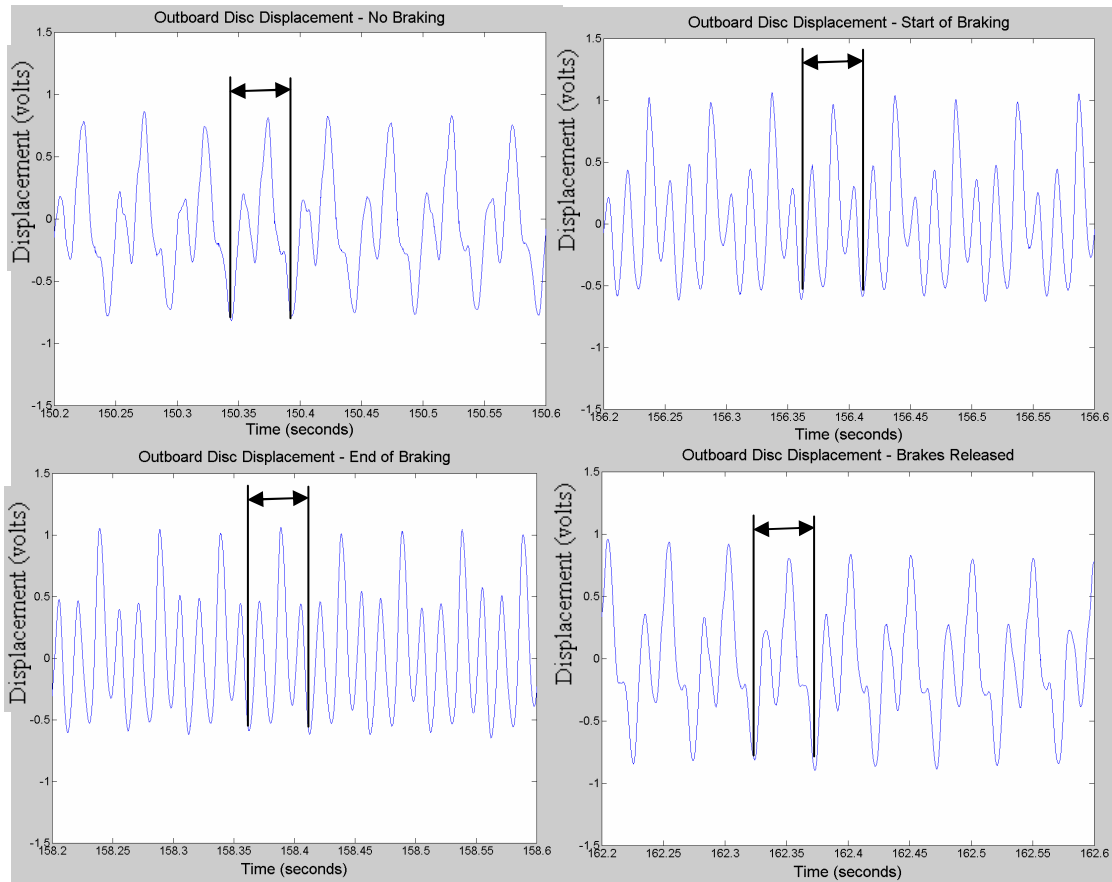


Figure 4.18: 12/02/08 Disc 4 graphs of outboard disc displacement for the 13th braking event. Reading from top left; No braking, start of braking, end of braking, brakes released.

Correlation has been found between the deformation (or run-out) of the brake disc and the frequency of the brake judder seen in the brake pressure variation. Figure 4.19 shows overlaid plots of outboard disc displacement and brake pressure variation. The judder in this case was severe, with the brake pressure variation being in the region of 2bar, or 13% of the applied pressure. The brake pressure variation was predominantly third order, characterised by one large and two smaller peaks. The outboard disc displacement was third order deformation with again one large and two smaller peaks.

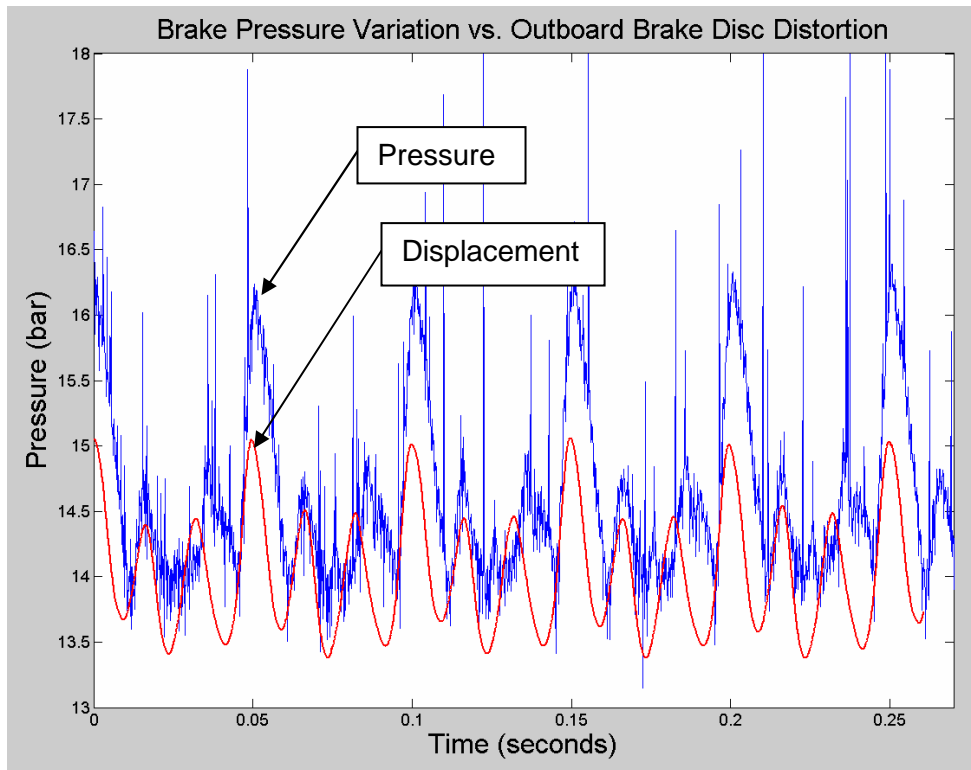


Figure 4.19: Correlation between disc distortion and BPV showing apparent 3rd order deformation and BPV.

Figure 4.20 shows the correlation between disc distortion and brake pressure variation. In this case the outboard disc displacement has been plotted against BPV and indicates predominant second order deformation. The BPV in this instance was predominantly first order, however there were also some smaller peaks present between the larger ones. The smaller peaks were somewhat masked by the signal noise, however a Fourier analysis of the signal allowed identification of these components. The Fourier analysis of the displacement and pressure signals is shown in figure 4.21 and figure 4.22, and in both it can be seen that second order content is a major component, which in this instance is indicated by a frequency of 60Hz. The pressure signal has components of first, second, fifth, sixth and tenth order, whilst the displacement signal has dominant components of first, second, third, ninth, tenth and eleventh order. Importantly this disc later went on to display 11 hot regions equispaced around each friction ring after undergoing higher speed high energy braking which is detailed in section 4.3. The eleventh order frequency picked up by the displacement transducers was a precursor to the formation of the visual hotspots. Again the wave-like deformation of the brake disc and the eleventh order deformation frequency was a result of buckling of the brake disc as introduced in

section 3.2.6.3. The predominant second order deformation was caused by circumferential buckling of the disc as a result of the thermal expansion due to the bulk friction ring temperature, whilst the superimposed higher order frequency was likely to be a result of a hot band on the friction ring surface causing higher order circumferential buckling.

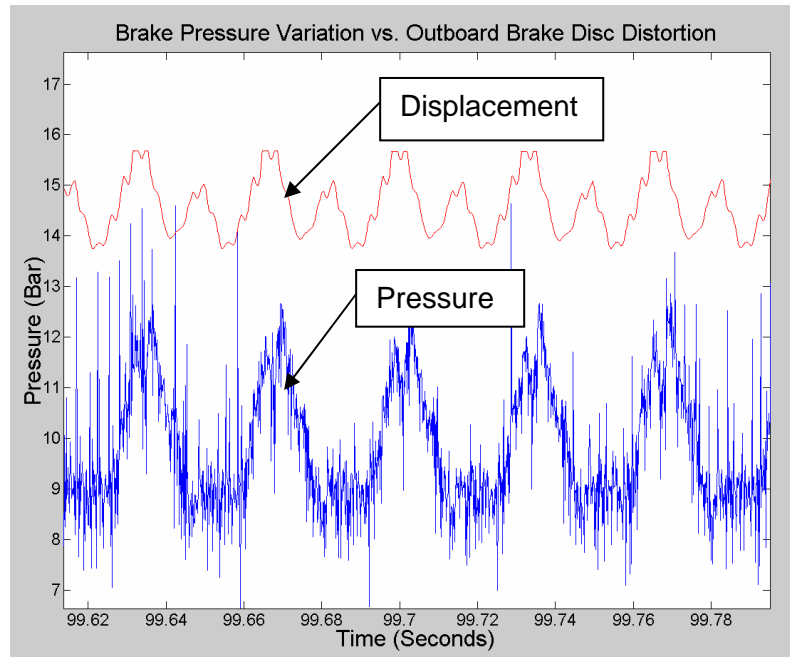
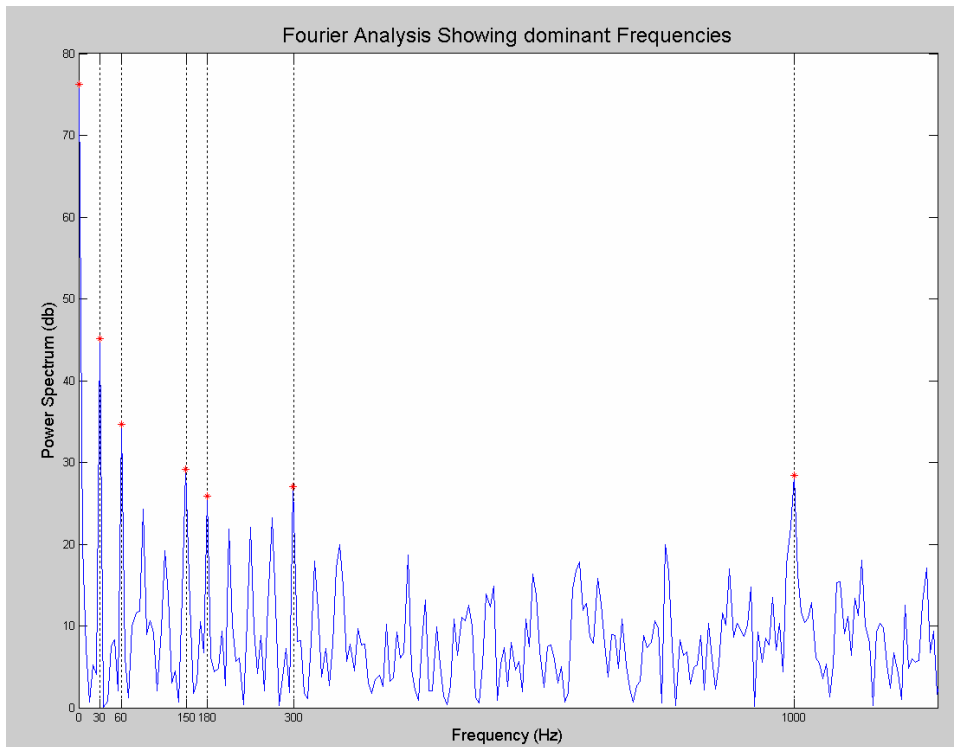
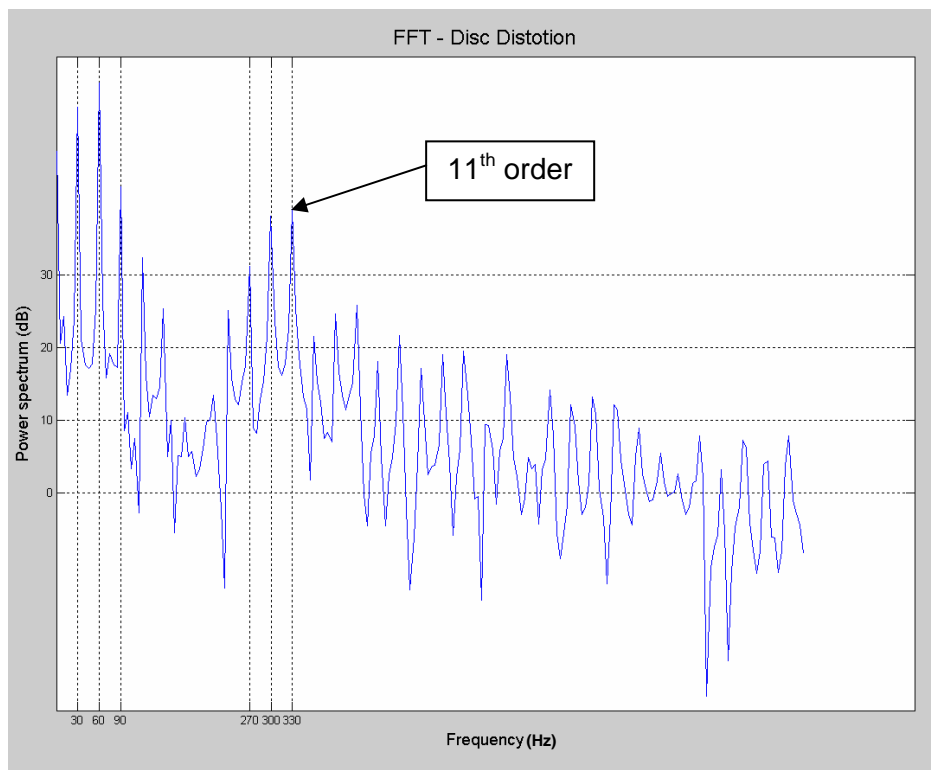


Figure 4.20: Correlation between disc distortion and BPV showing dominant 2nd order deformation and possible 2nd order BPV.



**Figure 4.21: Fourier analysis of the brake pressure variation – speed of disc rotation
30Hz**



**Figure 4.22: Fourier analysis of the outboard brake distortion – speed of disc rotation
30Hz**

Correlation between BPV and brake disc surface temperature can be seen in figure 4.23 which shows the variation over a full dynamometer test. In the test shown the brake disc had already developed quite severe judder from previous running as indicated by the large BPV amplitude of 6 bar at the beginning of the test. As the test progressed there was a steady increase in the BPV amplitude to a maximum value of 8 bar with significant judder being observed via the analogue pressure gauge, as drone, and as vibrations through the floor. The BPV amplitude can be seen to correlate with the maximum in-stop surface brake temperature and corresponded well with the analysis performed on the on-vehicle test data shown in section 3.2.4.2.

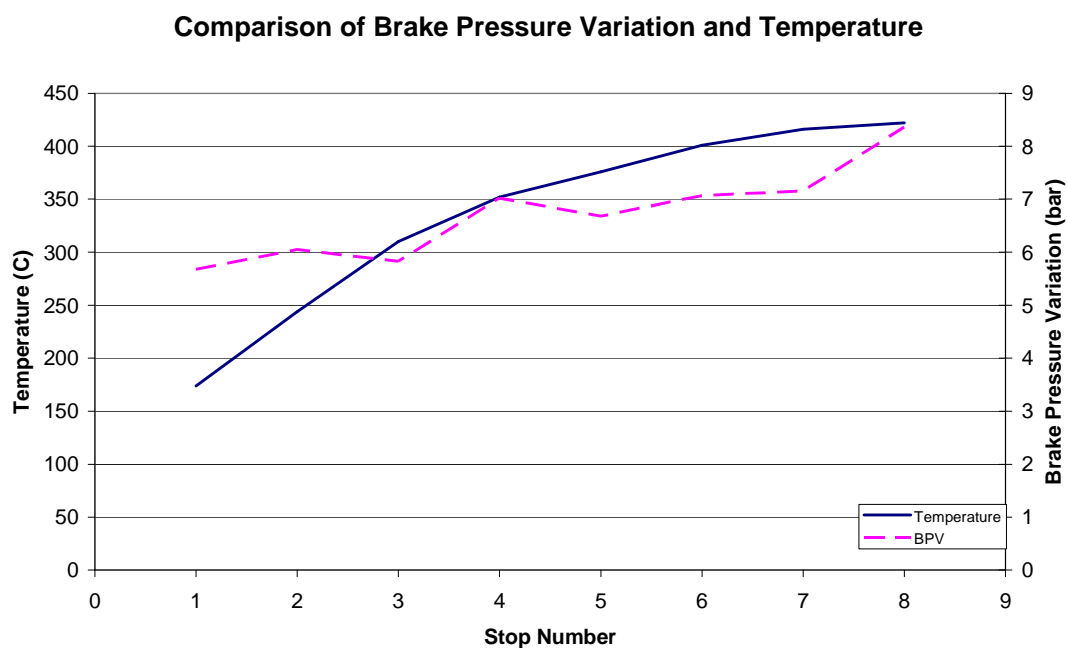


Figure 4.23: Development of brake pressure variation through a single 8 stop test showing correlation with disc surface temperature.

Extending this analysis to the off-brake periods it was evident that as the surface temperature of the brake disc increased the order of deformation during the off-brake periods could be seen to change. Figure 4.24 displays off-brake deformation correlated with brake disc surface temperature for a single test. The results indicated that the off-brake deformation was related to surface temperature with second order deformation generally appearing at disc surface temperatures above 60°C, and third order appearing above 180°C.

Temperature vs. order of brake disc displacement

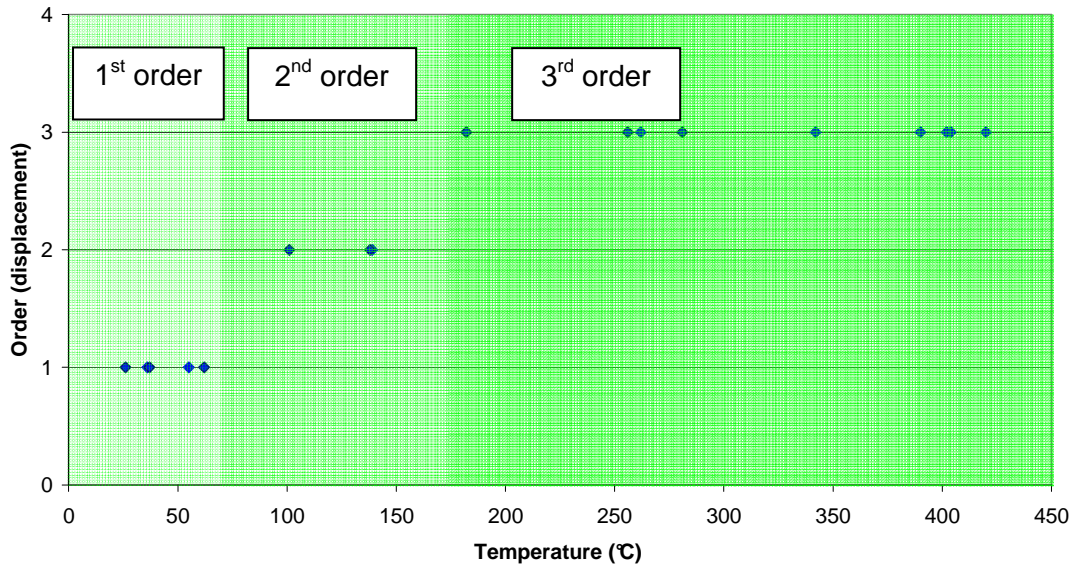


Figure 4.24: Graph comparing the mode order of off-brake disc distortion to temperature.

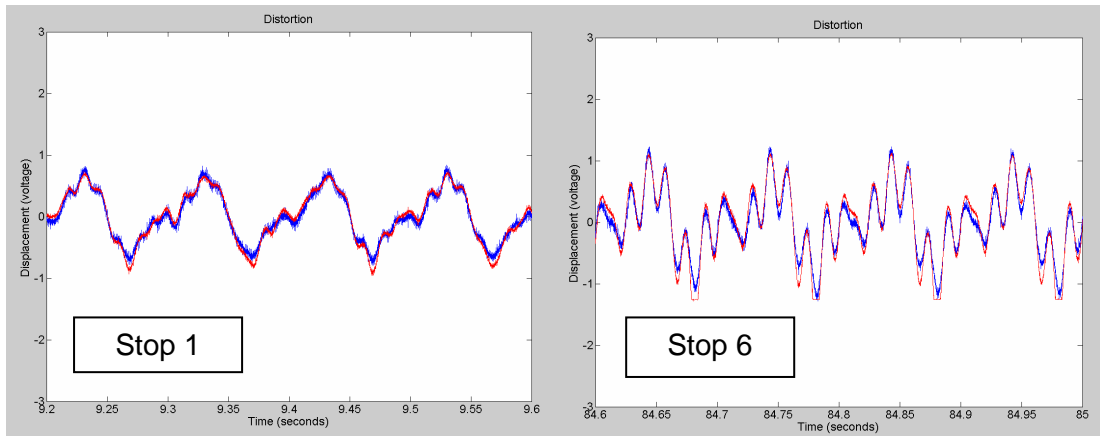


Figure 4.25: Inboard and outboard displacement showing the difference between stop 1 and stop 6 in a braking sequence.

As already discussed and identified earlier in figure 4.17 and figure 4.18, the in-stop distortion of the brake disc varied dramatically and was highly dynamic, however the difference between braking events was also notable. Shown in figure 4.25 are the inboard and outboard displacement plots for two different braking events; the first and the sixth. The first stop indicated predominant first order deformation with some

smaller peaks, however, by the sixth braking event the deformation had now completely changed. The smaller peaks were dominating the signal and had swelled due to the thermal input of the six braking events. What is of importance was the fact that both the inboard and outboard displacement transducers were identifying an overall waveform built up by the individual peaks, and that the peaks were not peaks on a single surface. This, together with the data previously discussed was good evidence of wave-like deformation of the brake disc resulting in brake judder. The wave deformation was caused by a number of factors, these being:

- Thermo-elastic deformation due to rapid heat dissipation through the brake disc causing buckling of the brake disc.
- Combined thermo-mechanical deformation of the brake disc due to both the heating effect, and the clamping action of the brake pads causing the disc wave to alter as it is fed between the two brake pads.
- Thermo-plastic deformation resulting from stress relieving allowing the disc to relax back to its natural shape. Evidence has shown (see below) that a brake disc can revert to a different state of cold deformation following a series of braking events in a brake test. The heating of the disc to over 500°C followed by slow cool down would give the conditions for a stress relieving operation. More details of this can be found in section 4.2.3.2.

The discs used for the dynamometer testing relaxed back to either first or second order deformation when cold. Figure 4.26 shows displacement measurements taken between high speed tests while the disc was cold. It shows that second order deformation was present. However figure 4.27 shows later testing where the same disc had relaxed back to first order deformation. The cause of this phenomenon was that the heating of the disc and subsequent cooling allowed the removal of some of the plasticity or retained stress which the disc previously experienced. This stress would have been retained during the casting process and further stresses would have been developed in the disc material during the machining process. It is important to note that if cold judder i.e. off brake wear, were the cause of the third order wave, the disc would remain in a third order state of deformation upon cooling. However, since the order of disc deformation increased with rising temperature and subsequently reverted back to a lower order of deformation during cooling it was therefore a result of hot judder occurring.

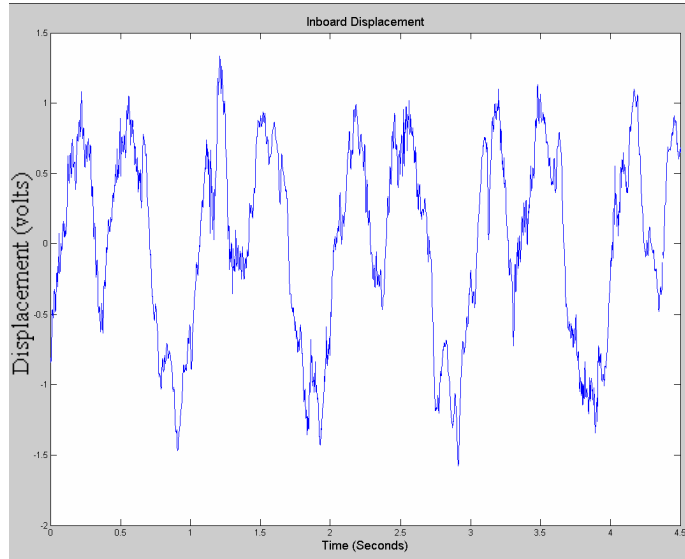


Figure 4.26: Graph of disc run-out (cold) showing second order deformation.

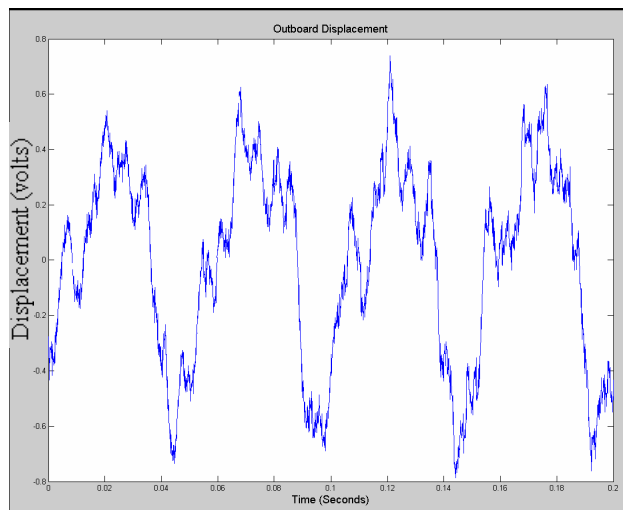


Figure 4.27: Graph of disc run-out (cold) showing dominant first order run-out.

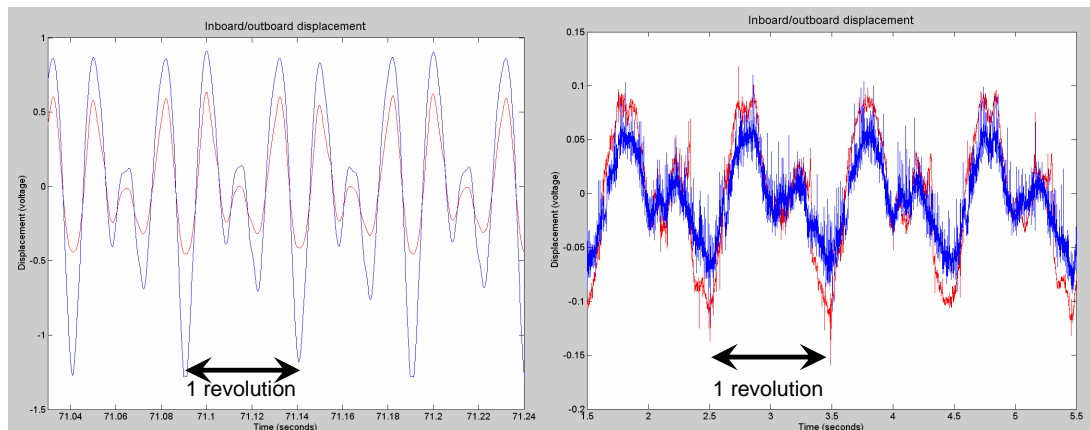


Figure 4.28: Comparison between in stop 'hot' deformation (left) and post test 'cold' deformation (right).

Finally the last observation of importance from the mid speed testing was the difference between the 'hot' disc shape and the 'cold' disc shape. Traditionally run-out and DTV data is measured post test by vehicle manufacturers (although this trend is now changing with the use of commercial brake dynamometers with non contacting displacement measurement systems [74][75][76]), however as the graphs in figure 4.28 suggest, this is not an accurate representation of the disc when it is actually causing brake judder. The graph on the left indicated third order deformation in-stop while the brake was hot. Compare this to the cold shape of the brake disc post test (right hand image), where the disc had adopted a predominantly second order 'cold' wave with some smaller peaks. The brake pressure variation has been shown in figure 4.10, figure 4.19 and figure 4.20 to be a result of the in-stop waveform of the disc. Therefore the disc should be measured and analysed in-stop to get an accurate representation of the conditions causing brake judder as was performed in this thesis. Cold DTV measurements would relate to wear of the dynamic in-stop wave form peaks as a result of the increased contact pressure between the disc and pad at the peak of the waves

4.2.3.1. Clamping Method

A mid-speed dynamometer study was performed to assess the possible interaction between the clamping area between the hub, brake disc and wheel, and the brake pressure variation due to brake judder. It is generally known that the run-out of a brake disc can be altered by the clamping action of the wheel and associated torque applied to the wheel bolts [49], and therefore it was possible that the arrangement of the wheel bolts was having an effect on the shape and deformation of the brake disc

during use. An initial 'quick' analysis involved slackening one of the five wheel bolts, however this proved to have no effect on the brake pressure variation.

A second method was devised to analyse the effect of the clamping area between the wheel, disc and hub. The mating face of the wheel had five main contact platforms, and therefore it was possible that these were affecting the disc deformation when the assembly was fully clamped together. To identify if this was the case a spacer with three contact platforms was designed to fit between the disc and hub, with the aim of altering the cold run-out of the disc. The aim of this was that if the dynamic wave or the brake judder itself could be influenced for better or for worse, it would give some indication as to what was causing the dynamic wave and thermal judder. The spacer can be seen in figure 4.29 with three contact platforms raised 0.25mm above the surrounding material.

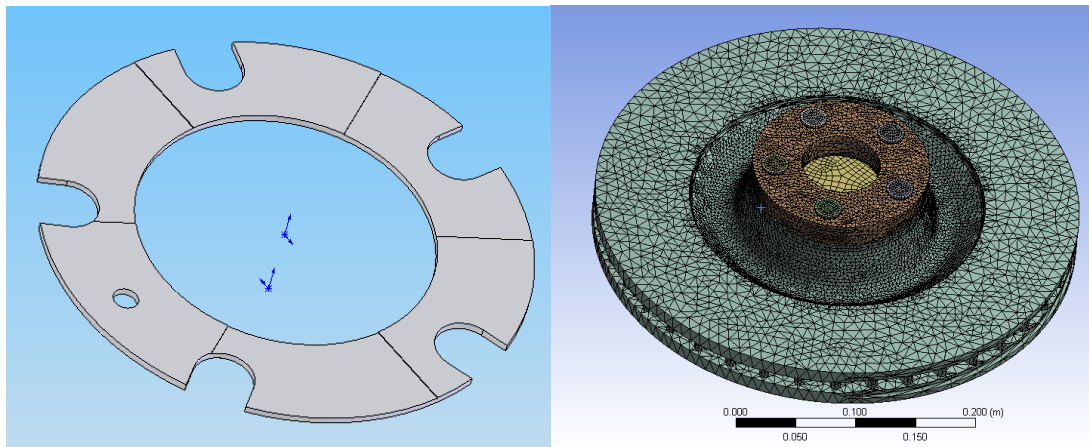


Figure 4.29: Spacer to alter the clamping area of the brake disc, hub and wheel (left) and associated finite element assembly with high mesh density in critical areas.

An initial finite element analysis of the hub-disc-spacer-wheel-wheel bolt assembly identified that the spacer would induce first order run-out of magnitude 12 microns in a perfectly machined and mated assembly contrasted with zero run-out for an assembly without the spacer. The largest deflection was seen where a bolt coincided directly with a recess in the spacer as can be seen in figure 4.30.

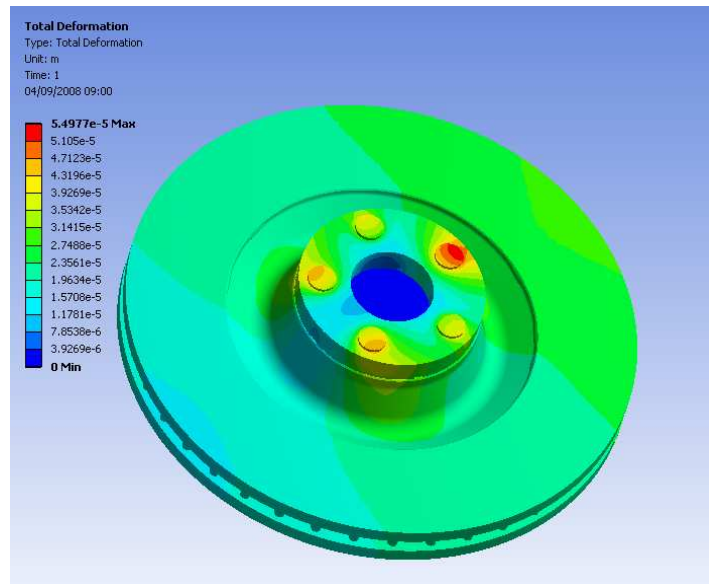


Figure 4.30: Deformation of the brake disc due to clamping force with spacer fitted. Largest disc deflection is seen on the right hand side.

Mounting of the spacer on the brake dynamometer changed the installed run-out from 55 microns to 140 microns (max-min) as was expected based on the FE study. The magnitude of the installed run-out was larger than the predicted FE values due to the inherent run-out of the brake disc itself prior to installation. The nature of the run-out was also altered when compared to the mounting of the disc without the spacer. Almost the reverse image was presented, as shown in figure 4.31, when the disc was installed in an identical position. Based on the general guide of less run-out is better, it was anticipated that the brake judder would be worse as a result of the run-out which was more than doubled. This was likely to cause large off-brake vibrations due to off brake contact with the brake pads, but also the run-out was likely to increase in-stop due to thermal deformation.

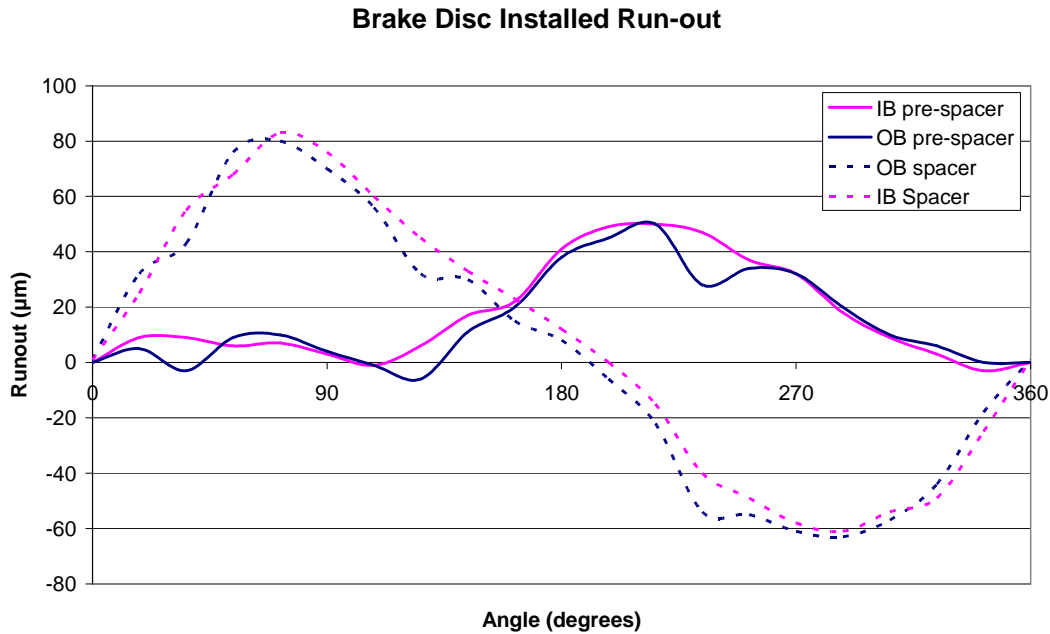


Figure 4.31: Effect on the installed run-out of the brake disc of altering the clamping area between disc and wheel.

Large off-brake vibrations were present during testing of the brake disc with the spacer installed. This as mentioned above was due to off brake contact between the brake pads and disc as a result of the increased run-out. The test procedure had to be altered slightly with the displacement transducer offset having to be increased due to the large and unpredictable vibration and deflection of the brake disc during running. The test speed was reduced to 600r/min where an acceptable level of off-brake vibration was present. Analysis of the brake pressure variation during the test showed no significant change in the overall magnitude. As a comparison, during the 7th braking event there was 1.7bar of pressure variation with the spacer, whilst without the spacer there was 1.6bar. This suggested that there was minimal link between the mounting geometry and clamping action of the bolts and the deformation of the brake disc on this particular braking system. Analysis of the brake disc distortion showed in-stop distortion to be mirrored as with the measured run-out when compared with the assembly without the spacer fitted. No significant increase in the relative magnitude or shape of the in-stop distortion was apparent as was highlighted by the coinciding peaks in figure 4.32. Since there was a large variation in the cold run-out between the two tests, shown in figure 4.31, but no significant variation between the magnitude or shape of the in-stop deformation of the two tests, shown in figure 4.32, it indicated that the clamping action of the brake pads together

with the change from low order deformation to higher order thermal deformation during braking was reducing the variation in the disc run-out between the two tests.

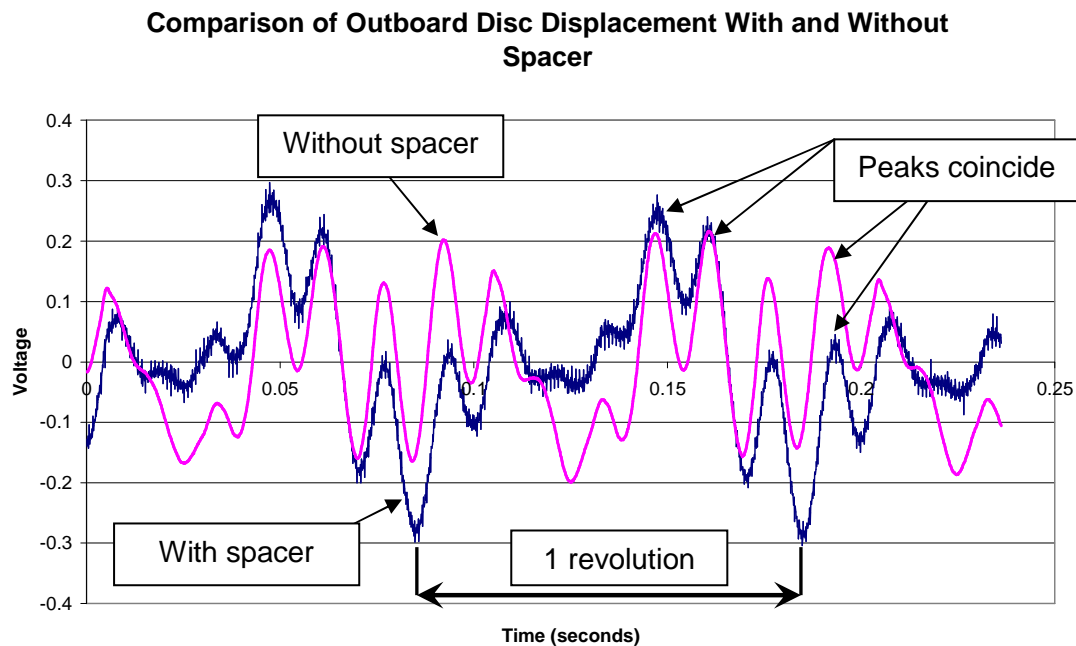


Figure 4.32: Graph showing the similarities in the disc waveform during braking with and without the spacer fitted.

4.2.3.2. Stress Relieving

The mid speed dynamometer testing shown in section 4.2.3 identified a possible stress relieving process occurring during hot running of the brake disc (specifically figure 4.26 and figure 4.27). The repeated heating and cooling of the brake disc during testing was removing retained stress which had built up during both the casting and machining processes. This process has been suggested by Gassmann *et al* [47] however there has been no published evidence which identified the effect it had on the distortion of the brake disc specifically with reference to brake judder. Therefore the aim of the following investigation was to give a better understanding of the stress relieving effect in relation to brake judder.

Evidence of this stress relieving process has been shown whereby a disc will initially have a first order deformation when new. Testing of the brake disc has shown this to then transform to third order upon braking and second order between braking events. As the test progressed the disc adopted a third order wave in the off-brake periods, and following cooling at the end of a test either second order or first order

deformation was present. A disc which had previously cooled to second order deformation could, following subsequent testing, cool to first order deformation. More often it was the case that a disc would adopt a second order mode of deformation following testing, suggesting that this was the natural shape that the disc was trying to assume. This was clear evidence that the stress relieving process has been occurring as a direct result of the heating and cooling of the brake disc during brake testing. To identify whether this was the case, bare metal discs were delivered for measurement without a protective zinc flake coating (Geomet) applied; it was therefore possible to have the brake discs stress relieved. The stress relieving process was performed by Wallwork Heat Treatment Ltd.; a specialist heat treatment company based in the UK, and involved heating the discs to 550°C within a vacuum followed by a controlled cool-down. The discs were measured on a Zeiss CMM before and after stress relieving and the results can be seen presented below. The absence of the protective coating increased the accuracy of the measured results by allowing the true surface of the brake disc to be measured without any influence from thickness variations of the zinc flake coating.

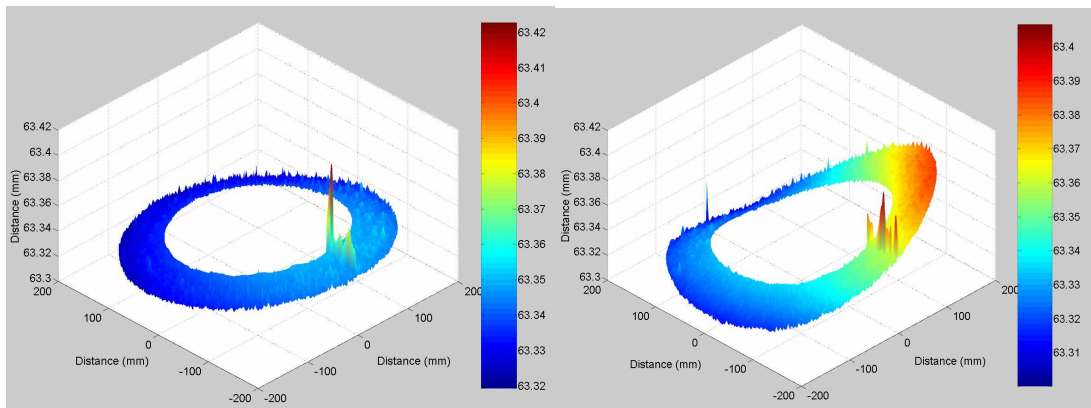


Figure 4.33: Disc 3 (inboard friction ring) pre stress relieving (left) and post stress relieving (right) – Same scale.

Figure 4.33 showed that following stress relieving the disc had deformed with the right hand edge deflecting upwards by approximately 40 microns when compared to the pre-stress relieved condition. The graph shown in figure 4.34 shows a scan at the mean rubbing radius of the brake disc pre and post stress relieving. It is evident that the disc had changed from low (15 microns) first order run-out to a large (65 microns) predominantly first order wave, with a secondary peak as shown.

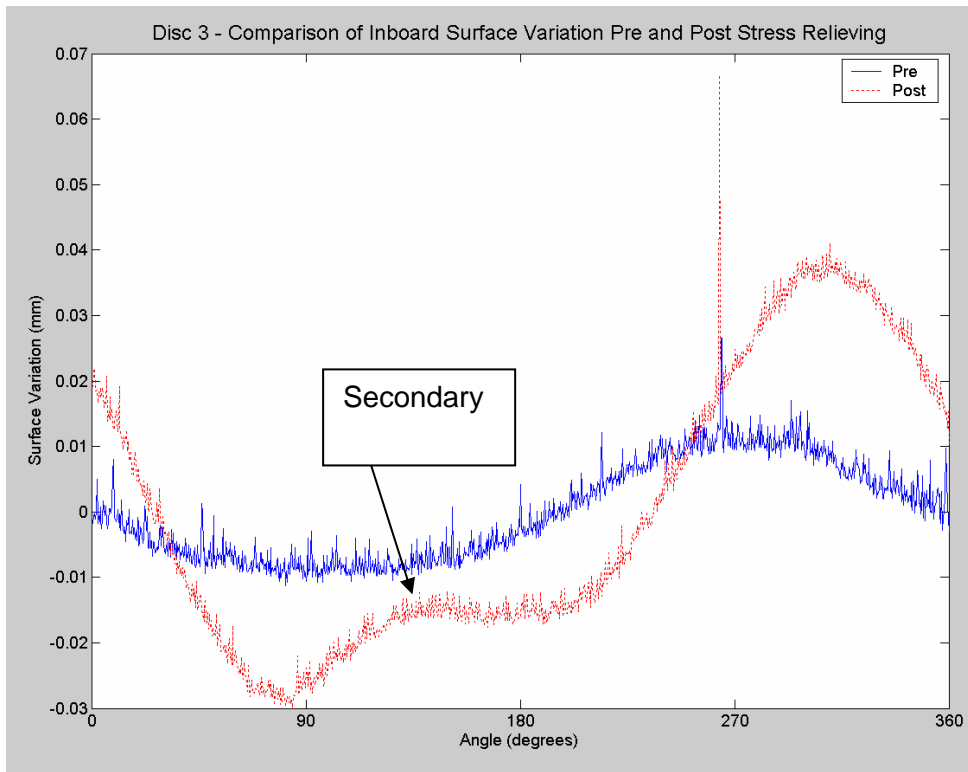


Figure 4.34: Disc 3 aligned inboard surface scan at a radius of 167mm

The reverse (outboard) side of the disc is shown in figure 4.35 and figure 4.36 with much the same effect being seen again as would be expected as the two friction rings must deform to a common shape otherwise fracturing of the disc vanes would occur. This friction ring was transformed from 18 microns to 57 microns of run-out with again the secondary peak being evident after stress relieving.

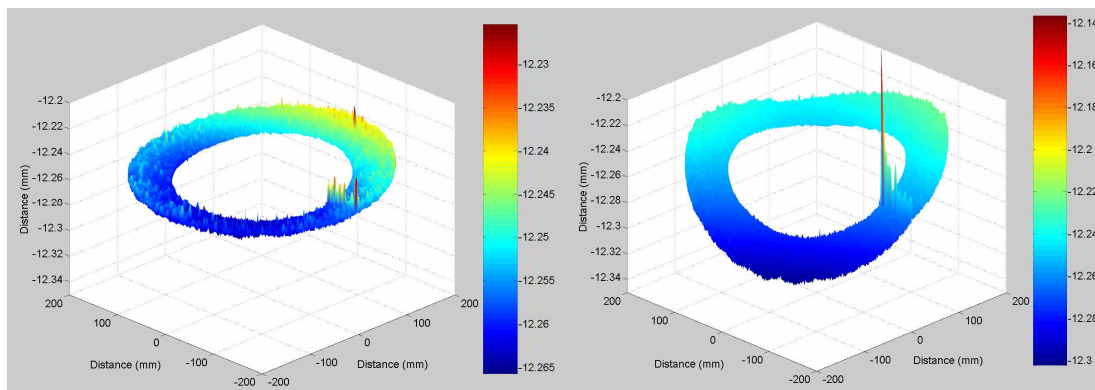


Figure 4.35: Disc 3 (outboard friction ring) pre stress relieving (left) and post stress relieving (right) – Same scale

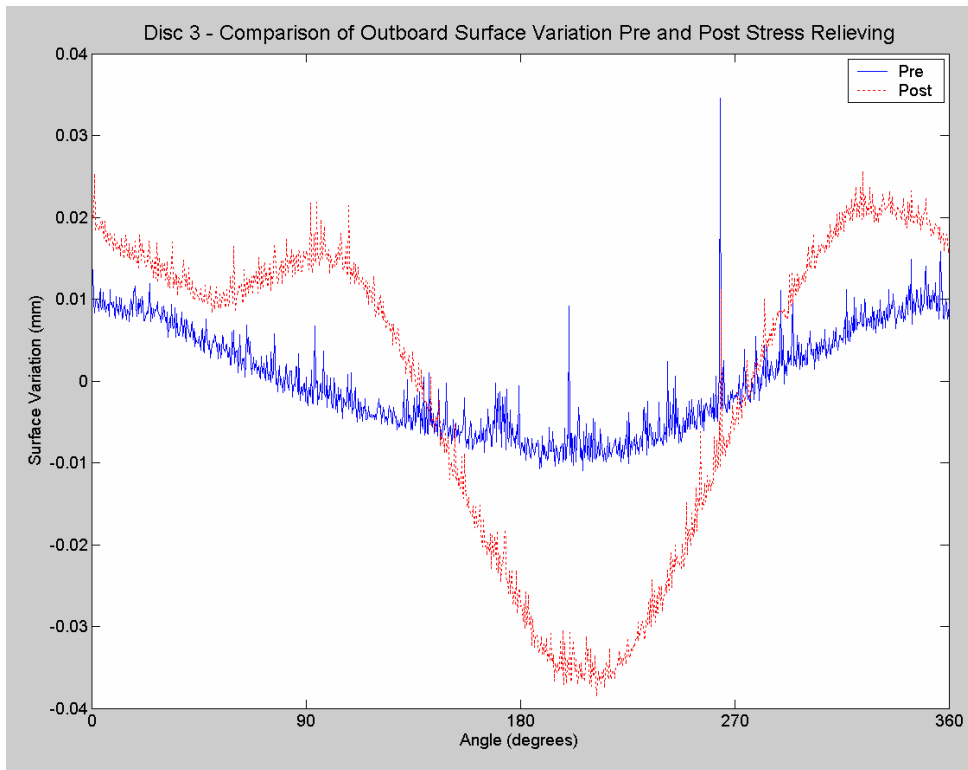


Figure 4.36: Disc 3 aligned outboard surface scan at a radius of 167mm

Surface CMM scans from a second disc can be seen in figure 4.37 and figure 4.38. These again showed a second order mode of deformation present within the disc following the stress relieving process. This was showing that during the casting and machining process significant stresses were retained within the disc material which prevented the disc from taking up its natural shape. Both brake discs took up a second order wave-like mode of deformation following stress relieving, however the orientation of the deformation was different for the two discs shown here when using a common reference point on the casting. The results presented above in figure 4.33 to figure 4.38 identified that large changes in the deformation of the brake disc could occur following a stress relieving process. The elevated disc temperatures seen during use of the brake disc, which could be in excess of 550°C (see figure 3.34 and figure 3.35), followed by cooling provided the correct conditions for the stress relieving process to occur. Therefore wave-like deformation of the brake disc resulting in a second order mode of cold deformation would occur during use as a result of this stress relieving process.

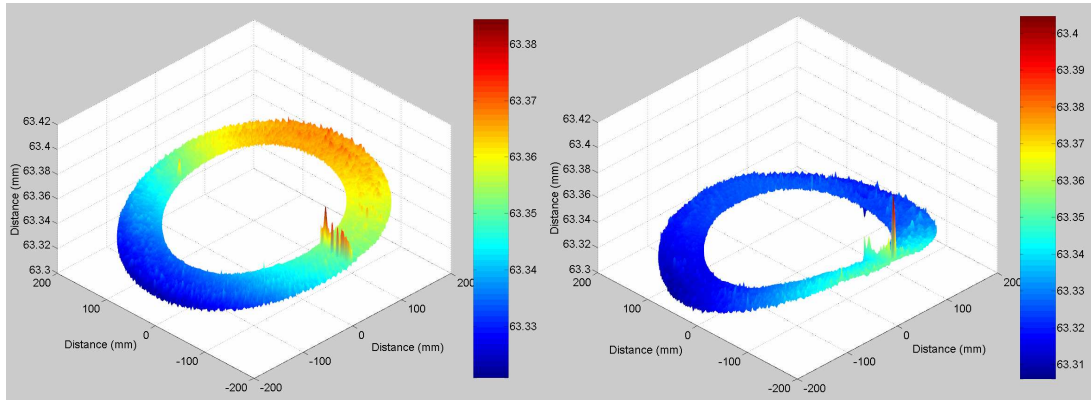


Figure 4.37: Disc 6 (inboard friction ring) pre stress relieving (left) and post stress relieving (right) – Same scale

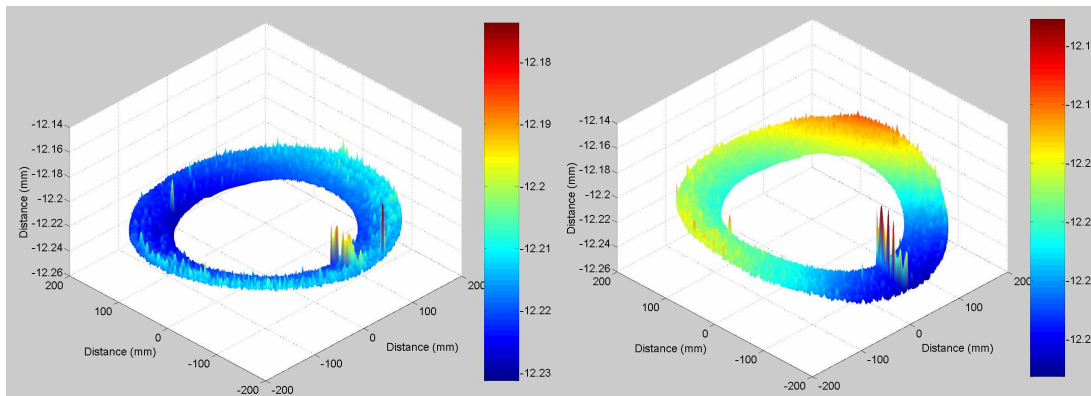


Figure 4.38: Disc 6 (outboard friction ring) pre stress relieving (left) and post stress relieving (right) – Same scale

A dynamometer test was carried out using the stress relieved discs to identify if there was any change in the type of in-brake distortion or the thermo-plastic deformation. It was anticipated that there would be little or no change between the pre and post test cold deformation of the brake disc. This was because the pre-stress relieving of the brake disc would remove the initial process which has been shown to occur during braking. Initial tests indicated that there was little change between the pre and post test run-out of the brake disc in both magnitude and shape of the run-out graph as shown in figure 4.39. Results from testing of un-stress relieved brake discs have shown that the run-out would change from first to second order and that it would also grow in magnitude for a non-stress relieved brake disc. Therefore these test results confirmed that pre-stress relieving a brake disc allowed the disc to deform to second order wave-like shape before testing, in doing so this step was removed from the overall process of disc deformation during brake testing. Therefore was concluded

that the second order wave-like deformation occurring on an un-stress relieved brake disc was a result of stress relieving during braking. Stress relieving during braking has been known about for some time [47], however its effect on wave-like disc deformation has not been documented until now. Repeat testing using a brake disc which has been stress relieved after casting but prior to machining is proposed in order to maintain the dimensional accuracy of the brake disc; however this has fallen out of the timeframe of this research.

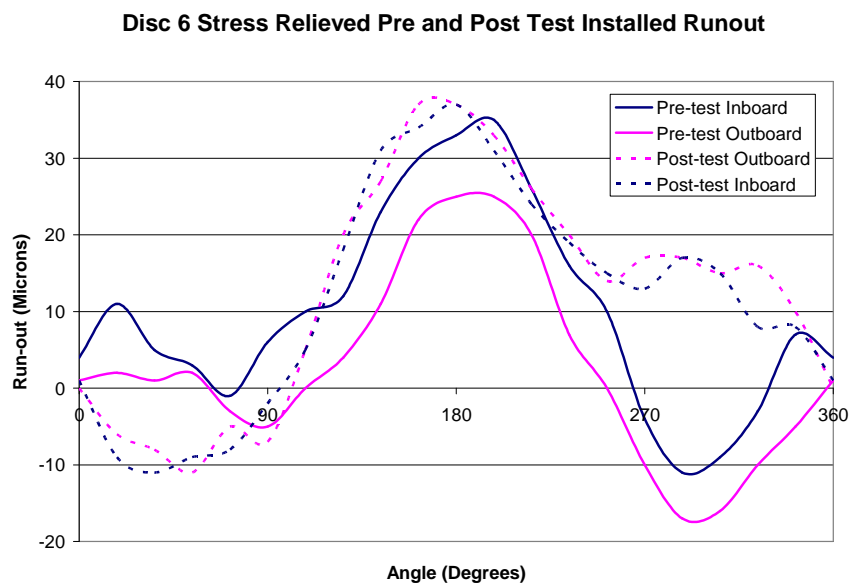


Figure 4.39: Graph showing the similarities between the pre and post test installed run-out of a stress relieved brake disc.

4.2.4. Mid-Speed Dynamometer Testing Discussion

The research carried out on the brake dynamometer at speeds of 1200r/min identified the brake pressure variation and therefore the brake judder to be linked to wavelike distortion of the brake disc. The distortion of the brake disc has been seen to change from first to third and back to first order deformation during a single brake application, whilst correlations have been made between temperature, BPV and off-brake deformation. The shape of the hot deformation of the brake disc has been shown to be vastly different from the cold deformation, with third order deformation commonly appearing during a braking application whilst the disc would cool to first or second order deformation. Explanations have been given to show why this should occur. The third order deformation has been previously identified by Anderson and Knapp [48] to occur on other braking systems, therefore it appears to be a common

trend. The correlation between the pulsation of the brake pressure variation and the disc wave-like deformation has been shown in section 4.2.3 and backs up the mechanism suggested by Lang [1], and detailed in section 3.2.6.3, of circumferential disc buckling due to rapid constrained thermal expansion of the friction rings.

Three different modes of deformation have been identified during a brake test, all having an effect on brake judder. Elastic wave-like deformation has been identified at the onset of braking, due to the mechanical loads of the brake pads together with the rotation of the brake disc. Thermo-elastic deformation occurs during any braking event and has the effect of intensifying brake judder and creating the buckled wave-form. It occurred due to the rapid heating and subsequent constrained expansion of the disc material. Thermo-plastic deformation identified over a series of braking events had the effect of “setting in” the wave deformation which maintained the level of brake judder. This was occurring due to the rapid heating and cooling of the brake disc. Of these three, thermo-elastic deformation of the brake disc was considered to be the most important factor with regard to brake judder. The reason for this can be explained by considering the first braking event in any test: at the onset of braking there was no brake judder, however the disc had already deformed due to the clamping of the brake pads. It is only after heat builds up in the brake disc that brake judder begins to intensify due to the thermo-elastic wave-like deformation resulting from rapid thermal expansion. Therefore an important conclusion can be drawn that minimising thermo-elastic deformation will reduce brake judder on the vehicle. This can be tackled by one or more of the following methods:

- Adopt a disc design which has more buckling stiffness and therefore resists circumferential buckling.
- Adopt a disc design which has less buckling stiffness and therefore promotes higher order circumferential buckling.
- Reduce the thermal gradients to allow the disc more freedom for thermal expansion and therefore avoid buckling.
- Design the disc so that it can distribute the heat more evenly and have a lower temperature.
- Reduce the thermal loading on the brake disc by reducing the vehicle mass.

Of the above methods, the one that would have the most benefits would be to reduce the thermal loading on the brake disc by reducing the vehicle mass. This would reduce the kinetic energy which would need to be transferred into the braking system to decelerate the vehicle as kinetic energy is directly proportional to mass. A reduction in speed would be more beneficial as kinetic energy is proportional to the square of the vehicle speed; however this is very much down to the driver unless a speed limiter is installed on the vehicle. Reducing the thermal gradients would be difficult as energy must still be transferred to the brake disc, often rapidly in emergency braking situations, however a reduction in vehicle mass would also help this as it would reduce the kinetic energy required to be transferred into the braking system. As described in section 3.2.6.3, if low order disc buckling were the root cause of judder on a particular braking system, then the buckling stiffness of the brake disc should be increased to reduce the propensity for the disc to buckle. However, if high order buckling was an issue (in the case of hot spotting), the disc design should be changed so that higher order buckling was promoted to distribute the influx of heat over more waveform peaks and therefore reduce the individual hot spot temperature and to reduce the brake pressure variation. Designing a disc that could distribute the heat more evenly throughout the brake disc and therefore have a lower maximum temperature would reduce both the thermal gradients and the thermal expansion of the disc and therefore reduce the propensity toward buckling. Section 5.4 of this thesis has looked at modifications made to the disc design which reduced its maximum operating temperature and thermal gradients.

Section 4.2.3.1 looked at modifications to the clamping area between disc and hub to assess the effect this had on the brake disc distortion during braking. Providing a non-uniform clamping area affected the cold run-out of the disc by inducing a distortion at the hub mounting face. The magnitude of this distortion was amplified at the mean rubbing radius, due to the large radial distance of 166mm, creating increased run-out. However this had minimal effect on the in-stop brake judder as did altering the wheel bolt torque. Therefore it was concluded that disc clamping area and bolt torque only had a major influence on cold judder not hot judder. This would indicate that the elastic, thermo-elastic and thermo-plastic deformation causing hot judder was influenced more by the rapid thermal expansion of the brake disc as a result of the thermal energy during braking, and also due to the brake disc geometry and its ability to resist the thermal buckling, but not due to the clamping area geometry or force.

A stress relieving process was seen to occur during braking which was a result of the high disc temperatures and subsequent cooling. It has been shown that this had the effect of changing the disc distortion from first order 'cold' deformation to second order 'cold' deformation following brake testing. Stress relieving a pair of new discs has identified this mechanism, leading to the conclusion that there were significant stresses retained in the disc following casting and machining, and that the removal of these stresses allowed the disc to deform significantly. In both cases the mode of disc deformation was second order, although the waveforms were not identical between the two analysed discs. Preliminary testing of this disc indicated that the post test deformation was similar to the pre test deformation. This was a sign that pre-stress relieving a brake disc removes the initial stress relieving process which would normally occur during braking. As the disc had already deformed as a result of the stress relieving process, there was no change in the cold deformation state following braking. It was proposed that repeat testing should be carried out to fully back up this process, together with testing of a disc which has been stress relieved prior to machining. This testing has fallen outside of the timeframe for this thesis. It has been shown that stress relieving a disc following machining allowed the disc to deform back to its intended shape, however the run-out of the disc was more than trebled (from 15 microns to 65 microns), leaving the disc susceptible to cold judder via off-brake wear. Stress relieving prior to machining would remove this problem and also give a very good base disc to further analyse the elastic deformation of the brake disc during braking without any other influential factors.

The results presented within this section have given a new and important understanding into the thermo-elastic and thermo-plastic wave-like deformation of the brake disc. Future testing and analysis has been proposed where necessary to either back up or build upon some of the more significant findings, for example the stress relieving process which results in second order wave-like deformation. With the completion of the analysis of the mid-speed testing, section 4.3 examines the nature of brake judder, drone and hot spotting at higher speeds on the brake dynamometer.

4.3. Dynamometer High Speed Testing

4.3.1. Methodology

High speed testing was carried out in an attempt to induce both drone and hot spotting on the braking system. High speed testing was carried out at 1800r/min and 2400r/min, equivalent to road speeds of 232 and 309km/h, to transfer up to 428kJ of energy into the braking system per braking event.

4.3.2. Results

Higher speeds of disc revolution have indicated higher orders of disc deformation whereby there were multiple waveform peaks per disc revolution. For these tests the displacement transducers could not be used due to the higher temperatures involved which would damage the transducers. The images shown in figure 4.40 display pad deposition and burnishing as a result of hot spotting and/or wave-like deformation. The pad deposition clearly displayed the characteristics of a tenth order waveform with 10 peaks on either side. The inboard side of the brake rotor displayed the reverse image of the outboard side, whereby high points on the inboard side were represented by low points on the outboard side – an antisymmetric distribution. A surface scan of the brake disc is shown in figure 4.42

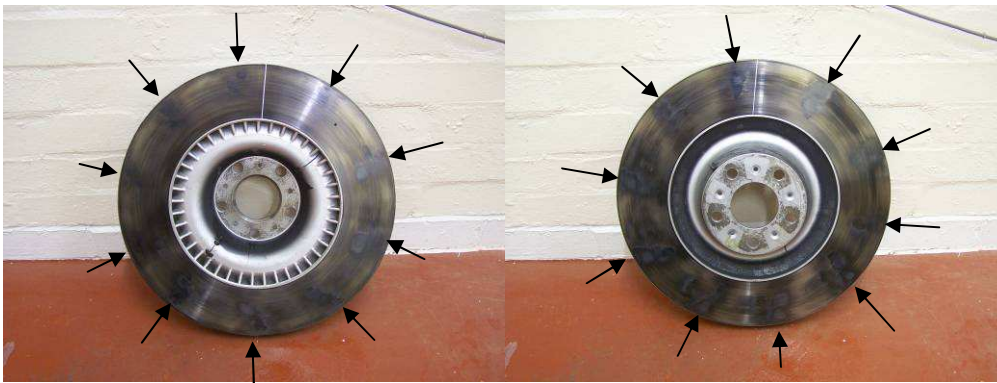


Figure 4.40: Friction material deposition/hot spotting resulting from 10th order disc deformation. Inboard (left) and outboard (right) disc images shown with reference line.

The tenth order waveform was more apparent when a combined image is created as shown in figure 4.41. The inboard disc image has been mirrored, rotated and finally overlaid on the outboard disc image. Colours highlight the highpoints of the disc with green showing high points on the outboard friction ring and red showing the high points on the inboard side. It is now easier to see that the high points on one friction

ring represented the low points on the other and therefore gave a characteristic waveform/antisymmetric pattern. This was similar to the findings of Kubota *et al* [4], whereby swellings appeared at alternate points on the inner and outer friction rings.



Figure 4.41: Combined image highlighting the high points on the inboard (red) and outboard side (green).

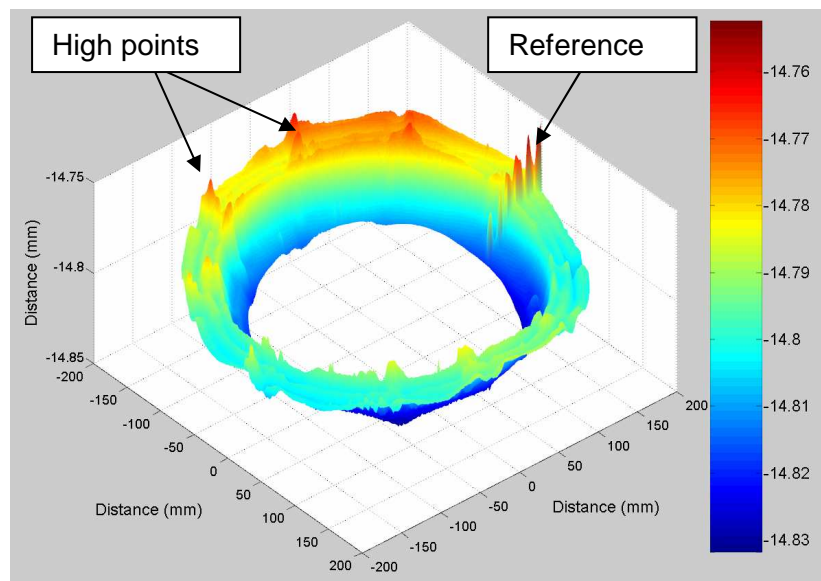


Figure 4.42: CMM surface scan of the brake disc showing high and low points.

Surface variation due to pad deposition was found to be as much as 11.4 microns above the surrounding surface when measured at the mean rubbing radius as seen in figure 4.43. This was easily enough to cause brake judder on its own before the overall DTV was taken into account.

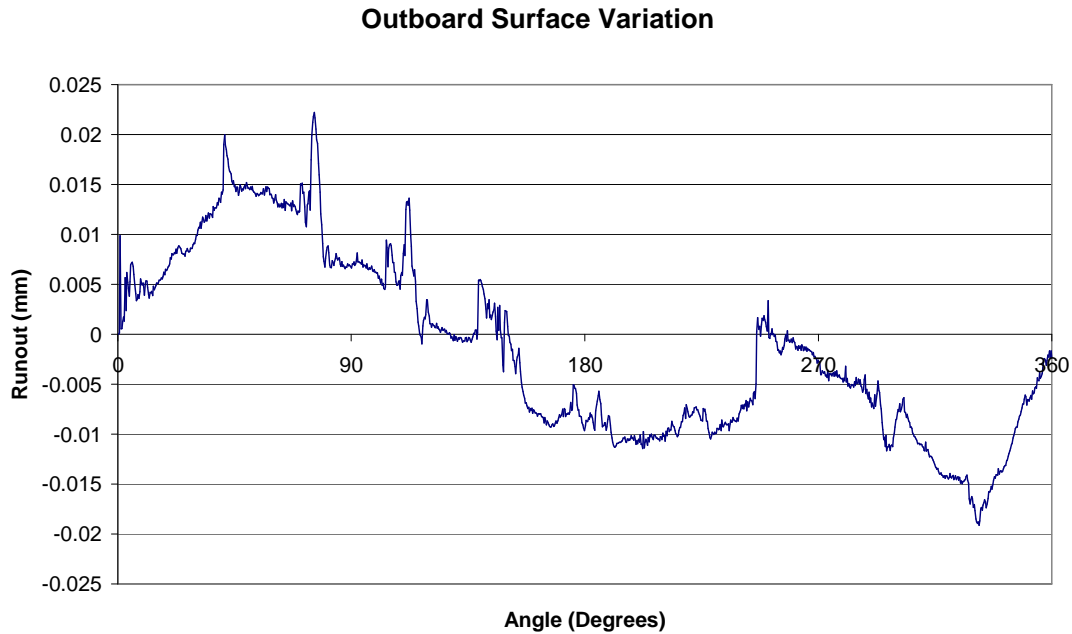


Figure 4.43: Outboard surface variation due to pad deposition as a result of hot spotting.

Three separate tests were carried out on brake discs which previously did not exhibit hot spots. Two tests carried out at 2400r/min caused both 9 and 10 hot spots to appear, whilst a further test at a reduced speed of 1800r/min caused 11 hot spots to appear on the brake disc, however this test involved eight braking events, each six seconds long, compared to the tests at 2400r/min which were all performed with four braking events, each four second long. Therefore the total energy dissipated during the test at 1800r/min was higher than the test performed at 2400r/min (2.89MJ and 1.71MJ respectively). The data from these tests is presented in table 4-2. The frequency of the hot spots were all in the region of a drone frequency (200-500Hz) and it must be noted the relatively small frequency window of 70Hz in which all of the hot spots were occurring. A corresponding audible drumming noise was observed during testing which was characteristic of brake drone.

Disc speed (r/min)	Number of Hot Spots	Hot Spot Frequency (Hz) (Disc speed/hot spots)	Total energy (MJ)
1800	11	330	2.89
2400	10	400	1.71
2400	9	360	1.71

Table 4-2: High speed tests showing number of hot spots, disc speed and hot spot frequency

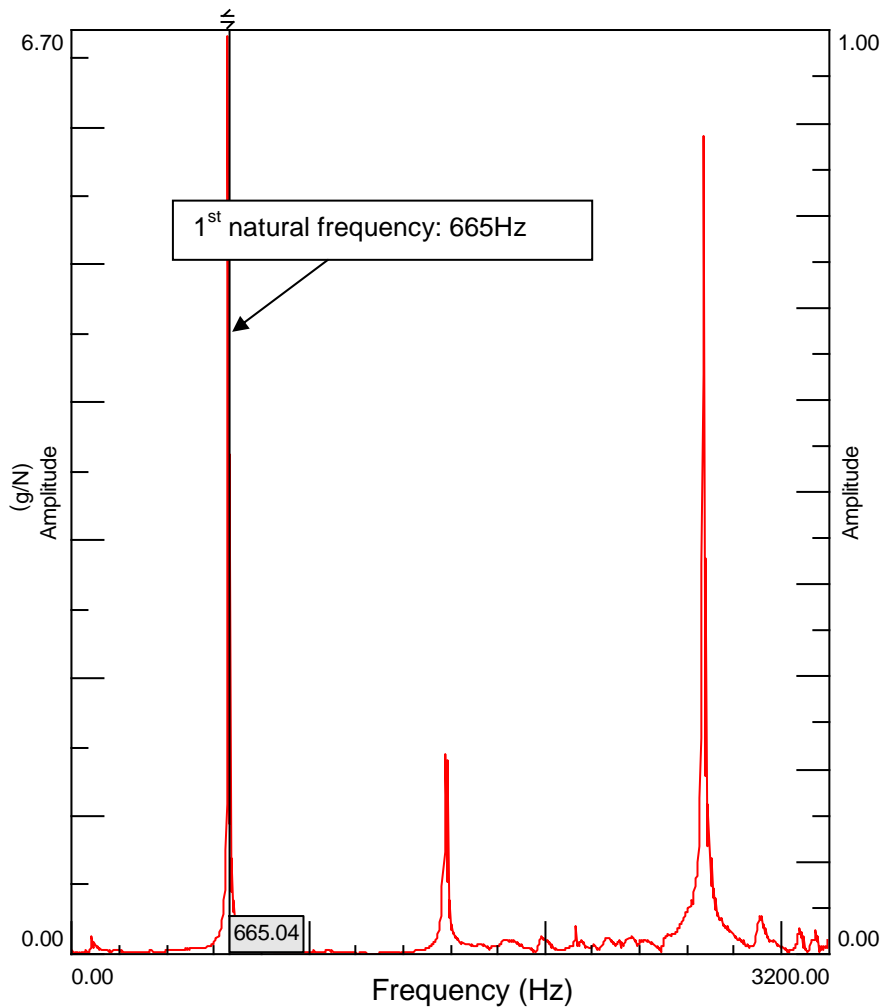


Figure 4.44: Modal analysis of the brake disc showing the first 3 natural frequencies.

Modal analysis is often used to identify the natural frequencies and associated modes of vibration of a component. For brake disc analysis this process is regularly used to identify squeal frequencies when analysing brake noise [11],[77]. Modal analysis can be carried out using various techniques including finite element analysis whereby the frequencies and mode shapes are predicted using mathematical models within the software, or tap-testing (also known as impact testing) where the component of interest is struck (tapped) with a modal hammer and the response measured with an accelerometer mounted on the component. Other methods exist including using a shaker to vibrate the component over a particular frequency range. For the purpose of this research the natural frequencies of the brake disc were of interest to identify if they correlated with the hot spot frequencies shown in table 4-2 and therefore had any relation to the formation of hot spots on the system as indicated by Afferrante *et al* [8]. A tap-test was selected as the most appropriate method as it required little set-up time and would produce accurate measurements of the natural frequencies of the brake disc when mounted on the dynamometer. The single-point tap-test identified only the natural frequencies and not the mode shapes, the mode shapes could be identified using FEA or a multi-point tap-test. The single-point tap-test involved mounting a single Kisler 9.54mV/g accelerometer on the surface of the brake disc using bees wax as the adhesive and then tapping the disc with a modal hammer which contained a load cell with a sensitivity of 2.25mV/N. Both the hammer and accelerometer were connected to a LMS data acquisition system. The LMS computer software used the signal from the modal hammer and accelerometer to identify the natural frequencies of the brake disc. In the above test the first natural frequency was identified as 665Hz; this did not correspond with the hot spot frequency which was calculated to be 330-400Hz as shown in table 4-2. Therefore it was not necessary to investigate the associated mode shape of the disc using FEA or more detailed multi-point tap-testing. It is proposed that the presence of hot spots on the brake disc surface was a result of high order disc buckling as described in section 3.2.6.3. Third order deformation was identified during braking in section 4.2.3 when the disc rotational speed was 1200r/min, whereas in the high speed testing of this section, the rotational speed was up to 2400r/min which caused up to 11th order wave-like deformation as indicated by the antisymmetric pad deposition. With the higher rotational speed of the high speed testing, more energy was being transferred into the brake disc. The heat generated caused large thermal expansion; however large thermal gradients were developed between the hot annulus, where heat was being generated, and the cooler surrounding material which constrained this expansion in the radial direction. This generated higher order

buckling. Evidence from the test at 1800r/min also backs up this mechanism. The total energy dissipated in this test was higher, as can be seen in table 4-2, due to the higher number and longer duration of the braking applications. The buckling equation (equation 3-15, section 3.2.6.3) showed that a higher tangential load (caused by thermal expansion due to higher thermal energy) would give a higher order of buckling, the dynamometer testing confirmed this with 11th order deformation.

4.3.3. Discussion

High speed testing has been identified as a quick and effective method of generating hot spots on the brake disc. The test data and analysis has importantly identified a trend whereby as the speed of rotation decreased the number of hot spots appeared to increase maintaining the hot spot frequency in the region of 330-400Hz. Three brake discs were tested on the dynamometer to show this finding due to the semi-destructive nature on the disc surface, so as yet this can only be classed as a tentative association. A tap test showed no correlation between the first natural frequency of the brake disc and the hot spot frequency, this indicated that vibration of the brake disc was having no dominant effect on the hot spot frequency. More importantly the test data has identified a link between the energy dissipated during a test and the number of hot spots when considering the buckled mode shape of the disc. Higher total energy dissipation resulted in more hot spots being generated. High speed dynamometer tests have shown the presence of 9th, 10th and 11th order disc wave forms. It is proposed that the higher order wave forms were a result of higher order buckling due to the higher thermal input into the brake disc. This resulted from the increased disc speed of rotation when compared to the mid-speed testing of section 4.2 which typically gave a 3rd order mode of deformation. Thermal imaging was used to aid the analysis of the observable hot regions on the brake disc and has been described in the next section of this thesis.

4.3.4. Thermal Imaging

The non uniform contact between the brake pad and disc can have significant effect on the surface temperature of the brake disc [53]; this has been observed in the thermal images recorded by the thermal camera of the brake dynamometer. This would in part be due to the difference between the apparent and real contact area of the brake pad, the effect of which has been shown by Qi *et al* [53], however other

factors which would affect this are the surface roughness of the brake disc and effects such as blue spotting [5] and the thermal distortion of the disc.

Thermal imaging was used to analyse the heat distribution and build-up within the brake disc to further understand what causes the disc to deform. Shown in figure 4.45 is a thermal image of the brake disc after repeat short duration drag braking applications during bedding-in of the pad and disc (8 bar brake pressure, each application 3 seconds long at 600r/min) which has elevated the disc surface temperature to 100°C. The underlying vane pattern can be seen to have had an influence on the temperature distribution on the surface of the friction ring. This vane pattern was due to the increased local thermal mass available to the friction ring where there was a vane beneath the friction ring surface. This allowed the disc to conduct heat from the surface to a vane faster than surrounding areas. Note that the apparent hot ring around the wheel centre was due to the low emissivity (0.04-0.05 [79]) of the protective zinc paint combined with the high reflectivity of the surface.

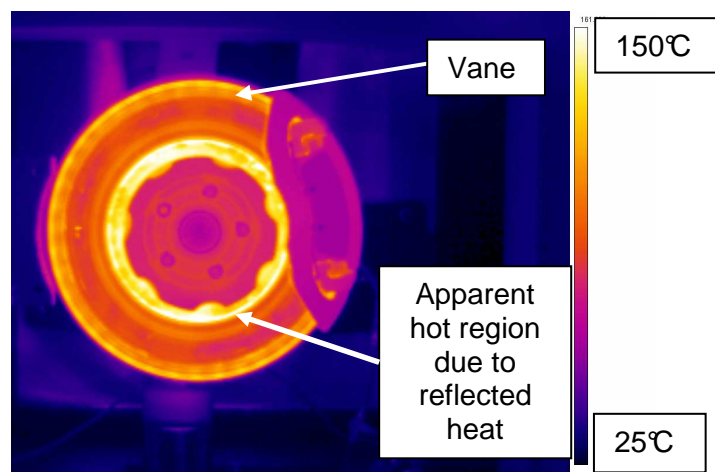


Figure 4.45: Thermal image of brake disc showing the vane pattern

Shown in figure 4.46 is the temperature profile around the disc at a radius of 187mm. The profile equated to an included disc angle of 262°, omitting the portion of disc obscured by the caliper. The number of peaks in the temperature profile correlated exactly with the number of disc vents in the included angle. It can clearly be seen that the vent profile was influencing the temperature on the surface of the disc, with a recorded temperature variation of 16°C. This variation is 21% of the average profile temperature and 20% of the maximum profile temperature recorded at this radius. It is temperature effects such as these which contribute to the cause of disc hot

spotting by causing an initial variation in the surface temperature profile. When combined with higher order disc deformation, the temperature variation would rise exponentially as a result of the localised thermal expansion and increased localised pressure distribution resulting in hot spotting.

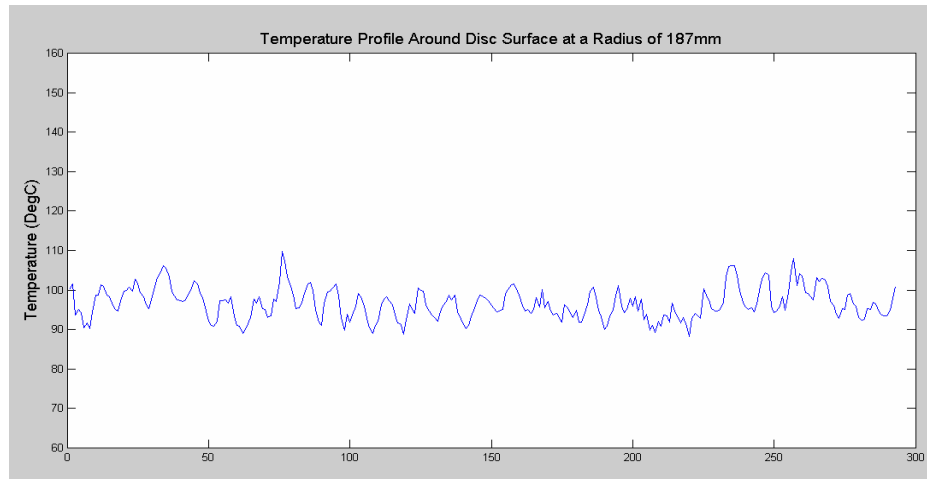


Figure 4.46: Temperature profile around the disc surface at 187mm. The number of peaks correlates with the number of vanes in the visible portion of the disc

Figure 4.47 shows a thermal image of a disc that has undergone repeated mid-speed testing on the brake dynamometer as defined in section 4.2.2. The test involved eight repeat braking events at 1200r/min with 1.5MPa pressure application, analysis of the brake pressure variation and associated disc distortion from this test has previously been described in section 4.2.3. Thermal banding of the disc can be seen, but also apparent are hot regions associated with pad deposition. This has occurred where the disc has become hot enough to deposit pad material onto the surface. This condition would only get worse as the disc was repeatedly heated. The hot area would expand causing increased contact with the pad which would result in increased heating and expansion which further worsens the problem.

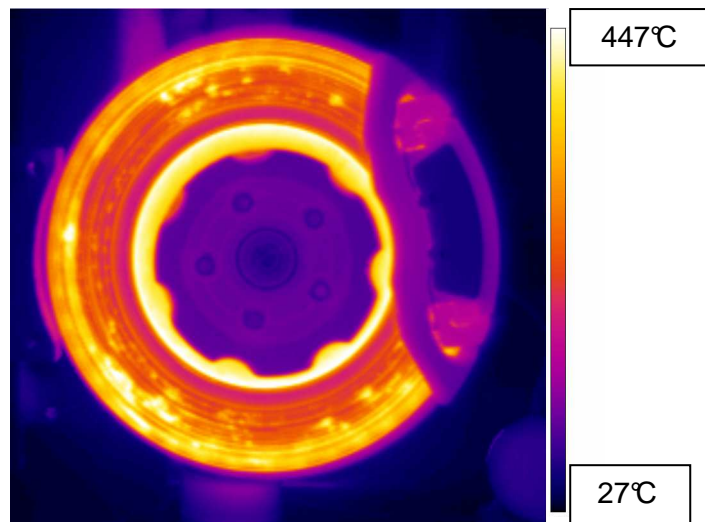


Figure 4.47: Thermal image showing thermal banding and regions of pad deposition.

Hot spotting of the brake disc surface has been seen to occur as was introduced in section 4.3.2. Figure 4.48 gives a thermal image of a disc showing hot spotting. This disc was tested at 2400r/min, equivalent to 309km/h (193mph), with an application pressure of 1.5MPa for continuity. The brakes were applied in short four second drag brake applications with four seconds of cooling between each application. As the image shows there was a link between the underlying vane geometry with the white lines on the image following the same angle as the vanes and the hot spot edges. All the brake discs used in this thesis had 40 vanes and the hot spots were equispaced about the disc which gave 10 hot spots spaced once every 4 vanes. Observation of the disc showed there to have been slight shifting of some of the associated regions of pad deposition which would indicate movement of the hot regions themselves. This disc had previously been tested at mid-speed using the test procedure described in 4.2.2, however no evidence of hot spotting had appeared under these test conditions which were performed at 1200r/min which was half the rotational speed of the test described in this section. Therefore it can be determined that there was not enough energy being dissipated into the brake disc in the form of heat at the lower speed of 1200r/min to generate the higher order wave-like distortion and subsequent focal hot spots on the friction ring surfaces. At the higher speed of 2400r/min however, the thermal energy was significant enough to generate the higher order deformation and resulting hot spots.

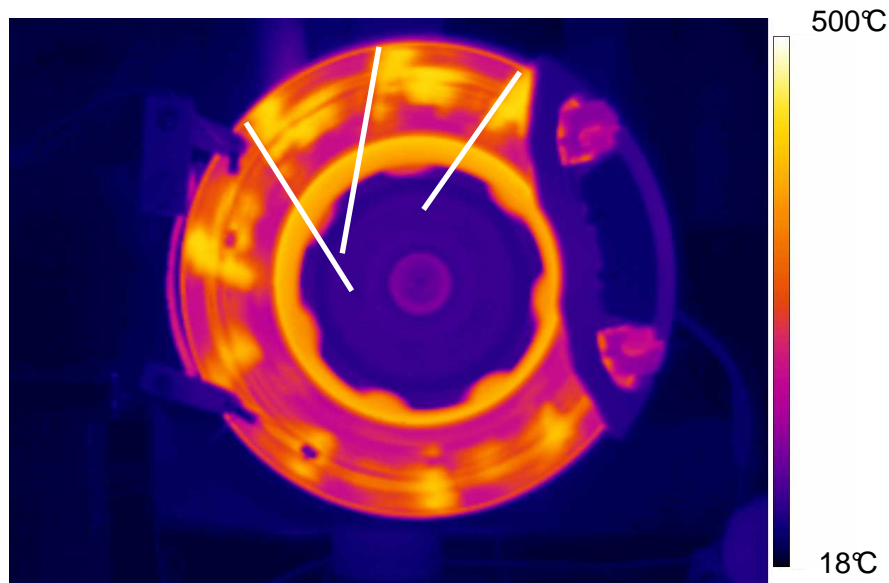


Figure 4.48: Thermal image of disc showing 10 areas of concentrated heat. The reverse side indicated the same number but positioned between the opposite side areas. Rotation CCW.

In a different test, with a new disc, 9 hot areas were established with extrapolation of the leading edge converging upon the centre of the disc, as shown in figure 4.49. This test followed identical heating conditions to the previous disc with the only difference being this disc had undergone no previous testing. Following further testing of this disc the number of hot areas increased to 18 when the testing was extended.

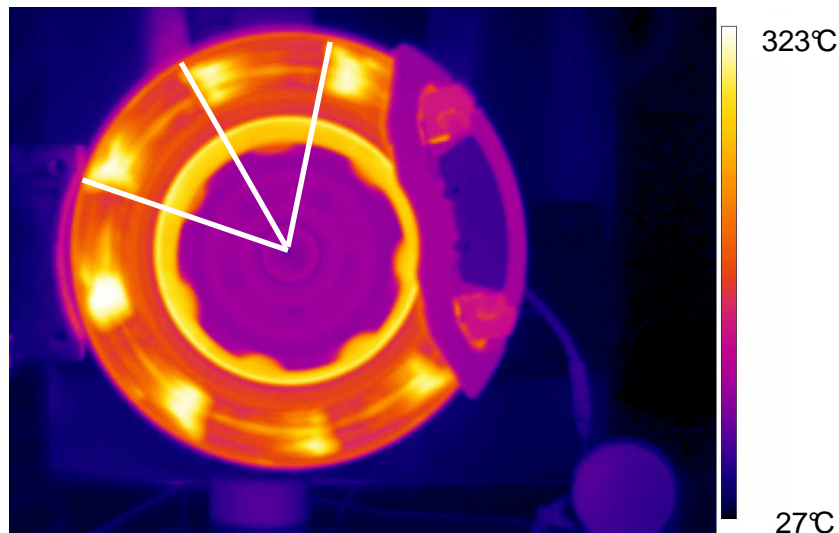


Figure 4.49: Thermal image of disc showing 9 areas of concentrated heat. The reverse side indicated the same number but positioned between the opposite side areas. Note leading edge of “hot spots” were radial, CCW rotation.

4.4. Dynamometer High Speed Testing Discussion

The antisymmetric nature of the hot spots suggested that higher order wave-like deformation of the brake disc was occurring with the peaks of these waves being unevenly heated due to increased contact pressure. This has also been suggested by Altuzarra *et al* [80] that the number of hot spots was influenced by the tangential vibration of the brake pad and the rotational speed of the brake disc; hot spots appear when the rotational speed of the disc is an integer factor of the tangential vibration. It has been proposed in section 4.3.2 of this thesis that antisymmetric hot spotting of the brake disc was a result of high order buckling (up to 11th order for the braking system used in this thesis) of the brake disc. The hot spot locations would correspond to the peaks of the buckled waveform on each side of the brake disc. Pad geometry was also likely to play a role with previous authors identifying correlations between hot spot numbers and pad length [27]. The initial patterns of hot regions identified in this research have spacing which is quite close to that of the pad arc length, therefore there could only be one hot spot beneath the brake pad at any one time. Only one test stands out as being different, however the 18 hot regions were formed on a disc which had already experienced hot spotting with associated pad burnishing and deposition and therefore cannot be used in a like for like comparison. If the disc mean circumference to pad ratio (see equation 3-19) was

reduced then the hot spotting of the brake disc would be reduced as the frictional energy would be distributed between more than one waveform peak, therefore reducing the temperature of each hot spot. This would also reduce the brake pressure variation as the brake pad would not have to ride up over each peak, instead it would slide across the top of a pair (or more) of peaks. The research has shown that hot spotting on this particular braking system is potentially influenced by the underlying vane geometry as has been shown in figure 4.48. This was a result of the buckled waveform of the brake disc being influenced by the circumferential stiffening effect of the angled vanes, but also the thermal mass of the vane. On the friction ring, there was an axisymmetric pattern of regions of higher and lower temperature, as shown in figure 4.45, this was directly caused by the presence of the thermal mass of the underlying vanes. This allowed heat to be removed from the surface and stored more quickly in the regions of larger thermal mass creating a fluctuating temperature profile on the surface of the disc. This can lead to hot spotting, as shown in figure 4.48 and figure 4.49, and in chapter 5, Finite Element (FE) simulations are presented which looked at the effect the vane geometry had on the surface temperature distribution.

4.5. Experimental Design and Testing Summary

On-vehicle testing has shown the magnitude of brake pressure variation to increase with worsening subjective judder ratings. Analysis of the pressure variation during individual braking events and individual disc revolutions has shown the nature of the pressure variation to alter dramatically as judder increases.

Dynamometer analysis has shown that the brake disc adopts a waveform during brake application which was a result of the rapid thermal expansion of the brake disc. This, as has been introduced in section 3.2.6.3 and investigated in chapter 4, caused buckling of the brake disc as a result of the compressive stress and loads caused by the rapid constrained thermal expansion of the friction rings. Brake disc deformation has been shown to be highly dynamic during a single braking event with different orders of deformation seen to develop during the first braking period alone. Increasing temperature caused thermo-plastic wave-like disc deformation which has been observed during off-brake periods with second order off-brake deformation consistently appearing on a 'hot' brake disc. Evidence has also suggested stress relief of the brake disc occurring during hot running and this has been shown to result in a 2nd order waveform. The heating and subsequent cooling of the brake disc was

removing some of the retained stresses allowing the disc to relax back to lower orders of deformation. This was allowing the phenomenon whereby the disc would adopt a second order cold shape following initial testing, however after subsequent testing the disc would then revert to a first order cold shape. Brake pressure variation has been shown to correlate with brake temperature, whilst the disc waveform has been identified as a source of brake judder and was correlated to the brake fluid pressure variation. Analysis has shown the cold state of the disc to bear little resemblance to its hot in-stop state.

Anti-symmetric hot spots have been shown to appear on the brake disc surface resulting from higher order waveforms. Hot regions appeared to be related to the speed of the disc with higher number of spots appearing with reducing disc speed as has been shown in table 4-2. Displacement transducer measurements back up this theory with higher order peaks and troughs appearing opposite each other on either side of the brake disc. The mode order of the waveform has been shown to be linked to the amount of energy transferred into the braking system, with higher mode orders occurring with larger thermal inputs. It was proposed that hot spotting of the brake system was a result of high order disc buckling.

The data and analysis performed in this chapter has provided an excellent insight into the deformation of the brake disc during use which results in thermal judder. Data from both the on-vehicle testing and the dynamometer testing has been used for FE modelling of the transient heating of the brake disc which can be found in chapter 5.

5. Finite Element Analysis

5.1. Introduction

Finite element analysis (FEA) is a very powerful tool to the brake engineer. It allows simulation and calculation of temperature, stress, strain and deflection of the brake disc. With the aid of FEA various brake disc designs can be analysed to determine whether the brake has acceptable stress and strain levels and whether it is capable of handling the required energy input during repeat braking without excessive thermal distortion or potential for failure. Factors to be considered in this are even distribution of temperature and good thermal transfer routes such as vane and vent profiles.

FEA is not a direct replacement for the testing of brake discs on brake dynamometers or by other means as the results obtained from complex finite element simulations can be meaningless without accurate validation of the applied loads and results from the simulation. Unrealistic results from a FE simulation can occur if care has not been taken to ensure that the input data, and calculations performed to derive the input data, were accurate. Assumptions and simplifications often have to be made to the model during both the modelling and application of loads. Ensuring that these assumptions and simplifications do not have a detrimental effect on the results is essential in order to produce a simulation with acceptable accuracy and a reliable solution. The initial thermal analysis performed as part of this research was focussed upon increasing the accuracy of the calculations used to define the input data, followed by an analysis of the heat distribution through the disc. These models then allowed an investigation to take place into the heat transfer through the brake disc with the aim of reducing the variation of the disc surface temperature and also providing a reduction in the maximum operating temperature. This provided a basis whereby either increased performance was available from the brake disc, or potential to reduce the mass of the brake disc whilst retaining the same heat transfer and storage performance. Reducing the variation of the brake disc surface temperature would reduce or eliminate this factor from the formation of hot spots.

5.2. Procedure

The procedure for this section of the research was to use the ANSYS 11 Workbench FEA software to simulate the heating and cooling of a whole brake disc. The method of heat application to the brake disc first had to be defined with the use of

calculations to identify the magnitude of the heat flux to be applied to the brake disc rubbing surfaces. It was necessary to identify the convective heat transfer coefficients of the brake disc, this was done using data from an associated CFD project [69][2] combined with testing on a spin rig to identify the correlation of the CFD results with measured data from a brake disc which was uniformly heated and then rotated in still air.

The FE model was constructed of a mesh of tetrahedral elements and represented a single brake disc as used by the research vehicle. The brake disc features have previously been described in section 1.4, but to summarise, the disc was 405mm in diameter, 36mm thick and had 40 vanes. The only simplification to the geometric representation of the disc in the FE model was that it had smooth interior vent walls rather than the rough cast walls of the actual brake disc. This simplification was made as no accurate CAD geometry was available which modelled the rough walls, and, even if it were available, the mesh required to represent it would need to be so small that the solution time and computing power required would be huge. The FE model also included the machined balance region – a region of the disc periphery which had a slot machined out of it in order to dynamically balance the brake disc following casting and machining.

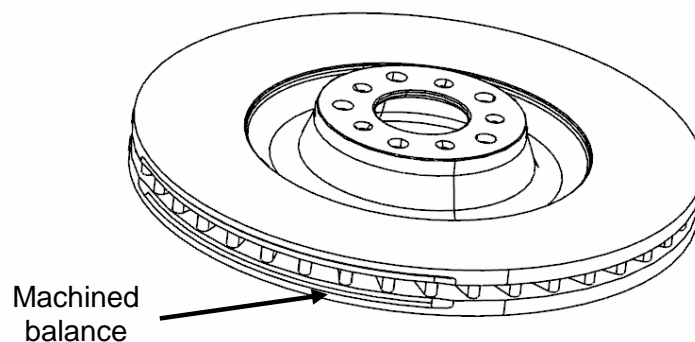


Figure 5.1: General image of the brake disc CAD model showing the machined balance

The thermal FEA simulations were validated against measured data from on-vehicle testing with a material property sensitivity analysis to improve the correlation of the results with the measured data. Simulations were then performed to identify the heat distribution through the brake disc and a new design was created to reduce the brake

disc operating temperature and to improve the heat distribution through the brake disc to reduce the propensity towards hot spotting and thermal distortion. More specific details of the procedure for each stage can be found in the associated section.

5.2.1. Heat Flux

Highly detailed finite element models can take up a long time to both create, with a structured mesh of high density elements, and to solve [53]. There is always a trade off between the accuracy of the model and the resources available, be they computational or time. Therefore simplifications invariably have to be made to the models to account for either limits on computational resources or time. The method used in this thesis to perform a thermal analysis of a brake rotor required a heat input to be applied to the friction ring surfaces of the rotor in the form of heat flux. Other methods of simulating the heat distribution were available, such as a fully coupled thermo-mechanical analysis whereby the rotation of the disc is simulated together with contact interactions between disc and pad, however generating such a simulation is a highly time consuming process and the work required is sufficient for a thesis in itself as the frictional heating, wear and deformation of a disc and pad interaction is highly complex. For simplification purposes, in the simulations performed as part of this thesis, the heat was applied to the entire friction ring surface covered by the brake pad in one revolution of the disc, rather than the area covered by the stationary pad. This simplification was carried out as it was assumed that the heat was swept around the disc surface by the pads to give full coverage of the disc in one revolution.

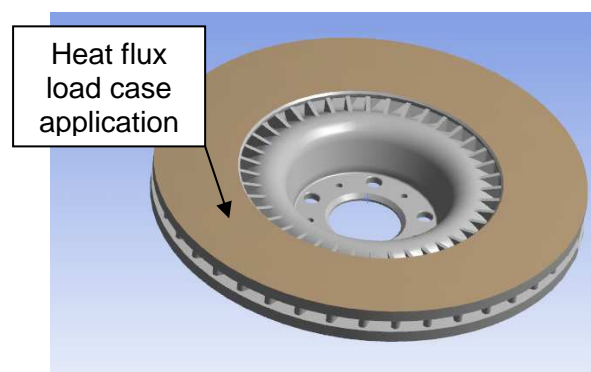


Figure 5.2: Image showing heat flux application to the friction ring surfaces (inboard friction ring shown)

For the purpose of this research a simplified transient thermal model of a stationary brake disc with heat flux being applied to each friction ring was modelled. Transient simulations were chosen because the purpose of the investigation was to identify temperature distribution over time; with a steady state analysis only constant heat flux loads could be applied, this was not representative of the actual system where the heat flux loads were non-linear due to the aerodynamic drag force on the vehicle which was proportional to the square of the vehicle speed and aided vehicle deceleration. With a transient model the heat flux loads were non linear and therefore more representative of the actual system. This allowed for investigation of heat flow through the brake disc due to the transient heat flux loads, whilst identifying any areas of concern. By taking this approach a much wider outlook could be accomplished which encompasses many different research approaches to combine both testing and simulation. Whilst this was not a like for like simulation, the results presented in section 5.2.3 demonstrate that this method has good correlation with measured data.

5.2.2. Energy Calculations

During deceleration, the vehicle brakes dissipate the kinetic energy of the vehicle mainly by converting it to heat. Some energy will be dissipated in the form of chemical reactions and noise, however these are negligible [82] when compared to the amount of thermal energy.

Heat flux is defined as power per unit area. Therefore to calculate the heat flux one must obtain the energy dissipated by the vehicle during a braking event:

At a steady speed on a level surface, knowing the vehicle mass (m_v) and velocity (V) the kinetic energy (KE) can be calculated as

$$KE = \frac{1}{2} m_v V^2 .$$

5-1

So to decelerate from velocity V_1 to velocity V_2 , the kinetic energy at velocity V_2 must be subtracted from the kinetic energy of the vehicle at velocity V_1 with the result being the energy dissipated during braking

$$KE = \left(\frac{1}{2} m_v V_1^2 \right) - \left(\frac{1}{2} m_v V_2^2 \right). \quad 5-2$$

However the rotating inertia of the driveline components also needed to be considered, these added their own kinetic energy to the system. This could be defined knowing the inertia (I_D) and angular velocity (ω) of the components

$$KE_I = \left(\frac{1}{2} I_D \omega_1^2 \right) - \left(\frac{1}{2} I_D \omega_2^2 \right). \quad 5-3$$

This gave the total kinetic energy as

$$KE_T = \left(\left(\frac{1}{2} m_v V_1^2 \right) - \left(\frac{1}{2} m_v V_2^2 \right) \right) + \left(\left(\frac{1}{2} I_D \omega_1^2 \right) - \left(\frac{1}{2} I_D \omega_2^2 \right) \right). \quad 5-4$$

However for this both the inertia of the individual rotating components and their radii must be known. For the vehicle in question, data for the inertia of the rotating components was not available, therefore a constant, k , was used and its value was used to match the output from the equations to the experimental data. For the simulations performed in this thesis, k had a value of 1 which gave good correlation.

Assuming constant deceleration, mean braking power (P_b) was equal to kinetic energy (KE_T) divided by stopping time (t_s)

$$P_b = \frac{KE_T}{t_s}. \quad 5-5$$

Stopping time was found from the relationship whereby final velocity was equal to the initial velocity minus the product of deceleration and braking time. The rate of deceleration during a vehicle braking test performed for this thesis was constant, therefore it was not necessary to take into account the additional resistances to motion, such as aerodynamic drag force and rolling resistance acting on the vehicle, when calculating stopping time. Therefore the relationship was

$$V_2 = V_1 - at_s. \quad 5-6$$

Rearranging for time and expressing the vehicle acceleration, a , as a function of gravity (g) gave

$$t_s = \frac{(V_1 - V_2)}{z \times g}. \quad 5-7$$

Taking into account the proportion of braking force acting on the front axle x_f , the braking power at one side of one front rotor P_{bf} , was proportional to the product of the braking power and the proportion of braking force acting on the front axle

$$P_{bf} = P_b \times x_f \times 0.5 \times 0.5. \quad 5-8$$

Heat flux is defined as power per unit surface area; in this case the surface area of one friction ring (A_D), this gave

$$\dot{q} = \frac{P_{bf}}{A_D}. \quad 5-9$$

At high velocity and low rates of deceleration aerodynamic drag force played an important role and comprised a significant proportion of the forces which aided the vehicle deceleration. It must therefore be taken into account to yield accurate results. Knowing the coefficient of drag (C_D), the density of air (ρ), the vehicle velocity (V_n) and the frontal area of the vehicle (A_V) the aerodynamic drag force (D) on the vehicle was defined as

$$D = \frac{1}{2} C_D \rho V_n^2 A_V \quad [81]. \quad 5-10$$

This gave a drag force at a specific speed which can be equated to a deceleration using Newton's 2nd law of motion to give the acceleration due to drag (a_D) as

$$a_D = \frac{D}{m_V} \quad 5-11$$

or

$$a_D = \frac{C_D \rho V_n^2 A_V}{2m_V}. \quad 5-12$$

It was also necessary to take into account the rolling resistance of the tyres which exhibited a resisting force to the forward motion of the vehicle

$$R_R = m_V g R_C. \quad 5-13$$

For the purpose of the calculations a value for the coast down deceleration of the vehicle was used which took into account driveline drag and rolling resistance, therefore a constant of 0.07g was used, this was provided from vehicle manufacturer data [23] and was termed r_r . Using the coast down deceleration and the deceleration due to aerodynamic drag, the proportion of vehicle deceleration due to the brakes was obtained. This was then used to calculate the heat flux.

Finally the brake pads absorb some of the energy during braking. Past research carried out by Tirovic [84] has generally identified 1% of the energy to be absorbed by the brake pads. However Day *et al* [82] have identified that varying temperature distributions between disc and pad occur due to changing interface pressure distribution as a result of wear and thermal expansion. However for simplification in this study a constant value has been used based on the research by Tirovic [84], therefore a value of 0.99 was used for η_d . This gave the following equation for the instantaneous heat flux for a single friction ring of a disc on the front axle of the vehicle

$$\dot{q}_n = \frac{(0.125m_V k (V_n^2 - V_{n+1}^2) x_f \eta_d)}{((t_{n+1} - t_n) A_D)} \times \left(1 - \frac{\left(\left(\frac{C_D \rho V_n^2 A_V}{2m_V g} \right) + r_r \right)}{a} \right). \quad 5-14$$

The initial ramp up in heat flux has not been modelled. This was the initial period where the brake pads came into contact with the brake disc. Investigations by Tirovic [84] have indicated that the time when maximum heat flux is achieved had little influence on the overall simulated disc temperature, however stability of the FE solution may be affected using this idealised modelling resulting from the “high and instantaneous power jump”. Idealised modelling of the initial contact between disc

and pads has been used for this research, that is the disc and pads were assumed to achieve maximum braking power instantaneously; this has shown good correlation with experimental data and is shown in section 5.2.3.1. The effect of tyre slip has also been ignored in this equation; tyre slip can be as much as 20% at high rates of deceleration [83][84], however the rates of deceleration in this study were low (typically 0.3g) and therefore the energy dissipated through tyre slip was negligible.

5.2.3. Modelling

The heat flux history generated using equation 5-14 is shown in figure 5.3 using the speeds recorded during three consecutive braking events from the on-vehicle testing. The heat flux fell to zero at the end of each braking event, rather than steadily decreasing, because the braking force was released before the vehicle came to rest in the on-vehicle testing, therefore to model this the heat flux had to be zero at the time when the brakes were released.

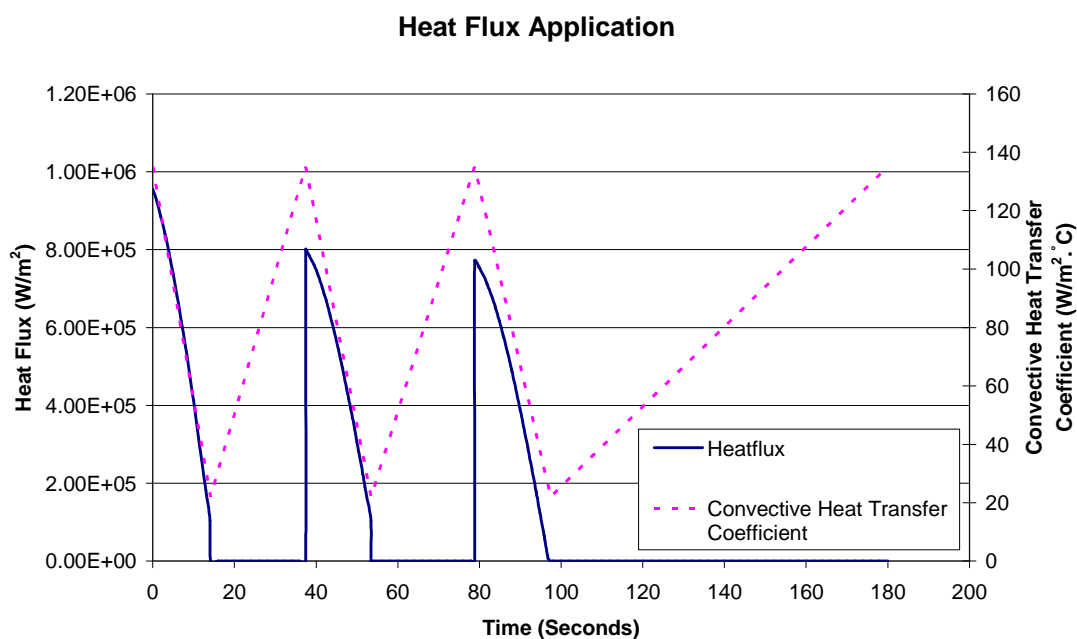


Figure 5.3: Standard heat flux application for a 3 stop test based on-vehicle data.

For the type of thermal simulation being performed, the convective heat transfer coefficients were obtained from a collaborating computational fluid dynamics study [2] and combined with measured data from the vehicle manufacturer [23]. The applied convective heat transfer data is also plotted on figure 5.3, and it can be seen that the application of the data was linear. This was a large simplification as

convective heat transfer was speed dependent; however the method used has provided results with suitable accuracy. Convective coefficients would also vary along the length of the vent walls, however to simplify the simulation this was not modelled as localised convective coefficients for the vent walls were not available within the timeframe of this section of the research. Application of a global convective heat transfer coefficient gave good correlation with on-vehicle test data as can be seen later in this section in figure 5.10.

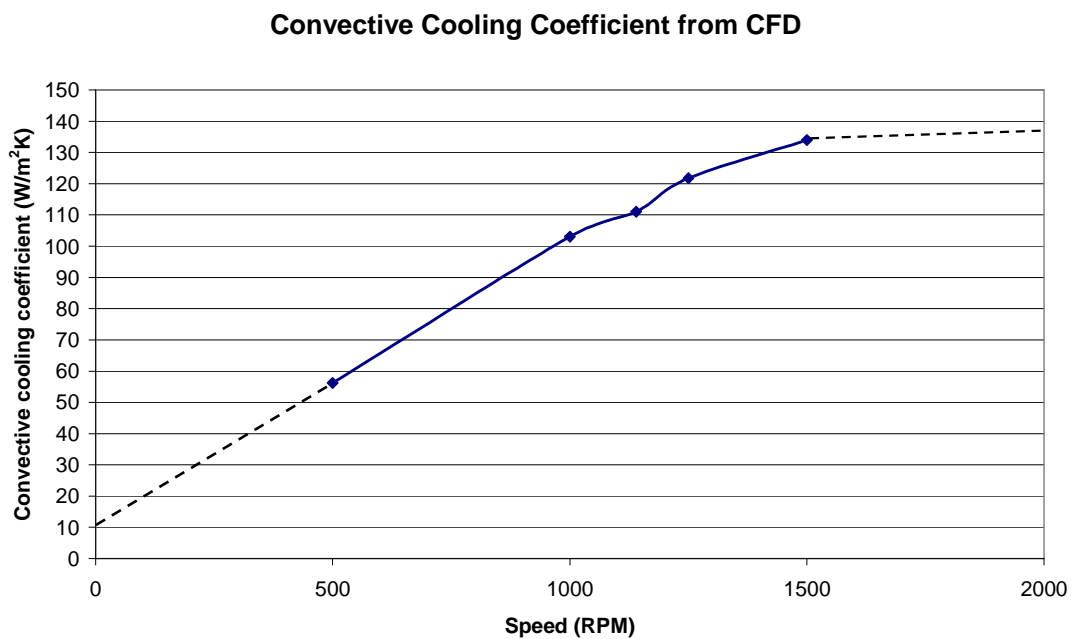


Figure 5.4: Convective cooling coefficient graph with data obtained from CFD.

The cooling coefficient curve can be seen in figure 5.4. It must be noted that data was only available for the speed range between 500-1500r/min. The curve has been linearly extrapolated outside of these ranges based upon measured data from the vehicle manufacturer which gave the maximum convective heat transfer coefficient of the brake disc as $136\text{W.m}^{-2}.\text{K}^{-1}$ [23]. At zero rotational speed the graph has been linearly extrapolated to give a heat transfer coefficient of $10\text{W.m}^{-2}.\text{K}^{-1}$. There was no simulated variation in cooling coefficient between the friction rings and vanes; however the cooling data varied linearly with speed.

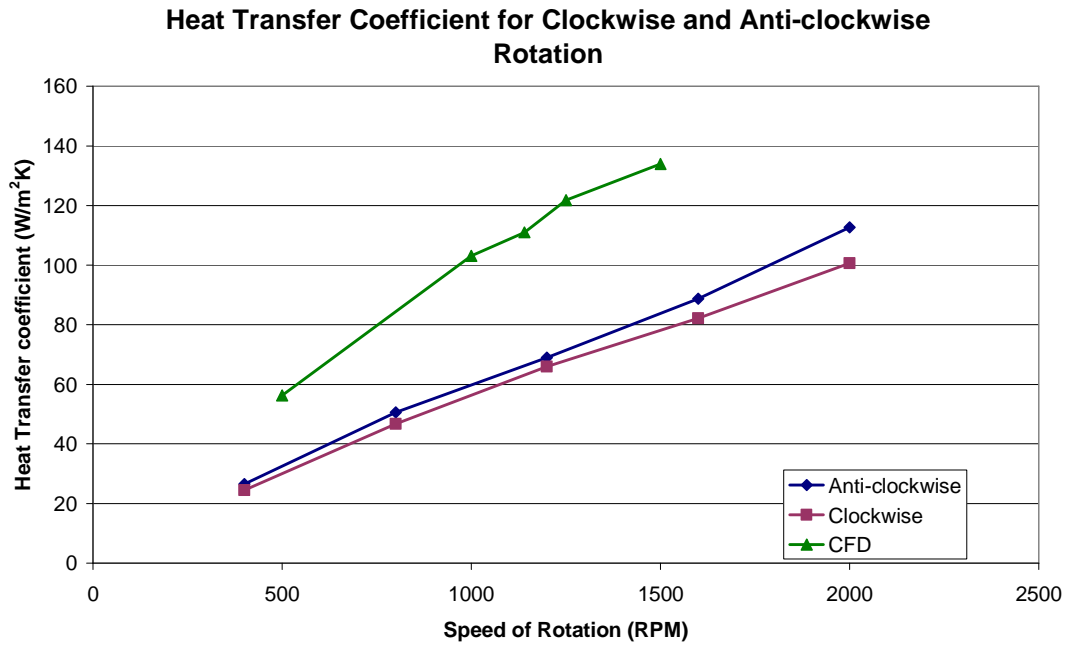


Figure 5.5: Heat transfer coefficient for clockwise and anti-clockwise rotation.

Shown in figure 5.5 is a graph of heat transfer coefficient which was measured on the Cranfield University spin rig. The procedure for the 'spin rig' study involved heating of the brake disc using an induction heater to an even temperature of 400°C. The disc was then rotated at a constant speed whilst the surface temperature was recorded with four rubbing thermocouples. Insulation between the disc and motor shaft minimised heat loss through conduction, limiting heat transfer to convection and radiation. The test was repeated at speeds of 1200, 1600 and 2000r/min both clockwise and anti-clockwise. This method allowed the idealised cooling performance of the brake disc to be characterised. The contrasting heat transfer coefficient obtained from the CFD study [2] is also shown for comparison. It can be seen that the CFD study simulated a higher convective cooling curve than that of the spin rig. However the test conditions must be taken into account. Firstly the disc was rotated in a contained environment with no wind effects or cross-flow across the brake disc as would be seen on-vehicle, however the conditions were very similar to that of a dynamometer simulation. Another more important factor is the method of heat application. On the spin rig an induction heater was used to heat all of the disc material, this induces eddy currents within the cast iron and also causes hysteresis heating due to the alternating magnetic field. Both of these effects caused rapid heating of the whole brake disc inside and out. As a result there was no initial temperature gradient and heat could only be transferred away by convection.

Whereas on-vehicle and on the dynamometer, heating was caused at the interface between the brake pad and friction ring surface. The heat then transferred by conduction through the material from the surface as a result of the temperature gradient between the hot surface of the disc and the cooler vent walls before being transported away by convection and radiation. As described in section 1.4, the brake disc used for this thesis had a 'handed' design, whereby the vanes cranked through an angle. The results presented in figure 5.5 show that there was a difference between the clockwise and anti-clockwise convective heat transfer coefficients of the whole brake disc. This difference increased with rotational speed and was found to be at a maximum at 2000r/min where there was a 10% difference between the two.

To further reduce the complexity of the FE analysis and speed up solution time the model only represented a brake disc; none of the other components of the brake assembly were modelled, therefore conduction to the wheel and hub was not modelled. A further simplification was that the disc was stationary and did not rotate. In reality heat would be swept around the rotating brake disc by the brake pads. Therefore the assumption has been made that the heat would be distributed evenly around the surface of the brake disc by the pads. On the actual braking system heat transfer via radiation increased with disc temperature with the heat loss due to radiation being proportional to the disc surface temperature to the power of 4 [84]. This could be defined using the Stefan-Boltzmann formula for a grey body in which the radiant emittance, W , is equal to the product of the emissivity, ϵ , the Stefan-Boltzmann constant, σ , and the temperature, T , to the power of four [79]

$$W = \epsilon\sigma T^4 \text{ (Watts/m}^2\text{)}. \quad \mathbf{5-15}$$

For this study the convective heat transfer coefficients obtained from the CFD study [2] included the effects of heat loss by conduction and radiation as they were validated using brake disc temperature data from on-vehicle testing (Figure 3.34) which included heat loss via convection to the air, conduction through the disc to the hub and radiation from the exposed brake disc surfaces. Therefore the convective coefficients used for the FE study represented the whole disc heat transfer coefficient (convection + conduction + radiation) and therefore were larger than those obtained from the spin-rig study seen in figure 5.5 which were solely a result of heat loss through convection.

Vehicle Front Brake Disc Temperatures

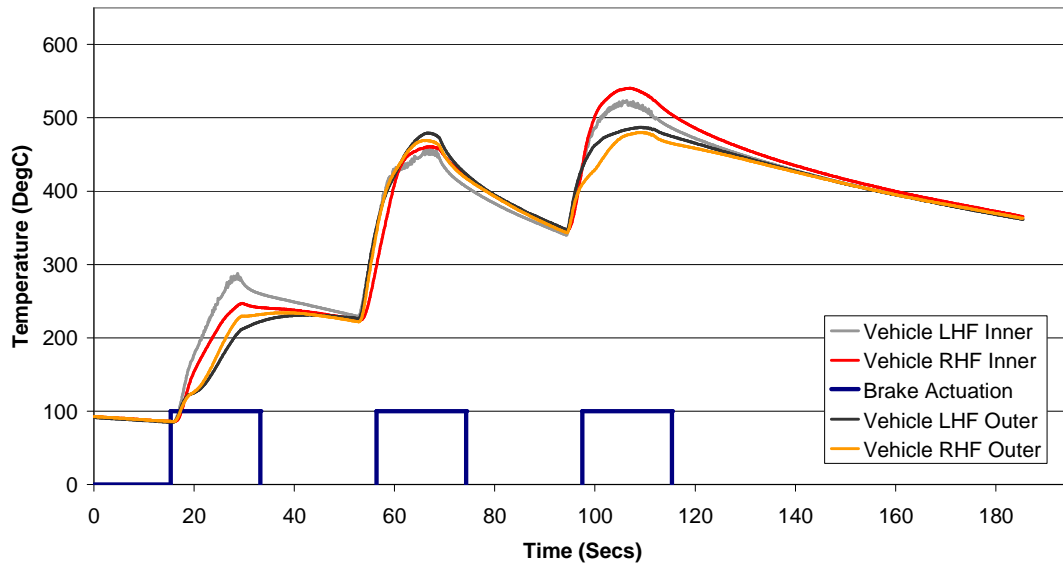


Figure 5.6: Brake disc temperatures from vehicle testing.

Figure 5.6 presents data from actual on-vehicle testing. Shown are temperature plots for the front brake discs measured using embedded thermocouples mounted in the inner and outer friction ring on each of the two discs. Each braking event was performed from 240km/h to 50km/h at a constant 0.3g rate of deceleration. The data identified that the inner friction ring was the hotter of the two rubbing surfaces. This was an expected effect as the outer friction ring was directly connected to the hub mounting face which acted as a heat sink therefore lowering its temperature. The inboard disc face was only connected to the hub and swan neck via the thin vanes and therefore had thermal mass and less direct conductive heat transfer path. A common design trend is to have a thicker friction ring on the inboard side to allow it to offset the lower thermal mass when compared to the outboard friction ring and swan neck; however the brake disc design used for this thesis, shown in figure 5.7, did not employ this design.

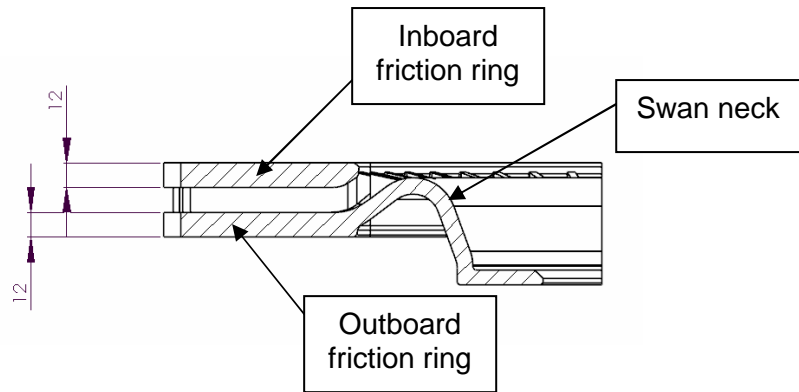


Figure 5.7: Cross section through brake disc showing equal friction ring thicknesses.

This could pose problems with buckling of the disc or even disc cracking due to uneven thermal gradients between the inner and outer friction ring giving different thermal expansion. These three braking events were selected for validation of the finite element simulations as they caused large temperature rises of over 200°C during each individual braking event followed by a long cooling period as can be seen in figure 5.6. Simulation of these braking events allowed for an analysis of the rapid build up and subsequent dissipation of heat in the brake disc and enabled an analysis of the surface temperature distribution resulting from the disc vent profile, this is described more detail in sections 5.3 and 5.4.

5.2.3.1. Material Property Sensitivity Analysis

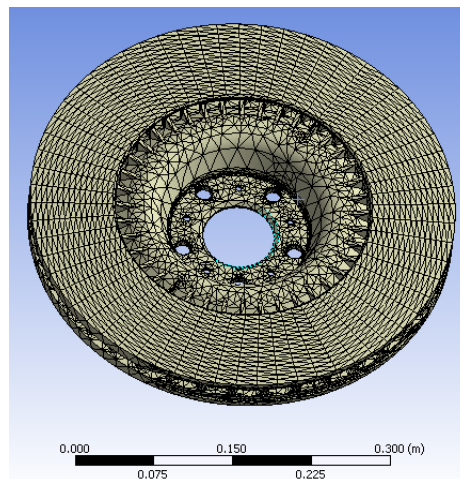


Figure 5.8: Mesh for the finite element model.

As part of the FE modelling procedure a material property sensitivity analysis was performed. The purpose of this analysis was to identify the effect which fully temperature dependent material properties had on the correlation of the FE results when compared to the data obtained from the on-vehicle testing. Each FE model

contained a structured mesh of 250000 elements as seen in figure 5.8. The initial disc temperature was set to 80°C to correspond with the start temperature of the measured data, whilst the ambient temperature was set at 20°C. The initial FE models used isotropic constant material properties for cast iron; these material properties were then modified in subsequent simulations to produce models which used temperature dependant material properties for comparison. The results and details from this study are presented in figure 5.9 and the discussion follows on the next page. The temperature dependent material properties were for a GG15HC grey cast iron and were supplied by the brake disc supplier and can be seen in table 5-1. Data for the temperature range of 600-1200°C was interpolated automatically by the FEA software.

Temperature (°C)	Young's Modulus (MPa)	Poisson's ratio (-)	Coefficient of thermal expansion 1.00E-06	Thermal conductivity (W.m ⁻¹ k ⁻¹)	Specific heat capacity (J.kg ⁻¹ K ⁻¹)	Density (kg.m ⁻³)
0	96725	0.25	8.84	53.3	457	7250
20	96000	0.25	9	53.1	460	7250
100	93100	0.25	9.65	52.5	474	7250
200	89600	0.25	10.46	51	488	7250
300	86300	0.25	11.23	49.5	502	7250
400	83000	0.25	11.99	49	516	7250
500	79900	0.25	12.75	48	530	7250
600	76900					
700	74100					
800	71300					
900	68100					
1000	66000					
1100	63000					
1200	61200					
1300	58900	0.25	18.83	40	642	7250

Table 5-1 – GG15HC cast iron material properties.

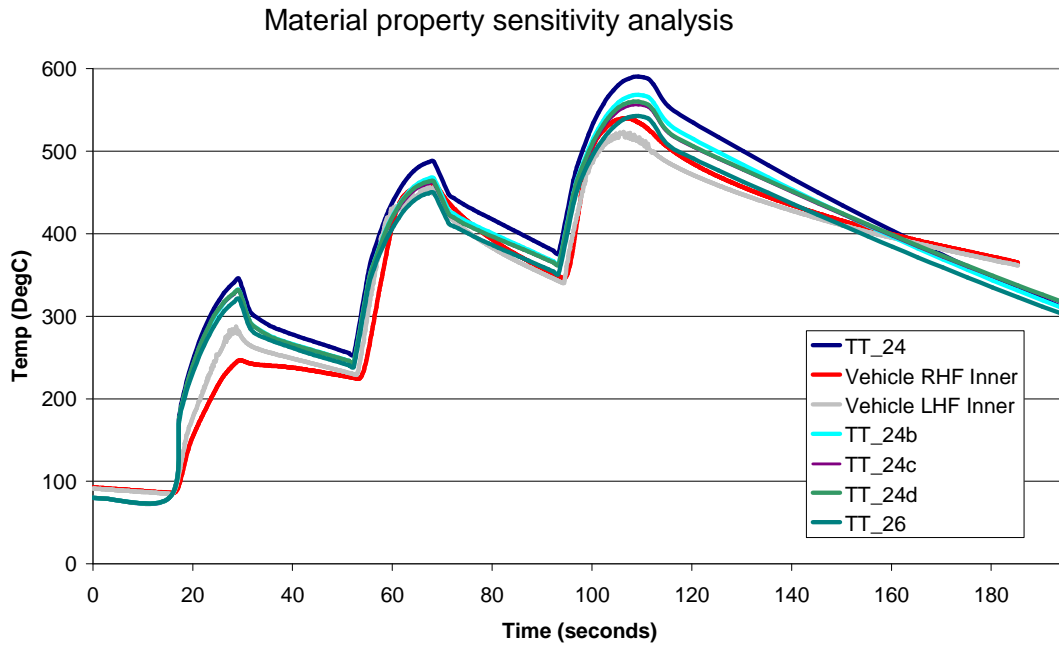


Figure 5.9: Graph showing simulated brake disc temperature resulting from varying the brake disc material properties.

Figure 5.9 shows the effects of varying the brake disc material properties and the effect of taking drag into account as part of the vehicle deceleration. The graph line TT_24 was generated using the results from a simulation which used constant material properties which did not vary with temperature. The material properties used were the default values for a grey cast iron provided by the ANSYS software and can be seen in table 5-2.

Young's Modulus (MPa)	Poisson's Ratio	Coefficient of Thermal Expansion	Conductivity (W.m ⁻¹ K ⁻¹)	Specific Heat Capacity (J.kg ⁻¹ K ⁻¹)	Density (kg/m ³)
110000	0.28	1.1x10 ⁻⁵	52	447	7200

Table 5-2: Constant material properties provided by the ANSYS 11 software.

It can be seen that there was an over prediction in the brake disc surface temperature of around 50°C when compared to the on-vehicle test data. In comparison the graph line TT_24b was generated using the results from a simulation which used a higher specific heat capacity. The value used was 488J.kg⁻¹.K⁻¹, which was obtained from the manufacturer data for 200°C shown in table 5-1. Using this value for the specific heat capacity gave a maximum temperature drop of 20°C when

compared to the previous value of $448 \text{ J.kg}^{-1}.\text{K}^{-1}$. Temperature dependent specific heat capacity was introduced in TT_24c using the data from table 5-1, and showed again more improvement in the correlation, whilst in TT_26 fully temperature dependent material properties were used based on manufacturer supplied data from table 5-1. Overall this showed that temperature dependent material properties had a significant effect on the simulation calculated temperature and its correlation with the measured data. The variation of the simulated data from the measured data can be seen in figure 5.10, with typically a $\pm 5\%$ variation seen during the second and third braking event. The first braking event had a much higher variation associated with it, in the order of $\pm 15\%$, however it must be noted that the temperature measured by each thermocouple for the recorded data varied by approximately $\pm 10\%$ for this particular braking event. The reasons for this have already been discussed in section 3.2.6.2, that it was due to the brake system being allowed to cool prior to the set of braking events shown. As a consequence the thermal contraction of the pads caused them to no longer conform uniformly to the brake disc surface – the hotter region of the pad at the centre of pressure would experience higher wear resulting from the increased contact pressure caused by localised thermal expansion. Upon cooling this region would become concave due to thermal contraction and wear, giving a non-uniform contact area upon the next brake application. Therefore the heat generation was also non-uniform on each braking face creating the temperature variation between each friction ring.

Comparison of FE model to Vehicle Data

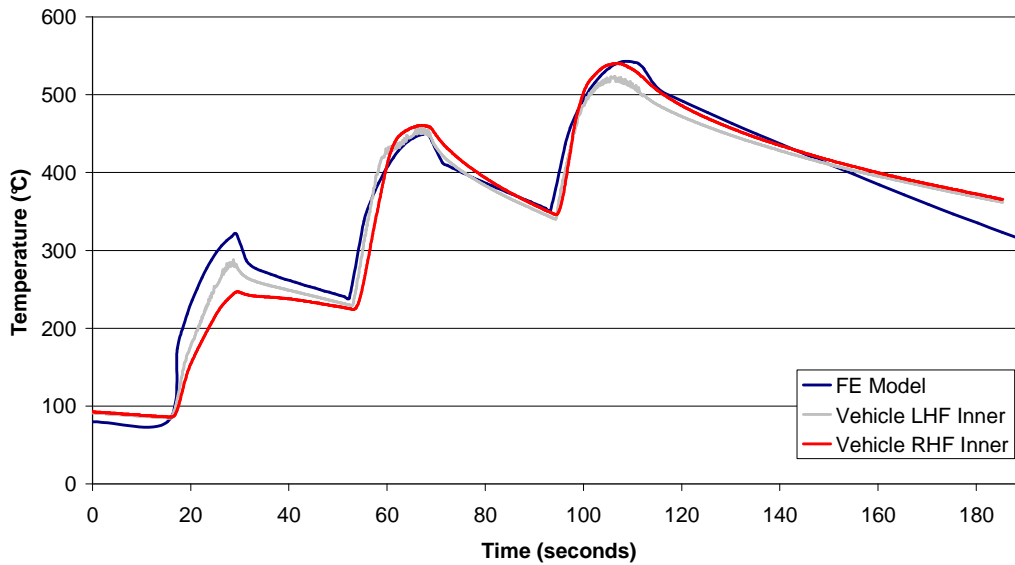


Figure 5.10: Graph showing simulated temperature against measured data.

All the above models used blanket convective cooling coefficients obtained from a collaborating project [2], the graph of these values can be seen in figure 5.4. It can be seen in figure 5.10 that the simulated disc temperatures in the final cooling phase fell quicker than the measured data. This indicated that the linear cooling curve, shown in figure 5.3, used for the simulation did not fully represent the actual vehicle conditions in the final cooling phase. However the FE study in this thesis was mainly focussed upon the heating phase and the simulated data showed good correlation for the three braking events therefore no modification to the convective heat transfer coefficients was required.

5.3. Results

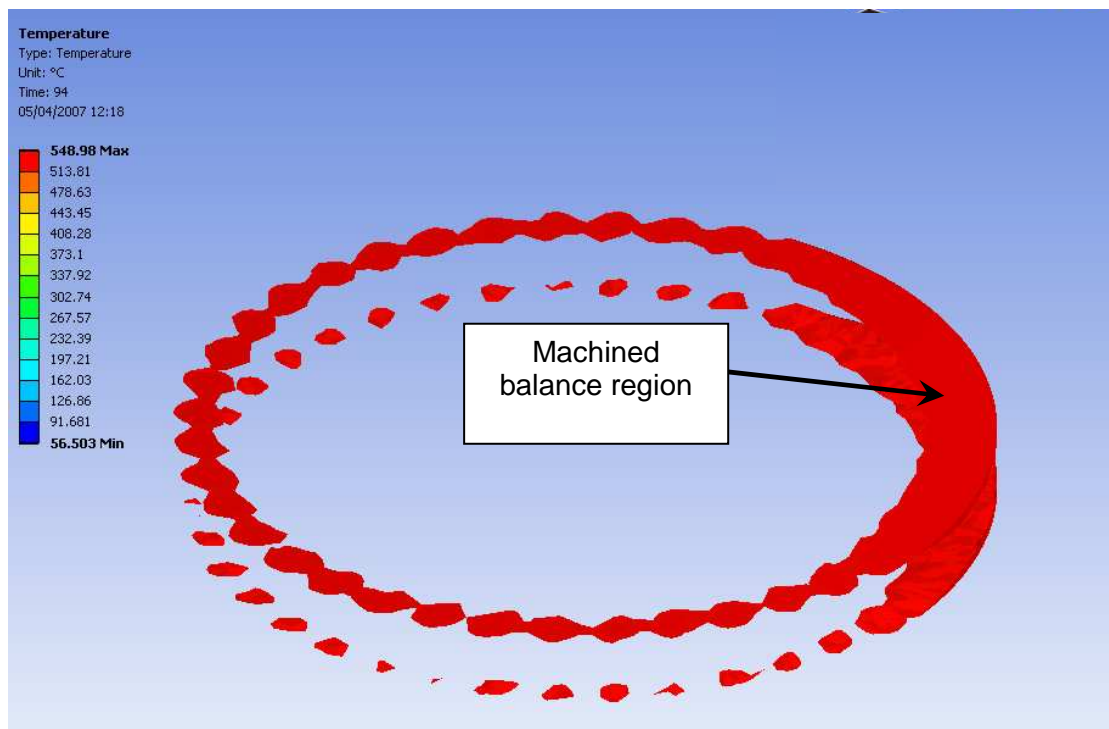


Figure 5.11: Simulated disc surface temperature following three high speed stops.

The transient simulation of repeated high speed braking events shown in figure 5.10 has identified thermal gradients beginning to form within the vanes (figure 5.12) and on the surface of the brake disc. These simulations have been validated against measured data on a vehicle. Figure 5.11 shows hot spots which formed on both friction ring surfaces as a result of the thermal gradient caused by the disc vanes, whilst figure 5.12 shows a cross section through the disc showing the thermal gradient within the vane structure. The image shown in figure 5.11 showed hot regions forming on the disc surface, whilst only 5°C hotter than the surrounding material (not shown) it was important to note that this was occurring after only three braking events. These hot spots coincided with the position of the vane gaps (or vents). Also shown was the tendency for a hot region to form which coincided with the position of the machined balance. The machined balance was a section of material which was removed from the outer periphery of the brake disc to dynamically balance it during manufacturing. The rough cast surfaces on the interior vent walls caused an imbalance within the disc which had to be counteracted by machining an arc from the outer disc diameter. In the FE simulation this region of the brake disc experienced hotter temperatures due to the reduced thermal mass caused by the removal of metal for balancing purposes. This caused a reduction in the rate

of heat conducted away from the surface in the localised region of the machined balance. In the above case the surface temperature around the machined balance was 10°C hotter than the surrounding material after three braking events.

This slight temperature variation could become important at elevated disc temperatures. Should the surface temperature of the disc rise to around 720°C followed by rapid cooling then the additional 10°C localised surface temperature variation could cause localised martensitic transformation of the cast iron grain structure. This would occur as the localised surface temperature would be in excess of the martensite start temperature of 726°C; this coupled with rapid conduction of heat to cooler regions of the brake disc would cause the martensitic transformation.

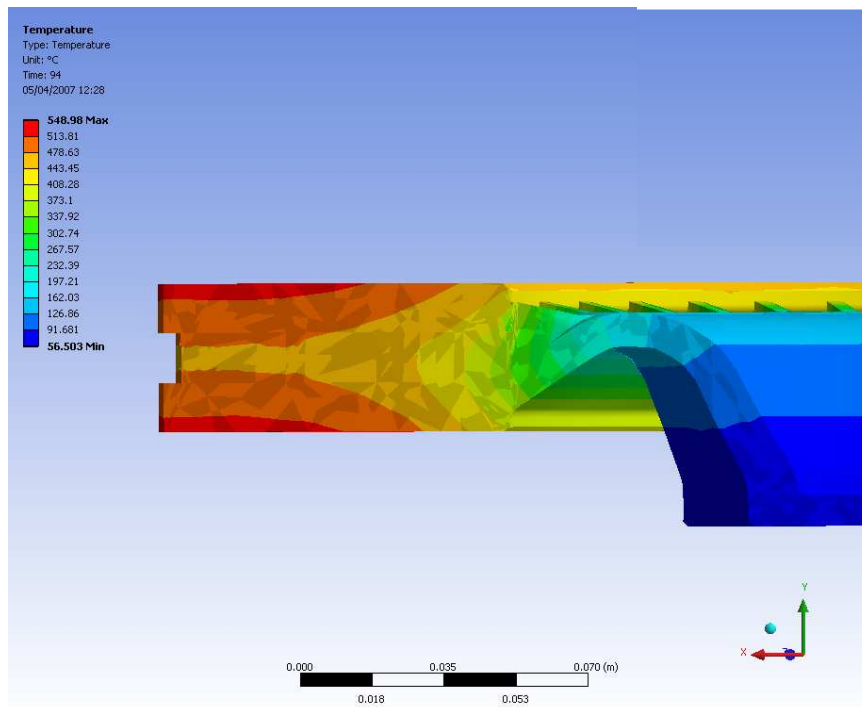


Figure 5.12: Simulated temperature gradient through a vane cross-section.

Shown in Figure 5.12 is the temperature gradient which was present within a vane cross section after the 3rd braking event. The centre of the vane had a temperature of 460°C, whilst the friction ring surfaces were some 70°C hotter. Following a one minute simulated period of cooling there was still a 10°C temperature gradient between the centre of the vane and surface of the friction rings.

A reduction in both disc temperature and surface temperature variation and lower thermal gradient through the disc thickness would help to reduce brake judder. As

was described in section 3.2.6.3, the large thermal gradients that were caused during braking, constrained the thermal expansion of the friction ring. This caused disc buckling which could lead to brake judder and hot spotting as shown in section 4.3.2. By creating a lower thermal gradient within the thickness of the friction ring the brake disc could distribute the heat through the brake disc more evenly; this would reduce the maximum disc temperature and therefore reduce the thermal expansion and subsequent distortion of the brake disc. Section 5.4 has looked at modifications to the disc design to achieve this.

It has been suggested that the convective cooling provided by the vanes of the brake disc provide the main benefit of cooling between brake applications with heat transfer coefficients not typically high enough to provide significant cooling during braking [36]. The following analysis aimed to identify the dominant modes of heat transfer and at what point during the braking cycle they occurred.

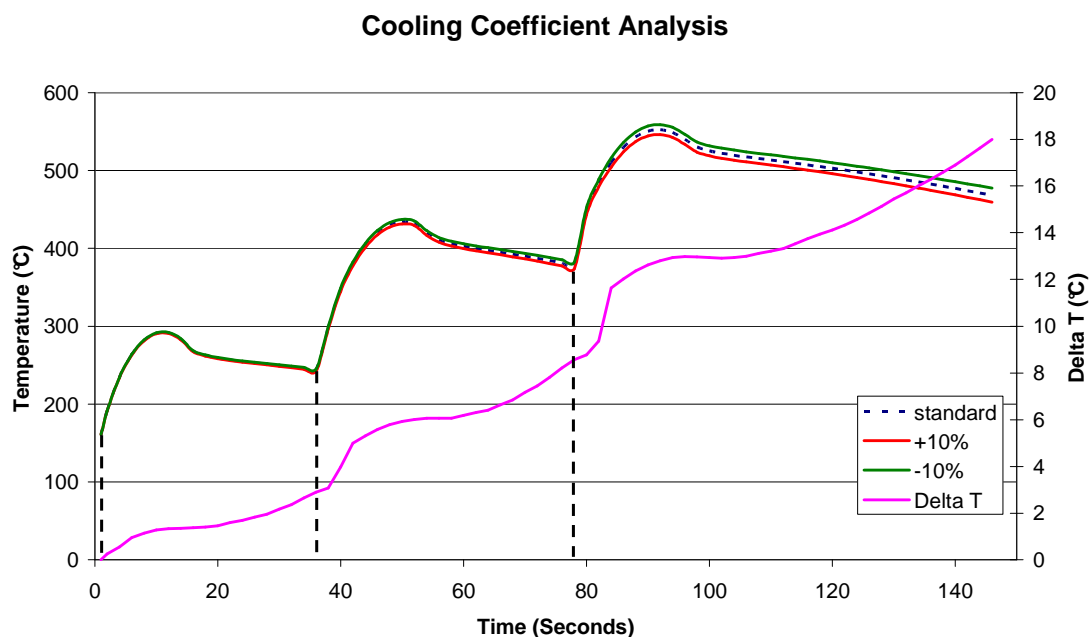


Figure 5.13: Results of adjusting the convective heat transfer coefficient by $\pm 10\%$, application of braking loads indicated by dotted line

A cooling sensitivity analysis was performed to assess the effect of a $\pm 10\%$ change on the convective heat transfer coefficient, the results of which can be seen in figure 5.13. The convective coefficients for each of the three simulations can be seen in table 5-3. The baseline data was determined by correlating vehicle speeds, from the

on-vehicle test data, with the graph of convective heat transfer coefficients shown in figure 5.4. The $\pm 10\%$ coefficients were derived from the baseline data.

Convective heat transfer coefficient Time (seconds)	-10%	Baseline	10%
0	121.5	135	148.5
14.18	19.8	22	24.2
37.44	121.5	135	148.5
53.51	19.8	22	24.2
78.85	121.5	135	148.5
97.47	19.8	22	24.2
180	121.5	135	148.5

Table 5-3: Convective heat transfer coefficients used for the cooling sensitivity analysis

The graph in figure 5.13 showed that the convective coefficient had its most dominant effect at high speed as would be expected because the coefficient was speed dependant and increased with increasing vehicle speed. This could be seen in the time period between 53-78 seconds. The vehicle had performed its second braking event and was now accelerating back up to speed, with peak speed being achieved at approximately the 78 second mark. At this point there was a noticeable difference between the +10% and -10% plots with +10% being 8°C cooler as would be expected due to the increased cooling coefficient. During the subsequent braking phase however, shown between 78-97 seconds, the gradient of the delta T plot (temperature difference between the +10% and -10% plots) did not increase significantly until 2 seconds into the braking period; this could also be seen for the previous braking event at 36 seconds. This was due to the applied thermal loads dominating the heat transfer mechanism in the early stages of braking, i.e. the heat flow in was far greater than the heat flow out of the disc and the increase in cooling had no overall effect. After this initial period the 10% increased cooling coefficient began to have an increasing effect as was indicated by the increasing gradient of the Delta T plot. Towards the end of the braking period the effect of the increased cooling began to tail off with the delta T gradient being zero at the release of the braking loads. At this point, indicated at the 14, 53 and 96 second mark, the zero gradient indicated that conduction was the dominant mode of heat transfer since the

increase in heat transfer coefficient had no effect on the delta T plot during the first few seconds after braking.

This was of interest because it identified where increased disc convective cooling was of benefit. The data identified that for this particular braking simulation convective cooling was most dominant 2 seconds into the braking period and tailing off heavily towards the end of the braking event with little effect for the first 3 seconds after the braking loads were applied. This highlighted that during the first few seconds of braking in order to achieve an even surface temperature, improving the heat transfer through conduction should be the primary aim to manage the large rate of heat flow into the disc, this was also the case at low speeds when the braking loads have been released and convection was low. Another point of note was that despite the 20% difference in heat transfer coefficient between the +10 and -10% curves, there was only an 18°C reduction in temperature at the end of the simulation, or to put it another way only 3.8% of the standard disc temperature. This was an indication that effort should be placed on managing the heat flow in combination with increasing the convective cooling, and in doing so a reduction in maximum disc temperature may also follow. Therefore section 5.4 of this thesis has looked into the effect of modifying the internal vent profile. The aim of this was to improve the heat flow through the brake disc, to reduce the thermal gradients on the surface of the brake disc and to reduce the overall disc temperature in an effort to reduce thermal distortion of the brake disc.

5.4. Improvement to Current Disc Design

5.4.1. Introduction

It is generally known that a non uniform temperature field around the friction ring on a brake disc can have a detrimental effect with regards to brake judder. A non uniform temperature distribution around the rubbing path would be the initial perturbation necessary for hot spotting [27]. Regions of high temperature would experience larger thermal expansion than the surrounding material and in turn give rise to higher temperatures due to increased contact/pressure as the brake pad slides over the swelling. This would give rise to the hot spotting phenomenon which creates high frequency brake judder. It was likely that the non uniform disc heating/expansion contributed to wave-like brake disc deformation which has been shown in section 4.2.3 to be a direct cause of brake judder, evidence of this was indicated by the anti-

symmetric pattern of the hot spots found in dynamometer testing in section 4.3. It was therefore important to try to reduce the variation of the surface temperature of the brake disc to avoid the above described problems.

5.4.2. Procedure

The problem of non-uniform surface temperature distribution and high disc temperature has been tackled here in this thesis from the approach of a thermal analysis and also with collaboration from an associated aerodynamic analysis project on the same brake disc [2]. The aim of which was to both promote convective heat transfer and conductive heat transfer through interpretation of information from both a thermal and aerodynamic analysis. Using this information, modifications to the brake disc vent profile design have been made. The aim of which was to reduce the surface temperature variation and to reduce the maximum disc temperature. FEA thermal simulations of the standard brake disc have been performed, based on the analysis of these results combined with analysis of brake disc thermal images modifications to the vent profile were made. FEA simulations of the modified design were then carried out to benchmark the performance benefit. Information from the associated aerodynamic project has been shown where appropriate. Back-to-back on-vehicle testing of the standard disc and a prototype of the modified design was also carried out using an identical test procedure for each test. More specific details can be found in the description of each section.

5.4.3. Current Design Analysis

Finite element simulations of the brake disc have shown variation of the disc surface temperature around its circumference which was directly related to the underlying vane geometry, this can be seen in figure 5.14. Disc surface temperature variation was in the region of 5°C after a three stop transient simulation of a brake disc based upon vehicle data. This was based upon uniform heat flux application to each friction ring surface whereby the instantaneous heat flux was constant across the whole friction ring area. In reality the heat would be swept around the disc surface and this would exacerbate the “rippling” temperature field shown in figure 5.14 due to increased surface contact at the hotter, and therefore swollen, regions which would in turn raise the localised temperature. Furthermore, the brake disc has been shown in sections 4.2.3 and 4.3 adopt a wave-like mode of deformation resulting from constrained thermal expansion causing disc buckling. The peaks of these waveforms would experience an increased localised pressure distribution from the

brake pad as it slides over peaks, this would cause a localised elevated disc temperature profile. If any of these waveform peaks coincided with a disc vent which already had a slightly higher temperature as shown from the FE study the temperature would be increased further. Therefore to reduce the potential for hot spotting to occur the buckling mode shape of the disc should be controlled (either by increasing it to distribute the thermal energy across more peaks, or decreasing it to eliminate hot spotting as suggested in section 3.2.6.3) and the variation of the disc surface temperature profile should be reduced by minimising the effect of the disc vent geometry. The following work has focussed on both minimising the disc surface temperature variation and reducing the maximum disc temperature to reduce the thermal distortion and to reduce the propensity towards hot spotting caused by an initial surface temperature variation.

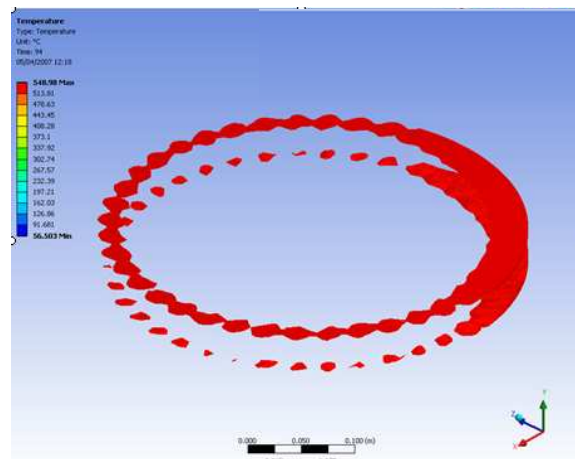


Figure 5.14: Simulated surface temperature variation due to underlying vane geometry and balance

Thermal imaging, as seen in section 4.3.4 and figure 5.15, has been used to analyse the heat distribution and build-up within the brake disc in an attempt to further understand what causes the disc to deform. Shown in figure 5.15 is a thermal image of the brake disc from section 4.3.4 after light brake applications which have elevated the disc surface temperature to 100°C (8 bar brake pressure, each application 3 seconds long at 600r/min). The underlying vane pattern was shown to influence the temperature distribution on the surface of the brake disc. This vane pattern was due to the increased thermal mass available to the disc where there was a vane beneath the disc surface. This allowed the disc to conduct heat from the surface to a vane faster than surrounding thinner areas which were already thermally saturated.

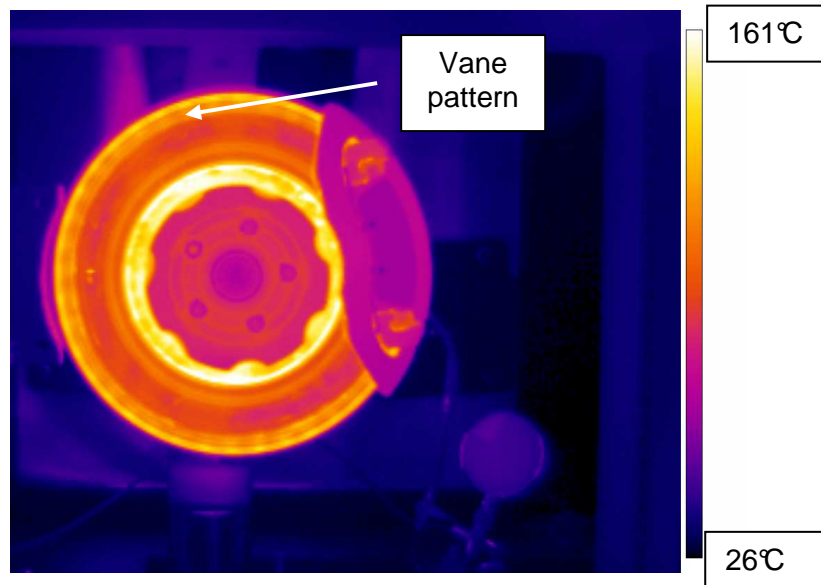


Figure 5.15: Thermal image of brake disc showing the vane pattern

Shown in figure 5.16 is the temperature profile around the disc at a radius of 187mm. The profile equated to an included disc angle of 262°, omitting the portion of disc obscured by the caliper. The number of peaks in the temperature profile correlated exactly with the number of disc vents (30) in the included angle. It was concluded that the vent profile was influencing the temperature on the surface of the disc, with a recorded temperature variation of 16.2°C. This variation was 21% of the average profile temperature and 19.7% of the maximum profile temperature recorded at this radius. It was temperature effects such as these which were concluded to be the cause of disc hot spotting and higher order disc deformation.

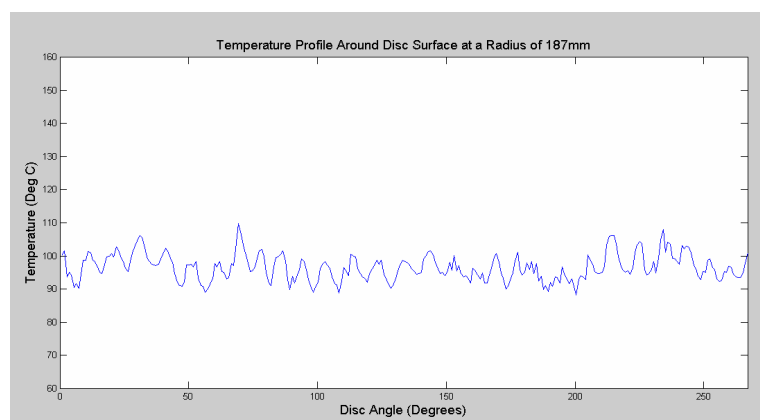


Figure 5.16: Temperature profile around the disc surface at 187mm clearly showing the variation due to the disc vanes

Uneven temperature gradients through the friction ring thickness were also observed from finite element simulations as shown in figure 5.12. This was seen when comparing the gradient above a vent to the gradient above a vane. While these gradients would never be uniform due to the thermal mass of the vane having a large effect on the friction ring material above it; effectively acting as a heat sink, some effort should be taken to minimise the difference between the two gradients in an attempt at maintaining an even friction ring surface temperature.

5.4.4. Design Development

As described in section 5.4.1 the main aim of the prototype disc design was to promote a more even temperature distribution around the brake disc. The prototype design centred around modifications to the vent profile of the standard brake disc to achieve the improved temperature profile and reduced disc temperature. The main design parameters of this prototype were to maintain the 40 vanes identical friction ring size and spacing. The reasons behind this were to prevent changing too many parameters which would affect the structural integrity and mask the effect on the judder performance of the disc; therefore the need for thermo-mechanical analysis of the stress and strain in the disc was eliminated.

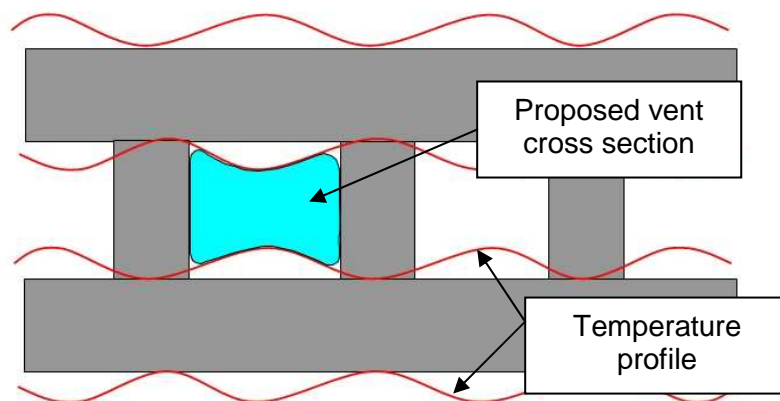


Figure 5.17: Temperature profile (exaggerated scale) due to vent geometry and proposed vent cross section

When observing the temperature profile on both the top friction ring surface and the vent ceiling of the standard brake disc, the distribution was of the trend shown in figure 5.17. It could be seen that the temperature of the friction ring surface and vent ceiling peaked at the 'mid-vent' position. Therefore this suggested that there was insufficient cooling and/or thermal mass in this region.

Taking this into account the prototype vent design incorporated a wave design with a dimple or “false vane” at the mid point between two vanes; the cross section of this profile can be seen in figure 5.17. The aim of this was to add mass mid way between the vanes to try and draw heat more evenly from the surface of the disc and to avoid build-up of the hot regions on the surface and vent ceiling. Initial trial simulations indicated good results and so various design iterations were performed to indicate an optimum solution.

The prototype design incorporated two wavy profiles, both symmetrical about their own mid planes. For simplicity of geometry, the dimensions of the profile at the inner radius remained fixed while the outer profile was modified. The outer extremes of the profile fitted within the standard vent shape or in other words material was added to the vent not removed. The main parameter which was adjusted was the radius of the centre dimple.

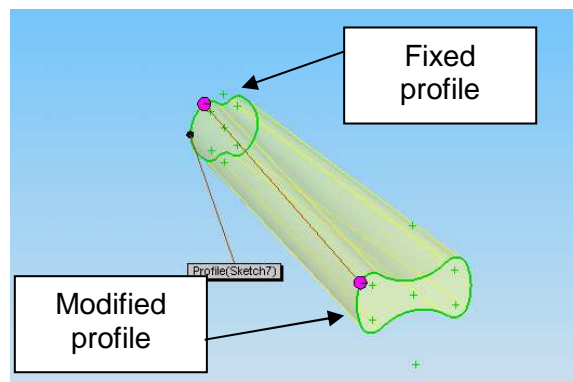


Figure 5.18: General view of vent design

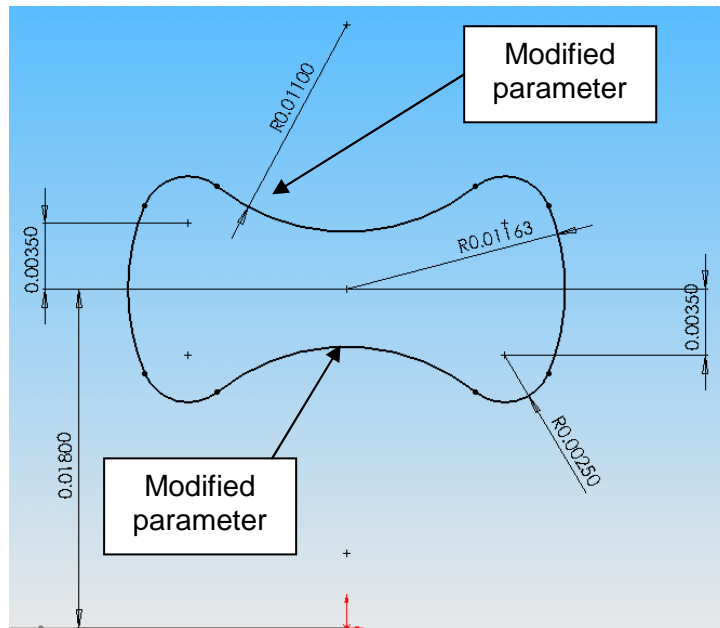


Figure 5.19: General view of the vent end profile

Whilst the thermal analysis focussed on modifications to the vent cross section shown in figure 5.19, the CFD analysis, performed as part of the associated research project [2], focussed on improving the airflow along the vent in the radial direction by introducing aerodynamic profiles to the disc vanes. The two designs were then merged to combine both aerodynamic benefits of the CFD design with the thermal benefits of the FEA design. The FEA procedure is presented in section 5.4.5, and the FEA and CFD results are presented in section 5.4.6.

5.4.5. Thermal Analysis Procedure

The same 3-stop thermal FE simulation as has been described in 5.2.3 was carried out on the brake disc based on data from the on-vehicle testing; the heat flux load can be seen in figure 5.3. The simulation matched the energy dissipation through the brake disc as seen in stops 11-13 of the vehicle test. CFD modelling and meshing of the modified FE disc designs which incorporated the wavy vent profile proved problematic. The disc curvature and geometry at the transition region between the wavy vent entrance and swan neck was complex and prevented a CFD model and mesh from being constructed in the GAMBIT software. Therefore no realistic measure of the convective coefficients could be made. Therefore the convective heat transfer coefficients implemented were identical to those used for the standard disc and can be seen in figure 5.3. Whilst the convective coefficients would have been different it was expected that this would have been minimal due to the disc

having the same cross section about the mid vane point as the standard disc. Also removal of the sharp standard vane corners was expected to improve airflow and prevent separation. Initial FE simulations focussed upon the effect of recessing the new vane profile at the outer radius to match that of the standard disc and to assess the effect this had on the overall disc temperature. The second aspect of the study focussed upon identifying the effect of the change in vane profile alone. This involved equalising the mass of the prototype disc design with that of the standard disc by thinning the inboard and outboard friction rings, details of this can be found in section 5.4.6. By equalising the mass of the brake disc the effect of the vent design change alone was benchmarked against the thermal performance of the standard disc as the overall effect of the increase in mass of the prototype disc had been eliminated. Therefore any change was attributed to the distribution of the mass. The third and final analysis involved varying the profile radius to find an optimum solution.

5.4.6. Thermal Analysis Results

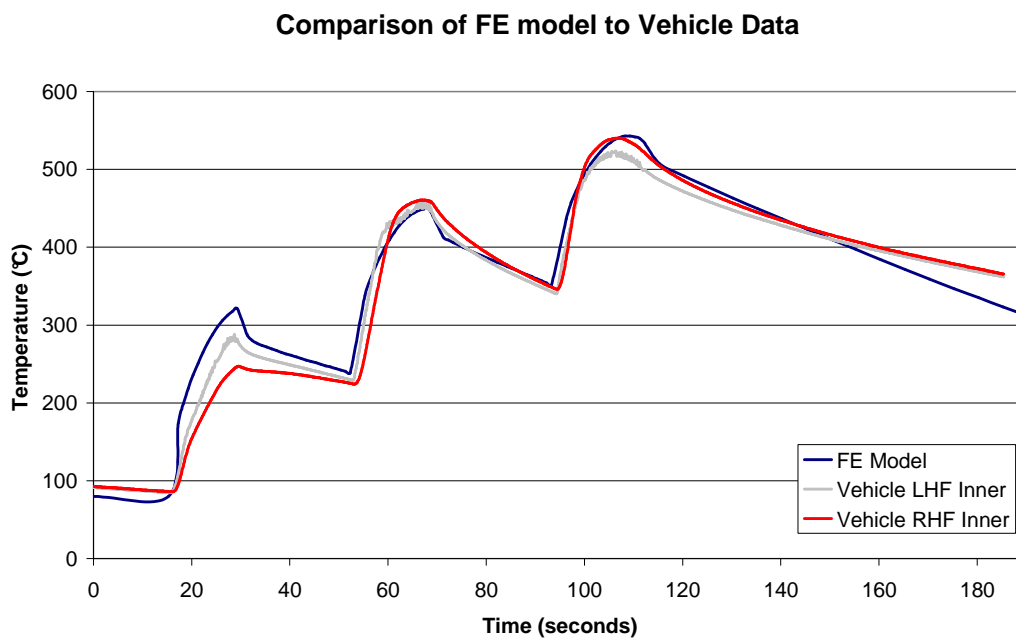


Figure 5.20: Graph showing comparison between simulated and actual data for the standard brake disc.

Figure 5.20 shows the accuracy of the simulation when compared to data obtained from vehicle testing. The simulated data correlated well with the measured data in the three braking events. The instance in time at which the maximum disc temperature occurred in the third braking event was used for analysis of the

prototype disc design and to compare its performance with the standard brake disc. It can be seen that the simulated disc temperatures in the final cooling phase fell quicker than the measured data; however as has previously been discussed in section 5.2.3.1, this was due to the simplified convective cooling curve in this phase. This region of the graph was not the main focus of this analysis and therefore no modification was required to the cooling coefficients.

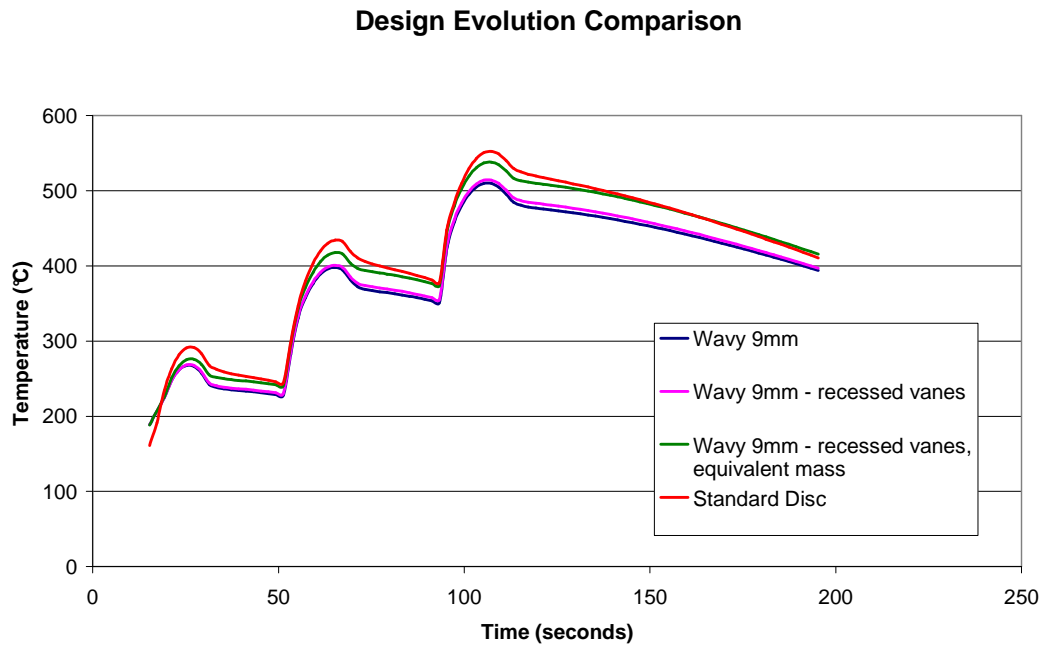


Figure 5.21: Graph showing evolution of the wavy brake disc design

Figure 5.21 shows the evolution of the design. The initial wavy 9mm design (9mm mid-vent radius) did not have recessed vanes at the outer disc radius, and therefore nowhere to clamp when machining the disc, however it gave an average reduction in the maximum disc temperature of 26°C over the three braking events when compared to the standard disc, and a maximum reduction of 43°C. The addition of recessed vanes increased the maximum disc temperature by an average of 4°C over the three braking events when compared to the initial 9mm design. Also shown was the effect of removing material from the friction rings to equalise the mass of the disc to that of the standard design. This increased the maximum disc temperature by an average of 22°C over the three braking events when compared to the initial 9mm design. This was due to the reduction in thermal mass of the brake disc caused by both the recessed vanes and the thinning of the friction rings to achieve the equivalent mass, therefore the maximum disc temperature increased. However, the

9mm design with recessed vanes and equivalent mass still gave an average disc temperature reduction of 3°C over the three braking events and a 14°C reduction in the maximum disc temperature when compared to the standard disc. This indicated that more scope for temperature reduction was possible by maintaining the 36mm disc thickness and removing material from other non critical areas of the disc to maintain the same disc mass as the standard design. The only other region available for removal of material was the swan neck region, however this was already relatively thin and therefore the potential to remove material from this region was limited as it would have impacted on the structural integrity of the brake disc.

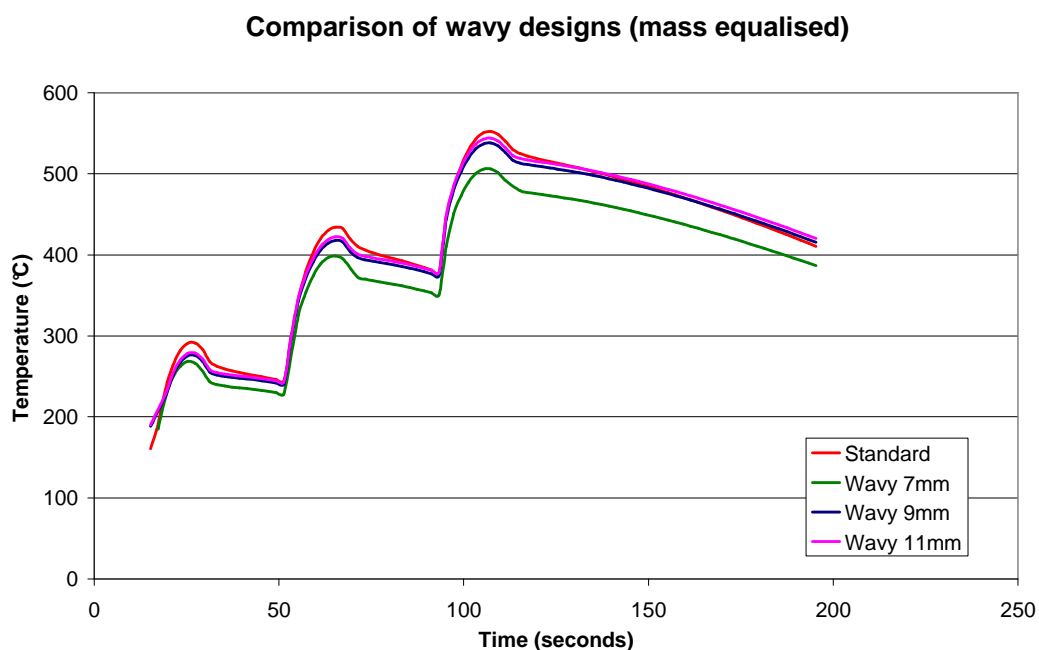


Figure 5.22: Graph showing comparison of wavy design iterations and the standard disc design (all identical mass)

Shown in figure 5.22 are the results from the final design iterations. It is clear from the graph that the 7mm design was the best from a temperature reduction point of view. With this design the dimple protruded the furthest into the vent and therefore had the largest wetted area exposed to the airflow. It also had the highest mass in the vent region once the overall disc mass was equalised and therefore was good for both conduction and convection of heat. Of interest was the fact that the maximum disc temperature decreased as the vent cross sectional area decreased. This was where the limits of the FE study came into play. During the heating phase a disc with a reduced vent area would benefit from improved heat capacity due to the extra

mass, however there will become a point where this would become detrimental to the cooling capacity of the brake disc during the cooling phase.

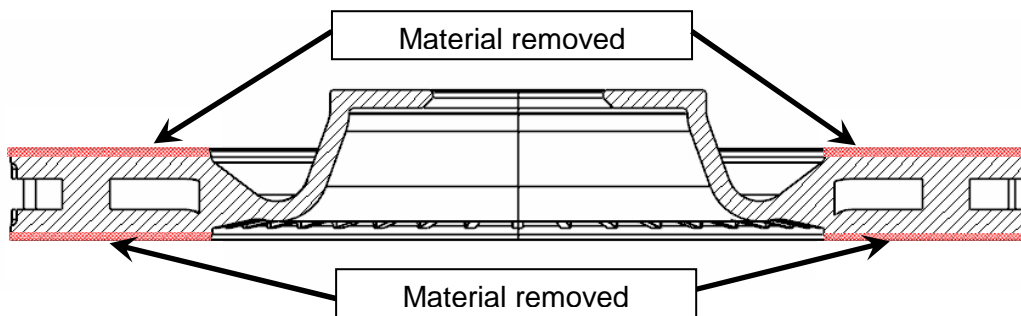


Figure 5.23: Cross section through brake disc. “Slices” removed from the friction ring surfaces to equalise the disc mass shown hatched.

Note: “Original mass” is the mass of the disc before the friction rings were thinned to equalise the mass as shown in figure 5.23. The FE simulations were carried out on discs with identical mass to the original standard design. “Design” refers to the mid vent (or dimple) radius that was used – see figure 5.19.

Design	Original Mass	Wetted Area (single vent)	Cross Sectional Area (measured at disc outer radius)	Max. Disc Temperature
Standard	19.448kg	0.00577m ²	0.00027816	552°C
11mm	20.492kg	0.00490m ²	0.0002m ²	544°C
9mm	20.567kg	0.00497m ²	0.00019m ²	538°C
7mm	20.722kg	0.00505m ²	0.00016m ²	506°C

Table 5-4: Thermal analysis results

From looking at the results in table 5-4 it can be seen that all of the proposed designs had both a smaller cross sectional area but also smaller wetted area than the standard design, however they all exhibited a lower maximum disc temperature. All of the proposed designs originally had a higher mass than the standard disc, however to eliminate the effect of added mass, the friction rings were thinned by removing material from the rubbing surfaces to equalise the mass prior to running the simulations. Therefore the reduction in surface temperature was attributed to the

design of the vent section alone, and it was clear that as the radius of the dimple decreased so did the maximum disc temperature. The 7mm design exhibited a maximum temperature reduction of 46°C compared to the standard disc and a 31°C average reduction in temperature which was equivalent to 7%.

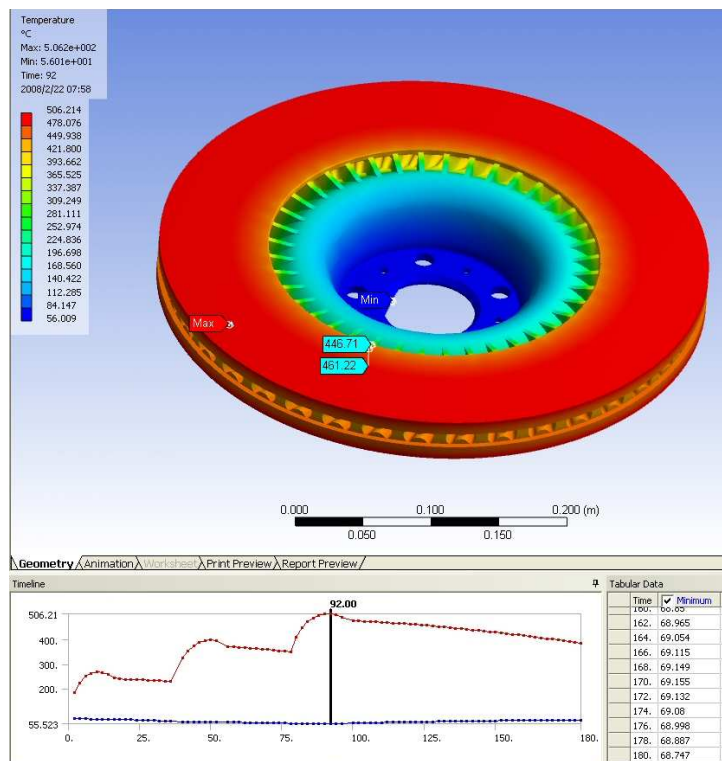


Figure 5.24: Wavy design 7mm thermal simulation

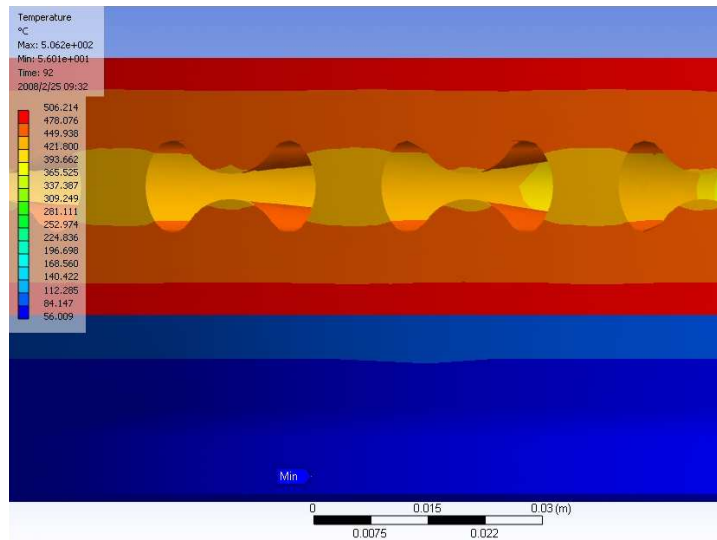


Figure 5.25: End view of disc showing thermal gradient (wavy 7mm)

The 7mm wavy design exhibited a thermal gradient through the first 4.7mm of 4.8°C/mm, compare this with the standard design which gave 6.8°C/mm over the first 5.41mm and this was seen as an improvement. This reduction in thermal gradient, together with the reduced disc temperature, provided more stability for the surface temperature of the brake rotor. The region of material near the disc surface could now accept more thermal energy due to the reduced thermal gradient and maximum disc temperature before any “rippling” of the surface temperature profile would occur. The reduction in maximum disc surface temperature would also reduce the possibility of martensitic transformation occurring as the bulk disc surface temperature was now further away from the martensite start temperature of 726°C in the three simulated braking events. The reduction in maximum disc surface temperature would also reduce the propensity for the disc to adopt higher modes of deformation due to buckling as the thermal expansion, and therefore the compressive stress caused by this, would be reduced.

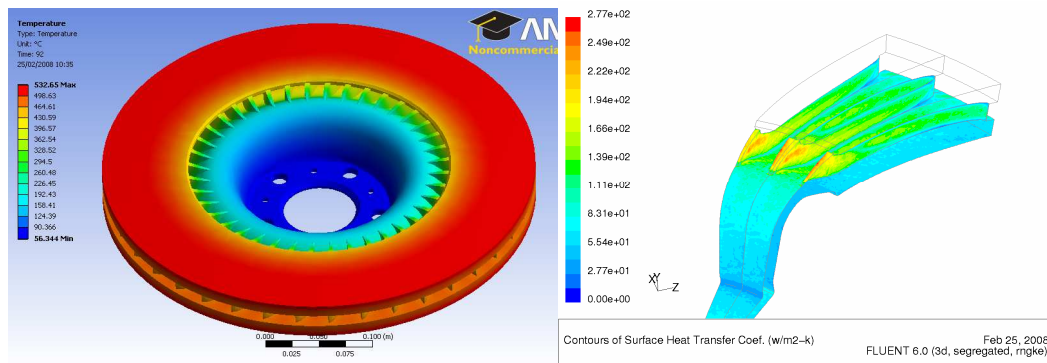


Figure 5.26: Aero design 1 showing temperature distribution (left) and convective heat transfer coefficient (right) [2]

A simultaneous aerodynamic study of the brake disc was carried out by a collaborating project [69][2], the aim of which was to improve the airflow and heat transfer characteristics of the brake design with the overall aim of combining features from both the thermal solution and the aerodynamic solution. Shown in figure 5.26 is the temperature distribution for the proposed aerodynamic design along with a CFD image showing the convective heat transfer coefficient. The convective heat transfer coefficient was obtained from a CFD study of the brake disc in the FLUENT software package which used rotating reference frames to simulate the rotation of the brake disc. The aerodynamic design incorporated an aerofoil profile to the disc vane to reduce airflow separation and therefore promote convective heat transfer. From a thermal analysis point of view this design exhibited a reduction in the maximum disc surface temperature of 20°C and an equivalent temperature distribution around the surface of the disc without any severe gradients at the vane attachment points. The thermal gradient for this design through the thickness of the friction ring was 5.5°C/mm over the first 5mm; this was an improvement over the standard disc design. The CFD study found that by incorporating the aerofoil vent profile the airflow through the vents exhibited less separation and therefore improved heat transfer characteristics with overall less variation in the heat transfer coefficient through the disc vent. A comparison of the standard and aerodynamic vent solution can be seen in figure 5.27.

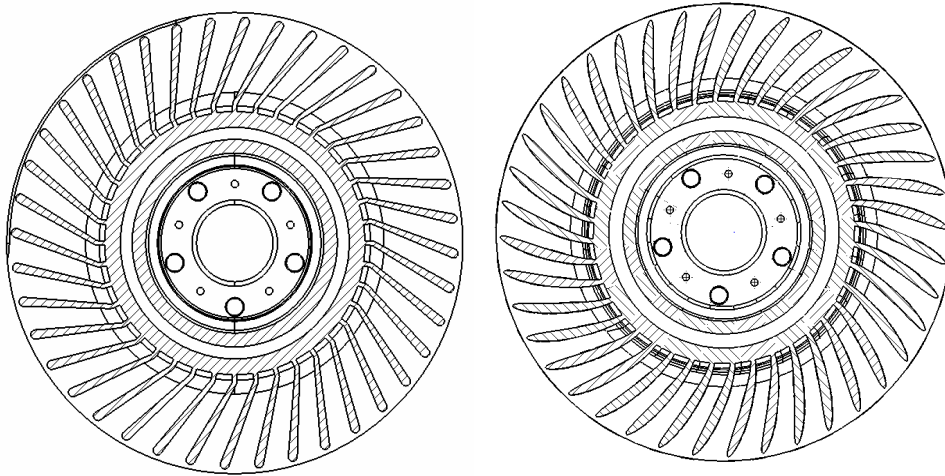


Figure 5.27: Image showing the original vane structure (left) and the proposed aerodynamic vane structure (right)

Meshing issues, which have been discussed in section 5.4.5, prevented a CDF study on the Wavy 7mm design, however as has been discussed in section 5.4.5, due to both the wavy design and standard disc sharing the same cross sectional geometry at 50% thickness they would have had similar airflow properties.

Attempts to combine the features from both suggested designs; that is an aerofoil vane shape and wavy vent profile, proved unsuccessful due to limitations with both the CAD system being unable to generate the complex geometry and the CAD modelling abilities of the author of this research. Based upon the evidence which showed that the wavy design would reduce the surface temperature variation and maximum disc temperature, whilst the aerodynamic profile would reduce separation and provide less variation of the convective heat transfer coefficient, combining the features from both of these designs would provide the best solution with regards to temperature reduction and improved heat distribution. To that extent a prototype disc model was manufactured modelling as closely as possible the best features from each design.

Testing of the prototype disc was carried out on-vehicle at the Millbrook proving grounds facility. The vehicle testing followed the test procedure shown in table 3-1 using a lower maximum vehicle speed of 240km/h to account for the maximum achievable speed on the Millbrook speed bowl circuit. Back-to-back tests of the prototype and standard disc were performed so that comparisons between the two discs could be made. The vehicle testing of the prototype design gave positive

results with a maximum 25% temperature reduction in back-to-back tests with a standard brake disc, and an average of 14% temperature reduction over the whole test duration equating to an average temperature reduction from 279°C to 241°C. The results from this test can be seen in figure 5.28.

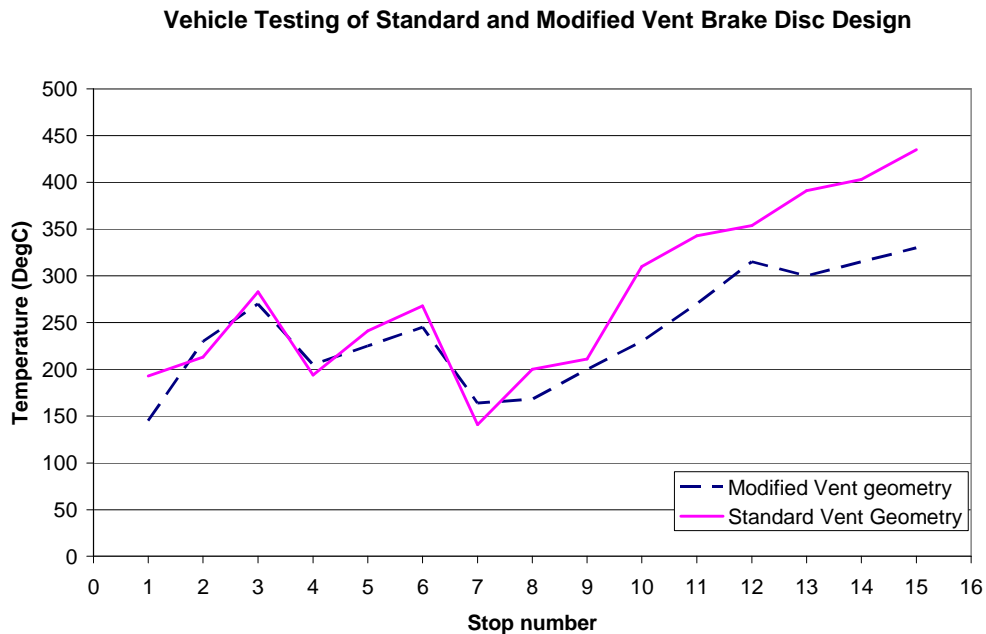


Figure 5.28: Back-to-back vehicle testing of the prototype disc and the standard disc

5.5. Finite Element Analysis Discussion

The finite element analysis of the heating and cooling of the brake disc has shown that the simplified modelling of the brake disc, with heat flux applied to both friction ring surfaces, provided good results which correlated well with measured data. Also shown was the effect that temperature dependent material properties had on the correlation of the simulation with measured data.

Conduction has been identified as the dominant mode of heat transfer from the friction ring surfaces both immediately after the onset of braking and immediately after the braking loads were removed. This was an important consideration as it indicated that managing the heat flow via good conduction paths played a significant effect in the overall disc temperature distribution during and after braking. As a result of this an improved design solution was sought out which incorporated both improved airflow through the disc and improved conduction of heat away from the friction surface of the disc to reduce the surface temperature variation.

It has been shown that the wavy 7mm design exhibited the most promising solution from a thermal aspect. The design showed a predicted temperature reduction of 46°C, a reduced thermal gradient through the disc thickness close to the friction ring surface and a reduction in the surface temperature variation circumferentially around the brake disc. It has been shown in section 5.4.6 by performing FE simulations of the standard and prototype disc with equal mass, that these improvements were due to better distribution of thermal mass around the vent floor and ceiling which promoted both conduction and convection.

Initial vehicle testing of the new brake disc design has given promising results, which have been shown in figure 5.28, with an indicated average 14% reduction in brake disc temperature. This equated to a reduction in average maximum disc temperature over the test duration from 279°C to 241°C. The cooler running of the brake disc will reduce the thermal deformation of the brake disc to some extent whilst the reduction in the surface temperature variation will reduce the possibility of hot spotting occurring as a result of an initial temperature variation. There was also increased scope to reduce the mass of the brake disc while maintaining the same thermal performance as that of the standard disc, for example having the same operating temperature with a lighter brake disc.

6. Conclusions

To date research carried out into the field of brake judder by other authors has focussed on analysing DTV growth as a cause of brake judder. However, comparatively little research had been carried out into the wave-like disc deformation which was believed to generate brake judder [11]. The novel findings of the research undertaken in this thesis have shown that significant brake judder can be caused due to thermal distortion of the brake disc which resulted in wave-like disc deformation. Good correlation was shown between in-stop thermal distortion and the brake pressure variation pulsation which was recorded as a measure of brake judder. The wave-like distortion of the brake disc showed both elastic and plastic properties with highly dynamic wave-like thermo-elastic deformation taking place within a single braking event alone which generally typified a third order mode of distortion. The wave-like deformation, shown in the dynamometer testing of chapter 4, backed up the mechanism of disc buckling which was suggested by Lang [1]. This circumferential buckling was caused by the thermal expansion of each friction ring surface resulting from the rapid influx of heat into the brake disc. The disc was unable to expand radially due to the constraining cooler regions of surrounding material, and was unable to expand circumferentially as it was constrained by itself as a result of being annular. Therefore compressive stresses were caused due to the tangential load on the disc which resulted in disc buckling. The waveform mode order was related to the buckling mode which was calculated from Euler's buckling theory [68]. Off-brake distortion was shown to be vastly different to the in-stop distortion due to thermo-elastic deformation which resulted from wave-like buckling.

One of the primary and novel benefits that this research has shown is that of analysing brake disc deformation in-stop whilst the brake was experiencing judder. The generally accepted method in industry for analysing and classifying brake judder has been that of disc thickness variation measurement. The DTV classifications nearly always show that as DTV increases so does the subjective level of brake judder. However DTV measurements do not always show any other correlation or give any insight into the source. This research has identified that elastic deformation occurred at the onset of braking, thermo-elastic wave-like deformation occurred during a single braking event and thermo-plastic wave deformation occurred throughout the duration of a sequence of braking events. This caused a wave-like deformation to occur during braking which subsequently relaxed back to a lower order of deformation following release of the brakes and cooling. This wave-like in-

stop disc deformation has been shown to have a direct link to brake judder which has been identified through brake pressure variation measurements. It was believed that the post test DTV was linked to the dynamic in-stop disc wave deformation; hence why it showed no link to the cold disc shape.

One of the conclusions of this thesis was that post test DTV would be linked to wear of the dynamic waveform peaks of the brake disc formed during a braking event. Higher contact pressures would be present at the peaks of these waves leading to accelerated wear profiles which would become evident in post testing DTV analysis. The brake disc waveform was shown to be dynamic in that it changed shape (or order) between braking events. Therefore whilst the DTV would relate to the in-stop waveform of each braking event, differing waveforms in separate braking events would give different DTV patterns. The same would also apply for hot spot and blue spot generation, the hot spot locations would move around the disc dependent upon the waveform present within each braking application. In severe cases this would generate blue spotting as seen in figure 2.3 in section 2.1.3, where multiple waveforms would have given the blue spotting shown. An important finding of this thesis has been that the cold shape of the brake disc has been shown to be completely different to the in-stop and post braking event 'hot' shape, and therefore post brake DTV was unlikely to show any correlation to the cold shape of the brake disc.

Furthermore it has been confirmed that there was a stress relieving process occurring during hot running and subsequent cooling of the brake disc. This thesis has identified that the stress relieving process allowed the disc to relax into a second order mode of deformation following testing on both the brake dynamometer and on-vehicle. This was an important finding as it identified that the stress relieving process influenced the disc wave-like deformation during braking, and would therefore have an influence on brake judder. Stress relieving of a pair of brake discs showed that the discs adopted a second order wave following stress relieving, having previously had a first order shape prior to the process. Initial dynamometer testing of stress relieved brake discs identified that the stress relieving process removes the initial deformation process and that there was no subsequent change in cold disc shape.

The initial on-vehicle testing and analysis identified brake pressure variation as an accurate method of judder measurement and investigation. The pressure variation was seen to correlate well with subjective scores recorded by the vehicle test

engineer. Not only this, but the pressure signal was sufficiently detailed at this early stage to enable frequency extraction using Fourier analysis to identify the development of the dominant frequencies resulting from brake judder.

A modified disc vent geometry was designed, the aim of which was to minimise the disc surface temperature variation so as to reduce the propensity towards hot spotting or thermo-elastic instabilities. Finite element analysis simulations of the proposed design identified a reduction in the surface temperature variation and a reduction of 46°C from 552°C to 506°C in overall maximum disc temperature based on an equivalent mass analysis. The proposed design was combined with an optimum vane profile from an aerodynamic study aimed at reducing flow separation to enhance the convective heat transfer from the disc to the air. This design was cast, and initial testing gave positive results.

In summary this thesis has shown clear and original contributions to the knowledge and understanding of the deformation of vented brake discs and its association to the brake judder phenomenon. Novel components of this research have shown in detail the dynamic nature of brake disc wave-like deformation, the link between wave-like in-stop brake disc deformation and brake pressure variation, the link between wave-like deformation and circumferential disc buckling, the possibility to measure on-vehicle brake judder represented as brake pressure variation, the stress relieving process of a brake disc during braking, the benefits of a modified vent geometry and finally and possibly most importantly the clear benefits of analysing the brake disc deformation in-stop whilst it is causing brake judder. All of these findings represent research that was either new in its entirety or built upon prior work from other authors to create an increased understanding of brake disc deformation and brake judder.

7. Recommendations for Further Work

The dynamic nature of brake disc distortion has been identified in this research, with elastic, thermo-elastic and thermo-plastic wave-like deformation all identified as a contributing factor. The research in this thesis has shown that the wave like deformation was linked to circumferential disc buckling. It is suggested that a multi-point analysis of the disc distortion on each side of the brake disc is performed. In doing so an increasingly accurate representation of the dynamic distortion of the brake disc can be formed. This analysis should look more deeply into the mechanism proposed in this research that DTV is due to accelerated wear of the dynamic in-stop waveform peaks.

A stress relieving process has been identified during testing of the brake disc. Manually performing this stress relieving process prior to any testing has shown that the brake disc takes up a second order mode of deformation similar to that seen during and after brake testing. It is proposed that a more in depth study of this process is performed to enable a clearer picture of the nature of brake disc deformation. Stress relieving a brake disc prior to testing will eliminate the initial deformation process and remove one factor from the equation of determining the source of the third order wave that is repeatedly seen during braking. The stress relieving process causes excessive run-out in a brake disc, it is therefore proposed that the disc be re-ground following this process.

The results from dynamometer testing of the prototype brake disc have yet to be obtained. The on-vehicle test data for the prototype disc showed a maximum temperature reduction of 25% with an average reduction of 10% over the whole test. It is anticipated that the temperature reduction will have a positive effect on the overall thermal deformation of the brake disc and this may go some way to reducing the level of brake judder.

The collected results and comparative data have identified that the FE models used for this study correlate well with the on-vehicle test data. A fully coupled thermo-mechanical analysis of the contact between pad and disc would yield more accurate surface temperature distributions, however identifying the boundary conditions which define the coulomb friction between two sliding bodies together with the associated contact interactions is not a simple problem and was out of the scope of this research.

8. References

- [1] Lang, A.M., (nd), "The Distribution of Temperature in Brakes", Mintex Don
- [2] Palmer E., (nd), "The Optimization of Aerodynamic Characteristics of Ventilated Brake Discs", University of Huddersfield, (PhD thesis to be submitted 2010)
- [3] Okamura T., Yumoto H., 2006, "Fundamental Study on Thermal Behaviour of Brake Discs", 25th Annual Brake Colloquium & Exhibition, SAE 2006-01-3203
- [4] Kubota M., Suenaya T., Doi, K., 1998, "A Study on the Mechanism Causing High Speed Brake Judder", SAE International Congress & Exposition 1998, SAE 980594
- [5] Fieldhouse, J., Beveridge, C., 2001, "An experimental Investigation of Hot Judder", SAE 2001-01-3135, 2001
- [6] Little, E., Kao, T., Ferdani, P., Hodges, T., 1998, "A Dynamometer Investigation of Thermal Judder", SAE, 982252
- [7] Yi Y., Barber J.R., Zagrodzki P., 2000, "Eigenvalue solution of thermoelastic instability problems using Fourier reduction", Proc.Roy.Soc. (London), Vol. A 456 (2000), pp. 2799-2821.
- [8] Afferrante L., Ciavarella M., Barber J.R., 2006, "Sliding thermoelastodynamic instability", Proceedings of the Royal Society (London), Vol.462, pp.2161-2176.
- [9] Jacobsson, H., 1999, "Analysis of Brake Judder by use of Amplitude Functions", Noise & Vibration Conference & Exposition, Michigan, 1999-01-1779
- [10] Heppes P., 1998, "Noise Insulators for Brake Squeal Reduction – Influence and Selection of the Damping Material", Automotive Braking – Recent Developments and Future Trends, Professional Engineering Publishing Limited, pp15-47
- [11] Fieldhouse J.D., 2006, "Brake Noise, Vibration and Judder", Braking of Road Vehicles 2006, University of Bradford, pp.281-300
- [12] Breuer B., Bill K.H., 2008, "Brake Technology Handbook", SAE International, pp35-36

- [13] Haigh M.J., Smales H., Abe M., 1993, "Vehicle judder under dynamic braking caused by disc thickness variation" IMechE C444/022/93
- [14] Suganuma, Y., Howse, F., Thornton, C., 2001, "Dynamometer Simulation Study for Market Brake Judder", SAE 2001-01-3191
- [15] Jacobsson H., 2003, "Aspects of disc brake judder", Proceedings of the Institution of Mechanical Engineers Vol. 217 Part D: Journal of Automobile Engineering.
- [16] De Vries A., Wagner M., 1992, "The Brake Judder Phenomenon", SAE, 920554
- [17] Curry E., 2006, "Design, Installation and Production of Brake Rotors", Braking of Road Vehicles 2006, University of Bradford
- [18] Barton D.C. 2006, "Materials Design for Disc Brakes", Braking of Road Vehicles 2006, University of Bradford
- [19] Chatterley T.C., Macnaughtan M.P., 1999, "Cast Iron Brake Discs – Current Position, Performance and Future Trend in Europe", SAE 1999-01-0141
- [20] Marshall P.H., 2006, "Brake Design Analysis", Braking of Road Vehicles 2006, University of Bradford
- [21] Beveridge, C.A., Fieldhouse J. D., 2000, "Noise Investigations of a Commercial Disc Brake Using Holographic Interferometry", Brakes 2000, IMechE
- [22] Robert Bosch GmbH, 2000, "Brake System Complaints by Problem Symptom" Data compiled from J.D. Power and Associates, New Car Quality Survey data MY2000, wave 2
- [23] Bentley Motors Limited – Private communications
- [24] Lang, A.M., Smales, H., 1983, "An Approach to the Solution of Disc Brake Vibration Problems", Braking of Road Vehicles. IMechE
- [25] Okamura T., Hasegawa K., Herai J., 2005, "High-Precision Brake Discs to Reduce Judder", 23rd Annual Brake Colloquium & Exhibition, 2005-01-3924
- [26] Eggleston, D., Eurac Technical Bulletin 0034056 – Thermal Judder. (n.d), Precision Disc Castings LTD

- [27] Steffen, T., 2006, "Hot Spot Simulation", Braking 2006, IMechE
- [28] Hillier V.A.W, Coombes P., 2004, "Hillier's Fundamentals of Motor Vehicle Technology, Book 1", 5th edition, ISBN 0748780823, Nelson Thornes, pp432
- [29] Lee K., Dinwiddie R.B., 1998, "Conditions of Frictional Contact in Disk Brakes and Their Effects on Brake Judder, SAE International Congress and Exposition 1998, SAE 980598
- [30] Angus, H. T., 1978, "Cast Iron: Physical and Engineering Properties", Butterworths, 2nd Edition, pp295
- [31] Honeycombe, R., Bhadeshia, H. K. D. H., 1995, "Steels: microstructure and properties" 2nd Edition, ISBN 0340589469, Edward Arnold
- [32] Afferrante L., Ciavarella M., 2006, "Thermo-elastic dynamic instability (TEDi) – how frictional heating excites the thermoelasto-dynamic modes in a simple 1D model" IMechE, Braking 2006 - Advances in Vehicle Braking Technology, pp189-198
- [33] Litos, P., Honner, M., Lang, V., Bartik, J., Hynek, M., 2006, "The measuring system for the experimental research of thermo-mechanical instabilities of disc brakes" Braking 2006, pp208-217, IMechE
- [34] Williams N.A., 2007, "Commercial Vehicle Brakes", Braking of Road Vehicles 2007, University of Bradford, pp. 501-540
- [35] Barber, J.R., 1969, "Thermoelastic instabilities in the sliding of conforming solids", Proceedings of the Royal Society of Engineers, Vol. A312, pp.381--394
- [36] Yi, Y., Barber, J.R., Hartstock, D.L., 2001, "Thermoelastic Instabilities in Automotive Disc Brakes – Finite Element Analysis and Experimental Verification", Proc. 3rd Contact Mechanics International Symposium, Peniche, Portugal,.
- [37] Barber, J.R., 2002, "Instability of thermoelastic contact", Friction and Instabilities, Springer-Verlag, Vienna, pp. 1-37
- [38] Majcherczak D., Dufrénoy P., 2006, "Dynamic analysis of a disc brake under frictional and thermomechanical internal loading", Archive of Applied Mechanics Vol. 75 pp. 497-512

- [39] Fieldhouse J.D., Bryant D., Crampton A., Talbot C., Layfield J., 2008, "A Study of Thermal Judder on a Laboratory Dynamometer", 26th Annual Brake Colloquium & Exhibition, SAE 2008-01-2542
- [40] Valvano, T., Lee, K., 2000, "An analytical method to predict thermal distortion of a brake rotor", SAE 2000-01-0445
- [41] Jacobsson, H., 2000, "Modeling of disc-brake judder in passenger cars", Brakes 2000, IMechE, pp68-69
- [42] Jacobsson, H., 1998, "Frequency Sweep Approach to Brake Judder", Thesis, Chalmers University of Technology
- [43] Jacobsson, H., 1998, "The Brake Judder Phenomenon Classification and Problem Approach", The 2nd International Seminar on Automotive Braking, IMechE
- [44] Rhee, S. K., DuCharme R. T., Spurgeon W. M., 1972, "Characterization of cast iron friction surfaces" SAE 720056
- [45] www.linkeng.com, November 2009
- [46] Kiyotaka Obunai, Kazuya Okubo, Toru Fujii, Tsuyoshi Nakatsuji, 2006, "Study on Low Speed Judder of Wave Type Brake Discs for Motorcycles", SAE 2006-32-0026
- [47] Gassmann S., Engel H.G., 1993, "Excitation and Transfer Mechanism of Brake Judder", SAE 931880
- [48] Anderson, A.E., Knapp, R.A., 1990, "Hot Spotting In Automotive Friction Systems", Wear, 135 (1990) 319-337
- [49] Suryatama, D., Stewart, D.J., Meyland, S.C., Hou, L.J., 2001, "Contact Mechanics Simulation for Hot Spots Investigation", SAE 2001-01-0035
- [50] Yeo T.I., Choi H., Kim J.H., 2006, "Equivalent Axisymmetric Finite Elements Applied to Undercut Shape Design of Ventilated Brake Disk", Braking 2006, pp135-144, IMechE
- [51] Day, A.J., Ahsi, A.B., 1990, "Heat Flow and Temperatures in Friction Material During Braking", Proceedings of the 17th Leeds-Lyon Symposium on Tribology Leeds, UK, September (1990), pp. 183-191

[52] Tirovic M., Day A.J., 1990, "The Calculation of Temperatures in Brakes", Second Brakes Workshop, University of Bradford

[53] Qi H.S., Day A.J., Kuan, H.K., Rosala G.F., 2004, "A Contribution Towards Understanding Brake Interface Temperatures", Braking 2004, Vehicle Braking and Chassis Control, pp.251-260

[54] Qi, H.S., Day, A.J., 2007, "Investigation of disc/pad interface temperatures in friction braking", Wear, 262 505–513

[55] Hussain K., Yang S.H., and Day A., 2007, "A study of commercial vehicle brake judder transmission using multi-body dynamic analysis", Proceedings of the Institution of Mechanical Engineers, Part K: Journal of Multi-body Dynamics, Volume 221, Number 2

[56] Singh A., Lukianov G., 2007, "Simulation Process to Investigate Suspension Sensitivity to Brake Judder", SAE World Congress & Exhibition, SAE 2007-01-0590

[57] Tan, M., Wang, A., Zhang, L., Blaschke, P., 2002, "Parametric Study of Brake Roughness", Conference on structural dynamics No.20, Los Angeles

[58] Breuer B., Bill, K.H., 2008, "Brake Technology Handbook", SAE International, pp442

[59] "Thermal Judder" EURAC Technical Bulletin 00034056, www.eurac-group.com, (nd)

[60] Rumold W., Keiper W., 2003, "Brake Noise – A Comparison of Subjective and Objective Evaluations" Advanced Brake Technology, SAE, pp275-297

[61] Pohlmann K.C., 2005, "Principles of Digital Audio", 5th Edition, McGraw-Hill, pp22-28

[62] Hanselman D., Littlefield B., 2001, "Mastering MATLAB 6 – A Comprehensive Tutorial and Reference", Prentice Hall, pp299-308

[63] Breuer B., Bill, K.H., 2008, "Brake Technology Handbook", SAE International, pp451

[64] Bryant D., Fieldhouse J., Talbot C., Crampton A., Mishra R., 2006, "The development of a design methodology to reduce the probability of brake judder and drone due to thermo-elastic instabilities of the brake rotor", FISITA World Automotive Congress, F2006V077

[65] Degenstein Th., Winner H., 2007, "New Methods of Force and Temperature Measurement in a Wheel Brake During the Braking Process", XXVII International μ Symposium, pp164-188

[66] Harding P.R.J, Wintle B.J., 1978, "Flexural Effects in Disc Brake Pads", Proceedings of the Institute of Mechanical Engineers, Volume 192

[67] Fieldhouse J.D., Bryant D., Palmer E., and Mishra R., 2007, "A study of the thermo-elastic effects of braking on high performance cars", 21st JUMV International Automotive Conference - Science and Motor Vehicles, Belgrade, Serbia.

[68] Hibbeler R.C., 2008, Mechanics of Materials, 7th edition, Pearson

[69] Palmer E., Mishra R., Fieldhouse J., Layfield J., 2008, "Analysis of Air Flow and Heat Dissipation from a High Performance GT Car Front Brake", SAE World Congress, 2008-01-0820

[70] Thompson J.K, Marks A., Rhode D., (nd) "The Use of Inertia Simulation in Brake Dynamometer Testing" Link Engineering, www.linkeng.com

[71] Newcomb T.P., Day A.J., Tirovic M., 1989, "Thermal Effects and Pressure Distribution in Brakes", First Brakes Workshop, University of Bradford.

[72] Link Engineering, "Link Engineering Newsletter", Link Engineering, Issue No. 8 - Vol. 1, 2003

[73] Agudelo C.E., Ferro E., (nd), "Technical overview of brake performance testing for Original Equipment and Aftermarket industries in the US and European markets", Link Technical Report FEV205-01, Link Testing Laboratories, Inc.

[74] www.capacitec.com/auto.htm, November 2009

[75] www.micro-epsilon.co.uk/applications/objects/Bremsscheibe-Konzentrizitaet/index.html, November 2009

[76] www.linkeng.com/brakefrictionmaterial/Model3070BrakeEvaluationSystem.htm, November 2009

[77] Breuer B., Bill K.H., 2006, "Brake Technology Handbook", SAE, pp. 430

[78] Meyer R., 2005, "Brake Judder – Analysis of the Excitation and Transmission Mechanism within the Coupled System Brake, Chassis and Steering System", SAE 2005-01-3916

[79] ThermaCAM™ Researcher, Users Manual, FLIR Systems, Professional Edition. Version 2.7 SR-1, Publication Number: 1 557 773, Revision: a48, Issue date: April 13th 2004

[80] Altuzara O., Amezua E., Avilés R., Hernández A., 2002, "Judder Vibration in Disc Brakes Excited by Thermoelastic Instability", Engineering Computations Vol. 19 No.4

[81] Katz J., 1995, "Race Car Aerodynamics: Designing for Speed", Bentley Publishers, pp47

[82] Day A.J., Newcomb T.P., 1984, "The Dissipation of Frictional Energy from the Interface of an Annular Disc Brake", Proceedings of the Institute of Mechanical Engineers, Vol. 198D No.11

[83] Day A.J., 2006, "Tyres and Tyre Adhesion", Braking of Road Vehicles 2006, University of Bradford, pp65-85

[84] Tirovic M., 2006, "Thermal Effects", Braking of Road Vehicles 2006, University of Bradford

9. Bibliography

Braking of Road Vehicles 2006, Day A.J., Shilton B.R., University of Bradford, 2007

Brake Design and Safety second edition, Limpert R., SAE, 1999

Brake Technology Handbook, Breuer B.J., Bill K., 2008, SAE

Advanced Brake Technology, Breuer B.J., Dausend U., 2003, SAE

10. Appendix

10.1. On-Vehicle Test Equipment

Sensor Data	
Thermal Measurement Information	
All K-type thermocouples, of various construction and insulation types. Maximum range -50°C to 1100°C	
Transducer Information	
Channel 6 - LHF Caliper Line Pressure	
Type used:	Kulite ETM-345FE-375M-200BARA
Range:	0 to 200 Bar A
Serial number:	6632-10-199
Gain setting:	23.387 mV / Bar A
Offset:	236 mV @ zero pressure
Inaccuracy:	< 1% across range
Sign orientation:	+ Pressure increase
Channel 7 - RHF Caliper Line Pressure	
Type used:	Kulite ETM-345FE-375M-200BARA
Range:	0 to 200 Bar A
Serial number:	6632-10-200
Gain Setting:	23.033 mV / Bar A
Offset:	327 mV @ zero pressure
Inaccuracy:	< 1% across range
Sign orientation:	+ Pressure increase
Channel 8 - Vehicle deceleration	
Type used:	Datron 2D S AC1-105
Range:	± 5 g
Serial number:	A642
Gain Setting:	500 mV / g
Offset:	2496 mV @ zero pressure
Inaccuracy:	< 2% across range
Sign orientation:	+ Vehicle Deceleration
Channel 9 - LHF brake pad inner back plate movement across-car	
Type used:	PCB Piezotronics 356A25
Range:	± 200 g
Serial number:	51906
Gain Setting:	26.22 mV / g (z-axis)
Offset:	Zero Offset
Inaccuracy:	< 2% across range
Sign orientation:	+ Movement towards centre line of car (right)
Channel 10 - LHF brake pad inner back plate movement circumferential	
Type used:	PCB Piezotronics 356A25
Range:	± 200 g
Serial number:	51906
Gain Setting:	26.35 mV / g (x-axis)
Offset:	Zero Offset
Inaccuracy:	< 2% across range
Sign orientation:	- Movement vertically up

Sensor Data (continued)	
Channel 11 - RHF brake pad inner back plate movement across-car	
Type used:	PCB Piezotronics 356A25
Range:	± 200 g
Serial number:	51904
Gain Setting:	25.51 mV / g (z-axis)
Offset:	Zero Offset
Inaccuracy:	< 2% across range
Sign orientation:	+ Movement towards centre line of car (left)
Channel 12 - RHF brake pad inner back plate movement circumferential	
Type used:	PCB Piezotronics 356A25
Range:	± 200 g
Serial number:	51904
Gain Setting:	24.31 mV / g (x-axis)
Offset:	Zero Offset
Inaccuracy:	< 2% across range
Sign orientation:	- Movement vertically up
Channel 13 - LHF caliper back plate - circumferential	
Type used:	PCB Piezotronics 356A25
Range:	± 200 g
Serial number:	51905
Gain Setting:	26.01 mV / g (x-axis)
Offset:	Zero Offset
Inaccuracy:	< 1.5% across range
Sign orientation:	- Movement vertically up
Channel 14 - RHF caliper back plate - circumferential	
Type used:	PCB Piezotronics 356A25
Range:	± 200 g
Serial number:	51915
Gain Setting:	25.18 mV / g (x-axis)
Offset:	Zero Offset
Inaccuracy:	< 2% across range
Sign orientation:	- Movement vertically up
Channel 15 - Pedal Effort	
Type used:	Datron Pedal Force Meter 72200201
Range:	0 to 1500 N
Serial number:	289
Gain Setting:	1.004 mV / N
Offset:	20 mV @ zero pressure
Inaccuracy:	< 1% across range
Sign orientation:	+ Force increase
Channel 22 - Pedal Travel	
Type used:	Celesco MT2A-15E-9-10K-S
Range:	0 to 355.6 mm
Serial number:	L1409164B
Gain Setting:	24.805 mV / mm
Offset:	61 mV @ zero displacement
Inaccuracy:	< 1% across range
Sign orientation:	+Displacement increase

Data Logging System	
Ipetronik KIM4-DMS / DIAdem 9.1	
Recording Frequency	
Channels 6 & 7 and 9 to 14:	1000 Hz
All Other Channels:	10 Hz
Signal Conditioning Equipment	
PCB Piezotronics 481A01 Conditioner. Serial No: 421	

10.2. On-vehicle Testing - Accelerometer Datasheet

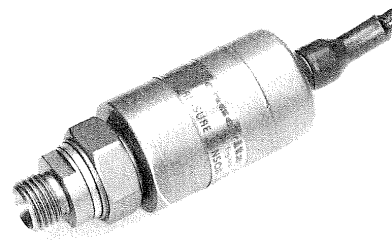
Model Number 356A25	ACCELEROMETER, ICP [®] , TRIAXIAL		Revision D ECN #: 25024
<p>Performance</p> <p>Sensitivity (±10%) Measurement Range Frequency Range (±5%) Frequency Range (±10%) Resonant Frequency Broadband Resolution (1 to 10000 Hz) Non-Linearity Transverse Sensitivity</p> <p>Environmental</p> <p>Overload Limit (Shock) Temperature Range (Operating) Temperature Response Base Strain Sensitivity</p> <p>Electrical</p> <p>Excitation Voltage Constant Current Excitation Output Impedance Output Bias Voltage Discharge Time Constant Settling Time (within 10% of bias) Spectral Noise (1 Hz) Spectral Noise (10 Hz) Spectral Noise (100 Hz) Spectral Noise (1 kHz) Spectral Noise (10 kHz)</p> <p>Physical</p> <p>Sensing Element Sensing Geometry Housing Material Sealing Size (Height x Length x Width) Weight Electrical Connector Electrical Connection Position Mounting Thread Mounting Torque</p>	<p>ENGLISH</p> <p>25 mV/g ±200 g pk 1 to 5000 Hz 0.5 to 6500 Hz ≥25 kHz 0.0002 g rms ±1% 51%</p> <p>±7000 g pk -65 to +250 °F See Graph 0.001 g/µe</p> <p>20 to 30 VDC 2 to 20 mA ≤100 ohm 8 to 12 VDC 0.5 to 2.0 sec <5 sec 70 µg/√Hz 15 µg/√Hz 5 µg/√Hz 3 µg/√Hz 2 µg/√Hz</p> <p>Ceramic Shear Titanium Hermetic</p> <p>0.55 in x 0.80 in x 14.0 mm x 20.3 mm x 14.0 mm 0.37 oz 10.5 gm 1/4-28 4-Pin Side 10-32 Female 10 to 20</p>	<p>SI</p> <p>2.6 mV/(m/s²) ±1960 m/s² pk 1 to 5000 Hz 0.5 to 6500 Hz ≥25 kHz 0.002 m/s² rms ±1% 51%</p> <p>±68600 m/s² pk -54 to +121 °C See Graph 0.01 (m/s²)/µe</p> <p>20 to 30 VDC 2 to 20 mA ≤100 ohm 8 to 12 VDC 0.5 to 2.0 sec <5 sec 686 (µm/s²)/√Hz 147 (µm/s²)/√Hz 49 (µm/s²)/√Hz 29.4 (µm/s²)/√Hz 19.6 (µm/s²)/√Hz</p> <p>Ceramic Shear Titanium Hermetic</p> <p>14.0 mm x 20.3 mm x 14.0 mm 10.5 gm 1/4-28 4-Pin Side 10-32 Female 113 to 225</p>	<p>Optional Versions (Optional versions have identical specifications and accessories as listed for standard model except where noted below. More than one option maybe used.) HT - High temperature, extends normal operation temperatures Frequency Range (±5%) Frequency Range (±10%) Broadband Resolution (1 to 10000 Hz) Temperature Range (Operating) Excitation Voltage Output Bias Voltage Discharge Time Constant Spectral Noise (1 Hz) Spectral Noise (10 Hz) Spectral Noise (100 Hz) Spectral Noise (1 kHz) T - TEDS Capable of Digital Memory and Communication Compliant with IEEE P1451.4 TLA - TEDS LMS International - Free Format TLB - TEDS LMS International - Automotive Format TLC - TEDS LMS International - Aeronautical Format TLD - TEDS Capable of Digital Memory and Communication Compliant with IEEE 1451.4 Temperature Range Excitation Voltage Output Bias Voltage</p> <p>2 to 5000 Hz 1.4 to 6500 Hz 0.0003 g rms -54 to +163 °C 23 to 30 VDC 7 to 16 VDC 0.1 to 0.6 sec 1864 (µm/s²)/√Hz 345 (µm/s²)/√Hz 196 (µm/s²)/√Hz 29.4 (µm/s²)/√Hz</p> <p>-10 to +200 °F 20 to 30 VDC 8.5 to 13 VDC</p> <p>[1] Typical. [2] TEDS option adds 1.0 VDC to bias voltage. [3] Valid from +250 to +325 °F (+121 to +163 °C), with HT option only. [4] Zero-based, least-squares, straight line method. [5] See PCB Declaration of Conformance PS023 for details.</p> <p>Supplied Accessories 080A109 Petro Wax (1) 080A12 Adhesive Mounting Base (1) 081B05 Mounting Stud (10-32 to 10-32) (1) ACS-1T NIST traceable triaxial amplitude response, 10 Hz to upper 5% frequency. (1) M081B05 Mounting Stud 10-32 to M6 X 0.75 (1)</p>
			<p>Entered: BLS Date: 11/10/2006</p> <p>Engineer: BAM Date: 11/10/2006</p> <p>Sales: WDC Date: 11/10/2006</p> <p>Approved: JJB Date: 11/10/2006</p> <p>Spec Number: 12854</p> <p>PCB PIEZOTRONICS VIBRATION DIVISION</p> <p>3425 Walden Avenue Depew, NY 14043 UNITED STATES Phone: 888-684-0013 Fax: 716-685-3886 E-mail: vibration@pcb.com Web site: www.pcb.com</p>
			<p>Typical Sensitivity Deviation vs Temperature</p>

10.3. Dynamometer Test Equipment

10.3.1. Pressure Transducer (P751-0001)

PRESSURE TRANSDUCER TYPE P700 Series

- * PRESSURE RANGES 0—10 TO 0—10,000 PSI (0.7 to 700 bars)
- * LOW & HIGH LEVEL OUTPUT
- * HIGH PRESSURE OVERLOAD PROTECTION
- * ALL WELDED CONSTRUCTION
- * INTEGRAL SHUNT CALIBRATION
- * 2 WIRE 4—20 mA OPTION BASEEFA & CENELEC APPROVAL CLASS Ex ia IIC T4



INTRODUCTION

These transducers have been designed for high reliability and stability. The all welded construction incorporates a double cantilever beam with bonded foil strain gauges. Coupling to the pressure diaphragm which is made via a force rod, gives excellent thermal isolation from the fluid or gas being measured and high overload protection is an integral part of the design. Though capable of sensing extremely small changes of applied pressure, the transducers are relatively insensitive to vibration, altitude and shock.

GENERAL SPECIFICATIONS – ALL MODELS

Pressure Ranges	Gauge or absolute reference
High Range (psi)	0, 75, 100, 150, 200, 250, 350, 500, 750, 1000, 1500, 2000, 2500, 3500, 5000, 7500, 10,000
(bar)	0, 5, 0.7, 10, 15, 20, 25, 35, 50, 70, 100, 150, 200, 250, 350, 500, 700
Medium Range (psi)	0, 10, 15, 20, 25, 35, 50
(bar)	0, 0.7, 1.0, 1.5, 2.0, 2.5, 3.5
Pressure Limit	≤ 5 x full range pressure or 12,000 psi whichever is less.
Burst Pressure	> 10 x full range pressure or 20,000 psi whichever is less.
Pressure Media	Liquids or gases compatible with 17 – 4PH & 17 – 7PH stainless steel or Inconel 625
Residual Unbalance	≤ ± 1% FRO P700 ≤ ± 2% FRO P720
Shunt Calibration	80% ± 5% full range pressure

ENVIRONMENTAL

Temperature Range	
Compensated	0°C to 100°C
Operable	– 55°C to + 120°C
Humidity	
Plug Outlet	95% Relative Humidity
Cable Outlet	Immersible to 1000 feet
Natural Frequency	Approx 2.5 KHz for 10 psi to approx 40 KHz for 10,000 psi
Acceleration Response	≤ 0.10% FRO/g (Medium range) ≤ 0.02% FRO/g (High range)
Insulation Resistance	≥ 500 Mohm at 50V D.C.

Notes:

1. A low current consumption version is available (1000 ohm bridge) at extra cost.

Seven classes of the P700 are currently available:—

1. P721/4 low cost version operating from 10V DC with 25mV output.
2. P701/9 basic version operating from 10V DC with 25mV output.
3. P741/9 integrated circuit amplifier variant operating from a regulated 10V DC supply with a 5V output.
4. P751/9 integrated circuit amplifier with integral regulator variant operating from an 11 to 18V DC supply with 2.5V output.
5. P761/9 integrated circuit amplifier with integral regulator variant operating from an 18 to 32V DC supply with 5V DC output.
6. P781/9 2 wire intrinsically safe variant to operate from a 10 to 36V DC with 4 – 20 mA output.
7. P791/9 integrated circuit amplifier variant operating from a regulated ± 15V DC supply with 5V DC output.

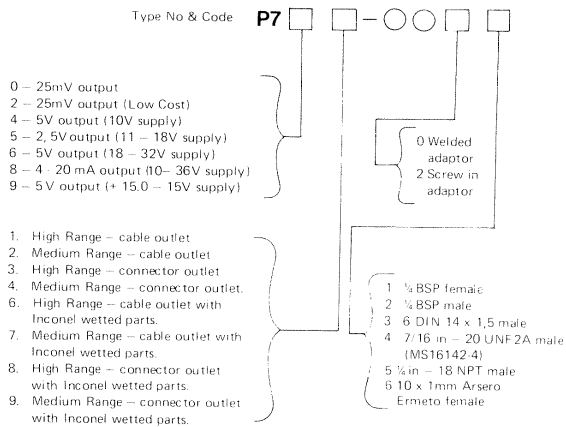
Should your requirements differ from our standard products, please contact us regarding customised transducers.

DETAILED SPECIFICATIONS

MODEL NUMBER	LOW LEVEL OUTPUT			HIGH LEVEL OUTPUT			
	P721/4	P701/9	P741/9	P751/9	P761/9	P781/9	P791/9
INPUT SUPPLY	10V DC/AC RMS	10V DC/AC RMS	10V DC				
Voltage	12V maximum	12V maximum	12V maximum	11 – 18V DC	18 – 32V DC	10 – 36V DC	+ 15.0, – 15V DC
Impedance	350 ohms ± 5%	350 ohms ± 5%	—	—	—	—	—
Current	—	—	30 – 35 mA	20 – 40 mA	30 – 40 mA	—	30 mA
OUTPUT AT +25°C							
Full range output with 1 metre cable	25 mV ± 2%	25 mV ± 1%	5V ± 1%	2.5V ± 1%	5V ± 1%	4 – 20 mA	5.0 ± 1%
Impedance	350 ohms ± 5%	350 ohms ± 5%	< 10 ohm	< 10 ohm	< 10 ohm	Load resistance 1.0 kohm max at 36V DC	< 10 ohm
Current (Maximum)	N.A.	N.A.	5mA	5mA	5mA		5mA
Residual Unbalance % FRO	≤ ± 2 FRO	≤ ± 1 FRO	≤ ± 1 FRO	≤ ± 1 FRO	≤ ± 1 FRO	≤ ± 1 FRO	≤ ± 1 FRO
ACCURACY:							
Combined Non-Linearity Hysteresis and Non Repeatability % FRO	± 0.2 Typical	± 0.18 Typical	± 0.18 Typical	± 0.18 Typical	± 0.18 Typical	± 0.18 Typical	± 0.18 Typical
	± 0.5 Max	± 0.25 Max	± 0.25 Max	± 0.25 Max	± 0.25 Max	± 0.25 Max	± 0.25 Max
Combined Thermal Zero and Sensitivity Error %FRO/°C	M.R. ± 0.03	± 0.02	± 0.02	± 0.02	± 0.02	± 0.02	± 0.02
	H.R. ± 0.03	± 0.015	± 0.015	± 0.015	± 0.015	± 0.015	± 0.015
PHYSICAL							
Max. Height (L)							
Cable version	83mm (3.27)	83mm (3.27)	99mm (3.90)	114mm (4.49)	114mm (4.49)	129mm (5.07)	99mm (3.90)
Connector version	83mm (3.27)	83mm (3.27)	99mm (3.90)	114mm (4.49)	114mm (4.49)	129mm (5.07)	99mm (3.90)
Weight	230 gm	230 gm	250 gm	250 gm	250gm.	250 gm.	250gm.

DESIGNATION AND ORDERING INFORMATION:

Specify by transducer Type number, coding and pressure range.



Example: P702 0025 10 bar A signifies "Pressure transducer cable outlet and 5/8 in - 18NPT male screw pressure connector, ranged 10 bar absolute."

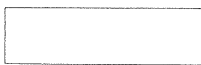
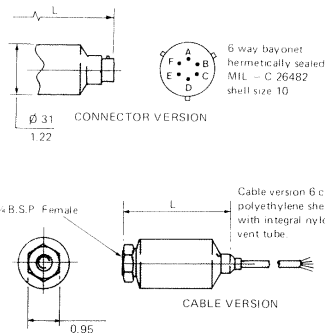
The company reserves the right to alter products without notice.

CONNECTIONS:

CABLE
 RED*
 WHITE
 YELLOW
 BLUE*
 VIOLET
 GREY

CONNECTIONS
 PIN A* EXCITATION (+)
 PIN D EXCITATION (-)
 PIN B OUTPUT (+)
 PIN C* OUTPUT (-)
 PIN E } 80% shunt calibration
 PIN F }

* 2 - Wire transmitter connections.
 • 0 Volt P791/4



Schaevitz-EM Ltd
 543 Ipswich Road
 Slough, Berks SL1 4EG England
 Tel: (0753) 37622
 Fax: (0753) 823663
 Telex: 847818 G.

Schaevitz Engineering
 U.S. Route 130 & Union Avenue
 Pennsauken, NJ 08100
 Tel: (609) 662 – 8000
 Fax: (609) 662 – 6281
 Telex: (230) 887208

10.3.2. Displacement Transducer

Product Data

Capacitive Transducer — MM 0004

FEATURES:

- No physical contact with structure under test
- Negligible static and dynamic influence on test specimen
- Small mechanical dimensions
- High sensitivity
- No interaction with magnetic transducers
- No influence from magnetic fields
- Operating temperatures up to 250°C (480°F)

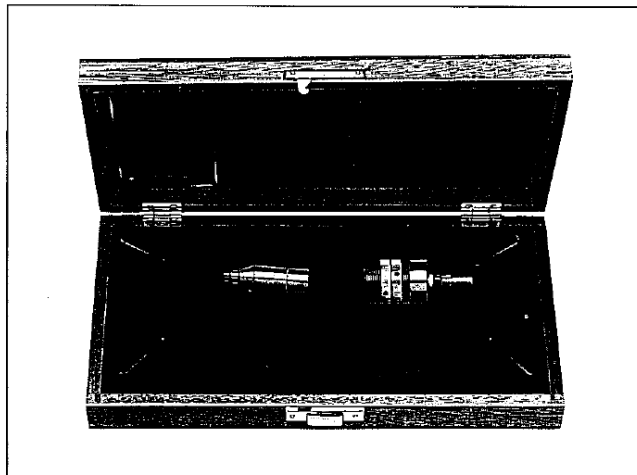
USES:

- Contact free displacement detection
- Vibration measurement
- Counting mechanical events or time between events with electronic counter
- As triggering device for stroboscopes, oscilloscopes, etc.

The Capacitive Transducer MM 0004 is a contact free displacement sensitive pick-up. It finds application where mechanical motion must be detected without loading the test specimen. The Transducer should be used with Preamplifier Type 2639 which receives its necessary supply voltage when connected to one of the Power Supplies 2804, 2807, or to a B & K Measuring Amplifier or Frequency Analyzer.

Description

The capacitive transducer consists of a gold plated electrode which is shielded by the housing to prevent stray capacitance from influencing the measurements. A double screened cable connects the MM 0004 to the preamplifier. The conductor and outer screen of this cable carry the signal while the inner screen is connected to the internal shield (guard ring) of the preamplifier. This means that the cable capacity has no influence on the measurements and the transducer is only loaded by the very high input impedance of the preamplifier (10 GΩ).



When the capacitive transducer is mounted with the plane of the electrode parallel to and at a suitable distance from the test specimen, an air-gap capacitor is formed which is charged by the polarization voltage

(200 V) of the preamplifier. When the plate distance, d_0 , changes due to vibrations, an alternating voltage will occur proportional to the vibration displacement. A static attraction between the electrodes exists due to the

voltage differential across them. This force is very small (approximately $56\mu\text{N}$ with a $0,5\text{ mm}$ gap), so the influence on measurements will be negligible.

The distance between the transducer and the test specimen is not critical,

and a distance which is approximately ten times the test specimen displacement is satisfactory in most cases.

If the test object to be measured upon is made from a non-conducting material, the other electrode of the air-gap capacitor can be made as

shown in Fig.2. One end of a thin metal foil is fixed to the vibrating object while the other end is electrically connected to the housing of the transducer via the clamping arrangement.

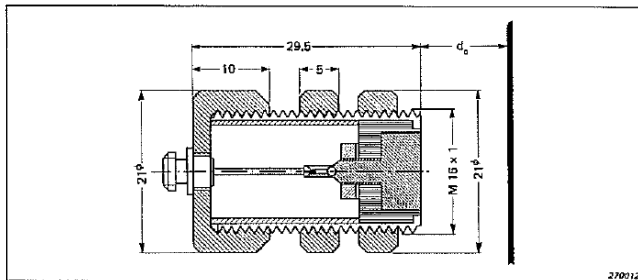


Fig.1. Cross section view of the Capacitive Transducer with indication of the main dimensions in mm (1 mm = 0,0394 in)

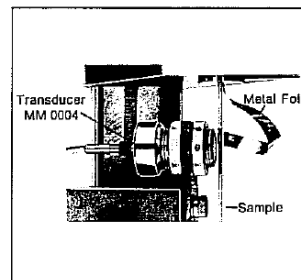


Fig.2. The Capacitive Transducer used to detect the motion of an object made from a non-conducting material

Specifications MM 0004


<p>SENSITIVITY: Inversely proportional to the square of the distance (d_0) between the electrode of the MM 0004 and the test specimen Typically: $0,8\text{ V RMS}$ at $d_0 = 0,5\text{ mm}$ and peak-to-peak displacement $0,1\text{ mm}$</p>	<p>STATIC FORCE: Inversely proportional to the square of d_0 Typically: $56\mu\text{N}$ at $d_0 = 0,5\text{ mm}$</p> <p>WORKING TEMPERATURE (continuous): Max. 250°C</p>	<p>POLARIZATION VOLTAGE: 200 V</p> <p>ELECTRODE AREA: $0,78\text{ cm}^2$ (in^2)</p>
<p>FREQUENCY RANGE: 20 Hz to 200 kHz</p>	<p>DISTORTION: Inversely proportional to d_0 Therefore d_0 should be more than 10 times the maximum displacement and not less than $0,5\text{ mm}$ to keep distortion below 5%</p>	<p>WEIGHT (excl. cable): $46,9\text{ g}$ ($1,66\text{ oz}$)</p>
<p>CAPACITANCE: Inversely proportional to d_0 Typically: $1,5\text{ pF}$ at $d_0 = 0,5\text{ mm}$</p>		<p>ACCESSORIES INCLUDED: Cable.....AO 0054</p>

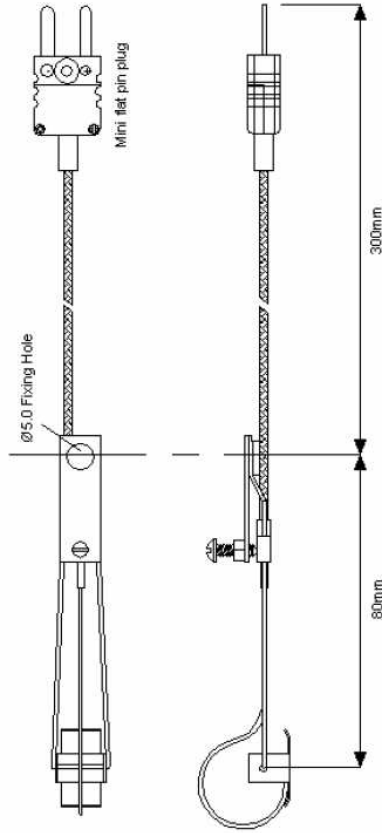
Brüel & Kjær 

WORLD HEADQUARTERS: DK-2050 Nærum · Denmark · Telephone: +45 42 80 05 00 · Telex: 37316 bruka dk · Fax: +45 42 80 14 05

Australia (02) 450-2066 · Austria 02235/7550 · Belgium 02-242-97 45 · Brazil (011) 246-8149/246-8166 · Canada (514) 695-8225 · Finland (80) 80 17 044
France (1) 64 57 20 10 · Federal Republic of Germany (04105) 4055 · Great Britain (01) 954-2356 · Holland 03 402-39 994 · Hong Kong 5-487406 · Italy (02) 52 44 141
Japan 03-438-0761 · Republic of Korea (02) 554-0605 · Norway 02-78 70 96 · Portugal (1) 65 92 56/65 92 80 · Singapore 225 6533 · Spain (91) 269 10 00
Sweden (08) 711 27 30 · Switzerland (042) 85 1 1 61 · Taiwan (02) 713 8303 · USA (508) 461-7000 · Local representatives and service organisations world-wide

10.3.3. Rubbing Thermocouple





Drawing Ref:	HTA 1001		
Description:	Type K, Rubbing or Contact Thermocouple		
Drawn By:	Tim King		
Date:	23/10/2006	Issue No:	01

Copyright of this drawing belongs to Tim King, High Tech Sensors and TCSensors and should not be copied or used without the explicit consent of Tim King

- 0.5mm (0.020") diameter, Mineral Insulated (M.I.), thermocouple.
- 310ss sheath material.
- Insulated Junction (ungrounded) from sheath at temperature measuring tip.
- Type K thermocouple conductors (wires).
- Simplex Circuit (single circuit) (2 wire).
- Fully adjustable tensioning of the ss floating rubbing shoe to reduce friction heat.
- Accuracy of thermocouple output generally $\pm 1.5^{\circ}\text{C}$ or 0.007% of the temperature.
- Thermocouple temperature range: -40°C to $+ 1100^{\circ}\text{C}$ at rubbing shoe.
- Mini flat pin thermocouple plug in IEC Colours (green).
- 5mm (0.20") diameter fixing hole.

10.4. FFT MATLAB code

```
%input data from excel into variable s
clear
close all
filename='29.xls';
s = xlsread(filename);
[m n]=size(s);
%make length of signal even
if m/2-floor(m/2)~=0
    m=m-1;
end
s=s(1:m);

%sampling frequency & Time
Fs=1000;
Ts=1/Fs;

%plot signal
time=Ts*(1:m)';
plot(time,s)
xlabel('time')
title(filename)

%calculate fft
y=fft(s);
yy=abs(y);
ff=(Fs/m)*(0:m/2-1)'; %frequency up to half sampling freq
Y=20*log10(yy); %power spectrum

%plot fft
figure,plot(ff,Y(1:m/2));
xlabel('frequency')
ylabel('power spectrum (dB)')
title(filename)

maxY = max(abs(Y));
minY = min(abs(Y));

h = floor( (maxY + minY) / 15 );
%Sets frequencies with power less than tol1 to zero
for tol1 = minY:h:maxY
    T=y;
    T( find(abs(Y)<tol1) ) = 0; %tol1ONE
    S = real( ifft(T) );
    figure,
    subplot(2,1,1), plot(time,S);
    title(['For tol1: abs(dB) < ', num2str(tol1)]);
    subplot(2,1,2), plot(time,(s-S))
    title('Error between original and filtered signal');
end
```

10.5. On-Vehicle BPV Development

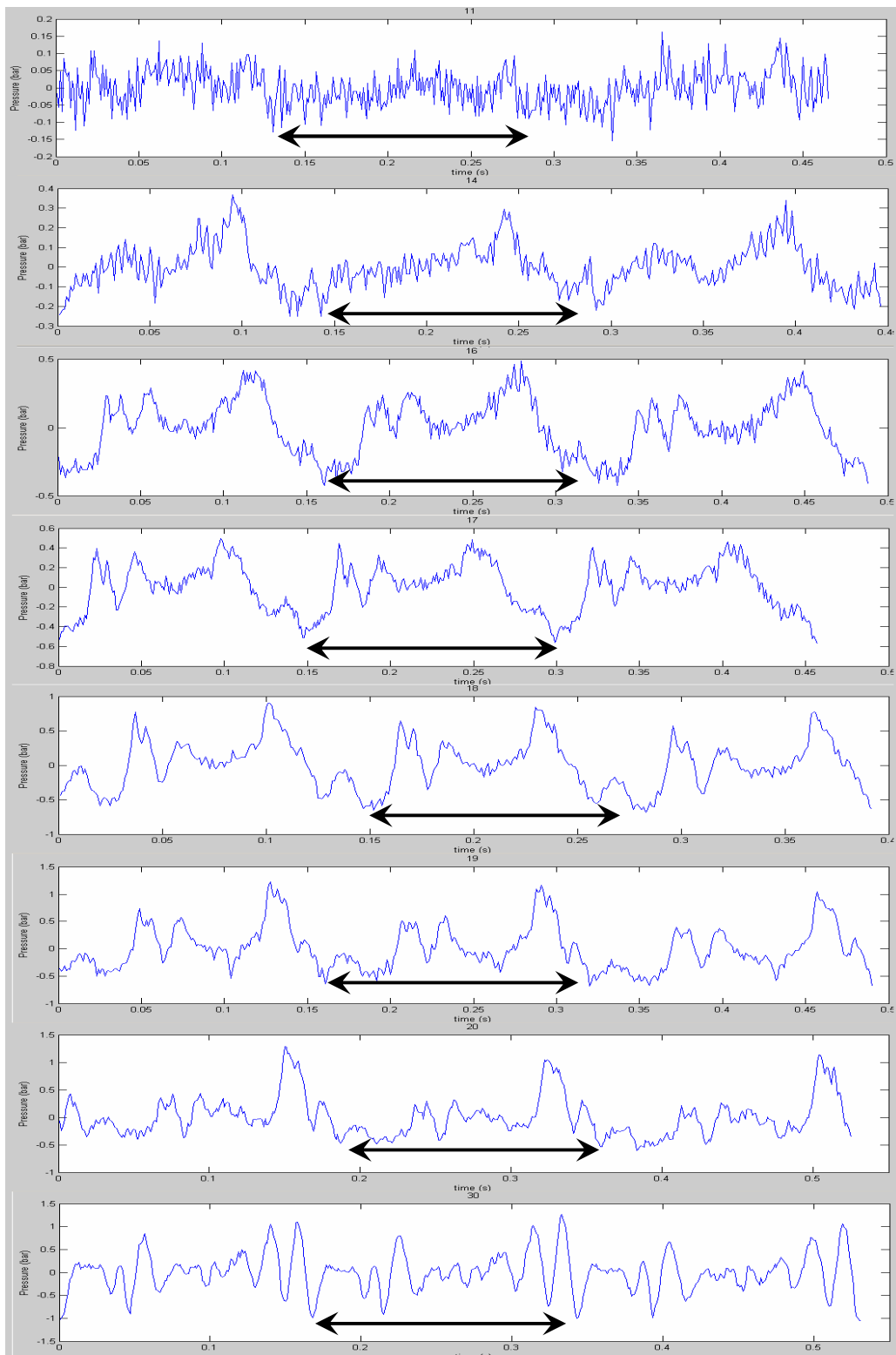


Figure 10.1: On-Vehicle BPV Development for left hand front brake disc following on-vehicle testing; selected braking events between stops 11 to 30, one revolution indicated by arrow.